Vol. 126, May 1, 1981
Complete in one issue

ISSN 0003-2670

ANALYTICA CHIMICA ACTA

International journal devoted to all branches of analytical chemistry

ELSEVIER SCIENTIFIC PUBLISHING COMPANY

ANALYTICA CHIMICA ACTA

International journal devoted to all branches of analytical chemistry
Revue internationale consacrée à tous les domaines de la chimie analytique
Internationale Zeitschrift für alle Gebiete der analytischen Chemie

PUBLICATION SCHEDULE FOR 1981 (incorporating the section on Computer Techniques and Optimization).

	J	F	M	A	M	J	J	A	S	O	N	D
Analytica Chimica Acta	123	124/1	124/2	125	126	127	128	129	130/1	130/2	131	132
Section on Computer Techniques and Optimization		133/1			133/2			133/3			133/4	

Scope. *Analytica Chimica Acta* publishes original papers, short communications, and reviews dealing with every aspect of modern chemical analysis, both fundamental and applied. The section on *Computer Techniques and Optimization* is devoted to new developments in chemical analysis by the application of computer techniques and by interdisciplinary approaches, including statistics, systems theory and operation research. The section deals with the following topics: Computerized acquisition, processing and evaluation of data. Computerized methods for the interpretation of analytical data including chemometrics, cluster analysis, and pattern recognition. Storage and retrieval systems. Optimization procedures and their application. Automated analysis for industrial processes and quality control. Organizational problems.

Submission of Papers. Manuscripts (three copies) should be submitted as designated below for rapid and efficient handling:

Papers from the Americas to: Professor Harry L. Pardue, Department of Chemistry, Purdue University, West Lafayette, IN 47907, U.S.A.

Papers from all other countries to: Dr. A. M. G. Macdonald, Department of Chemistry, The University, P.O. Box 363, Birmingham B15 2TT, England.

For the section on *Computer Techniques and Optimization:* Dr. J. T. Clerc, Universität Bern, Pharmazeutisches Institut, Sahlistrasse 10, CH-3012 Bern, Switzerland.

American authors are recommended to send manuscripts and proofs by INTERNATIONAL AIRMAIL.

Submission of an article is understood to imply that the article is original and unpublished and is not being considered for publication elsewhere. Upon acceptance of an article by the journal, the author(s) resident in the U.S.A. will be asked to transfer the copyright of the article to the publisher. This transfer will ensure the widest dissemination of information under the U.S. Copyright Law.

Information for Authors. Papers in English, French and German are published. There are no page charges. Manuscripts should conform in layout and style to the papers published in this Volume. Authors should consult Vol. 121, p. 353 for detailed information. Reprints of this information are available from the Editors or from: Elsevier Editorial Services Ltd., Mayfield House, 256 Banbury Road, Oxford OX2 7DE (Great Britain).

Reprints. Fifty reprints will be supplied free of charge. Additional reprints (minimum 100) can be ordered. An order form containing price quotations will be sent to the authors together with the proofs of their article.

Advertisements. Advertisement rates are available from the publisher.

Subscriptions. Subscriptions should be sent to: Elsevier Scientific Publishing Company, P.O. Box 211, 1000 AE Amsterdam, The Netherlands. The section on *Computer Techniques and Optimization* can be subscribed to separately.

Publication. *Analytica Chimica Acta* (including the section on *Computer Techniques and Optimization*) appears in 11 volumes in 1981. The subscription for 1981 (Vols. 123–133) is Dfl. 1639.00 plus Dfl. 198.000 (postage) (total approx. U.S. $942.00). The subscription for the *Computer Techniques and Optimization* section only (Vol. 133) is Dfl. 149.00 plus Dfl. 18.00 (postage) (total approx. U.S. $86.00). Journals are sent automatically by airmail to the U.S.A. and Canada at no extra cost and to Japan, Australia and New Zealand for a small additional postal charge. All earlier volumes (Vols. 1–121) except Vols. 23 and 28 are available at Dfl. 164.00 (U.S. $84.00), plus Dfl. 13.00 (U.S. $6.50) postage and handling, per volume.

Claims for issues not received should be made within three months of publication of the issue, otherwise they cannot be honoured free of charge.

Customers in the U.S.A. and Canada who wish to obtain additional bibliographic information on this and other Elsevier journals should contact Elsevier/North Holland Inc., Journal Information Center, 52 Vanderbilt Avenue, New York, NY 10017. Tel: (212) 867-9040.

MERCK solvents – an imposing array

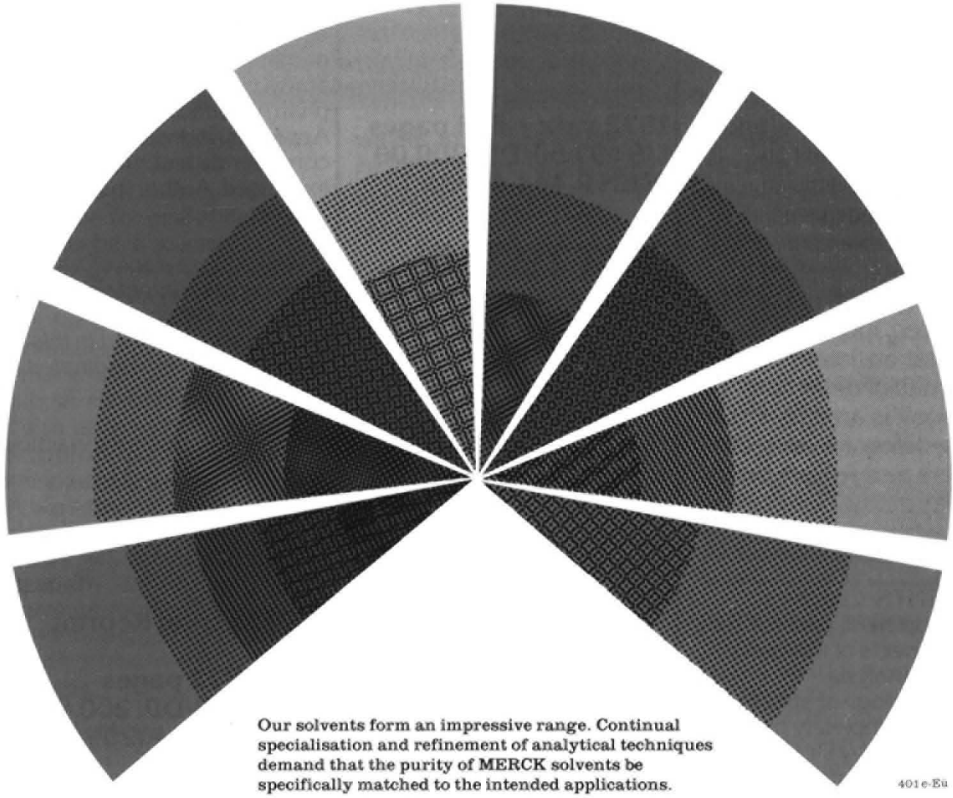

Our solvents form an impressive range. Continual specialisation and refinement of analytical techniques demand that the purity of MERCK solvents be specifically matched to the intended applications.

401e-Eu

Our range includes:

pro analysi solvents
pro analysi solvents, dried (max. 0.01% H_2O)
solvents for pesticide residue analysis
solvents for extraction analysis
Uvasol® solvents for spectroscopy
Uvasol® solvents for fluorescence spectroscopy
solvents for scintillation measurements
solvents for chromatography LiChrosolv®
solvents for synthesis
The Merck box system enables you to save up to 22%.
Please send for our brochures.

E. Merck, Darmstadt
Federal Republic of Germany

SPOT TESTS IN INORGANIC ANALYSIS

Sixth English Edition, Completely Revised and Enlarged.

By FRITZ FEIGL in collaboration with VINZENZ ANGER.

This standard work investigates the application of specific, selective, and sensitive reactions to research problems in qualitative inorganic analysis. It examines all pertinent information relating to each of the 742 tests cited, including details of operation, interferences and limits of detection. The book is an easy-to-use research tool for laboratory workers and researchers in analytic inorganic chemistry and related fields.

CONTENTS: Chapters. 1. Development, present state and prospects of inorganic spot test analysis. 2. Methodology of spot test analysis (completely revised and enlarged by Dr. G. Skalos). 3. Preliminary orientational tests. 4. Tests for the elements, their ions and compounds. 5. Application of spot reactions in tests of purity, examination of technical materials, studies of minerals. 6. Tabular summary.

"... will doubtlessly remain the authoritative book on the subject for a long time."

- Journal of the Electrochemical Society

"The book should be in chemistry libraries at all levels."

- Choice

"The volume contains a wealth of useful information and belongs on the reference shelf of every chemist who has occasion to carry out simple, rapid and selective detection tests without resorting to the use of a $40,000 instrument.

- Journal of Chemical Education

1972 xxix + 698 pages
US $97.50/Dfl. 200.00
ISBN 0-444-40929-7

SPOT TESTS IN ORGANIC ANALYSIS

Seventh English Edition, Completely Revised and Enlarged.

by FRITZ FEIGL in collaboration with VINZENZ ANGER.

This volume deals with all theoretical and practical aspects of the applications of spot tests to organic analysis. Information is given on more than 900 tests. This book continues to be of great value to organic and analytical chemists in academic as well as industrial laboratories.

CONTENTS: Chapters: 1. Development, present state and prospects of organic spot test analysis. 2. Preliminary (exploratory) tests. 3. Detection of characteristic functional groups in organic compounds. 4. Detection of structures and certain types of organic compounds. 5. Identification of individual organic compounds. 6. Applications of spot tests in the differentiation of isomers and homologous compounds. Determination of constitutions. 7. Applications of spot reactions in the testing of materials, examination of purity, characterization of pharmaceutical products etc. Appendix. Individual compounds and products examined. Author index. Subject Index.

"Even in these days of physical instrumentation there is ample room for the techniques described in this book which were originated and largely developed by Prof. Feigl."

- Laboratory Practice

"It should be classified as a 'must' for every laboratory, regardless of its field of specialization."

- Talanta

1966 Second Reprint 1975
xxiii + 772 pages
US $97.50/Dfl. 200.00
ISBN 0-444-40209-8

ELSEVIER

P.O. Box 211, 1000 AE Amsterdam, The Netherlands

52 Vanderbilt Avenue, New York, NY 10017

The Dutch guilder price is definitive. US $ prices are subject to exchange rate fluctuations.

ANALYTICA CHIMICA ACTA
VOL. 126 (1981)

ANALYTICA CHIMICA ACTA

International journal devoted to all branches of analytical chemistry

ELSEVIER SCIENTIFIC PUBLISHING COMPANY

Anal. Chim. Acta, Vol. 126 (1981)

Printed in The Netherlands.

Analytica Chimica Acta, 126 (1981) 1—13
Elsevier Scientific Publishing Company, Amsterdam — Printed in The Netherlands

TRANSPORT PHENOMENA IN FLOW INJECTION ANALYSIS WITHOUT CHEMICAL REACTION

J. M. REIJN*, W. E. VAN DER LINDEN[a] and H. POPPE

Laboratory for Analytical Chemistry, University of Amsterdam, Nieuwe Achtergracht 166, 1018 WV Amsterdam (The Netherlands)

(Received 20th October 1980)

SUMMARY

Dispersion phenomena play a very important role in flow injection analysis. In this paper, physical transport phenomena in flow injection methods are discussed. Three different types of reactor — a straight tube, a helically coiled tube and a new single bead string reactor — are compared. Under similar flow conditions, the dispersion in the single bead string reactor is the lowest. The specific advantages of single bead string reactors are their very simple preparation and maintenance and the good reproducibility of the peaks. It is shown that in open capillary tubes (coiled or not) the Taylor dispersion equation is of very limited use, because the residence times are too short, and because secondary flow occurs in the case of coiled tubes.

One of the less understood aspects of flow injection analysis (f.i.a.) is the dispersion process which takes place during the transport of the sample from the injection device towards the detector. The total peak broadening contains contributions from three sources

$$\sigma^2_{\text{peak}} = \sigma^2_{\text{injection}} + \sigma^2_{\text{transport}} + \sigma^2_{\text{detection}} \quad (1)$$

In a previous article [1] attention was focussed on the contribution of the injection to the total peak broadening, whereas in the present study the role of transport is investigated. If very small sample volumes are injected, and injection and detection devices causing negligible additional peak broadening are used, eqn. (1) can be reduced to $\sigma^2_{\text{peak}} = \sigma^2_{\text{transport}}$. In this study only the physical aspects of the dispersion will be considered, and it is assumed that no chemical reaction between the sample and reagent stream takes place.

Two types of model have been frequently used to describe the dispersion process. The first model is the tanks-in-series model which is closely related to the concept of age distribution functions and was introduced by Danckwerts [2]. This model has the advantage of mathematical simplicity and elegance (see, e.g., [1]). The second model is the axial dispersion model of Levenspiel and Bischoff [3]. This model has the advantage of analogy to

[a]Present address: Technical University, Laboratory for Chemical Analysis, Afd. CT-THT, P.O. Box 217, 7500 AE Enschede, The Netherlands.

0003—2670/81/0000—0000/$02.50

the differential equation which describes a diffusion process in the presence of convection. In some cases this model leads to direct solutions [4], for which reason it will be used in the subsequent argument. For a full discussion of the merits of the two models, reference is made to Levenspiel and Bischoff [3] and Froment and Bischoff [5].

THEORY OF THE AXIAL DISPERSION MODEL

Basically the axial dispersion model is described by a one-dimensional diffusion equation containing a convective term. The mass balance for the axial dispersion model is (for the symbols used, see Table 1)

$$(\partial C/\partial t) + (\langle v\rangle \partial C/\partial z) = D_L \partial^2 C/\partial z^2 \quad (2)$$

The system is, as usual, assumed to be infinitely long; boundary conditions have been discussed [3]. For a delta injection (total mass M present at $z = 0$ for $t = 0$), this equation has the solution

$$C(z,t) = (M/\pi R^2)\,(4\pi D_L t)^{-1/2} \exp[-(z - \langle v\rangle t)^2/4D_L t] \quad (3)$$

which is a modified Gaussian function. When a detector is placed at $z = L$, eqn. (3) describes the concentration as a function of time, i.e., the elution curve. Important parameters of this curve are the first and second statistical moments, i.e., the mean m and the variance σ_t^2. From eqn. (3), these parameters can be derived as

$$m = (L/\langle v\rangle) + (2\,D_L L/\langle v\rangle^3) \text{ and } \sigma_t^2 = (2\,D_L L/\langle v\rangle^3) + (8\,D_L/\langle v\rangle^4)$$

The dimensionless group $\langle v\rangle L/D_L$ is referred to as the axial or longitudinally-

TABLE 1

List of symbols

A	absorbance	h	reduced plate height	$\langle v\rangle$	true mean fluid velocity
C	concentration	M	total mass injected		
C_m	mean value concentration	L	reactor length	$\langle v_0\rangle$	superficial mean fluid velocity
D_L	axial dispersion coefficient	m	mean	z	axial coordinate
		N	number of beads	ϵ	void fraction
D_m	molecular diffusion coefficient	N_{th}	plate number	κ	peak width reduction coefficient
		ΔP	pressure drop		
Dn	Dean number (Dn = Re/$\lambda^{1/2}$)	Pe_L	axial Peclet number	λ	aspect ratio (d_h/d_t)
		Pe_r	radial Peclet number	ν	kinematic viscosity
d_c	column diameter	R	tube radius	ρ	column-to-particle diameter ratio (d_c/d_p)
d_h	helix diameter	Re	Reynolds number		
d_M	equivalent hydraulic diameter	Re_p	Reynolds number based on particle diameter	ρ_s	specific gravity
				σ_t^2	variance
d_p	particle diameter	r	radial coordinate	τ	dimensionless time ($\tau = tD_m/R^2$)
d_t	tube diameter	Sc	Schmidt number		
f_v	volumetric flow rate	t	time	τ_v	dimensionless residence time
H	plate height	t_v	residence time		

based Peclet number Pe_L. When $Pe_L > 100$, $m = L/\langle v \rangle$ and $\sigma_t^2 = 2D_L L/\langle v \rangle^3$, and eqn. (3) can be simplified to

$$C_{(L,t)} = C_{max} \exp[-(m - t)^2/2\,\sigma_t^2] \tag{4}$$

where $C_{max} = (M/\pi R^2)\,(\langle v \rangle/4\pi L D_L)^{1/2}$.

It must be stressed that D_L (or Pe_L) is still an entirely empirical parameter, as is the number of tanks in the tanks-in-series model [1]. In the subsequent paragraphs, the physical meaning of D_L will be investigated in some detail for various reactor types.

Straight tube

For the case of laminar flow in a round tube, a direct solution of the convective diffusion equation was given by Taylor [4]. The convective diffusion for this case reads (in cylindrical coordinates)

$$(\partial C/\partial t) + 2\langle v \rangle(1 - r^2/R^2)\,(\partial C/\partial z) = D_m\,[(\partial^2 C/\partial r^2) + (r^{-1}\,\partial C/\partial r) + (\partial^2 C/\partial z^2)] \tag{5}$$

If the time elapsed from the time of injection is long enough to stabilize the radial concentration changes, eqn. (5) can be simplified to

$$D_L \partial^2 C_m/\partial z_1^2 = \partial C_m/\partial t \tag{6}$$

The symbols in this equation are defined by $z_1 = z - \langle v \rangle t$; $C_m = 2R^{-2} \int_0^R Cr\,dr$; and $D_L = R^2\langle v \rangle^2/48\,D_m$.

In fact, eqn. (6) describes the dispersion as a diffusion process relative to a point moving with the mean velocity $\langle v \rangle$ of the fluid stream. The apparent diffusion coefficient is D_L. When again a delta injection is applied to eqn. (6) the solution is equal to eqn. (3). However, the axial dispersion coefficient D_L is no longer an empirical parameter, but is directly connected to physical quantities via the above definition of D_L.

Later, Aris [6] gave a refined treatment and found

$$D_L = D_m + R^2\langle v \rangle^2/48\,D_m \tag{7}$$

However, under f.i.a. conditions, the second term on the right-hand side of eqn. (7) is always much larger than the first term, and so the first term can be neglected. For low D_L values, eqn. (7) can then be rewritten

$$\sigma_t^2 = R^2 m/24\,D_m \tag{8}$$

An important question arises about the time which is necessary to fulfil the condition for stabilization of the radial concentration changes. For this, Taylor gives the condition $t \gg R^2/(3.8)^2 D_m$ or $\tau \gg 0.07$, where τ is a dimensionless time defined by $\tau = t\,D_m/R^2$. Later investigators gave more exact criteria. Lighthill [7] gives $\tau > 0.5$ and Ananthakrishnan et al. [8] give $\tau > 0.8$. Recently, Golay and Atwood [9] reported a computer simulation of the early stages of the development of the concentration profile in

laminar flow; the criterion $\tau > 0.8$ can again be derived from this work. As will be shown later, τ is less than 0.8 in nearly all published f.i.a. work. For this reason, the Taylor theory is of limited use for f.i.a.

In the same study, Golay and Atwood demonstrated the possible occurrence of double peaks which were also predicted by the numerical analysis of Gill and Ananthakrishnan [10]. It also follows from [10] that the detection process (mean value or cup-mixing detection) can greatly influence the shape of the elution curve at small values of τ. For the case of pure convection, this was shown theoretically by Reijn et al. [1].

Coiled tubes

In a helically coiled tube, secondary flow phenomena cause a decrease in the peak broadening because of increased radial mass transport. As was pointed out by Tijssen [11] and Van den Berg et al. [12], this improves the analytical usefulness of tubular reactors. According to Van den Berg et al.

$$D_L = R^2\langle v\rangle^2 \cdot \kappa / 48\, D_m \tag{9}$$

where $\kappa = 5.6\ (\mathrm{DnSc}^{1/2})^{-0.67}$ (for $12.5 < \mathrm{DnSc}^{1/2} < 200$) (10a)

$$\kappa = 1 \qquad \text{(for } \mathrm{DnSc}^{1/2} < 12.5\text{)} \tag{10b}$$

(for listing of symbols, see Table 1). For a liquid with Sc = 500 ($D_m = 2 \times 10^{-9}$ m^2s^{-1} in water), condition (10a) becomes $0.56 < Dn < 8.9$.

As the Dean number Dn is given by $Dn = Re/\lambda^{1/2}$ (λ is the aspect ratio, i.e., coil diameter/tube diameter) and practical f.i.a. is carried out in the range $10 < Re < 500$, it can be seen immediately that even for a very slight coiling with say $\lambda = 1000$, serious deviations from Taylor dispersion caused by secondary flow are to be expected in f.i.a. As the trend in f.i.a. is towards miniaturization, the secondary flow effects are even more likely to be present (in tightly coiled tubes λ is much smaller, so Dn is much larger). Only for very low flow rates where $Dn < 0.56$, can Taylor dispersion be expected (provided that the residence time requirements are fulfilled).

Packed bed reactors

Packed bed reactors have been used both by engineers and by chromatographers. As has been indicated by Horne et al. [13], the influence of the ratio ρ of the column diameter to particle diameter has been investigated for chromatography in the range $5 < \rho < 50$. Recently Scott et al. [14] used a reactor with $\rho \to 1$. These authors used porous beads (pellets) and introduced the term "single pellet string reactor" SPSR. For the case of non-porous beads and $\rho \to 1$, the name "single bead string reactor", (SBSR) is proposed.

According to Horne et al. [13], the axial dispersion coefficient D_L for liquids in a packed bed ($5 < \rho < 50$) is given by

$$\langle v\rangle d_p < D_L < 2\langle v\rangle d_p \tag{11}$$

where $\langle v\rangle$ is the mean interparticle fluid velocity and d_p the particle diameter.

In chromatography the plate height H is generally used to describe dispersion phenomena. In order to facilitate comparisons, some chromatographic terms are defined here. For a given column (reactor) of length L, plate height H is defined by $H = L\,\sigma_t^2/m^2 = L/N_{th} = 2L/Pe_L$, where N_{th} is the number of plates in the column. From this definition it follows that $D_L = H\langle v\rangle/2$. In packed beds, a reduced plate height is introduced: $h = H/d_p$, and so, in chromatographic terms, expression (11) can be written as $2 < h < 4$. Further details are given by Horne et al. [13]. It must be stressed here that expression (11) for D_L and the expression $2 < h < 4$ are valid only for $5 < \rho < 50$. For the behaviour of D_L and h when $\rho \to 1$, no results seem to have been published for liquids.

Pressure drop

For the case of laminar flow in a straight tube, the pressure drop ΔP is given by the Hagen-Poiseuille relation

$$\Delta P/L = 8\eta\langle v\rangle/R^2 = 8\eta f_v/\pi R^4 \tag{12}$$

As pointed out by Tijssen [11] this relation remains valid for helically coiled tubes provided that $Dn < 100$, as will nearly always be the case in f.i.a.

For packed bed reactors, a well known equation for the pressure drop is the Ergun relation

$$\Delta P/L = \rho_s(\langle v_0\rangle^2/d_p)\,[(1-\epsilon)/\epsilon^3]\,[150\,(\nu/\langle v_0\rangle d_p)\,(1-\epsilon) + 1.75] \tag{13}$$

For the case of gases, Scott et al. [14] found that the pressure drop for a SPSR could be described adequately when the Ergun relation was used with a modified particle diameter d_M, which these authors defined as

$$d_M = d_p/[1 + (d_t L/d_p^2 N)] \tag{14}$$

In this definition wall effects have been taken into account. For the case of liquids this modified Ergun relation has not yet been verified.

FLOW CONDITIONS IN FLOW INJECTION ANALYSIS

It is convenient to use dimensionless quantities for the description of the flow conditions in f.i.a. experiments. The Reynolds number relates the mean fluid velocity $\langle v\rangle$, the tube radius R and the kinematic viscosity ν

$$Re = 2R\langle v\rangle/\nu = 2f_v/\nu\pi R \tag{15}$$

In the case of packed beds and for the SBSR, a modified Reynolds number is used

$$Re_p = \langle v\rangle\, d_p/\nu = \langle v_0\rangle d_p/\nu\epsilon \tag{16}$$

For the case of very dilute aqueous solutions, eqn. (15) can be simplified to $Re = 21.2\,f_v/d_t$ when the volumetric flow rate f_v is expressed in ml min^{-1} and the tube diameter d_t is given in mm. The Schmidt number, Sc, is the ratio of

the kinematic viscosity, ν, and the molecular diffusion coefficient, D_m: Sc = ν/D_m.

Time is made dimensionless by the transformation $\tau = t\, D_m/R^2$. Time is thus "reduced" to a molecular diffusion scale.

For a number of single-line f.i.a. experiments reported in the literature, some relevant dimensionless quantities were calculated (Table 2). All sample and reagent solutions were assumed to be very dilute aqueous solutions with a kinematic viscosity $\nu = 10^{-6}$ m^2 s^{-1}. For the molecular diffusion coefficient D_m, the value taken was 2×10^{-9} m^2 s^{-1} (so that Sc = 500). To date, most flow injection procedures have involved flow rates higher than 0.5 ml min^{-1} and tube diameters smaller than 1 mm. From the recalculated data in Table 2 it can be seen that the lower limit of Re is 12. As the Schmidt number for pure water is 200, the product ReSc will be higher than 2000. This means that the first term on the right-hand side of eqn. (7) can indeed be neglected.

Furthermore, it can be seen that nearly all determinations are made at τ_v values <0.8. Therefore in the case of straight tubes, the validity of the Aris—Taylor model is questionable. As was pointed out above in the case of helically coiled tubes, the Aris—Taylor model is not valid because of the secondary flow (even when $\tau_v > 0.8$).

TABLE 2

Flow conditions in f.i.a.[a]

Flow rate (ml min^{-1})	Line length (m)	Tube diameter (mm)	Re	ReSc	t_v (s)	τ_v	Ref.
7.06	3.00	0.766	195	97000	11.7	0.16	[11]
3.36	10.00	0.25	283	142000	35	4.48	[12]
1.5	0.05	0.50	63	31500	0.4	0.012	[15]
1.5	0.25	0.50	63	31500	2.0	0.062	[15]
1.5	0.75	0.50	63	31500	5.9	0.188	[15]
1.5	1.25	0.50	63	31500	9.8	0.314	[15]
1.5	1.75	0.50	63	31500	13.7	0.439	[15]
1.5	2.50	0.50	63	31500	19.6	0.628	[15]
1.5	3.00	0.50	63	31500	23.6	0.754	[15]
1.5	3.50	0.50	63	31500	27.5	0.880	[15]
18	2.50	1.00	350	175000	6.5	0.052	[16]
10	1.50	1.00	212	106000	7.1	0.057	[16]
8.6	4.90	1.00	182	91000	26.8	0.21	[17]
8.6	5.00	1.00	182	91000	27.4	0.22	[18]
0.6	0.50	1.00	12	6000	39.3	0.31	[19]
4.0	0.85	1.00	84	42000	10.0	0.08	[20]
3.0	1.06	1.00	63	31500	16.7	0.13	[21]
1.0	0.80	1.00	21	10500	23.6	0.188	[22]
2.0	0.30	1.00	42	21000	7.1	0.056	[23]
1.0	0.37	0.80	37	18500	11.2	0.139	[24]

[a]Some of the data for this table were obtained from a review by Betteridge [25].

EXPERIMENTAL

Three different reactors were used in a f.i.a. arrangement: (1) a straight tube, which was not bent at all, with the dimensions $L = 1.48$ m, $d_t = 0.592 \times 10^{-3}$ m, and $V = 407 \times 10^{-9}$ m^3; (2) a helically coiled tube of the same dimensions with an aspect ratio $\lambda = 10$; (3) a SBSR, for which the relevant data are summarized in Table 3, and which was dry-packed; the design of the SBSR is shown in Fig. 1(a).

The carrier stream was a 0.1 mol l^{-1} solution of potassium nitrate. The sample solution was also a 0.1 mol l^{-1} solution of potassium nitrate that contained potassium permanganate (10^{-3} mol l^{-1}). The potassium nitrate was added to reduce the concentration dependence of the molecular diffusion coefficient of the potassium permanganate. The injection volume was ca. 14×10^{-9} m^3. The injection was of the slug type and was done with an Altex injection valve. This valve was automatically switched by means of a pneumatic actuator (Durrum).

The detector was a home-made borosilicate glass optical cell (Fig. 1b) with a pathlength of ca. 5 mm and an inner diameter of ca. 0.5 mm. Connections with the spectrophotometer (Zeiss PMQ II with a digital read-out and an analog absorbance output) were made with glass fibers, so that dead volumes from the connections were negligible. All measurements were made at a wavelength of 525 nm (the absorption maximum of potassium permanganate). The elution curves were digitized with a 12-bit A/D converter and punched on paper tape. Data processing was done on a Varian minicomputer (Varian V76).

RESULTS

Figures 2—4 show the peak shapes obtained in these experiments. In the case of the straight tube (Fig. 2) two extremes are clearly shown: the Taylor

TABLE 3

Hydrodynamic and geometric constants for the SBSR

Tube diameter, d_t	0.750×10^{-3} m	Number of particles/ unit length, N/L	1730 m^{-1}
Particle diameter, d_p	0.600×10^{-3} m		
Void fraction, ϵ	0.56	Equivalent diameter, d_M	2.72×10^{-4} m
Reactor length, L	1.64 m	Flow-rate range, f_v	0.2—1.5 ml min^{-1}
Open volume, Vo	724×10^{-9} m^3	Reynolds number, Re_p	4—35
Void volume, ϵVo	406×10^{-9} m^3	Specific gravity, ρ_s	998 kg m^{-3}
		Kinematic viscosity, ν	10^{-6} m^2 s^{-1}

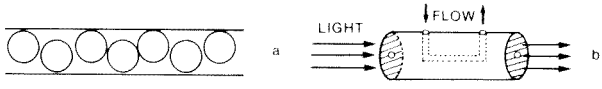

Fig. 1. Some experimental details. (a) Principle of the single bead string reactor; (b) home-made optical flow-through cell.

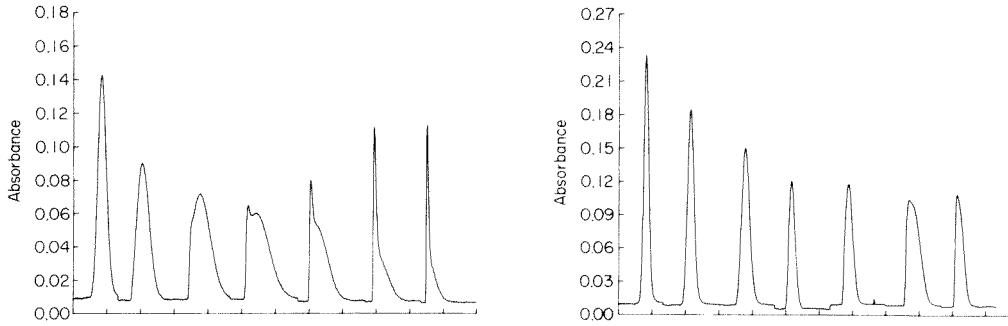

Fig. 2. Peak shapes in straight tubes. On the vertical axis, absorbance is plotted. For each peak a different time-scale is used on the horizontal axis: from left to right $\tau \approx 1$; $\tau \approx 0.7$; $\tau \approx 0.4$; $\tau \approx 0.3$; $\tau \approx 0.2$; $\tau \approx 0.1$; $\tau \approx 0.05$.

Fig. 3. Peak shapes in coiled tubes. See legend for Fig. 2.

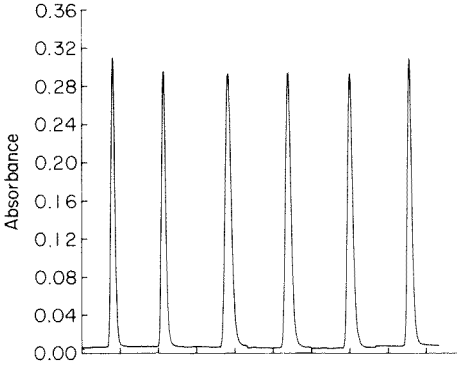

Fig. 4. Peak shapes in the SBSR. Flow conditions (from left to right): 0.2; 0.4; 0.6; 0.8; 1.0; 1.5 ml min^{-1}.

dispersion for large values of τ and convective dispersion for low values of τ. A transition region of τ can also be distinguished, indicated by the occurrence of double peaks. In the coiled tube (Fig. 3) double peaks are not observed, but for low values of τ convective dispersion again becomes more important. In the SBSR, approximately Gaussian peaks were found for all measurements (Fig. 4).

From these experimental data, several peak parameters were calculated. A statistical analysis program with a baseline correction procedure provided values for the peak height, the mean and the variance. In order to obtain some quantitative data on the peak shape, the peak widths at 60% of the height ($w_{0.6}$) and at 10% of the height ($w_{0.1}$) were also calculated. From the variance and the mean, the axial dispersion coefficient D_L was calculated. This parameter has no significance for double peaks or for convective peaks, because the axial dispersion model is not valid in these cases.

In order to facilitate comparison with other literature data, the axial Peclet number Pe_L and the inverse of the radial-based Peclet number $(Pe_r)^{-1}$ were also calculated.

All the calculated data are summarized in Tables 4—6 and Figs. 5—9 show

TABLE 4

Results for the straight tube[a]

Re	τ_v	ReSc	$(Pe_r)^{-1}$	Pe_L	D_L (m^2 s^{-1})
7.2	2.02	5040	25.4	96.5	1.87×10^{-4}
10.8	1.35	7560	36.2	66.0	4.09×10^{-4}
14.4	0.97	10100	50.0	47.5	7.58×10^{-4}
18.0	0.72	12600	66.7	35.0	1.29×10^{-3}
21.6	0.69	15100	71.4	32.5	1.66×10^{-3}
25.2	0.58	17600	76.9	27.5	2.29×10^{-3}
28.8	0.51	20200	80.6	26.5	2.71×10^{-3}
32.4	0.49	22700	98.0	25.5	3.17×10^{-3}
36.0	0.40	25200	109	23.0	3.91×10^{-3}
54.0	0.28	37800	139	18.0	7.50×10^{-3}
72.0	0.20	50400	161	15.5	1.16×10^{-2}
108	0.13	75600	192	13.0	2.08×10^{-2}
144	0.10	101000	238	10.5	3.42×10^{-2}
180	0.085	126000	263	9.5	4.74×10^{-2}
216	0.072	151000	263	9.5	5.68×10^{-2}
288	0.055	175000	313	8.0	7.88×10^{-2}

[a]Although the axial dispersion model is no longer valid for Re > 54.0, apparent values for $(Pe_r)^{-1}$, Pe_L and D_L are included here to indicate any possible trend in the dispersion behaviour.

TABLE 5

Results for the coiled tube

Re	τ_v	ReSc	$(Pe_r)^{-1}$	Pe_L	D_L (m^2 s^{-1})	$DnSc^{0.5}$
7.2	2.02	5040	9.3	270	6.67×10^{-5}	60
10.8	1.35	7560	11.9	210	1.29×10^{-4}	90
14.4	0.97	10100	14.7	171	2.11×10^{-4}	120
18.0	0.72	12600	15.7	160	2.81×10^{-4}	150
21.6	0.69	15100	18.2	137	3.94×10^{-4}	180
25.2	0.58	17600	20.0	125	5.10×10^{-4}	211
28.8	0.51	20200	21.5	116	6.21×10^{-4}	241
32.4	0.47	22700	23.7	106	7.64×10^{-4}	271
36.0	0.40	25200	26.0	96	9.38×10^{-4}	301
54.0	0.28	37800	35.7	80	1.69×10^{-3}	452
72.0	0.20	50400	42.7	60	3.00×10^{-3}	602
108	0.13	75600	51.5	50	5.40×10^{-3}	903
144	0.10	101000	51.0	50	7.20×10^{-3}	1204
180	0.085	126000	55.5	45	1.00×10^{-2}	1506
216	0.072	151000	53.7	47	1.15×10^{-2}	1807
288	0.055	175000	49.5	51	1.23×10^{-2}	2108

TABLE 6

Results for the SBSR

Re_p	τ_v	Re_pSc	$(Pe_r)^{-1}$	Pe_L	h	D_L (m^2 s^{-1})
6.1	1.94	4270	4.1	610	9.0	1.36×10^{-5}
9.1	1.26	6370	4.9	510	10.7	2.43×10^{-5}
12.1	0.97	8470	4.9	510	10.7	3.24×10^{-5}
15.1	0.77	10600	4.9	530	10.3	3.89×10^{-5}
18.2	0.70	12700	5.4	460	11.9	5.41×10^{-5}
21.2	0.58	14800	5.4	460	11.9	6.30×10^{-5}
24.2	0.51	17000	5.5	450	12.1	7.35×10^{-5}
27.3	0.47	19100	5.3	470	11.6	7.94×10^{-5}
30.3	0.41	21200	5.4	460	11.9	9.00×10^{-5}
45.4	0.30	31800	4.6	540	10.1	1.15×10^{-4}

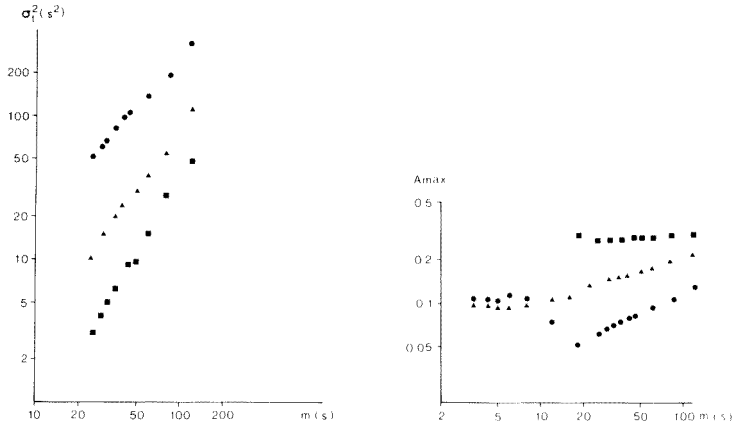

Fig. 5. Peak broadening in three different reactors. Variance of σ_t^2 plotted against mean residence time m: (•) straight tube; (▲) coiled tube; (■) SBSR.

Fig. 6. Peak height (in absorbance units) as a function of the mean residence time m; symbols as in Fig. 5.

graphical presentations of the results. $(Pe_r)^{-1}$ is plotted as a function of ReSc in Fig. 8.

From the measurements in the straight tube with long residence time ($\tau_v > 0.5$) the value for the molecular diffusion coefficient D_m of potassium permanganate was calculated by linear regression from eqn. (8): $D_m = (1.41 \pm 0.03) \times 10^{-9}$ m^2 s^{-1}. This value of D_m corresponds to Sc = 700. All tabulated values of τ_v were calculated with this value for D_m. The transformation factor D_m/R^2 equals 1.61×10^{-2} (s^{-1}).

DISCUSSION

Straight tubes

Taylor dispersion is observed for $\tau > 0.5$. When τ_v becomes smaller, convective dispersion starts to dominate the dispersion process. Theory for a purely convective case was given by Reijn et al. [1]. The transition region (with the double peaks) is very complicated to describe mathematically. From Fig. 7(a) it can be seen that $w_{0.6}$ suddenly decreases at $\tau_v \approx 0.3$. The transition region can also be detected from the discontinuous change in the peak height (Fig. 6) at $\tau \approx 0.3$. The changes in $w_{0.1}$ are less pronounced, mainly because the diffusion process is more effective in the tail of the peak.

For f.i.a. the use of straight tubes is very impractical, but it is a convenient tool for fast determinations of molecular dispersion coefficients, provided that a τ_v value of at least 0.5 is used (for the method, see also Huber and Van Vught [26]).

Coiled tubes

The expected secondary flow effects are unambiguously demonstrated under f.i.a. flow conditions. Reasonable agreement with the correlation of Van den Berg et al. [12] (eqns. 9 and 10) was obtained (Fig. 10). A possible explanation for the deviations at high flow rates is the small value of τ in the present experiments ($\tau \ll 1$) whereas Van den Berg et al. had $\tau > 1$ in all their experiments. Under f.i.a. conditions, the determination of D_m is not possible in a coiled tube because the values of $DnSc^{1/2}$ are too high. Tijssen [27] stated that for negligible deviations from straight tube behaviour, Dn^2Sc must be less than 30. In the present experiments the lowest value of Dc^2Sc was 3600.

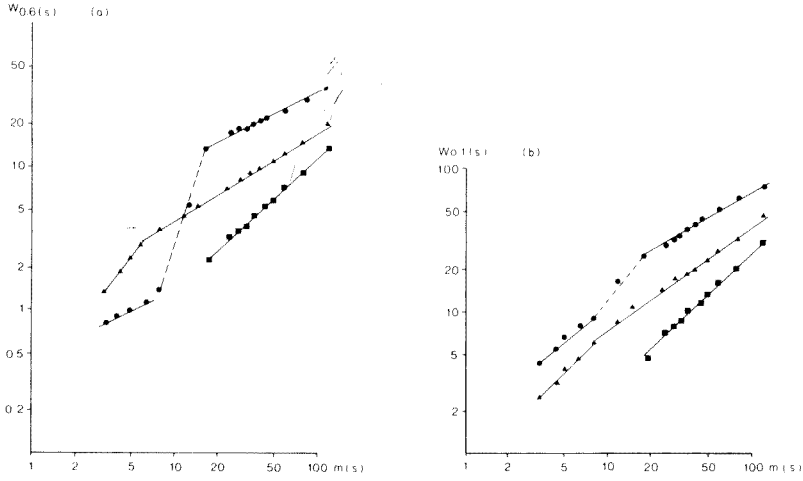

Fig. 7. Peak width at (a) 60% of peak height ($w_{0.6}$) and (b) 10% of peak height ($w_{0.1}$) as a function of the mean residence time m; symbols as in Fig. 5.

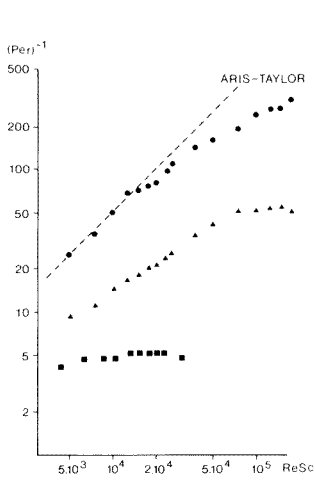

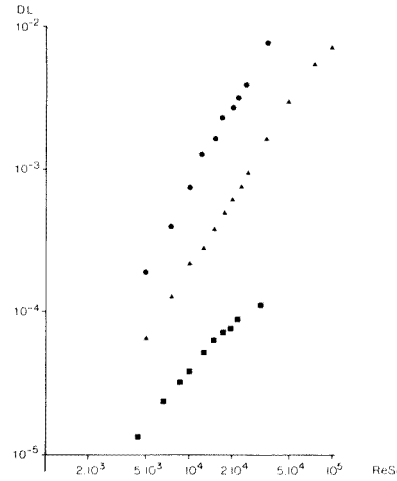

Fig. 8. Inverse radial Peclet number $(Pe_r)^{-1}$ as a function of ReSc. Broken line represents the Aris—Taylor dispersion theory. Symbols as in Fig. 5.

Fig. 9. Axial dispersion coefficient D_L as a function of ReSc. Symbols as in Fig. 5.

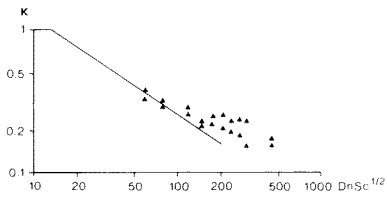

Fig. 10. Peak width reduction coefficient κ as a function of $DnSc^{1/2}$. Full line is the correlation of Van den Berg et al. (eqn. 9).

Single bead string reactor

For this reactor the dispersion behaviour was quite constant over the whole flow range as expected from the expression $2 < h < 4$. The flow rate was limited to f_v = 1.5 ml min^{-1} (Re_p = 45). Above this flow rate, leakage in the connections occurred because of the increased pressure. In a subsequent study, details of the hydrodynamic and dispersion behaviour of the SBSR will be presented. The peak height in the SBSR system was almost constant, independent of the flow rate, as can be seen in Fig. 6. This feature seems very advantageous for f.i.a.

Conclusion

The Aris—Taylor theory is valid in straight tubes only and provided that the residence time is long enough. An experimental criterion for the minimum required residence time was found to be $\tau > 0.3$. This value has to be compared with the theoretical values $\tau > 0.5$ found by Lighthill [7] and

$\tau > 0.8$ given by Ananthakrishnan et al. [8]. For coiled tubes the theory used should take secondary flow into account. Van den Berg [28] and Tijssen [29] have made valuable contributions to such theories.

In an attempt to fill the gap between open capillary tubes (coiled) and columns packed with small particles as used in chromatography, the SBSR was introduced [30]. The dispersion behaviour of this reactor was found to be better than that of comparable straight or coiled tubes. From preliminary experiments [30] the micromixing properties of the SBSR also appear to be very promising. The logical extension to this work is a study of the influence of chemical reactions on the dispersion; such a study is in progress.

The authors are greatly indebted to Dr. R. P. J. Duursma and Ing. H. Steigstra for their aid in instrumentation and data processing and to Dr. Ir. H.C. Smit for valuable discussions.

REFERENCES

1 J. M. Reijn, W. E. van der Linden and H. Poppe, Anal. Chim. Acta, 114 (1980) 105.
2 P. V. Danckwerts, Chem. Eng. Sci., 2 (1953) 1.
3 O. Levenspiel and K. B. Bischoff, Adv. Chem. Eng., Vol. 4, Academic Press, New York, 1963.
4 G. I. Taylor, Proc. R. Soc., Ser. A, 219 (1953) 186.
5 G. F. Froment and K. B. Bischoff, Chemical Reactor Analysis and Design, J. Wiley, New York, 1979.
6 R. Aris, Proc. R. Soc., Ser. A, 235 (1956) 67.
7 M. J. Lighthill, J. Inst. Math. Applics, 2 (1966) 97.
8 V. Ananthakrishnan, W. N. Gill and A. J. Barduhn, A. I. Ch. E. J., 11 (1965) 1063.
9 M. J. E. Golay and J. G. Atwood, J. Chromatogr., 186 (1979) 353.
10 W. N. Gill and V. Ananthakrishnan, A. I. Ch. E. J., 13 (1967) 801.
11 R. Tijssen, Anal. Chim. Acta, 114 (1980) 71.
12 J. H. M. van den Berg, R. S. Deelder and H. G. M. Egberink, Anal. Chim. Acta, 114 (1980) 91.
13 D. S. Horne, J. H. Knox and L. Maclaren, Sep. Sci., 1 (1966) 531.
14 D. S. Scott, W. Lee and J. Papa, Chem. Eng. Sci., 29 (1974) 2155.
15 J. Růžička and E. H. Hansen, Anal. Chim. Acta, 99 (1978) 37.
16 J. Růžička and E. H. Hansen, Anal. Chim. Acta, 78 (1975) 17.
17 J. Růžička, H. Bergamin F° and E. A. G. Zagatto, Anal. Chim. Acta, 81 (1976) 371.
18 J. Růžička and J. Stewart, Anal. Chim. Acta, 79 (1975) 79.
19 J. Růžička, E. H. Hansen, H. Mosbaek and F. J. Krug, Anal. Chem., 49 (1977) 1858.
20 H. Bergamin F°, B. F. Reis and E. A. G. Zagatto, Anal. Chim. Acta, 97 (1978) 427.
21 E. H. Hansen, J. Růžička and B. Rietz, Anal. Chim. Acta, 89 (1977) 241.
22 B. Karlberg and S. Thelander, Analyst, 103 (1978) 1154.
23 R. Lundin and T. Anfält, Proc. Workshop on FIA, Swedish Chemical Society, Uppsala, October 1977.
24 J. W. Dieker and W. E. van der Linden, Anal. Chim. Acta, 114 (1980) 267.
25 D. Betteridge, Anal. Chem., 50 (1978) 832A.
26 J. F. K. Huber and G. van Vught, Ber. Bunsenges. Phys. Chem., 69 (1965) 821.
27 R. Tijssen, Sep. Sci. Technol., 13 (1978) 681.
28 J. H. M. van den Berg, Ph.D. Thesis, Eindhoven University of Technology, 1978.
29 R. Tijssen, Ph.D. Thesis, Delft 1979.
30 J. M. Reijn, W. E. van der Linden and H. Poppe, Anal. Chim. Acta, 123 (1981) 229.

Analytica Chimica Acta, 126 (1981) 15—21
Elsevier Scientific Publishing Company, Amsterdam — Printed in The Netherlands

FLOW-THROUGH COULOMETRIC STRIPPING ANALYSIS AND THE DETERMINATION OF MANGANESE BY CATHODIC STRIPPING VOLTAMMETRY

A. TROJÁNEK and F. OPEKAR

J. Heyrovský Institute of Physical Chemistry and Electrochemistry, Czechoslovak Academy of Sciences, Jilská 16, 110 00 Prague 1 (Czechoslovakia)

(Received 11th November 1980)

SUMMARY

A simple flow-through system is described for collection of liquid samples into a closed loop. This arrangement can be used for coulometric determinations by the stripping method without previous calibration. The usefulness of the system is demonstrated on the determination of manganese (ca. 10^{-6} M) in acetate buffer by cathodic stripping voltammetry.

The demands for detectors in flow-through systems such as liquid chromatography, flow-through analyzers, etc., have gradually led to modification of classical electroanalytical techniques to unambiguous flow-through forms. Compared with other electrochemical methods, the application of stripping voltammetry has a distinct disadvantage in that the detection cannot be carried out continuously; the method is, by nature, discontinuous. The measuring period in which analytical data are obtained is always preceded by a preparation period: deposition of the test substance, conditioning of the electrode surface, and possibly deposition of a mercury film. However, the high sensitivity of the method and its relative irreplaceability in analysis for traces of heavy metals have led to this method being used successfully in a number of cases for measurement in flowing liquids.

For example, the use of a tubular electrode permits treatment of large solution volumes and thus attainment of high sensitivity in determinations [1]. In contrast, if only small sample volumes are available, a rotating electrode can be used; transport of the electroactive substance to this electrode is very good even at relatively low flow rates [2, 3]. The anodic stripping voltammetric method with collection [4] can be used in flowing systems, similarly to the ring-disc method [5]; this system allows suppression of the undesirable charging current, as in the differential mode of stripping voltammetry with a pair of identical electrodes [6]. Some new electrode materials, such as reticulated vitreous carbon (RVC), can be used for stripping determinations in flow-through arrangements; these materials permit construction of porous flow-through electrodes, on which up to 100% material conversion is attained under suitable conditions [7].

The work described here was carried out in order to construct a flow-through system which would allow simple collection of samples into a closed liquid loop and determination of their components by stripping coulometry.

EXPERIMENTAL

A schematic diagram of the liquid flow circuit is depicted in Fig. 1. The liquid flows through polyethylene tubes (1 mm i.d.) at a flow rate determined by a five-channel peristaltic pump (Zalimp 304, Poland). An important element, in addition to the electrolytic cell itself, is stop-cock 4, which is made of plexiglas (body) and teflon (internal part). This stop-cock separates the liquid circuit into two sections, the filling section and the working area. In position 4a (filling), the two parts of the circuit are connected by the filling channel in the stop-cock and the sample is drawn into the working area. Any air bubbles are removed through an auxiliary channel in the stop-cock (not shown). In position 4b (measuring) the filling and working parts are separated and form two separate loops. Thus the separated amount of sample can be treated without turning off the pump.

The body of the flow-through cell (Fig. 2), consisting of two parts joined by clamps, is made of plexiglas. The working electrode is a glassy carbon rod (40 mm long, 2.7 mm diameter; type GC 10, Tokai Electrodes, Japan) placed in the central hole of the auxiliary tubular electrode made of spectral carbon impregnated with paraffin. The diameter of the central hole is 3.1 mm and the electrolysis proceeds in an electrolyte layer about 0.2 mm thick. Exactly central placing of the working electrode is ensured by two plexiglas

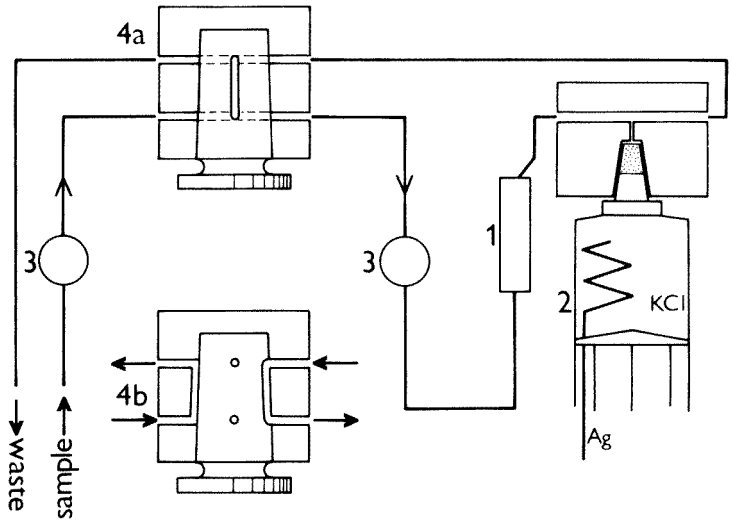

Fig. 1. The liquid flow circuit for coulometric stripping analysis: (1) flow-through electrolytic cell (see Fig. 2); (2) reference electrode (see text); (3) pump; (4) stop-cock shown in the filling position (4a) and during electrolysis (4b).

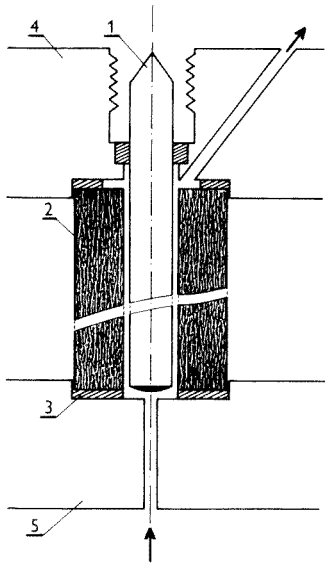

Fig. 2. The electrolytic cell: (1) working electrode; (2) auxiliary electrode; (3) seals; (4) top section of cell body; (5) bottom section of cell body. The arrows indicate the direction of liquid flow.

cylinders, which have internal grooves for entrance and exit of liquid and are fixed firmly at the ends of the auxiliary electrode. Escape of liquid around the working electrode is prevented by rubber seals which are pressed onto the electrode rod by a hollow screw which simultaneously forms the body of a spring contact. The Ag/AgCl reference electrode (Fig. 1) is made from a plastic hypodermic syringe, which is fitted at the tip with a porous ceramic stopper and filled with saturated potassium chloride; this was found to be very practical. Electrolytic contact with the liquid flow is ensured by a capillary channel with a diameter of 0.13 mm (Fig. 1), from which any air bubbles can be removed by gently pressing the syringe plunger. A classical potentiostat and an electronic circuit for potentiostatic-galvanostatic work in a three-electrode arrangement [9] were constructed from operational amplifiers.

The supporting electrolyte was 0.1 M acetate buffer (pH 5.5), prepared from analytical-grade chemicals. A stock solution (10^{-4} M) of manganese(II) sulphate (p.a.) was prepared and working solutions were made by appropriate dilution.

THEORY

The discontinuous character of stripping voltammetry is a good reason for the use of combined working techniques, where the substance to be determined is deposited during flow through a closed loop, previously filled from

the medium to be analyzed in an on-line system or from an individual vessel with samples. In the establishment of optimal working conditions, it is necessary to consider the rules valid for electrolysis in such an arrangement, where the amount of substance deposited corresponds to the height of the stripping current peak.

If the electrolysis is carried out with the flow-through electrolytic cell in the loop position, then the concentration of the electroactive substance c at time t from the beginning of the electrolysis is given by $(c/c_0)_t = A^i$, where c_0 is the initial concentration, exponent i corresponds to the number of flow cycles of the solution through the cell, and A is the ratio of the concentrations of the electroactive substance at the entrance to the electrolytic cell and at its exit at an arbitrary moment during the electrolysis. Number i is given by the relationship $i = t\bar{v}/V_0$, where $\bar{v}$ is the mean volume flow rate and V_0 is the liquid volume in the closed loop. The decrease in the concentration c_e, resulting from deposition of amount m_e (in moles) on the electrode, can be expressed by the height of the stripping peak I_p, $c_e = m_e/V_0 = k_1 I_p/V_0$, and similarly $c_0 = k_1(I_p)_0/V_0$, where $(I_p)_0$ is the peak height corresponding to dissolution of the substance after complete deposition from volume V_0. As $(c/c_0)_t = (1 - c_e)/c_0$, it is also true that $(c/c_0)_t = (1 - I_p)/(I_p)_0$ and thus $\log A = \log [1 - I_p/(I_p)_0]\ V_0/t\bar{v}$.

This relationship yields the efficiency of the electrolysis during passage of the solution through the flow-through cell, which generally depends on the flow rate. If a dependence in the form $A = 1 - k_2\bar{v}^{-n}$ is assumed [8], an equation is obtained which allows characterization of the flow-through cell by the values of constants k_2 and n, which can then be determined experimentally from

$$\log(1 - A) = \log k_2 - n \log \bar{v} \tag{1}$$

The equation

$$(c/c_0) = (1 - k_2\bar{v}^{-n})^{t\bar{v}/V_0} \tag{2}$$

then enables the degree of depletion of the electroactive substance to be determined at an arbitrary time and under various experimental conditions on the basis of the determined values of k_2 and n. The value of exponent n can also be found from the height of the stripping peak in an open flow-through system, where a fresh solution with a constant concentration of the electroactive substance c_0 is fed to the entrance to the electrolytic cell. The concentration of substance c at the outlet from the cell is given [8] by the relationship $c_0 - c = c_0 k_2 \bar{v}^{-n}$, where the decrease in the concentration can again be expressed by the amount deposited on the electrode and found from the height of the stripping peak: $c_e = m_e/V = k_1 I_p/V$, where V is the volume of electrolyte treated, given by the value of the product $t\bar{v}$. Substitution leads to the relationship

$$I_p/\bar{v} = tc_0 k_2 \bar{v}^{-n}/k_1 = B\bar{v}^{-n} \tag{3}$$

which yields the value of n by plotting the ratio $I_p/\bar{v}$ vs. $\bar{v}$ on a logarithmic scale for deposition for a constant time at various flow rates.

RESULTS AND DISCUSSION

The use of the simply constructed electrolytic cell without a separated reference electrode ensures that the products of the anodic reaction are accumulated in the solution volume during cathodic deposition on the working electrode. The presence of these products affects the amount of substance deposited and makes it practically impossible to deplete the solution completely. Thus a system which can be determined by cathodic stripping voltammetry, the Mn^{2+}/MnO_2 system [10, 11], was chosen to demonstrate the usefulness of the proposed arrangement.

The volume of liquid required to fill the working compartment of the liquid circuit was 0.9 ml and filling was done from a vessel with a volume of at least 3.5 ml. A flow rate of 21.3 ml min^{-1} was sufficient to fill the working part of the circuit and to remove all bubbles in time periods of less than 10 s. In Fig. 3, the dependence of the height of the stripping peak of manganese dioxide on the electrolysis time at a potential of +1.0 V, in a circuit filled with a 10^{-6} M solution of manganese(II) salt in acetate buffer, is depicted by points. The peak height is related to that corresponding to complete depletion of manganese(II) ions, here peak height $(I_p)_0$ after electrolysis for 9 min. The values of constants $k_2 = 1.4 \times 10^{-2}$ $ml^{2/3}$ $s^{-2/3}$ and $n = 0.65$ were found, by using eqn. (1), from the determined dependence of the efficiency of the electrolysis A on the flow rate in the range 1.2—30 ml min^{-1}. Measurement in an open circuit according to eqn. (3) yielded the value $n = 0.67$, in agreement with the assumed value [8] of $n = 2/3$. These constant values were then employed to calculate the curve corresponding to complete electrolysis for various volumes of treated solution. Figure 4 depicts the calculated dependence of the time necessary to achieve 95% $(I_p)_0$ in a volume of V_0 at various flow rates. The efficiency of the electrolysis (A) generally decreases with increasing flow rate. Here, for example, at a flow rate of 21.3 ml min^{-1}, only 4% of the substance is converted during flow through the cell, whereas almost 20% is converted at a flow rate of 1.2 ml min^{-1}. Nonetheless, the use of a larger flow rate results in an increase in the rate of complete electrolysis because of the increased number of times that the solution flows through the cell per unit time. It is apparent from Fig. 4 that this effect is not very marked at higher flow rates and that eventually an increase in the flow rate tends rather to introduce problems connected with work at increased pressures in the liquid circuit.

Coulometric determination of manganese

The technique based on quantitative deposition of all the material contained in a closed loop allows determination by the stripping method without prior calibration. This was confirmed by measurements on a set of

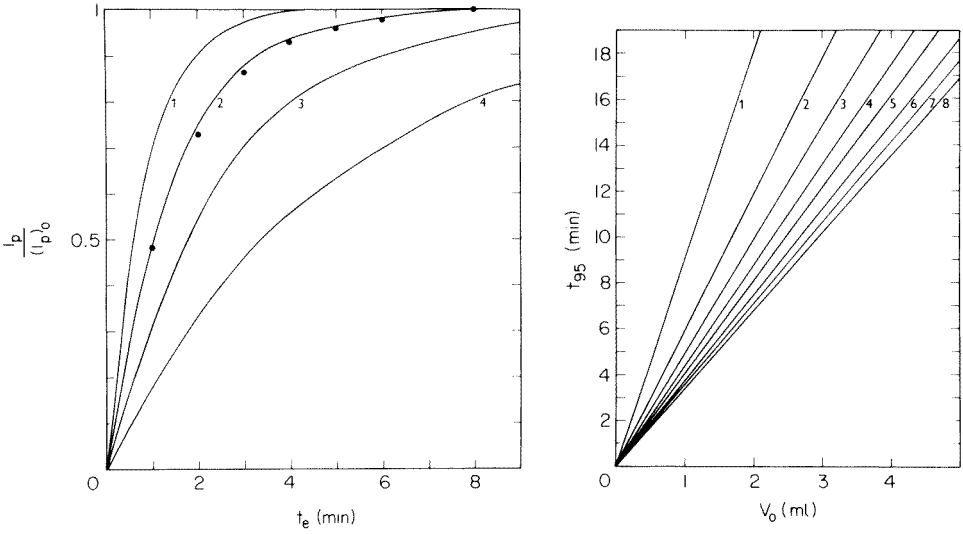

Fig. 3. Calculated time course of complete electrolysis for $k_2 = 1.4 \times 10^{-2}$ ml$^{2/3}$ s$^{-2/3}$ and $n = 2/3$ and various sample volumes V_0: (1) 0.5; (2) 0.9; (3) 1.5; (4) 3 ml. The points correspond to measured experimental values.

Fig. 4. Calculated dependence of the necessary time to achieve 95% conversion on the sample volume for $k_2 = 1.4 \times 10^{-2}$ ml$^{2/3}$, s$^{-2/3}$ and $n = 2/3$ for various flow rates (in ml min^{-1}): (1) 3; (2) 12; (3) 21; (4) 30; (5) 39; (6) 48; (7) 57; (8) 66.

samples with manganese contents of 5×10^{-7}—5×10^{-6} M at a flow rate of 21.3 ml min^{-1}. Because of the necessity of measuring the charge, a galvanostatic technique was chosen, using an apparatus which automatically counted the transition times [12]. This apparatus requires the differentiated form of the chronopotentiometric curve. The pulsing potential produced by the peristaltic pump made it impossible to differentiate the E—t curve in the classical manner, and so differentiation was achieved by measuring the difference between two subsequent values of the potential sampled synchronously with the pump pulses [13]. Thus the charge corresponding to the amount of deposited substance was found at a known value of the stripping current. The samples were subjected to electrolysis for 5 min at a potential of +1.0 V (cf. Fig. 4).

The concentration values found from Faraday's law for the range specified above generally differed from the expected values by less than 5%.

Conclusions

The proposed modification of the stripping voltammetric technique in flowing systems is an approach that can be used for mass treatment of chemically analyzed samples and for periodic collection of liquid samples from the analyzed medium. Coulometry, carried out as described, permits attainment of complete electrochemical conversion even when electrodes

with relatively low efficiency are used, and thus determinations are possible without the use of standard solutions. Galvanostatic stripping of the deposit lends the required degree of selectivity to the coulometric procedure.

It can be expected that the use of a more complicated electrolytic cell with separated electrodes would enable samples to be treated by the a.s.v. method in the same manner.

REFERENCES

1 S. H. Lieberman and A. Zirino, Anal. Chem., 46 (1974) 20.
2 J. Wang and M. Ariel, Anal. Chim. Acta, 101 (1978) 1.
3 J. Wang and M. Ariel, Anal. Chim. Acta, 99 (1978) 89.
4 G. W. Schieffer and W. J. Blaedel, Anal. Chem., 49 (1977) 49; 50 (1978) 99.
5 G. W. Tindall and S. Bruckenstein, J. Electroanal. Chem., 22 (1969) 367.
6 J. Wang and M. Ariel, J. Electroanal. Chem., 85 (1977) 289.
7 W. J. Blaedel and J. Wang, Anal. Chem., 51 (1979) 799; 1725.
8 V. G. Levich, Physico-Chemical Hydrodynamics, Prentice-Hall, Englewood Cliffs, New Jersey, 1962.
9 S. Bruckenstein and B. Miller, J. Electrochem. Soc., 117 (1970) 1040.
10 K. Z. Brainina, Zh. Anal. Khim., 19 (1964) 810.
11 H. Monien and K. Zinke, Fresenius Z. Anal. Chem., 240 (1968) 32.
12 F. Opekar, M. Herout and R. Kalvoda, Chem. Listy, 74 (1980) 542.
13 F. Opekar and A. Trojanek, Anal. Chim Acta, 127 (1981), in press.

Analytica Chimica Acta, 126 (1981) 23—34
Elsevier Scientific Publishing Company, Amsterdam — Printed in The Netherlands

MULTIPURPOSE ELECTRODE WITH DIFFERENT ENZYME SYSTEMS BOUND TO COLLAGEN FILMS

C. BERTRAND, P. R. COULET* and D. C. GAUTHERON

Laboratoire de Biologie et Technologie des Membranes du CNRS, Université Claude Bernard, Lyon 1, 43 Boulevard du 11 Novembre 1918, 69622 Villeurbanne Cédex (France)

(Received 14th July 1980)

SUMMARY

Selective, multipurpose electrodes have been developed from the previously described glucose electrode based on amperometric detection of hydrogen peroxide. Several single or multi-enzyme systems, including galactose oxidase, cholesterol oxidase, glucoamylase with glucose oxidase, and invertase with glucose oxidase, can be covalently bound to collagen membranes and attached to a platinum anode for monitoring the hydrogen peroxide generated. The probes allow fast and sensitive measurements of galactose, free cholesterol and maltose. Analogous electrodes are convenient for the assay of sucrose and lactose, with lower sensitivity. For disaccharide measurements, a comparative study of membranes produced by random co-immobilization, stacking of membranes and asymmetric coupling is reported. Asymmetric coupling improved the electrode performances in every case. One enzyme membrane is readily replaced by another in the electrode construction, and the sensors can be used for hundreds of assays.

Since the pioneering work of Katchalski and co-workers, enzyme immobilization on various carriers has been extensively developed [1, 2]. Numerous studies have been reported concerning the kinetic behaviour of bound enzymes and the achievement of new enzymatic devices, such as enzymatic reactors or analytical systems. Among the new analytical methods, enzyme electrodes, which consist of an enzymatic reaction taking place near an electrochemical sensor, appeared to be very promising [3]. Electrochemical monitoring of the reaction (by amperometry or potentiometry) leads to an attractive and reagentless technique, adaptable to numerous determinations of clinical or industrial interest [4].

In this laboratory, a mild method of general use for surface covalent binding of proteins on industrial collagen films has been developed [5, 6] and successfully applied to the design of polymembrane reactors [7, 8] and enzyme electrodes. In a first approach, such an electrode for trace glucose determination has been designed [9]. The device consists of a platinum anode which allows the detection of hydrogen peroxide at +650 mV vs. Ag/AgCl, KCl, covered by a collagen membrane bearing covalently immobilized glucose oxidase catalyzing the oxidation of glucose according to the reaction

0003—2670/81/0000—0000/$02.50

$$\beta\text{-D-glucose} + O_2 \xrightarrow{\text{glucose oxidase}} \beta\text{-D-glucono-}\delta\text{-lactone} + H_2O_2$$

A compensating electrode mounted with a non-enzymatic collagen membrane permits the detection of electrochemical interferences which can then be subtracted. The enzyme electrode response was routinely found to be proportional to glucose concentration in the range 10^{-7}—2×10^{-3} M. Such performances, allowing determinations within more than four orders of magnitude, led to an exploration of the possibility of obtaining a multipurpose electrode using the same basic amperometric sensor for hydrogen peroxide, associated with various mono- or polyenzymatic collagen membranes, provided that hydrogen peroxide was the final product to be detected.

EXPERIMENTAL

Chemicals

Glucose oxidase (EC 1.1.3.4, grade I, of fungal origin, 210 units mg^{-1}), alcohol oxidase (EC 1.1.3.13, from *Candida boidinii*, 5 units mg^{-1}), mutarotase (EC 5.1.3.3, from hog kidney, 5 000 units mg^{-1}), invertase (EC 3.2.1.26, from yeast, 150 units mg^{-1} of dry powder), β-galactosidase (EC 3.2.1.23, from *Escherichia coli*, 30 units mg^{-1}) and peroxidase (EC 1.11.1.7, from horseradish, 250 units mg^{-1}) were obtained from Boehringer, Mannheim. Galactose oxidase (EC 1.1.3.9, type IV, from *Dactylium dendroides*, 140 Sigma units mg^{-1}; Sigma Chemical Co.) cholesterol oxidase (EC 1.1.3.6, from *Mycobacteria*, 140 units ml^{-1} in a Triton X-100 solution; Miles Laboratories, France) and glucoamylase (EC 3.2.1.3, 50 units mg^{-1}; Merck) were obtained. These enzymes and all other reagents were used without further purification. All other reagents were of the highest grade commercially available. ABTS (*2,2′-azino-di-[3-ethylbenzthiazoline sulfonate] (6)) was obtained from Boehringer, Mannheim. Lyophilized normal control sera (Lyo-Trol N) were a gift from Bio-Mérieux, France. Each vial of serum was reconstituted with distilled water before use.

Immobilization of enzymes on collagen membranes

Films of highly polymerized insoluble collagen (20 cm wide, 0.1 mm thick in a dry state, F 70 type) were prepared in bulk quantities by the Centre Technique du Cuir, Lyon, France. Pieces of the required area were cut out from this crude film and activated as described previously [6] which consists of three steps: acidic esterification with methanol, hydrazine treatment, and formation of the acylazide with nitrous acid. After removal of all excess of reagents by washing, the activated membrane was ready for enzyme immobilization. Enzymes were linked by reaction with acylazide by direct immersion of the activated membrane in the enzyme solution at an alkaline pH [6]. In the case of a two-enzyme system, in addition to the random co-immobilization procedure on both membrane faces, it is possible to perform an asymmetric coupling, each enzyme being bound on only one face of the

membrane [10]. Unless otherwise stated, the concentration of enzyme in the coupling solution was 1.3 mg ml^{-1}. In every case, the coupling occurred spontaneously during 2—4 h at 4°C. Each membrane was washed in 1 M potassium chloride and stored in the buffer solution giving the optimal stability for the enzyme system considered according to the available technical data [11]. In these conditions, the enzyme membranes can be kept for years at 4°C without any leakage of enzyme. Thermal, operational and storage stability and resistance to denaturing reagents have been tested on enzyme collagen membranes. The proteinic environment provided by the carrier appears to be very favorable for the bound enzymes [12].

Immobilization for maltose electrode

Asymmetric coupling [10]. A special vessel was used into which 1 ml of glucose oxidase solution (1.3 mg ml^{-1}) in 0.2 M borate buffer, pH 9, was poured. One face of the activated collagen membrane was laid on this enzyme solution and to allow intimate contact between the membrane and the enzyme during coupling, a slight suction was applied by means of a peristaltic pump. This produced a small depression into which 0.6 ml of glucoamylase solution in the same buffer (13 mg ml^{-1}) was deposited. After coupling, the glucose oxidase face was pressed against the platinum surface, the glucoamylase face being exposed to the reaction mixture.

Random co-immobilization. In this case the coupling solution consisted of 1.3 mg of glucose oxidase and 13 mg of glucoamylase per ml in 0.2 M borate buffer, pH 9. After coupling, both enzymes are randomly co-immobilized on each face. Either face can be pressed against the platinum surface.

Two membranes stacked in the sensor cap. One membrane carried glucoamylase on both faces (coupling solution 13 mg ml^{-1}) and the other carried glucose oxidase on both faces (coupling solution 1.3 mg ml^{-1}), the latter being fitted directly to the platinum surface.

Apparatus and procedure

The enzyme electrode consisted of a platinum anode, the potential of which was fixed at +650 mV vs. Ag/AgCl, 0.1 M KCl, associated with an enzymatic collagen membrane maintained in close contact by a screwed cap.

The principle of the measurement is based on the general reaction

$$\text{substrate} + O_2 \xrightarrow{\text{oxidase}} \text{product} + H_2O_2$$

The hydrogen peroxide produced is oxidized to oxygen at the platinum disk by the well known two-electron reaction.

In a typical experiment, the enzyme electrode is immersed in 20 ml of the appropriate buffer (at 30°C) for optimal activity of the chosen enzyme (Table 1). The electrode is allowed to equilibrate for 30 min and after a baseline current is obtained electrode calibration is achieved by successive additions of substrate. To cover a wide range of final concentrations for the calibration graph, standard substrate solutions in the range 10^{-4}—10^{-1} M

TABLE 1

Immobilized enzyme activities

Enzyme	Buffer[a]	Optimal substrate concn.[b]	Specific immobilized activity (nmol min^{-1} cm^{-2})[c]
Oxidases			
Glucose oxidase	0.2 M Sodium acetate—acetic acid, pH 5.5	0.1 M Glucose	40—60
Alcohol oxidase	0.1 M Sodium phosphate, pH 7.4	0.25 M Methanol	≤ 1
Cholesterol oxidase	Buffer—detergent solution, pH 6.6 containing 0.3% Polyethylene glycol 0.4% Sodium cholate 0.3% Triton X-100 0.12 M NaCl 0.15 M K_2HPO_4 0.15 M KH_2PO_4	3.7×10^{-4} M Cholesterol	2—3
Galactose oxidase	0.1 M Potassium phosphate, pH 7.0	0.55 M Galactose	15—20
Disaccharidases			
Glucoamylase	0.2 M Sodium acetate—acetic acid, pH 4.7	25 mM Maltose	50—150
Invertase	0.2 M Sodium acetate—acetic acid, pH 5.5	75 mM Sucrose	3—5
β-Galactosidase	0.1 M Potassium phosphate, pH 7.0	35 mM Lactose	70—80

[a]Selected from [11] and suppliers' data. [b]For maximal enzyme activity. [c]Amount (nmol) of substrate reacted per minute per cm^2 of enzyme membrane surface.

are used; to avoid a large variation of the final reaction volume substrate additions of 5—100 μl are made. When the substrate is added to the buffer solution into which the electrode is immersed, hydrogen peroxide is produced and a current vs. time curve is recorded. A plateau is reached after a few minutes corresponding to the steady-state response time. When this plateau is reached, more substrate can be added to the same vessel, and so on. The reaction mixture is renewed only after a number of additions (see below).

The tighter is the fit between the platinum surface and the enzyme membrane, the shorter is the response time. With multienzyme systems the response time is generally larger because of the relative V_m/K_m ratios of the enzymes and diffusional limitations. In order to obtain a reliable value in a shorter time a differentiating amplifier was used, and $di_1/dt = f(t)$ was recorded simultaneously with $i_1 = f(t)$. A peak was obtained and its height, the dynamic response, which was proportional to the substrate concentration, was measured (Fig. 1). This response was obtained within 1 min.

When electrochemical interferences may occur in biological fluids, a compensating electrode mounted with a non-enzymatic collagen membrane is also used and the interfering current (i_2) is also recorded. A differential current amplifier allows the measurement of ($i_1 - i_2$). i.e. measurement of the enzymatically generated hydrogen peroxide, and then $d(i_1 - i_2)/dt$. As tested with a glucose oxidase membrane as a model, successive substrate determinations are possible, provided that the steady-state current is obtainable without washing out the reaction mixture. The number of determinations possible between washings depends on the concentration in the added sample solutions; at the upper limit of linearity of the calibration graph, the current increase on successive additions is no longer proportional to the increase of substrate concentration in the medium and the buffer in which the electrode is immersed must be renewed. These electrodes were used with the same membrane for months with periodic calibration.

Electrodes and electronics (PRG5 polarograph, Derivol differentiating amplifier and Deltapol differential current amplifier) were from Solea-Tacussel and recorders were from Sefram, France.

Measurement of membrane enzyme activities

Membrane enzyme activities were determined by either spectrophotometric or electrochemical procedure.

Spectrophotometric determination. This method was used for the measurement of disaccharidase activities (glucoamylase, invertase and β-galactosidase). The immobilized disaccharidase catalyses the reactions

$$\text{disaccharide} + H_2O \xrightarrow{\text{disaccharidase}} \text{glucose} + \text{-ose}$$

The reaction was initiated simply by dipping the enzymatic membranes into 9 ml of the suitable buffer [11] containing the disaccharide at optimal concentration (Table 1). The reaction mixture was carefully thermostated at 30°C and continuously stirred, while 0.2-ml aliquots were withdrawn every minute for 4 min. The glucose formed was measured by the use of two auxiliary soluble enzymes and a chromogenic reagent [13]

$$\beta\text{-D-glucose} + O_2 \xrightarrow{\text{glucose oxidase}} \beta\text{-D-glucono-}\delta\text{-lactone} + H_2O_2$$

$$H_2O_2 + (\text{ABTS})_{red} \xrightarrow{\text{peroxidase}} (\text{ABTS})_{ox} + H_2O$$

Glucose was determined by adding 0.8 ml of the glucose oxidase—peroxidase—ABTS reagent and measurement of the dye absorbance at 420 nm after 30 min. A calibration graph using glucose standard solutions was obtained in the same way at the same time.

Electrochemical determination [14]. This method was used for the measurement of oxidase activities. In this case, the electrode was mounted with a membrane not containing enzyme. It was immersed in 20 ml of reaction mixture at 30°C, containing the appropriate buffer and the substrate at optimal concentration (Table 1), under constant magnetic stirring.

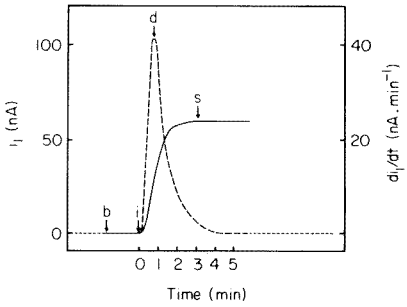

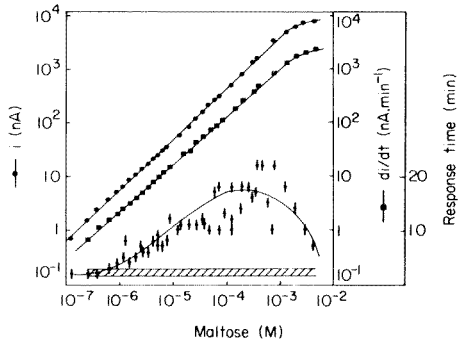

Fig. 1. Typical recording of steady-state (s) and dynamic (d) responses of the enzyme collagen electrode. After stabilization of the baseline current (b), a portion of substrate to be determined (here, 2×10^{-5} M glucose) is injected into the medium (i) and the current is recorded.

Fig. 2. Calibration graphs and response times for a maltose electrode with asymmetric glucoamylase/glucose oxidase collagen membrane. Calibration graphs correspond to the steady-state current (•) and the dynamic response (▪). Response times vs. log [maltose] are plotted for steady-state (♦) and dynamic (hatched area) signals. Other conditions as in Table 1.

After equilibration, the reaction was started by dipping into the reaction mixture a piece of active film. Hydrogen peroxide produced was oxidized at the platinum disk and the current obtained recorded vs. time. Since hydrogen peroxide is constantly increasing in the bulk phase, a linear variation of current is recorded, and after calibration of the electrode with hydrogen peroxide, the activity of the bound oxidases is determined.

RESULTS AND DISCUSSION

After the coupling of enzymes had been achieved, the activities of enzyme membranes were determined as described above. These activities are given in Table 1.

Monoenzyme electrodes

Three monoenzyme systems were tested, each of them producing hydrogen peroxide

$$\text{galactose} + O_2 \xrightarrow{\text{galactose oxidase}} \text{galactohexodialdose} + H_2O_2$$

$$\text{cholesterol} + O_2 \xrightarrow{\text{cholesterol oxidase}} \Delta^4\text{-cholestenone-3} + H_2O_2$$

$$\text{alcohol} + O_2 \xrightarrow{\text{alcohol oxidase}} \text{aldehyde} + H_2O_2$$

Response to galactose. Galactose oxidase, as demonstrated by Avigad et al. [15], is not specific for galactose but also oxidizes galactosides (such as lactose and raffinose) and polysaccharides containing galactose end-groups. However, when interfering sugars are not present, galactose determination

with such an enzyme is possible. The electrode was mounted with a galactose oxidase membrane and its calibration done by injection of galactose solutions. A steady-state response was obtained after 5—6 min and a dynamic response in 1 min. The lowest galactose concentration detected was 5×10^{-7} M. The sensor exhibited calibration linearity from 5×10^{-7}—6×10^{-4} M. Above the latter value, a response was still obtained but the current increase was no longer proportional to the galactose concentration. Similar calibration graphs were obtained with the previously described glucose electrode with linear ranges of 10^{-7}—2×10^{-3} M, the upper limit corresponding to the Michaelis constant of the immobilized enzyme [9]. The slope of the calibration curve was in the range 1—3 mA M^{-1} depending on the membrane activity.

Very few studies have been reported concerning galactose determinations with enzyme electrodes. Taylor et al. [16] described the use of galactose oxidase bound to a cellulose acetate membrane by glutaraldehyde and the amperometric detection of hydrogen peroxide. Their electrode could detect galactose at least up to 2.8×10^{-2} M, but the lower limit was not stated precisely.

Response to free cholesterol. In a similar way, a free cholesterol electrode has been designed using cholesterol oxidase bound to a collagen membrane [17]. Cholesterol was detected at a very low concentration, such as 10^{-8} M, and the calibration graph was linear over the range 10^{-7}—8×10^{-5} M. The steady-state response was obtained after 3—5 min whereas the dynamic response was a maximum within 1 min. Because of the great selectivity of cholesterol oxidase (only 3-β-sterols with a double bond in the Δ^5 or Δ^4 position are oxidized [18]) only electrochemical interferences have to be considered. The use of the differential system with the non-enzymatic compensating electrode enables the true response to cholesterol to be ascertained.

This electrode was used for free cholesterol determination in reconstituted human serum and exhibited good accuracy and reproducibility. Repeated (10) additions of 10 μl of serum to the reaction mixture gave an average serum level of free cholesterol of 1.46×10^{-3} M (with a standard deviation of 0.28×10^{-3} M), which was within the range (0.7—1.8×10^{-3} M) quoted by the supplier. Depending on the membrane activity, the slope of the calibration curve was 2—4 mA M^{-1}. Satoh et al. [19] have described a free cholesterol electrode giving a linear relationship up to 2×10^{-4} M of free cholesterol in serum. Huang et al. [20] have used immobilized cholesterol ester hydrolase and cholesterol oxidase for the amperometric determination of total cholesterol in serum. Their calibration graph for total serum cholesterol was linear from 0 to 5 g l^{-1}.

Response to methanol. Although alcohol oxidase catalyses the oxidation of many primary alcohols to the corresponding aldehydes, methanol is the best substrate. Therefore one could expect to produce a convenient electrode for this compound. However, an electrochemical response was obtained for methanol in the absence of enzyme. Furthermore, the enzyme membrane

exhibited a very low activity (1 nmol min^{-1} cm^{-2}). Guilbault and Lubrano [21], describing an amperometric enzyme electrode with alcohol oxidase, used the enzyme in solution, because the insolubilized enzyme had an activity too low to be useful in enzyme electrodes.

Multienzyme electrodes

The detection of several species by an enzyme electrode needs two or more enzymes. The compound to be determined is the substrate of the first enzyme of the sequence; one of the final products must be hydrogen peroxide. Most of the multienzyme systems described have had the enzymes randomly co-immobilized in a gel or on a membrane [22—24]. In addition to random co-immobilization, two other possibilities are considered here: stacking of several collagen membranes, each of them bearing a different enzyme and coupling of a different enzyme to each side of the membrane, a technique recently developed in this laboratory [10] (asymmetric coupling).

Two-enzyme electrode for maltose determination. Glucoamylase mainly hydrolyses α-1,4-glucan linkages in polysaccharides, removing successive glucose units from the non-reducing ends of the chains. In the case of maltose hydrolysis, two glucose units are released, which are oxidized in the presence of glucose oxidase. Several collagen membranes, chemically activated under the same conditions, were tested for maltose assay, using three different modes of enzyme co-immobilization: asymmetric coupling, random co-immobilization and two membranes placed one on the other. Calibrations for maltose were achieved with the three types of membrane electrodes. Their main characteristics are compared in Table 2 and a typical calibration curve obtained with an asymmetric membrane is given in Fig. 2. In this case, as for the other enzyme electrodes, the detection limit is defined as the lowest concentration which gives a detectable current (0.5 nA, here). As is well known, generally accepted conventions for expressing the performances of such sensors at the lower detection limit are not available. As shown in Table 2, the detection limit was 1.25×10^{-7} M and the response was linear up to 10^{-3} M.

TABLE 2

Two-enzyme electrodes for maltose determination

Membrane[a]	Membrane activity		Maltose determination				
	GOD (nmol min^{-1} cm^{-2}, glucose)	GA (nmol min^{-1} cm^{-2}, maltose)	Detection range (M)	Linear range (M)	Slope (mA M^{-1})	Response time (min)	
						Steady-state	Dynamic
Asymmetric GA/GOD	40	146	1.25×10^{-7} to 4×10^{-3}	1.25×10^{-7} to 1×10^{-3}	4.3	2—22	2—3
Co-immobilized GA + GOD	44	94	1.25×10^{-7} to 7×10^{-3}	1×10^{-6} to 2×10^{-3}	4.1	2—20	
Membrane GA + membrane GOD	63	48	3.75×10^{-7} to 4×10^{-3}	1×10^{-6} to 1×10^{-3}	3.3	2—22	2—3

[a]GOD, glucose oxidase; GA, glucoamylase.

A two-enzyme electrode for the determination of maltose using magnetic enzyme membranes and a pO_2 electrode was described by Cordonnier et al. [22]. Although the maximum linear range was not precisely stated, linearity was obtained from only 0.5×10^{-3}—2×10^{-3} M according to the reported calibration curve.

Three-enzyme electrode for sucrose determination. Amperometric determination of sucrose needs the use of three enzymes. The reaction sequence is

$$\text{sucrose} + H_2O \xrightarrow{\text{invertase}} \alpha\text{-D-glucose} + \text{fructose}$$

$$\alpha\text{-D-glucose} \xrightarrow[\text{(and spontaneous)}]{\text{mutarotase}} \beta\text{-D-glucose}$$

$$\beta\text{-D-glucose} + O_2 \xrightarrow{\text{glucose oxidase}} \beta\text{-D-glucono-}\delta\text{-lactone} + H_2O_2$$

A sucrose electrode was composed in three different ways: co-immobilization of invertase and glucose oxidase on the same collagen membrane (both faces); asymmetric coupling with invertase and mutarotase co-immobilized on one face, and glucose oxidase on the other; or of mutarotase and glucose oxidase co-immobilized on one face and invertase on the other.

Calibration curves were obtained for the three systems. Asymmetric coupling permitted better sensitivity than random co-immobilization (Fig. 3). The steady-state response was obtained in 8—12 min for asymmetric coupling, whereas it took about 30 min for the random co-immobilization electrode. The detection limits linear ranges and slopes of the calibration curves for the three systems are compared in Table 3. The addition of mutarotase, either soluble (2500 units) in the sensor cap or immobilized in the asymmetric systems does not significantly affect the response or the linear range.

The sucrose electrode was less sensitive than that for maltose. However, this device, especially when asymmetric membranes were used, had a wider linear range than the electrode described by Cordonnier et al. [22] (estimated linear range 1.4×10^{-3}—1.4×10^{-2} M). The present results are similar to those of Satoh et al. [23] (linear range 1×10^{-4}—2.5×10^{-3} M) who combined

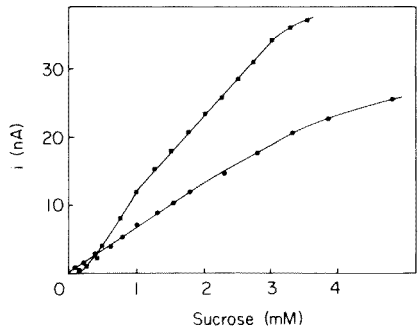

Fig. 3. Calibration graphs for the sucrose electrode using asymmetric membranes. (•) Glucose oxidase and mutarotase are bound to one face, and invertase to the other. (▪) Glucose oxidase is bound to one face, and mutarotase and invertase to the other. Steady-state current is measured. Other conditions as in Table 1.

TABLE 3

Characteristics of sucrose electrode for different types of immobilization on collagen membranes (GOD, glucose oxidase; MUT, mutarotase; INV, invertase)

Immobilization procedure	Detection limit (M)	Linear range (M)	Slope of calibration graph (mA M^{-1})
Random co-immobilization INV + GOD	6×10^{-3}	6×10^{-3}—1.5×10^{-2}	6.4×10^{-3}
Asymmetric coupling (INV + MUT) + GOD	2.5×10^{-4}	1×10^{-3}—3×10^{-3}	1.1×10^{-2}
Asymmetric coupling INV + (MUT + GOD)	1×10^{-4}	1×10^{-4}—2×10^{-3}	6.9×10^{-3}

invertase and glucose oxidase co-crosslinked on a collagen membrane and detected dissolved oxygen by amperometry. Barker and his group [24] developed enzyme electrodes for the determination of sucrose and amylose using the technique of titanium tetrachloride coupling on glass disks with invertase and glucose oxidase. A linear response was thus obtained in the range 0.1—1.0 mmol of sucrose.

Two-enzyme electrode for lactose determination. Lactose is hydrolysed to galactose and glucose in the presence of β-galactosidase. To obtain hydrogen peroxide as the final product glucose oxidase was chosen because it does not react with lactose and galactose. Calibration curves were obtained for lactose in two different systems: one with two membranes stacked in the sensor cap, one bearing β-galactosidase, and the other with a membrane with β-galactosidase on one side and glucose oxidase on the other side, facing the sensor (Fig. 4). The main characteristics of both lactose electrodes are compared in Table 4. Asymmetric coupling gave the better performances but the detection limit was rather high (3.5×10^{-5} M) and the linear range narrow. The slope was low compared to those obtained for other electrodes based on hydrogen peroxide measurement, even the two-enzyme system for maltose (Table 2).

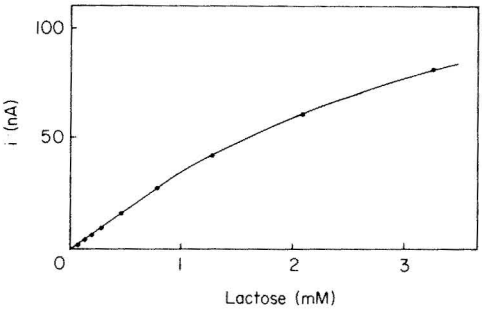

Fig. 4. Calibration graph for lactose electrode based on an asymmetric β-galactosidase/glucose oxidase membrane. Steady-state current is measured. Other conditions as in Table 1.

TABLE 4

Characteristics of lactose electrode for different types of membranes (GOD, glucose oxidase; β-gal, β-galactosidase)

Immobilization procedure	Detection limit (M)	Linear range (M)	Slope (mA M^{-1})	Steady-state response time (min)
Stacking of β-gal and GOD membranes in the sensor cap	3.5×10^{-4}	Non-linear		25—50
Asymmetric coupling	3.5×10^{-5}	6.7×10^{-5}—1×10^{-3}	0.03—0.35	4—10

CONCLUSIONS

The uses of the previously described glucose electrode based on amperometric detection of hydrogen peroxide [9] have been extended to the determination of various other species. The same basic electrochemical sensor, when associated with collagen membranes bearing different enzymes, leads to simple and reagentless methods for the determination of various substrates. Galactose, cholesterol, maltose, sucrose and lactose can be determined in this way, but other species able finally to yield hydrogen peroxide through a specific enzyme sequence, should be measurable by this method. Electrochemical interferences can be detected by a non-enzymatic electrode and the current subtracted, providing an accurate measurement of the hydrogen peroxide generated enzymatically.

For the determination of disaccharides, asymmetric coupling, recently developed in this laboratory [10], gave the best electrode performances, i.e., higher sensitivity and wider linear ranges. As previously emphasized by other authors, when multienzyme systems are used, the substrate for each enzyme may interfere [24]. In the present study, disaccharide electrodes were tested in glucose-free media. If glucose is present in the sample, its determination must be included in the overall procedure.

Few multienzyme electrodes have been described so far [21—24]. When proper comparisons can be made, i.e. when the detection limit is clearly indicated, and not merely stated as zero, the enzyme—collagen electrodes generally have a wider useful concentration range. For example, a range of 4 orders of magnitude was obtained with the glucoamylase—glucose oxidase system for maltose determination.

The enzyme electrode systems described here present numerous advantages arising from the collagen membranes themselves. Enzymatically active collagen disks which are placed close to the platinum anode allow the substitution of an active membrane by another in a few minutes. Furthermore the mechanical strength of these membranes is excellent and numerous assembling and disassembling procedures can be undertaken without damage.

For example, glucose oxidase collagen membranes could be used periodically for more than 500 assays within 300 days and even stored mounted in the electrode at room temperature (20—22°C). β-Galactosidase was found to be more sensitive to denaturation, losing 75% of its activity within one week. But it must be emphasized that even when the enzyme activity of the membrane decreases, leading to a decrease in the slope of the calibration graph, the linearity is retained and measurements remain possible. All these properties permit the construction of multipurpose enzyme electrodes which are very convenient for numerous routine assays that are normally time- and reagent-consuming.

The authors thank the DGRST for financial support (grant EGC 77-7-1617) and B. Duclot and E. Frey for skilful assistance. This work is part of the Docteur-Ingénieur thesis of C. Bertrand, Lyon, 1979.

REFERENCES

1 I. H. Silman and E. Katchalski, Annu. Rev. Biochem., 35 (1966) 873.
2 K. Mosbach (Ed.), Methods in Enzymology, Vol. 44, Academic Press, New York, 1976.
3 L. C. Clark, Jr. and C. Lyons, Ann. N.Y. Acad. Sci., 102 (1962) 29.
4 G. G. Guilbault and M. H. Sadar, Acc. Chem. Res., 12 (1979) 344.
5 P. R. Coulet, J. H. Julliard and D. C. Gautheron, French Patent, 1973, 2.235.133.
6 P. R. Coulet, J. H. Julliard and D. C. Gautheron, Biotechnol. Bioeng., 16 (1974) 1055.
7 J. M. Brillouet, P. R. Coulet and D. C. Gautheron, Biotechnol. Bioeng., 18 (1976) 1821.
8 P. R. Coulet, F. Paul, D. Dupret and D. C. Gautheron, in H. H. Weetall and G. P. Royer (Eds.), Enzyme Engineering, Vol. 5, Plenum, New York, 1980, p. 231.
9 D. R. Thevenot, R. Sternberg, P. R. Coulet, J. Laurent and D. C. Gautheron, Anal. Chem., 51 (1979) 96.
10 P. R. Coulet and C. Bertrand, Anal. Lett., 12 (1979) 581.
11 H. U. Bergmeyer (Ed.), Methods of Enzymatic Analysis, Vols. 1—4, Verlag Chemie, Academic Press, New York, 1974.
12 P. R. Coulet and D. C. Gautheron, Biochimie, 62 (1980) 543.
13 H. U. Bergmeyer and E. Bernt, in H. U. Bergmeyer (Ed.), Methods of Enzymatic Analysis, Verlag Chemie, Academic Press, New York, 1974, p. 1212.
14 R. Sternberg, Thèse de Doctorat de 3ème cycle, Université Paris Val-de-Marne, 1979.
15 G. Avigad, D. Amaral, C. Asensio and B. L. Horecker, J. Biol. Chem., 237 (1962) 2736.
16 P. J. Taylor, E. Kmetec and J. M. Johnson, Anal. Chem., 49 (1977) 789.
17 C. Bertrand, P. R. Coulet and D. C. Gautheron, Anal. Lett., 12 (1979) 1477.
18 W. Richmond, Scand. J. Clin. Lab. Invest., 29 (1972) abstract 3.25.
19 I. Satoh, I. Karube and S. Suzuki, Biotechnol. Bioeng., 19 (1977) 1095.
20 H. S. Huang, J. C. W. Kuan and G. G. Guilbault, Clin. Chem., 23 (1977) 671.
21 G. G. Guilbault and G. J. Lubrano, Anal. Chim. Acta, 69 (1974) 189.
22 M. Cordonnier, F. Lawny, D. Chapot and D. Thomas, FEBS Lett., 59 (1975) 263.
23 I. Satoh, I. Karube and S. Suzuki, Biotechnol. Bioeng., 18 (1976) 269.
24 A. S. Barker and P. J. Somers, in A. Wiseman (Ed.), Topics in Enzyme and Fermentation Biotechnology, Vol. 2, Ellis Horwood, Chichester, 1978, p. 120.

Analytica Chimica Acta, 126 (1981) 35—41
Elsevier Scientific Publishing Company, Amsterdam — Printed in The Netherlands

SELECTIVE KINETIC DETERMINATION OF PYRIDOXAL-5′-PHOSPHATE WITH AN AMMONIA GAS-SENSING ELECTRODE

SAAD S. M. HASSAN[a] and G. A. RECHNITZ*
Department of Chemistry, University of Delaware, Newark, DE 19711 (U.S.A.)
(Received 24th November 1980)

SUMMARY

The coenzyme pyridoxal-5′-phosphate (PLP) is determined by in situ measurement of the rate of ammonia production using a potentiometric gas-sensing membrane electrode. It is shown that the initial rate of ammonia liberation from L-tryptophan by action of tryptophanase apoenzyme and the coenzyme can be linearly related to PLP levels in the nanogram range with minimal interference from related compounds. Calibration data for the 1×10^{-7}—2.5×10^{-6} M range for PLP yielded a least-squares equation of rate (mV min^{-1}) = (0.64 ± 0.01) C — 0.01 ± 0.02 with a standard error of 0.02 mV min^{-1}, where concentration, C, is expressed in units of 10^{-7} mol l^{-1}.

Vitamin B_6 is a dietary constituent required for proper nutrition. In contrast to the great majority of vitamins, no pathological or clinical conditions in human beings can be directly related to its deficiency; however, the various members of the vitamin B_6 group and their derivatives are known to owe their vitamin activity to the ability of the organisms to convert them into the enzymatically active form pyridoxal-5′-phosphate (PLP) whose level is a characteristic manifestation of vitamin deficiency [1]. Several methods have been reported for the determination of PLP, but most of these suffer a lack of selectivity [2]. The most sensitive and selective methods are those based on the role of PLP as coenzyme in enzymatic reactions involving glutamic oxalacetic transaminase [3], tyrosine decarboxylase [4] and tryptophanase [5] apoenzymes.

Determinations of PLP by currently used methods based on tryptophanase apoenzyme [5—9] are based on the ability of PLP to restore the activity of tryptophanase apoenzyme for the degradation of tryptophan substrate followed by measurement of either indole [5—7] or pyruvate [5, 9] products. Extraction of indole followed by reaction with *p*-dimethylaminobenzaldehyde (Ehrlich's method) and reaction of pyruvate with 2,4-dinitrophenylhydrazine to form chromogenic adducts has been employed in all the available spectrophotometric methods. However, these procedures are applicable to concentrations of PLP higher than the microgram level and involve several manipulation steps resulting in low recoveries and poor precision.

[a]On leave from Ain Shams University, Cairo, Egypt.

0003—2670/81/0000—0000/$02.50

In an attempt to increase the sensitivity of these methods to cover the measurement of PLP at the nanogram level, radioactive and chromogenic substrates have been suggested. Reaction with radiolabeled tryptophan, removal of the excess by ion exchange, extraction of the radioactive pyruvate product as hydrazone, centrifugation, drying and activity counting have been described [10, 11]. A chromogenic substrate (S-*o*-nitrophenyl-L-cysteine) was also used [12] instead of tryptophan to permit direct spectrophotometric measurement of its degradation product (*o*-nitrothiophenolate). These methods, however, involve several time-consuming reaction and separation steps, preparation of the substrate [12] and the use of radioactive reagents and sophisticated instruments [10, 11].

In this paper, a simple, precise and rapid approach is described for determining PLP in concentrations as low as the nanogram level, by following the rate of the reaction of tryptophan with tryptophanase apoenzyme as a function of PLP concentrations. A novel aspect of the present procedure is the in situ potentiometric measurement of the initial rate of ammonia liberation using the ammonia gas-sensing electrode.

EXPERIMENTAL

Apparatus and reagents

The reaction was conducted in a 20-ml double-jacketed cell thermostatted at 30 ± 0.1°C by a Haake Model MF Magnibath. Potentiometric measurements were done with an ammonia gas sensor (Orion Model 95-10) and a Corning Model 12 Research pH-meter. The readings were recorded with a Heath-Schlumberger chart recorder (Model SR-255B).

All chemicals used were reagent grade and freshly deionized ammonia-free water was used to prepare all solutions.

Tryptophanase apoenzyme (80 U mg^{-1} protein) from *E. coli*, pyridoxal-5'-phosphate (PLP), pyridoxal hydrochloride, pyridoxamine-5'-phosphate hydrochloride, pyridoxine hydrochloride and pyridoxamine dihydrochloride were obtained from Sigma Chemical Co. (St. Louis, MO). Tryptophanase apoenzyme working solution (2.5 mg ml^{-1}) was prepared by dissolving 12.5 mg of the apoenzyme in 2 ml of 0.1 M Tris-HCl buffer of pH 8.1 containing 0.1 M KCl and dialyzing the solution in a cellophane bag for 7—10 h at 4°C against 2000 volumes of the same buffer. The contents of the bag were made up to 5 ml with the buffer and kept in crushed ice during measurements. The enzyme solution was freshly prepared daily and used directly. L-Tryptophan, 2×10^{-2} M at pH 8.1, was prepared by dissolving 0.408 g of L-tryptophan in about 50 ml of deionized water, and 0.1 M KOH was added dropwise to adjust the pH. The solution was then filtered and made up to 100 ml with deionized water. Pyridoxal-5'-phosphate (PLP) stock solution, 10^{-4} M, was prepared by dissolving 2.74 mg of PLP in 100 ml of deionized water, and kept refrigerated in the dark. Working solutions were prepared by 10-fold and 100-fold dilution from the stock solutions prepared freshly each day.

Procedure

A series of 10—100-μl aliquots of 10^{-5} M PLP standard solution (27-270 ng ml^{-1}) was transferred to the 20-ml thermostatted reaction cell containing a small teflon-covered spinbar. The tryptophanase apoenzyme working solution (100 μl, 2.5 mg ml^{-1}) was added and the total volume of the solution was made up to 1.8 ml with the 0.1 M Tris-HCl buffer containing 0.1 M KCl. After stirring, the ammonia gas sensor was immersed in the solution and the potential was allowed to reach a stable reading (15 min). The recorder speed was then adjusted to 0.1 in. min^{-1} and a 200-μl aliquot of 2×10^{-2} M L-tryptophan solution of pH 8.1 was added to initiate the reaction. The response curves were recorded and the maximum initial rate of potential change (mV min^{-1}) was determined. A blank experiment was done under identical conditions but without PLP. The initial rate was plotted as a function of PLP concentration in the range 10—135 ng ml^{-1}. Lower PLP concentrations were determined by following the same procedure, but with the use of 300 μl of the apoenzyme working solution, 10—100-μl aliquots of 10^{-6} M PLP (2.7—27 ng ml^{-1}) and 350 μl of 2×10^{-2} M L-tryptophan.

RESULTS AND DISCUSSION

The rate of ammonia liberation from excess of L-tryptophan by the action of tryptophanase apoenzyme as a function of PLP coenzyme (reaction 1) was effectively followed by using the ammonia gas sensor. The conditions were optimized to attain maximum reaction rates suitable for accurate potentiometric determinations of low levels of PLP.

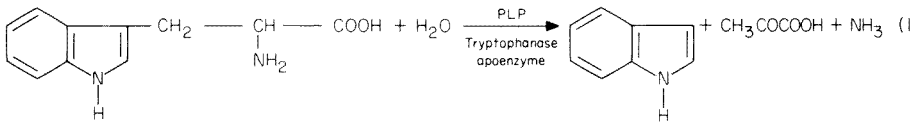

Under the optimum reaction conditions (see below), PLP catalyzed the cleavage of L-tryptophan with a 10^3-fold amplification in terms of ammonia production. The concentrations of ammonia released by the action of PLP at levels as low as 10^{-8} M were in the 10^{-4}—10^{-5} M range which is conveniently within the detection range of the ammonia sensor.

Reaction conditions

A preliminary investigation of the commercially available tryptophanase apoenzyme showed considerable contamination by ammonium salts. Complete elimination of the ammonia background was satisfactorily attained by dialysis at 4°C for 7—10 h using Tris-HCl buffer of pH 8.1 containing 0.1 M KCl. The presence of high potassium concentration was necessary to stabilize and activate the purified apoenzyme.

The effect of the purified apoenzyme concentrations on the rate of the reaction of 2.5×10^{-7} M PLP and 2×10^{-3} M L-tryptophan in a total volume of 2 ml of 0.1 M Tris-HCl buffer of pH 8.1 at 30°C was investigated. The

results (Fig. 1) showed that 0.25 mg of the enzyme was sufficient for the release of ammonia at a detectable rate by 2.5×10^{-6}—10^{-7} M PLP in the presence of excess of substrate. Moreover, an increase of the enzyme concentration to 0.8—1 mg was sufficient for substrate cleavage and ammonia liberation in the presence of as little as 10^{-8} M PLP.

The concentration of L-tryptophan substrate required to saturate 0.25 mg of the enzyme in the presence of 2.5×10^{-7} M PLP in 2 ml of 0.1 M Tris-HCl buffer (pH 8.1, 30°C) was 1.5×10^{-3} M (Fig. 2). A Lineweaver-Burk plot of the reciprocal of initial reaction rate vs. substrate concentrations revealed a K_m value of 0.33×10^{-3} M (Fig. 3) compared with the values of 0.32×10^{-3} M [13], 0.33×10^{-3} M [14] and 0.25×10^{-4} M [6] obtained by other workers. A 2×10^{-3} M concentration of tryptophan was used throughout this study.

The temperature dependence of the reaction in the range 25—40°C was investigated by measuring the initial rate of ammonia liberation from 2×10^{-3} M L-tryptophan using 0.25 mg of tryptophanase apoenzyme and 2.5×10^{-7} M PLP in 2 ml of 0.1 M Tris-HCl buffer (pH 8.1). A 10°C increase in temperature increased the reaction rate 1.3 times (Fig. 4). However, fluctuation of the potential readings and slow attainment of the steady readings (>30 min) by the electrode system were observed at temperatures higher than 30°C. Thus, the reaction was conducted at 30°C to allow fast and stable potential response.

The effect of pH in the range 7—8.5 on the reaction was examined by following the initial rate of ammonia released from the reaction of 2.5×10^{-7} M PLP, 0.25 mg of the apoenzyme and 2×10^{-3} M L-tryptophan in 2 ml of 0.1 M

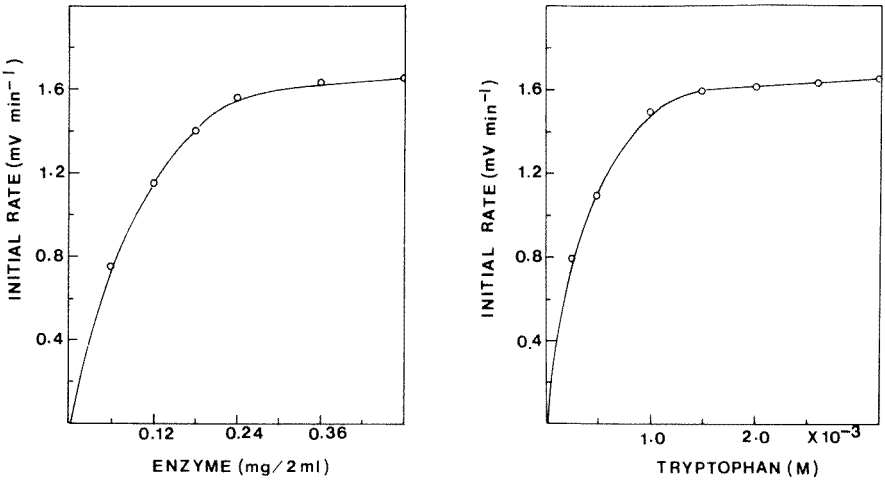

Fig. 1. Effect of tryptophanase apoenzyme concentration on the rate of the reaction of 2.5×10^{-7} M PLP and 2×10^{-3} M L-tryptophan at pH 8.1 and 30°C.

Fig. 2. Effect of L-tryptophan concentration on the rate of the reaction of 2.5×10^{-7} M PLP and 0.25 mg of tryptophanase apoenzyme at pH 8.1 and 30°C.

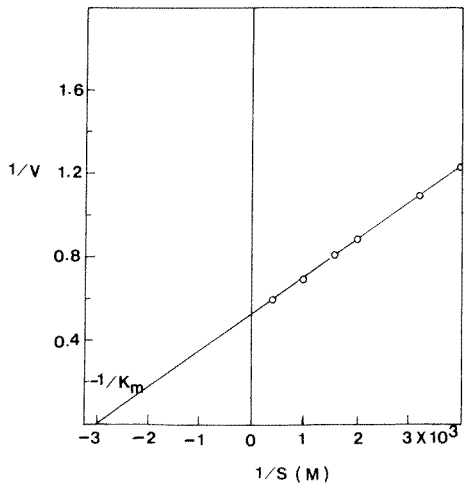

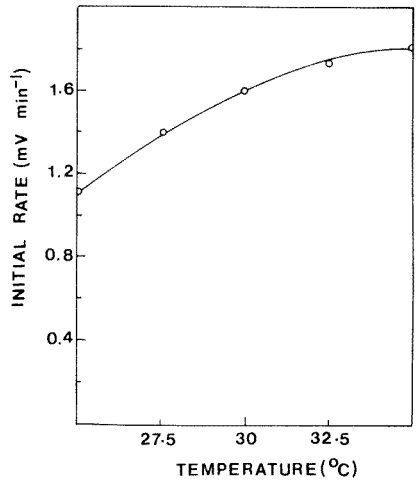

Fig. 3. Lineweaver-Burk plot of 1/S vs. 1/V for the deamination of L-tryptophan using 0.25 mg of tryptophanase apoenzyme and 2.5×10^{-7} M PLP at pH 8.1 and 30°C.

Fig. 4. Effect of temperature on the rate of the reaction of 2.5×10^{-7} M PLP, 0.25 mg of tryptophanase apoenzyme, and 2×10^{-3} M L-tryptophan at pH 8.1.

Tris-HCl buffer solutions at 30°C. The results showed that the reaction proceeded with reasonable efficiency over this pH range with a maximum rate (1.6 mV min^{-1}) at pH 7.8—8.2. Since the increase in pH improves the detection limit and expands the measurement range of the ammonia gas sensor, the present study was conducted at pH 8.1.

The effect of preincubation was investigated by following the initial rate of ammonia liberation by three parallel series of experiments using identical concentration of the reactants (2.5×10^{-7} M PLP, 0.25 mg of apoenzyme, and 2×10^{-3} M L-tryptophan) at pH 8.1 and 30°C. In the first series, PLP and the apoenzyme were incubated until a steady potential reading was reached (ca. 15 min); then tryptophan substrate was added to initiate the reaction. The second set of experiments was conducted by initially incubating the substrate and the apoenzyme followed by addition of PLP after attainment of a steady potential reading. The third set was carried out by incubating PLP and tryptophan to constant potential readings, and then adding the apoenzyme. The results showed that the initial rate obtained in the first set of experiments was two and three times those rates obtained in the second and third series of experiments, respectively. It is thus apparent that the association of the apoenzyme and PLP coenzyme to form the holoenzyme by preincubation for 15 min at 30°C prior to reaction with the substrate significantly affects the initial reaction rate. A further increase of the incubation time to 40 min did not change the reaction rate.

Determination of PLP

Pyridoxal-5′-phosphate in the concentration range of 1×10^{-7}—2.5×10^{-6} M was satisfactorily determined by using 0.25 mg of apoenzyme and 2×10^{-3} M tryptophan substrate at pH 8.1 and 30°C. Under these conditions, a linear relationship between the PLP concentration and the initial rate of ammonia liberation (mV min^{-1}) was obtained. Least-squares statistical evaluation of the data yielded a value of 0.64 ± 0.01 for the slope of the calibration curve, an intercept of −0.01 ± 0.02, and a standard error of 0.02 mV min^{-1}. The mean standard deviation, calculated from the repetitive assay of ten samples with 25 ng PLP ml^{-1}, was ±2.5%.

Even lower PLP concentrations, in the 1×10^{-8}—2.5×10^{-7} M range, were determined under conditions where the apoenzyme and substrate concentrations were increased 3—4 and 2 times, respectively. A linear relationship between the PLP concentration and the initial rate of ammonia liberation was also obtained under these conditions. The slope of this calibration curve was 0.66 ± 0.01 with an intercept of 0.1 ± 0.1 and a standard error of 0.02 mV min^{-1}. A precision of ±5.7% was obtained for determinations at the 5 ng PLP ml^{-1}. These concentration ranges would accommodate the low levels of PLP found in biological materials [15—17].

The selectivity of the method was demonstrated by measuring the rate of ammonia liberation at PLP levels of 25 ng ml^{-1} in the presence of other members of the vitamin B_6 group and their phosphate derivatives. No interferences were noticed in the presence of 100-fold amounts of pyridoxal hydrochloride, pyridoxamine-5′-phosphate hydrochloride, pyridoxine hydrochloride, pyridoxamine dihydrochloride, phosphate or sulphate ions.

The present method, which incorporates elements of earlier methods that employ tryptophanase apoenzyme, has many inherent advantages over most of the available procedures. Apart from its simplicity, selectivity, precision, and rapidity, few manipulation steps are involved owing to the in situ measurement of the ammonia. The limit of detection is lower than that obtained by the spectrophotometric methods [4, 6—8] and almost as good as that obtained by radiometric procedures [10, 11]. The assay time is about a quarter of that required by the other techniques.

We gratefully acknowledge support of this work by grant GM-25308 from the National Institutes of Health.

REFERENCES

1 W. Sebrell and R. Harris, The Vitamins, Chemistry, Physiology, Pathology, Vol. III, Academic Press, New York, 1954, pp. 220—298.
2 P. Gyorgy and W. Pearson, The Vitamins, Chemistry, Physiology, Pathology Methods, 2nd edn., Vol. VII, Academic Press, New York, 1967, pp. 197—198.
3 W. Umbbeit, W. Bellamy and J. Gunsalus, Arch. Biochem., 7 (1945) 185.
4 H. Wada, T. Morisue, Y. Sakamoto and K. Ichihara, J. Vitaminol. (Kyoto), 3 (1957) 183.

5 G. Schreiber and H. Halzer, in H.-U. Bergmeyer (Ed.), Methods of Enzymatic Analysis, Academic Press, New York, 1965, p. 606.
6 I. Gunsalus, C. Galeener and J. Stamer, in S. Colowick and N. Kaplan (Eds.), Methods in Enzymology, Vol. II, Academic Press, New York, 1955, pp. 238—242.
7 S. Gailani, Anal. Biochem., 13 (1965) 19.
8 B. Haskell and E. Snell, Anal. Biochem., 55 (1972) 567.
9 I. Nakahara, Y. Morino, T. Morisue and Y. Sakamoto, J. Biochem. (Tokyo) 49 (1961) 339.
10 S. Fujii, J. Osaka City Med. Center, 17 (1968) 443.
11 K. Okuda, S. Fujii and M. Wada, in S. Colowick and N. Kaplan (Eds.), Methods in Enzymology, Vol. XVIII, Part A, Academic Press, New York, 1970, pp. 505—509.
12 C. Suelter, J. Wang and E. Snell, Anal. Biochem., 76 (1976) 221.
13 T. Watanabe and E. Snell, J. Biol. Chem., 82 (1977) 733.
14 W. Newton, Y. Morino and E. Snell, J. Biol. Chem., 240 (1965) 1211.
15 B. Chabner and D. Livingston, Anal. Biochem., 34 (1970) 413.
16 H. Maruyama and D. Coursin, Anal. Biochem., 26 (1968) 420.
17 M. Chauhan and K. Dakshinamurti, Anal. Biochem., 96 (1979) 426.

Analytica Chimica Acta, 126 (1981) 43—50
Elsevier Scientific Publishing Company, Amsterdam — Printed in The Netherlands

CONSTRUCTION OF A GUANINE ENZYME ELECTRODE AND DETERMINATION OF GUANASE IN HUMAN BLOOD SERUM WITH AN AMMONIA GAS SENSOR

D. P. NIKOLELIS, D. S. PAPASTATHOPOULOS and T. P. HADJIIOANNOU*

Laboratory of Analytical Chemistry, University of Athens, Solonos 104, Athens (144) (Greece)

(Received 30th September 1980)

SUMMARY

The guanine electrode is based on guanase used with an ammonia gas-sensing membrane electrode; immobilization of the enzyme is optimized. Guanine in the range 10^{-4}—10^{-2} M gives a linear potential vs. log(concentration) plot with a response time of 4—1.5 min over the range specified. Guanase (0.12—12 I.U. l^{-1}) is determined in serum by adding guanine to the sample, and measuring the ammonia evolved with the gas-sensing electrode. Results compare favourably with the xanthine oxidase method.

Much attention has recently been given to the development of specific biosensors for various substrates of biomedical and biochemical interest by using immobilized enzymes in conjunction with potentiometric ion- or gas-sensing membrane electrodes [1, 2]. The possibility of devising enzyme—substrate sensors employing deaminating enzymes for the determination of various nucleotides has been explored [3], and the utility of ammonia gas-sensing electrodes in the determination of adenosine deaminase has been reported [4]. Such potentiometric sensors for purine compounds have not previously been described, despite the important role of these compounds in biochemical processes.

Selective methods for the determination of guanine have been based on polarographic [5], spectrophotometric [6] and gas chromatographic techniques [7]. Attention has also been given to estimation of the activity of serum guanase (guanine aminohydrolase) because it is a sensitive index of hepatic cell necrosis [8, 9]. Most of the proposed procedures are time-consuming and expensive [9—12].

This paper describes the development and evaluation of an immobilized guanase probe for guanine monitoring. The optimum operating conditions were established to ensure linearity and maximum slope of the calibration graph and minimum response time. Guanine was determined with this electrode in the range 10^{-4}—10^{-2} M. A potentiometric method was developed for the determination of guanase activity in human serum by using an ammonia gas sensor. The results obtained compare favorably with those obtained with the conventional xanthine oxidase method.

0003—2670/81/0000—0000/$02.50

EXPERIMENTAL

Apparatus

An Orion Model 95-10 ammonia gas-sensing electrode was employed in construction of the enzyme electrode. Potentials were measured with a Corning Model 12 pH/mV meter connected to a Heath-Schlumberger SR-255 B strip chart recorder. All measurements were done in a thermostatted cell at 37 ± 0.2°C.

Reagents

Guanase E.C.3.5.4.3, from rabbit liver (Sigma Chemical Co., St. Louis, MO) was obtained as a suspension in 3.2 M ammonium sulphate solution, pH 6.0, with an activity of about 1.2 I.U. ml^{-1}. One unit of guanase is the amount of enzyme which deaminates 1.0 μmol of guanine to xanthine per min at pH 8.0 and 25°C. The guanase activity was measured as recommended by the supplier. All other chemicals were of analytical grade. Distilled deionized water was used throughout.

A stock solution of 0.1000 M guanine was prepared by dissolving 1.510 g of free guanine in a few ml of 1 M sodium hydroxide solution and diluting to 100.0 ml with water; this solution was stored in a refrigerator. Working solutions were prepared daily by appropriate dilutions of the stock solution with 0.1 M Tris-HCl buffer, pH 8.0, just before the measurements. Calibration curves for the determination of guanase in human blood serum were constructed from results obtained by use of Wellcomtrol reference solutions (Wellcome Reagents Limited, Beckenham, England) to which known amounts of guanase had been added. Aqueous standard guanase solutions were prepared by appropriate dilution of the commercial enzyme preparation just before measurement.

Electrode preparation

The guanine electrode was constructed by placing 10 μl of enzyme suspension (approximately 0.012 I.U.) between an outer circular cellophane dialysis membrane and the gas-permeable membrane of the ammonia electrode. The enzyme suspension layer was about 0.2-mm thick. The electrode was preconditioned by soaking for 2 h in 0.1 M Tris buffer, pH 8.0, and was stored in this buffer at 4°C when not in use [3].

Procedures

Determination of guanine. Pipet 5.00 ml of standard guanine or unknown sample solution into the thermostatted cell, immerse the guanine electrode in the solution, start the stirrer and read the e.m.f. when it is constant to within ±0.1 mV (in 1.5—4 min). Calculate the guanine concentration from a calibration curve of e.m.f. vs. log (guanine concentration).

Determination of guanase. Pipet 5.00 ml of standard 0.01 M guanine solution (in 0.1 M Tris buffer, pH 8.0) into the thermostatted cell, immerse the

ammonia gas sensor in the solution, inject 100 μl of standard guanase or of unknown sample solution, start the stirrer and read the e.m.f. when it is constant to within ±0.1 mV. Calculate the guanase activity from a calibration graph of e.m.f. vs. log(guanase activity).

RESULTS AND DISCUSSION

The guanine electrode

The basis for the guanine electrode is the specific deamination of guanine according to the reaction

$$\text{Guanine} + H_2O \xrightarrow{\text{Guanase}} \text{Xanthine} + NH_3$$

Guanine diffuses into the immobilized enzyme layer of the electrode producing a stoichiometric quantity of ammonia which gives rise to a constant potential directly related to the logarithm of guanine concentration in the sample solution. This reaction is also the basis for the estimation of guanase activity. A small volume of the enzyme sample is mixed with a standard guanine solution and the ammonia produced gives rise to a potential directly related to log(guanase activity).

A typical calibration graph for the enzyme electrode in stirred guanine solutions, buffered at pH 8.0 with 0.1 M Tris buffer, is shown in Fig. 1A. The electrode has a linear response for about two decades of guanine concentration, 10^{-4}—10^{-2} M; the slope is 29 mV per decade at 37°C, with a correlation coefficient of −0.999.

Other procedures were investigated for the immobilization of the enzyme, such as cross-linking with glutaraldehyde on albumin as described by Brown et al. [13] or on activated glass beads [14]. The enzyme activities of the immobilized preparations were found to be about 20% and 50% of the

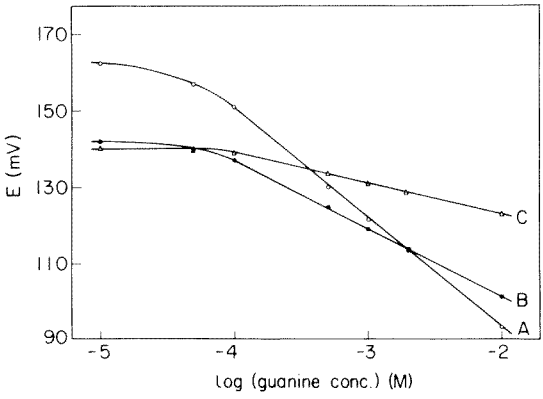

Fig. 1. Calibration graphs for guanine electrodes prepared with (A) the enzyme suspension; (B) the enzyme immobilized on activated glass beads; (C) cross-linked enzyme layers. Other conditions as in text.

initial enzyme activity, respectively. These preparations were used in the same way as the enzyme suspension for the guanine electrode construction. Calibration curves obtained with these guanine electrodes are also shown in Fig. 1. Both electrodes were less sensitive and had greater response times than the electrode prepared by direct use of the enzyme suspension; they were not studied further.

Effect of the amount of enzyme. The effect of variations in the amount of enzyme used for the enzyme layer on the sensitivity of the electrode is shown in Fig. 2. The slope of the calibration curve increases with the amount of enzyme used up to 10 μl (0.012 I.U.) of enzyme suspension, which was chosen for the construction of the electrode.

Dynamic response of the electrode. The response rate was tested for 10^{-4} and 10^{-2} M guanine solutions; it was 4 and 1.5 min, respectively, whether the sequence of measurements was from low to high concentrations or vice versa.

Effect of buffer, pH and interferences. Since the selection of optimum solution conditions represents, by necessity, some compromise between optimum conditions for the enzyme reaction [15] and those of the NH_3—NH_4^+ equilibrium [16] involved in the ammonia sensor, the effects of buffer composition and pH were studied in some detail. The buffers tested were

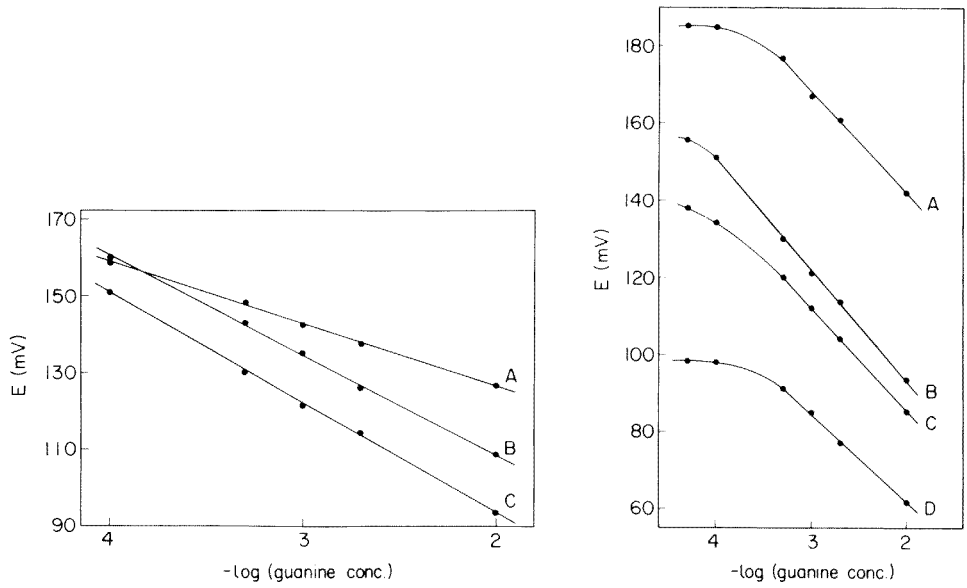

Fig. 2. Effect of amount of enzyme calibration graph: (A) 10 μl of enzyme suspension diluted 1:10; (B) 10 μl of enzyme suspension as purchased; (C) 25 μl of enzyme suspension. Other conditions as in text.

Fig. 3. Calibration curves for the guanine electrode in 0.1 M Tris-HCl buffer at (A) pH 7.5; (B) pH 8.0; (C) pH 8.5; (D) pH 9.0. Other conditions as in text.

phosphate, borate, glycine and Tris. The best sensitivity was obtained with the Tris buffer. Further investigations in this buffer system as a function of pH (Fig. 3) demonstrate that the widest linear range is obtained at pH 8.0 (curve B), which lies in the middle of a broad pH optimum in the range pH 6—10 for the enzymatic reaction.

Few interferences would be expected because guanase specifically hydrolyses guanine; guanosine and other purines are not attacked [17].

Temperature effect. The effect of temperature on the electrode performance was studied. The results obtained are summarized in Table 1. An increase of temperature in the range 27—37°C improved the performance of the enzymatic electrode (smaller response times and larger response slopes), so 37°C was chosen for the recommended procedure because no further improvement in electrode characteristics was observed at higher temperatures.

Long-term stability and operating life. The stability in performance and the operational lifetime of the guanine electrode depend on operational conditions and storage. The lifetime of the electrode was found to be about 6 weeks, if stored at 4°C when not in use. During this period the slope of the response curve of the electrode remained constant at 29.0 ± 0.4 mV per decade at 37°C. As the electrode began to age, an increased curvature in the upper limit region was noted, and the upper limit of the linear region decreased to 5×10^{-3} M, whereas the lower limit was unaffected. When the guanine electrode was stored at room temperature, its lifetime was shortened drastically; the slope of the response curve remained constant for only 4 days, thereafter decreasing continuously.

Application. Results for the determination of guanine in aqueous solutions are given in Table 2. It can be seen that guanine in the range 10^{-4}—10^{-2} M can be determined with an average error of ±1.6%. The relative standard deviation was 1.7% for a 1.0×10^{-3} M guanine sample (6 results).

Determination of guanase

Results for the determination of guanase in aqueous solutions are given in Table 3. The same procedure was used for the 0.12—1.2 and 1.2—12 I.U. l^{-1} ranges, but the slopes of the calibration curves were different for the two ranges. The results indicate that guanase in the range 0.12—12 I.U. l^{-1}

TABLE 1

Effect of temperature on response time and slope of the guanine electrode

Temperature (°C)	Response time (min)	Slope (mV/decade)
27	2.5[a]—6[b]	20.0
32	2—5	23.0
37	1.5—4	28.6
42	1.5—4	28.6

[a] 10^{-2} M guanine solution. [b] 10^{-4} M guanine solution.

TABLE 2

Determination of guanine in aqueous solutions

Guanine ($\times 10^{-5}$ M)		Relative error (%)
Taken	Found[a]	
10.0	9.86	−1.4
20.0	19.9	−0.5
50.0	51.3	+2.6
100	102	+2.0
200	202	+1.0
500	488	−2.4
1000	1010	+1.0
	Mean:	1.56

[a]From interpolation of calibration graph, average of two determinations. Regression equation: $E = -28.6 \log [\text{guanine}] + 35.8$; corr. coeff., −0.9990.

can be determined with an average error of 1.1%. The relative standard deviations for 0.5 and 6 I.U. l^{-1} guanase were 1.2% and 1.1%, respectively (6 results each).

The accuracy of the method was tested by adding guanase to a serum calibration reference and control (Wellcomtrol), formulated so as to approximate normal levels for frequently tested serum constituents. Accuracy and precision were very similar to those obtained in the determination of guanase in aqueous solutions. Typical results of recovery studies are shown in Table 4. Recovery experiments were also carried out with hospital serum samples, containing normal amounts of guanase. The recovery of guanase

TABLE 3

Determination of guanase in aqueous solutions

Guanase (I.U. l^{-1})		Relative error (%)	Guanase (I.U. l^{-1})		Relative error (%)
Taken	Found[a,b]		Taken	Found[a,c]	
0.120	0.123	+2.5	1.20	1.22	+1.7
0.300	0.304	+1.3	3.00	2.97	−1.0
0.500	0.496	−0.8	6.00	5.91	−1.5
0.800	0.810	+1.2	9.00	9.01	+0.1
1.00	0.997	−0.3	12.0	11.9	−0.8
1.20	1.19	−0.8			
	Mean:	1.15%		Mean:	1.02%

[a]From interpolation of calibration graph, average of two determinations. [b]Regression equation: $E = -28.8 \log [\text{guanase}] + 155.2$; corr. coeff., −0.9999. [c]Regression equation: $E = -47.5 \log [\text{guanase}] + 157.2$; corr. coeff., −0.9995.

TABLE 4

Determination of guanase added to a Wellcomtrol standard[a]

Guanase (I.U. l^{-1})		Relative error (%)	Guanase (I.U. l^{-1})		Relative error (%)
Taken	Found[a,b]		Taken	Found[a,c]	
0.120	0.121	+0.8	1.20	1.19	−0.8
0.300	0.298	−0.7	3.00	3.02	+0.7
0.500	0.492	−1.6	6.00	5.94	−1.0
0.800	0.819	+2.4	9.00	9.21	+2.3
1.00	0.992	−0.8	12.0	11.9	−0.8
1.20	1.21	+0.8			
					Mean: 1.12%
		Mean: 1.18%			

[a]Average of two determinations. Calibration graph obtained with four standard guanase solutions. [b]Regression equation: $E = -28.9 \log [\text{guanase}] + 135.1$; corr. coeff., −0.9999. [c]Regression equation: $E = -47.7 \log [\text{guanase}] + 135.5$; corr. coeff., −0.9998.

(amount added, 0.12—0.5 I.U. l^{-1}) ranged from 92 to 110% (average 101.2%).

The accuracy of the method was further tested by comparing values for serum from a calibration curve with those obtained with the conventional xanthine oxidase spectrophotometric method [18]. Comparison of the results for 50 individual serum samples analyzed by both methods, gave a linear plot, $y = 0.997x - 0.015$, with a correlation coefficient of 0.996, showing that there is satisfactory agreement between the two methods. The proposed method is faster than the spectrophotometric method (2 min compared with 15 min for a spectrophotometric determination). Also, the additional use of xanthine oxidase increases the cost of a determination. The reported normal values for ammonia nitrogen are in the range 0.75—1.95 μg N ml^{-1}; the free ammonia concentration in serum at pH 8.0 should be 3×10^{-6}—8×10^{-6} M. These small concentrations cause negligible interference.

The authors are indebted to Dr. E. Nikoleli-Sideri (IKA Hospital, Athens, Greece) for providing samples of human blood serum. This work was supported in part by grants from the University of Athens and the National Research Foundation of Greece. The paper was presented at the 1st Balkan Chemistry Days Conference, Athens, April 1980.

REFERENCES

1 K. Camman, Working with Ion-Selective Electrodes, Springer-Verlag, New York, 1979; pp. 98—104.
2 G. E. Baiulescu and V. V. Cosofret, Applications of Ion-Selective Membrane Electrodes in Organic Analysis, E. Horwood, Chichester, Sussex, 1977.
3 D. S. Papastathopoulos and G. A. Rechnitz, Anal. Chem., 48 (1976) 862.
4 C. E. Hjemdahl-Monsen, D. S. Papastathopoulos and G. A. Rechnitz, Anal. Chim. Acta, 88 (1977) 253.

5 G. Dryhurst, Anal. Chim. Acta, 57 (1971) 137.
6 W. L. Gyure, Anal. Bioch., 51 (1973) 421.
7 T. Vo-Dinh, E. L. Yen and J. D. Winefordner, Anal. Chem., 48 (1976) 1186.
8 I. Davidsohn and J. B. Henry, Clinical Diagnosis by Laboratory Methods, 15th edn., W. B. Saunders, Philadelphia, PA, 1974, p. 860.
9 G. Ellis and D. M. Goldberg, Clin. Chim. Acta, 37 (1972) 47.
10 M. Nyssen and J. Dorche, Clin. Chim. Acta, 22 (1968) 363.
11 B. G. Wolthers, B. J. Nusse, J. Bootsma and A. Groen, Clin. Chim. Acta, 41 (1972) 223.
12 G. Ellis, R. J. Spooner and D. M. Goldberg, Clin. Chim. Acta, 47 (1973) 75.
13 G. Brown, D. Thomas, G. Gellf, D. Domurato, A. M. Berjonneu and C. Guillon, Biotechnol. Bioeng., 15 (1973) 359.
14 D. L. Marshall, Biotechnol. Bioeng., 15 (1973) 447.
15 S. P. Colowick and N. O. Kaplan, Methods in Enzymology, 2nd printing, Vol. II, Academic Press Inc., NY, 1960, p. 480.
16 J. N. Butler, Ionic Equilibrium, A Mathematical Approach, Addison-Wesley, Reading, MA, 1964, p. 132.
17 H. M. Kalckar, J. Biol. Chem., 167 (1947) 461.
18 G. Näher, in H. V. Bergmeyer (Ed.), Methoden der Enzymatischen Analyse, Verlag Chemie, Weiheim, 1970, p. 1843.

Analytica Chimica Acta, 126 (1981) 51—56
Elsevier Scientific Publishing Company, Amsterdam — Printed in The Netherlands

DEVELOPMENT AND ANALYTICAL APPLICATIONS OF A NEW LIQUID-MEMBRANE 3,5-DINITROSALICYLATE-SELECTIVE ELECTRODE

T. P. HADJIIOANNOU and P. C. GRITZAPIS
Laboratory of Analytical Chemistry, University of Athens, Athens (Greece)
(Received 29th September 1980)

SUMMARY

A 3,5-dinitrosalicylate (DNS)-selective electrode with a liquid membrane of either tetraphenylphosphonium-DNSH dissolved in *p*-nitrocumene or dimethyldioctadecylammonium-DNSH dissolved in 1-decanol is described. The liquid membrane electrode exhibits rapid and near-Nernstian response to $DNSH^-$ activity from 10^{-2} to 10^{-5} M. The response is unaffected by pH in the range 2.5—6.5. The electrode has been successfully applied in the direct potentiometric titration of iron(III) and copper(II) with EDTA and in the indirect titrimetric determination of aluminium(III) and nickel(II). It is also useful in titrations of bulky quaternary cations such as cetyltrimethylammonium, cetylpyridinium and didodecyldimethylammonium ions with DNSHNa.

Several liquid-membrane ion-selective electrodes have been described which respond selectively to organic anions. Salts of bulky quaternary ammonium ions with various anions have been widely used for constructing liquid-membrane anion-selective electrodes. Several of these electrodes have been used as indicator electrodes in potentiometric complexiметric and precipitation titrations [1—4].

In this paper, new 3,5-dinitrosalicylate (DNS)-selective electrodes are described. Tetraphenylphosphonium 3,5-dinitrosalicylate, $Ph_4P^+DNSH^-$, dissolved in *p*-nitrocumene, or dimethyldioctadecylammonium 3,5-dinitrosalicylate, $(CH_3)_2(C_{18}H_{37})_2N^+$-$DNSH^-$, dissolved in 1-decanol is the electroactive substance in the DNS-selective electrode. These electrodes exhibit useful analytical characteristics for direct determinations of DNS and can be applied in potentiometric complexiметric and precipitation titrations of several metal ions and of bulky quaternary ammonium ions.

EXPERIMENTAL

Instrumentation and reagents

The electrodes, the reaction cell and the recording system were the same as previously reported [5], except where stated.

All solutions were prepared with deionized-distilled water from reagent-grade materials.

0003—2670/81/0000—0000/$02.50

A 0.02 M monosodium 3,5-dinitrosalicylate (DNSHNa) solution was prepared by dissolving 5.360 g of DNSHNa (Eastman Kodak) in water and diluting to 1 l; it was standardized against standard sodium hydroxide solution. More dilute standard solutions were prepared by dilution.

Solutions (0.0100 M) of dimethyldioctadecylammonium bromide, cetyltrimethylammonium bromide (CTAB), cetylpyridinium chloride (CPC) and didodecyldimethylammonium bromide (DDAB), were prepared by dissolving appropriate amounts of pure substances (Eastman Kodak) in 15% (v/v) or 5% (v/v) (for CTAB and CPC) water—isopropanol mixtures. A 0.1000 M solution of tetraphenylphosphonium chloride was prepared by dissolving the appropriate amount of salt in water.

Solutions (0.010 M) of iron(III) and copper(II) were prepared by dissolving appropriate amounts of ammonium iron(III) sulfate in 2% H_2SO_4, and of copper(II) sulfate pentahydrate in water. The molarity of these solutions was checked titrimetrically with EDTA. More dilute solutions were prepared as needed.

Preparation of the liquid ion-exchangers

Tetraphenylphosphonium 3,5-dinitrosalicylate was precipitated by mixing 3.0 ml of 0.100 M tetraphenylphosphonium chloride solution with 30 ml of 0.010 M monosodium 3,5-dinitrosalicylate solution. Similarly, dimethyldioctadecylammonium 3,5-dinitrosalicylate was precipitated by mixing 30 ml of 0.010 M dimethyldioctadecylammonium bromide solution with 30 ml of 0.010 M monosodium 3,5-dinitrosalicylate solution. The salts are readily soluble in *p*-nitrocumene and 1-decanol, respectively, which were therefore used for their extraction. The organic phases (ca. 30 ml) were washed twice with double-distilled water to remove traces of the chloride or bromide salts (and NaCl or NaBr), and then dried thoroughly with anhydrous sodium sulfate.

Construction of the electrode

The body of an Orion series 92 electrode equipped with a teflon membrane (Millipore LCWPO 1300) was used. The electrode was assembled as recommended by the manufacturer, and the internal reference and liquid ion-exchanger solutions were injected into the appropriate ports in the electrode body. The internal reference solution was 0.01 M monosodium 3,5-dinitrosalicylate in 0.1 M NaCl. A 0.01 M liquid-ion exchanger solution was used. The DNS electrode was conditioned by soaking in a stirred 0.01 M solution of DNSHNa for 12 h before use, and was also stored in this solution when not in use. The operative life of the electrode was more than 2 months, with daily usage of at least 5 h.

Procedures

Semi-automatic titration of iron(III) in presence of DNSHNa. (For the range 3.0×10^{-5}—10^{-3} M iron, with 1.000×10^{-2} M EDTA.) Pipet into a 100-ml beaker a 50.00-ml aliquot of the sample and 1.00 ml of 0.0100 M

DNSHNa solution. Start the stirrer, and after the potential has stabilized (ca. 1 min), start the burette and the recorder simultaneously to obtain the titration curve. For the greatest accuracy calibrate the recorder for each titration, using the burette reading.

Semi-automatic titration of copper(II) in presence of DNSHNa. (For the range 7.2×10^{-5}—1.8×10^{-3} M copper, with 1.000×10^{-2} M EDTA.) Pipet into a 100-ml beaker a 25.00-ml aliquot of the sample and 25.00 ml of acetate buffer (3 M, pH 4.3), and continue as in the titration of iron(III) from the point of adding the DNSHNa solution.

Semi-automatic titration of CTA, CP and DDA with DNSHNa. (For the range 2—12×10^{-4} M, with 1.000×10^{-2} M DNSHNa.) Pipet into a 50-ml beaker a 25.00-ml aliquot of the sample, and continue as in the titration of iron(III) from the point of starting the stirrer.

RESULTS AND DISCUSSION

Characteristics of the electrode

Linear response range. Typical calibration curves for the DNS-selective electrodes in stirred monosodium 3,5-dinitrosalicylate solutions showed linear response in the 10^{-2}—10^{-5} M range. The slope of the calibration curve was 58 mV/decade change in concentration at 25°C. After a few days, there was a decrease in slope in the 10^{-4}—10^{-5} M range.

Effect of pH. To check the pH-dependence of the potential of the DNS-selective electrode, potential—pH curves at various DNSHNa concentrations were constructed. The pH of the initial solution was altered by addition of very small volumes (less than 0.1 ml per 20 ml of test solution) of sodium hydroxide or sulfuric acid solutions. The plots (Fig. 1) show that between pH 2.5 and 6.5 the potential is practically independent of pH. At higher pH values there is an increase in potential because of the decrease in the $DNSH^-$ concentration caused by its dissociation to give DNS^{2-} ions (for $DNSH_2$: $pK_{a_1} = 0.70$, $pK_{a_2} = 7.25$) [6, 7]. During the operative life of the electrode, no discernible change in the potential—pH behavior was observed.

Dynamic response of the electrode. The dynamic response was tested for 10^{-2}—10^{-5} M monosodium 3,5-dinitrosalicylate solutions; the sequence of measurements was from low concentration to high concentrations and back. The response times were quite short (less than 3 s, including the mixing and recorder time) and depended on the concentration change, the stirring rate and efficiency of mixing. It was therefore possible to employ the DNS-selective electrodes in titrations with continuous addition of titrant and for the continuous monitoring of changing systems.

Potentiometric selectivity coefficients. The interference of various anions was studied by the graphical mixed solution method [8]. The concentration of the tested anion was kept constant, while the $DNSH^-$ concentration was varied in the range 10^{-2}—10^{-5} M. Selectivity coefficients are presented in Table 1. The two DNS electrodes respond to picrate ion in the range 10^{-2}—10^{-5} M with a slope of 55 mV/decade change in concentration.

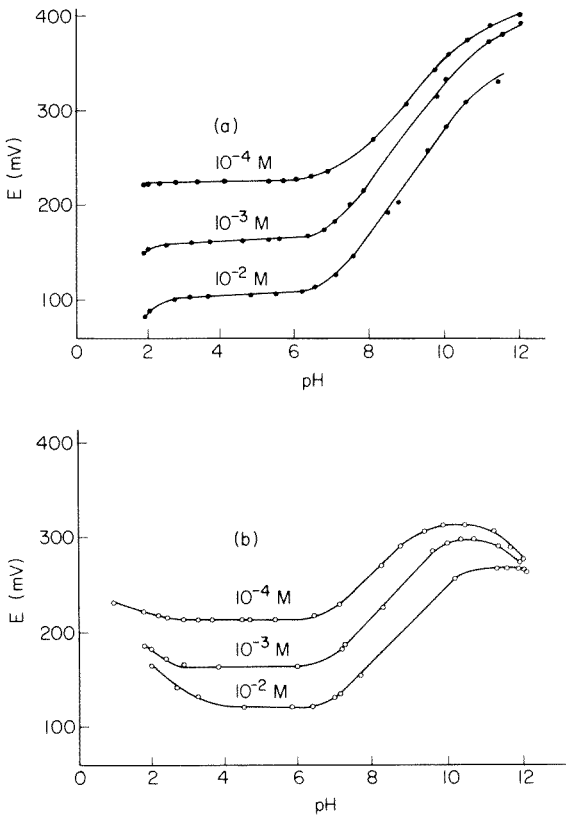

Fig. 1. Effect of pH on the potential of the 3,5-dinitrosalicylate-selective electrode at the different concentrations of monosodium 3,5-dinitrosalicylate marked: (a) $Ph_4P^+DNSH^-$ in *p*-nitrocumene; (b) $(CH_3)_2(C_{18}H_{37})_2N^+DNSH^-$ in 1-decanol.

TABLE 1

Potentiometric selectivity coefficients of DNS-selective electrodes

Anion[a] tested	$K^{pot}_{DNSH^-,j}$		Anion[b] tested	$K^{pot}_{DNSH^-,j}$	
	$Ph_4P^+DNSH^-$	$(CH_3)_2(C_{18}H_{37})_2N^+DNSH^-$		$Ph_4P^+DNSH^-$	$(CH_3)_2(C_{18}H_{37})_2N^+DNSH^-$
Periodate	1.5×10^{-2}	2.0×10^{-2}	Bromide	5.0×10^{-4}	3.0×10^{-3}
Perchlorate	1.3×10^{-2}	1.8×10^{-2}	Iodide	5.0×10^{-4}	6.0×10^{-4}
Chromate	4.0×10^{-3}	5.0×10^{-3}	Chloride	4.0×10^{-4}	6.0×10^{-4}
Benzoate	3.0×10^{-3}	2.3×10^{-2}	Nitrate	4.0×10^{-4}	5.0×10^{-4}
Citrate	3.0×10^{-3}	3.0×10^{-3}	Sulfate	3.0×10^{-4}	3.0×10^{-4}
Phthalate	3.0×10^{-3}	3.0×10^{-2}			

[a]The concentration of the anion, j, was 0.01 M. [b]The concentration of the anion, j, was 0.1 M.

Analytical applications

The DNS-selective electrode can be used as indicator electrode in potentiometric titrations of many metal ions with EDTA using 3,5-dinitrosalicylic acid as metallochromic indicator, and of bulky quaternary cations with DNSHNa. As examples, the titrimetric determinations of Fe(III), Cu(II), Al(III) and Ni(II), and of cetyltrimethylammonium, N-cetylpyridinium and didodecyldimethylammonium ions were examined.

Typical recorded curves for the direct titration of iron with EDTA in the presence of DNSHNa and the indirect titration of nickel are shown in Fig. 2. For the indirect titration of nickel or aluminum, a known excess of standard EDTA solution was added to the sample and the unreacted EDTA was back-titrated with standard iron(III) solution. In the case of aluminum, boiling for 1—2 min was necessary to ensure its quantitative binding, before the back-titration. Under the experimental conditions used, there was a blank of 0.02 ml of 0.01 M EDTA in the titration of iron in the range 3×10^{-5}—10^{-4} M. No blank was observed for more concentrated iron solutions or for copper. Results of determinations of iron, copper, aluminum and nickel in aqueous solutions are presented in Table 2. The data indicate that these ions can be determined with average errors of about 1% in the ranges specified.

Typical recorded curves for titrations of didodecyldimethylammonium, tetrapentylammonium and tetraphenylarsonium ions with DNSHNa are shown in Fig. 3. The point of maximum slope of the curves was taken as the end-point. There was a blank of 0.10 ml of 0.01 M DNSHNa solution in the titration of three organic cations tested (CTA, CP, DDA) at a titrant delivery

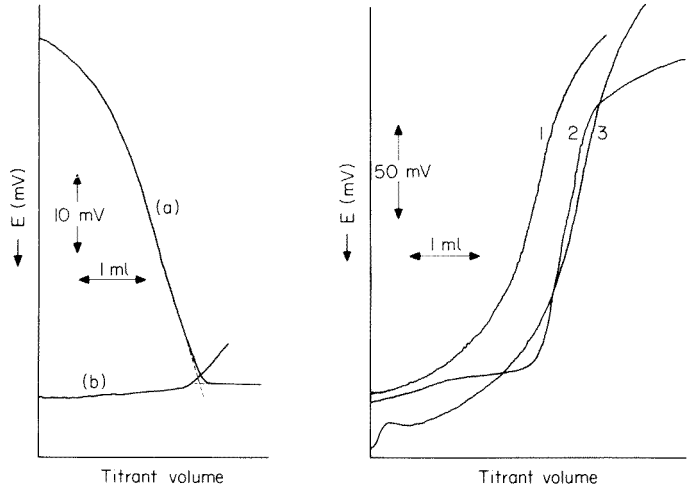

Fig. 2. Recorded curves for (a) direct titration of 5×10^{-4} M iron(III), and (b) indirect titration of 15.00 ml of 1.7×10^{-3} M nickel (+7.00 ml of 10^{-2} M EDTA) with 2×10^{-2} M iron(III) in presence of DNSHNa as indicator.

Fig. 3. Recorded curves for titration of 25 ml 10^{-3} M solutions of (1) tetrapentylammonium, (2) didodecyldimethylammonium and (3) tetraphenylarsonium ions with 10^{-2} M DNSHNa.

TABLE 2

Summary of results for aqueous solutions of Fe(III), Cu(II), Ni(II) and Al(III)

Ion	Amount in sample (mg)	Average error (%)
Fe(III)	0.08—2.8	1.2
Cu(II)	0.1—3.2	0.6
Al(III)	0.5—1.4	1.2
Ni(II)	1—3	1.3

TABLE 3

Semi-automatic potentiometric precipitation titration of quaternary cations with DNSHNa

Cation	Amount ($\times 10^5$ mol)		Error (%)	Cation	Amount ($\times 10^5$ mol)		Error (%)
	Taken	Found			Taken	Found	
CTA	0.530	0.530	—	CP	0.520	0.510	−1.9
	1.060	1.050	−0.9		1.040	1.020	−1.9
	2.12	2.10	−0.9		1.560	1.550	−0.6
	2.63	2.62	−0.4		2.09	2.12	+1.4
			Av. 0.6		2.59	2.58	−0.4
DDA	0.490	0.501	+2.2				Av. 1.2
	0.980	0.999	+1.9				
	1.72	1.74	+1.2				
			Av. 1.8				

rate of 0.33 ml min^{-1}. No blank was observed for the tetrapentylammonium and tetraphenylarsonium cations. Results for titrations of CTA, CP and DDA cations are given in Table 3. The data indicate that amounts of these cations in the range 0.5—2.5 $\times$ 10^{-5} mol can be determined with average errors of about 1%.

The authors are grateful to E. P. Diamandis for stimulating discussions. This research was supported in part by research grants from the Greek National Institute of Research and the Alexandros Onassis Public Benefit Foundation.

REFERENCES

1 E. P. Diamandis and T. P. Hadjiioannou, Mikrochim. Acta (Vienna), (1977, II), 255.
2 E. Pungor (Ed.), Ion Selective Electrodes, Akadémia Kiado, Budapest, 1973, p. 225.
3 M. Kataoka, M. Shin and T. Kambara, Talanta, 42 (1977) 261.
4 A. R. Rajput, M. Kataoko and T. Kambara, J. Electroanal. Chem., 66 (1975) 67.
5 T. P. Hadjiioannou and E. P. Diamandis, Anal. Chim. Acta, 94 (1977) 443.
6 L. G. Bray, J. F. Dippy, R. C. Hughes and W. W. Laxton, J. Chem. Soc., (1957) 2405.
7 C. Vassiliadis, G. Colovos and P. Karayiannidis, Chim. Chron., 31A (1966) 46.
8 G. J. Moody and J. D. R. Thomas, Selective Ion-Sensitive Electrodes, Merrow, Watford, 1971, p. 14.

Analytica Chimica Acta, 126 (1981) 57—64
Elsevier Scientific Publishing Company, Amsterdam — Printed in The Netherlands

THIN-LAYER DIFFERENTIAL PULSE VOLTAMMETRIC DETERMINATION OF CHLORPROMAZINE IN BIOLOGICAL FLUIDS

TAFEEDAH B. JARBAWI and WILLIAM R. HEINEMAN*

Department of Chemistry, University of Cincinnati, Cincinnati, OH 45221 (U.S.A.)

GASTON J. PATRIARCHE

Institut de Pharmacie, Université Libre de Bruxelles, Campus Plaine B.P. 205/1, 1050 Bruxelles (Belgium)

(Received 24th November 1980)

SUMMARY

The combination of a thin-layer electrochemical cell with differential pulse voltammetry can be used to determine chlorpromazine in plasma and urine. The thin-layer cell (23 μl capacity) has a wax-impregnated graphite electrode. Direct determination of chlorpromazine in urine gave a linear calibration curve for the range 4.8×10^{-8}—2.4×10^{-4} M with 97% recovery. No interference from glutethimide, dextropropoxyphene, meprobamate, diazepam, and methaqualone-HCl was detected. Direct measurement of chlorpromazine in plasma gave a linear calibration curve for the range 2.4×10^{-5}—4.8×10^{-4} M with 89% recovery. The procedure for plasma and urine requires only 2 min per determination. Detection levels are below that required for monitoring therapeutic levels of chlorpromazine in urine.

In 1952, Delay et al. [1] first reported the use of chlorpromazine (CPZ) for the treatment of psychoses. Two years later, chlorpromazine was recognized as a drug which radically alters the treatment, course and prognosis of various mental illnesses.

Since then various methods have been used for the determination of chlorpromazine: fluorescence [2—4], gas chromatography with electron-capture detection [5—7], thin-layer chromatography [8—10], mass fragmentography [11], spectrophotometry [12—14], and gas chromatography—mass spectrometry [15]. Each one of these methods has its own limitations, such as interference, insufficient sensitivity, or complexity of procedure or instrumentation.

Merkle and Discher [16] showed that chlorpromazine is electrochemically oxidized via two 1-electron steps. The first oxidation step produces the cation radical ($CPZ^{+\bullet}$). The second step involves oxidation of $CPZ^{+\bullet}$ to produce the sulfoxide. Patriarche and co-workers used chronopotentiometry to measure the $E_{\tau/4}$ for chlorpromazine oxidation [17, 18]. They also developed a method for the coulometric titration of chlorpromazine with electrogenerated cerium(IV) in which they were able to determine 0.25—20 mg of chlorpromazine.

Differential pulse polarography has been successfully used for the determination of drugs [19—25]. The feasibility of combining the low detection limit of differential pulse voltammetry (d.p.v.) with the small volume capability of thin-layer electrochemical cells for determining small amounts of metal ions and organic compounds has recently been demonstrated [26, 27]. Thin-layer d.p.v. measurements on the drug diazepam gave a linear calibration curve over the range 1—60 $\mu g\ l^{-1}$ with a detection limit of 0.1 $\mu g\ l^{-1}$ on 60 μl of sample [27].

This work demonstrates the capability of using a thin-layer electrochemical cell in conjunction with d.p.v. for the determination of chlorpromazine in phosphate buffer pH 7.00, plasma, and urine. The good detection limit of d.p.v. combined with the need of only a few microliters of fluid in the thin-layer cell makes this technique competitive with other methods.

EXPERIMENTAL

Instrumentation

Determinations were performed in the small volume (ca. 23 μl) thin-layer cell shown in Fig. 1. Holes for A, B, and C (diameters of 0.2390 in., 0.1610 in. and 0.1610 in., respectively) were drilled in a 1.75 in. diameter plexiglas rod (G). In order to connect the three holes, 0.0125 in. diameter channels (E) were drilled. Two teflon tubes (B, C) of 0.1452 in. diameter and 0.40 in. length were press-fitted into the cell body with silicone rubber. A wax-impregnated graphite electrode with a diameter of 0.181 in. was inserted into a piece of cylindrical teflon (D, 0.183 in. diameter) which served as a brace for adjusting the volume of the thin solution layer in the cell. The brace enabled a given volume to be easily reproduced when the electrode was removed for polishing. A standard calomel reference electrode and an auxiliary platinum electrode were positioned in B and C, respectively.

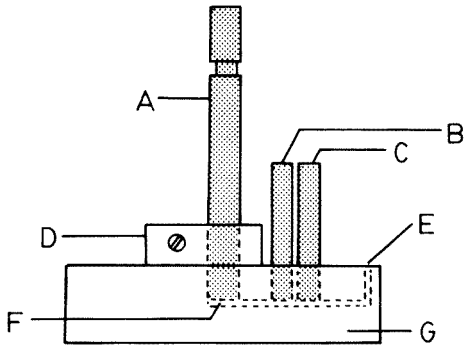

Fig. 1. Thin-layer cell. (A) Wax-impregnated graphite electrode; (B) reference electrode compartment; (C) auxiliary electrode compartment; (D) volume brace; (E) channel connecting the three compartments; (F) thin solution layer undergoing electrolysis; (G) cell body.

In all experiments, a Princeton Applied Research Model 174A Polarographic Analyzer was used with a Houston Instruments Omnigraphic 2000 x-y recorder. A Harrick plasma cleaner was used to clean the thin-layer cell prior to each determination. Instrument settings were as follows except where stated otherwise: differential pulse mode; 5 mV s^{-1} scan rate; 50 mV modulation amplitude; 1 s/drop clock time; 1.5 V range; positive scan; and 200 mV initial potential.

The wax-impregnated graphite electrode was made from POCO FXI spectroscopic graphite rods. The electrode was polished as previously described [26]. The electrode was cleaned by briefly polishing prior to each voltammetric run.

Reagents

Phosphate buffer was Buffer—Titrisol (EM Laboratories, Elmsford, NY). Plasma was obtained from Cincinnati General Hospital. Vials of freeze-dried urine control containing the drugs glutethimide, dextropropoxyphene, chlorpromazine, meprobamate, methaqualone-HCl and diazepam, plus one vial without drugs were obtained from Applied Science Laboratories, Inc. Each vial contained 50 μg of each drug and produced 5 ml of reconstituted urine when distilled water was added to the contents. Solutions of chlorpromazine were protected from light and heat by wrapping the containers with aluminum foil and refrigerating them.

Procedures

Two procedures were followed for determining chlorpromazine in plasma and urine. In the first procedure, two samples of 8×10^{-3} g of chlorpromazine were mixed with 3 ml of plasma or 25 ml of urine and were then extracted by the methods described earlier for plasma [28] and urine [8]. The extracted chlorpromazine was then dissolved in phosphate buffer pH 7.00 and determined by thin-layer d.p.v. The second procedure did not utilize any pretreatment or pre-extraction steps: chlorpromazine was dissolved in plasma or urine, and differential pulse voltammograms were recorded with no additional treatment of the sample.

The method of standard addition was used to determine the recovery of chlorpromazine in urine, freeze-dried urine control, and plasma. In the case of the freeze-dried urine control, the standard solution was prepared by making the urine control vial without drugs 1.00×10^{-5} M in chlorpromazine.

RESULTS AND DISCUSSION

Thin-layer cyclic voltammetry

Thin-layer cyclic voltammetry was used to determine the optimum solution conditions and electrode material for the determination of chlorpromazine. A typical voltammogram of chlorpromazine in pH 7.00 phosphate buffer at a wax-impregnated graphite electrode is shown in Fig. 2. The well-

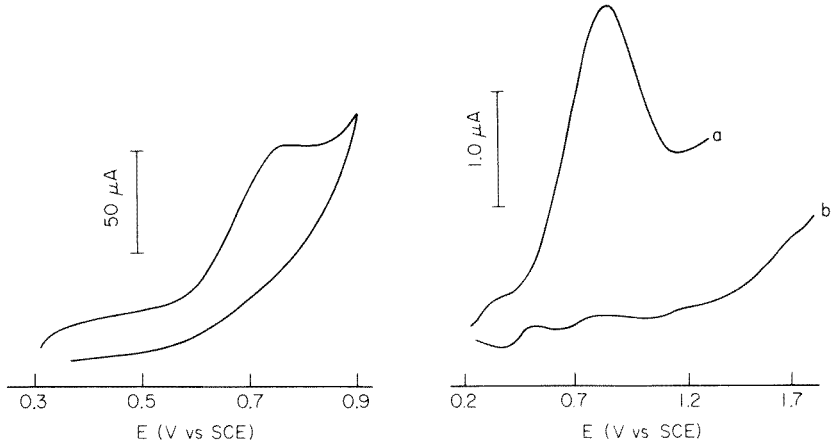

Fig. 2. Thin-layer cyclic voltammogram at wax-impregnated graphite electrode for 4.8×10^{-4} M chlorpromazine, phosphate buffer pH 7.00. Scan rate 5 mV s^{-1}.

Fig. 3. Thin-layer differential pulse voltammograms of (a) 5.0×10^{-5} M chlorpromazine in urine; (b) urine.

defined anodic peak (E_p = 757 mV vs. SCE) corresponds to the 1-electron oxidation of chlorpromazine to $CPZ^{+\bullet}$. Instability of the radical cation at this pH is indicated by the absence of a cathodic wave on the reverse scan. The radical cation is more stable in acidic solution as shown by a more reversible cyclic voltammogram obtained in 3 M H_2SO_4 at a gold minigrid optically transparent thin-layer electrode. However, this electrode was not chosen for the chlorpromazine determination since adsorption of $CPZ^{+\bullet}$ on the gold was troublesome. Use of the wax-impregnated graphite electrode in strongly acidic conditions resulted in its rapid deterioration.

Thin-layer differential pulse voltammetry

Well-defined thin-layer differential pulse voltammograms were obtained for the oxidation of chlorpromazine in phosphate buffer pH 7.00, plasma, and urine. A representative voltammogram for chlorpromazine in urine is shown in Fig. 3. The following values of peak voltage were found in the three media: 670 mV in phosphate buffer, 700 mV in plasma, 800 mV in urine. A sharper peak and a lower residual current were obtained with the phosphate buffer as supporting electrolyte. The well-defined waves for chlorpromazine in plasma and urine suggested that direct measurement in these media might be feasible.

The peak current for the chlorpromazine oxidation wave was optimized by systematic variation of modulation amplitude (pulse height), clock time (pulse length), and scan rate. The effect of modulation amplitude at different scan rates on peak current is shown in Fig. 4. The effect of clock time (pulse length) at a 5 mV s^{-1} scan rate and 50 mV modulation amplitude is

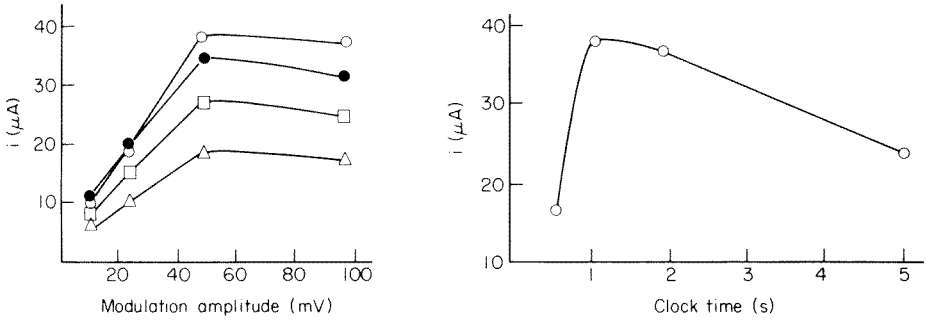

Fig. 4. Effect of modulation amplitude on peak current at varying scan rates for 4.8×10^{-4} M chlorpromazine in phosphate buffer pH 7.00 at the thin-layer electrode. Scan rates: (△) 1 mV s^{-1}; (□) 2 mV s^{-1}, (○) 5 mV s^{-1}, (●) 10 mV s^{-1}.

Fig. 5. Effect of clock time (pulse length) on peak height for 4.8×10^{-4} M chlorpromazine in phosphate buffer pH 7.00 at the thin-layer electrode. Scan rate 5 mV s^{-1}, modulation amplitude 50 mV, initial potential +200 mV.

shown in Fig. 5. Conditions for maximum sensitivity were as follows: 5 mV s^{-1} scan rate, 50 mV pulse height, and 1 s clock time.

Calibration curves

Calibration curves were obtained for standard solutions of chlorpromazine in the three media. Thin-layer differential pulse voltammograms were recorded in a non-sequential order. A linear relationship between peak height and concentration from 4.8×10^{-8} to 2.4×10^{-4} M chlorpromazine with a detection limit of 4.8×10^{-9} M was obtained in both phosphate buffer and urine. A calibration curve for chlorpromazine in urine is shown in Fig. 6. A

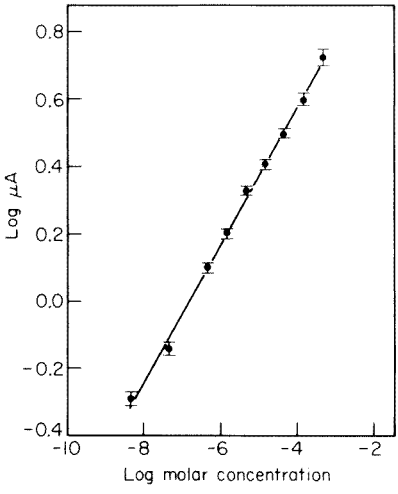

Fig. 6. Calibration curve for chlorpromazine in urine. Bars indicate range for three determinations.

more restricted linear range of 2.4×10^{-5}—4.8×10^{-4} M with a detection limit of 4.8×10^{-6} M was obtained for chlorpromazine in plasma. Least-squares results for all these data are included in Table 1. The smaller range in plasma is attributed to fouling of the electrode by components in the plasma. In all cases, optimum reproducibility resulted when the electrode was removed from the cell and polished briefly after each voltammogram was recorded. Failure to clean the electrode caused progressive decrease in peak currents, presumably due to fouling of the electrode by adsorbed $CPZ^{+\bullet}$ or other solution components in the case of plasma and urine.

Recovery and interferences

The recovery of chlorpromazine for a variety of samples by the two procedures is shown in Table 2. A recovery of 96% was obtained for chlorpromazine in urine when the commonly used extraction procedure was employed. By comparison, recoveries of 97.5% and 97.3% were obtained

TABLE 1

Linearity of the calibration curves for phosphate buffer, urine, and plasma[a]

Sample	Slope	Intercept	Standard error of estimate
Phosphate buffer	0.189 ± 0.004[b]	1.411 ± 0.023[c]	0.020
Urine	0.204 ± 0.003	1.389 ± 0.018	0.012
Plasma	0.126 ± 0.012	0.947 ± 0.059	0.031

[a]Based on 4 determinations for each calibration curve. [b]Standard deviation of slope. [c]Standard deviation of intercept.

TABLE 2

Recovery of chlorpromazine (CPZ)

Sample	Procedure	CPZ added (mg)	CPZ average found (mg)	Standard deviation (mg)	Number of trials	Recovery (%)
Urine	Extraction	8.00	7.68	0.83	6	96[b]
Urine	Direct	8.00	7.80	0.71	5	97.5[c]
Freeze-dried urine[a]	Direct	0.050	0.0487	0.0029	6	97.3[c]
Phosphate buffer	Direct	8.00	7.57	0.81	5	94.6[c]
Plasma	Extraction	8.00	5.94	0.97	6	74.3[b]
Plasma	Direct	8.00	7.11	0.87	5	88.9[c]

[a]Also contains glutethimide, dextropropoxyphene, meprobamate, diazepam, and methaqualone-HCl, 50 μg each. [b]Relative recovery. [c]Absolute recovery.

when measurements were made directly on urine and freeze-dried urine respectively with no sample treatment. This substantiates the feasibility of directly determining chlorpromazine in urine by thin-layer d.p.v. These results compare favorably with the 95.5% recovery reported for t.l.c. [8] and the 84.2% for fluorescence [4]. A recovery of 88.9% was obtained by direct measurement on plasma. Although this recovery is lower than that obtained for urine, direct determination is still feasible within the linear concentration range reported above. The low recovery by extraction of plasma (74.3%) is attributed to loss of chlorpromazine during the lengthy procedure.

The voltammogram for freeze-dried urine control containing 50 μg each of chlorpromazine, glutethimide, dextropropoxyphene, meprobamate, diazepam, and methaqualone-HCl exhibited a single oxidation wave which is attributed to chlorpromazine. Determination by a standard addition procedure gave 48.7 μg of chlorpromazine, indicating no measurable interference from the other drugs.

Conclusions

The feasibility of using thin-layer d.p.v. for the determination of electroactive drugs has been demonstrated with chlorpromazine. No sample pretreatment is necessary for urine over the chlorpromazine range 4.8×10^{-8}—2.4×10^{-4} M. This linear range extends well below the average urine level of 5.8×10^{-6} M found for patients receiving a therapeutic dose of 600 mg/day for 6 months [8]. The procedure is simple and rapid (ca. 2 min per determination) and requires only 23 μl of solution for filling the cell. Direct determination of chlorpromazine in plasma is also feasible over the linear range 2.4×10^{-5}—4.8×10^{-4} M. The average chlorpromazine blood level has been reported as 1.1×10^{-5} M [28] and 4.7×10^{-6} M [29] for patients receiving therapeutic doses of 400 mg and 200 mg (three times per day) respectively. Therefore, direct determination in blood is suitable for patients receiving more than 400 mg three times per day. The extraction procedure should be used for the lower concentrations of chlorpromazine in plasma.

We are grateful to P. T. Kissinger who suggested using the wax-impregnated graphite electrode and D. A. Roston who helped in constructing the thin-layer cell. This work was supported by the National Science Foundation. T. B. J. acknowledges support by a University of Cincinnati Summer Research Fellowship.

REFERENCES

1 J. Delay, P. Deniker and J. M. Harl, Ann. Med. Psychol., 110 (1952) 267.
2 P. N. Kaul, M. W. Conway and M. L. Clark, Nature, 226 (1970) 372.
3 P. N. Kaul, M. W. Conway, M. L. Clarck and J. Huffine, J. Pharm. Sci., 59 (1970) 1745.
4 J. B. Ragland, V. J. K. Wright and R. S. Ragland, Anal. Biochem., 12 (1965) 60.
5 S. H. Curry, Anal. Chem., 40 (1968) 1251.

6 S. H. Curry, Life Sci., 7 (1968) 9.
7 B. J. Gudziowicz, H. F. Martin and J. L. Driscoll, J. Gas Chromatogr., 2 (1964) 265.
8 Anon., Psychopharmacol. Bull., 6(1) (1970) 44.
9 C. L. Huang, Int. J. Neuropharmacol., 6 (1967) 1.
10 D. E. Johnson, J. D. Miller and H. P. Burchfield, Life Sci., 12 (1963) 959.
11 C. G. Hammer and B. Holmstedt, Anal. Biochem., 25 (1968) 532.
12 A. G. Bolt, I. S. Forrest and M. T. Serra, J. Pharm. Sci., 55 (1966) 1205.
13 A. G. Bolt, I. S. Forrest and M. T. Serra, J. Pharm. Sci., 56 (1967) 1208.
14 W. J. Turner, P. Turano and J. March, J. Clin. Chem., 16 (1970) 916.
15 E. Usdin, CRC Critical Reviews in Clin. Lab. Sci., 2 (1971) 347.
16 F. H. Merkle and C. A. Discher, Anal. Chem., 36 (1964) 1639.
17 A. G. Dumortier and G. J. Patriarche, Fresenius Z. Anal. Chem., 264 (1973) 153.
18 G. J. Patriarche and J. J. Lingane, Anal. Chim. Acta, 49 (1970) 25.
19 E. Jacobsen and M. W. Bjornsen, Anal. Chim. Acta, 96 (1978) 345.
20 D. G. Prue, F. Q. Gemmill, Jr. and R. N. Johnson, Anal. Chim. Acta, 107 (1979) 59.
21 A. G. Fogg and N. Fayad, Anal. Chim. Acta, 102 (1978) 205.
22 E. Jacobsen and B. Korvald, Anal. Chim. Acta, 99 (1978) 225.
23 J. C. Viré, G. J. Patriarche and J. P. Sépulchre, Anal. Lett., 11 (1978) 681.
24 M. A. Brooks, J. A. F. deSilva and L. M. D'Arconte, Anal. Chem., 45 (1973) 263.
25 H. A. Beckett, E. E. Essien and W. Franklin Smyth, J. Pharm. Pharmacol., 26 (1974) 399.
26 T. P. DeAngelis and W. R. Heineman, Anal. Chem., 48 (1976) 2262.
27 T. P. DeAngelis, R. E. Bond, E. E. Brooks and W. R. Heineman, Anal. Chem., 49 (1977) 1792.
28 D. H. Efron, S. R. Harris, A. A. Manian and L. E. Gaudette, Psychopharmacol., 19 (1971) 207.
29 L. C. Huang and A. A. Kurland, Arch. Gen. Psychiat., 5 (1961) 509.

Analytica Chimica Acta, 126 (1981) 65—70
Elsevier Scientific Publishing Company, Amsterdam — Printed in The Netherlands

CYCLIC VOLTAMMETRIC STUDY OF VANADIUM(V)/(IV) AS A REDOX CATALYST IN NON-AQUEOUS MEDIA

M. OTTO and G. WERNER*

Department of Chemistry, Analytical Centre, Karl-Marx-University, Liebigstrasse 18, 7010 Leipzig (German Democratic Republic)

(Received 30th December 1980)

SUMMARY

A basic study for possible kinetic-catalytic methods in non-aqueous solvents with vanadium as a redox catalyst is described. The redox behaviour of the V(V)/V(IV) couple is studied by cyclic voltammetry at a carbon electrode in acetonitrile. Vanadium oscillates between the two oxidation states without chemical side reactions, and is thus promising as a redox catalyst in non-aqueous media. The oxidizing power of the couple is increased with increasing *p*-toluenesulphonic acid concentrations and is decreased in the presence of solvents of increasing donor strength. The influence of common activators on the formal potential of the couple is discussed.

The most sensitive homogeneously catalyzed chemical reactions used for kinetic-catalytic determinations of trace metals are based on redox mechanisms [1—3]. In many examples, the catalyst acts as an electron mediator between the oxidizing and reducing agents. In its higher oxidation state the catalyst oxidizes the substrate (amines, phenols, azo dyes etc.) and is regenerated by oxidants such as peroxides and halates.

The redox behaviour of the catalyst is strongly influenced by its coordination sphere which can be affected by complexing agents as well as by the solvent. Kinetic-catalytic determinations are generally carried out in aqueous solutions. By change of the solvent, new features are to be expected with respect to the selectivity and sensitivity of homogeneously catalyzed reactions. An example of an analytically applicable homogeneously catalyzed reaction in non-aqueous media is the vanadium(V)/(IV)-catalyzed oxidation of *o*-dianisidine by organic peroxides such as *t*-butyl hydroperoxide or cumene hydroperoxide. This reaction proceeds in the presence of an organic acid in solvents such as acetonitrile or methylene chloride [4]. In order to characterize the redox behaviour of the catalyst in the presence of solvents of different donor ability in more detail, an electrochemical study of the vanadium(V)/(IV) couple became necessary.

Some voltammetric investigations of vanadium in non-aqueous solvents have been carried out. Michlmayr and Gutmann [5] studied the reduction of $VOCl_2$ polarographically in dimethylsulphoxide (DMSO) and dimethyl-

0003—2670/81/0000—0000/$02.50

formamide (DMF). The redox behaviour of bis(acetylacetonato)oxovanadium complexes in acetonitrile for oxidation states of vanadium less than (IV) was also described; polarography was used as well as voltammetry at a platinum electrode [6]. Electrochemical measurements of vanadium in mixed solvents have also been published [7]. Unfortunately, no data for the redox behaviour of the vanadium(V)/(IV) couple in non-aqueous media can be deduced from these studies. In order to gain detailed information, cyclic voltammetry was chosen for studying this redox system in acetonitrile as well as in the presence of other solvents with different donor abilities.

EXPERIMENTAL

The electrochemical studies were done at 22°C under an argon atmosphere by use of a conventional three-electrode compartment on a Beckman Electroscan 30. A carbon disc electrode (Radelkis, Budapest) or a glassy-carbon electrode (VEB Elektrokohle, Lichtenberg) served as working electrode. The saturated calomel reference electrode was separated from the measuring solution by a frit filled with agar gel. A platinum wire was the auxiliary electrode (Forschungsinstitut Meinsberg, G.D.R.). Because of the uncontrolled diffusion potential between the measuring solution and the aqueous SCE, all potentials were measured vs. the SCE and the ferrocene/ferricinium couple as a reference redox system [8]. The potentials could be reproduced to within 13 mV. Ferrocene was purified by sublimation.

Because no stoichiometric compound of a vanadium—acetonitrile solvate could be obtained [9], vanadium(IV) was used as $VOCl_2 \cdot 3DMSO$ which was prepared by the method of Gutmann and Laussegger [10], recrystallized in acetone—ethanol and stored in vacuum over phosphorus(V) oxide. The concentration of vanadium(IV) for the electrochemical measurements was adjusted to $1—5 \times 10^{-3}$ M from a 5×10^{-2} M stock solution in acetonitrile prepared daily from pure $VOCl_2 \cdot 3DMSO$. Acetonitrile was purified by fractional distillation [11]. The water content was checked by Karl Fischer titration. In view of the potential analytical applications of the redox system, the investigations were undertaken at a definite water content of 0.3% (v/v). Other solvents were reagent-grade or pure chemicals and were used without further purification.

All measurements were done in 0.1 M tetraethylammonium perchlorate (TEAP) which was prepared from tetraethylammonium hydroxide and perchloric acid and recrystallized from acetonitrile. The hydroxide was obtained from commercial tetraethylammonium halides by ion exchange on a strong anion exchanger (Wofatit-SBK, VEB Chemiekombinat Bitterfeld, G.D.R.). Anhydrous *p*-toluenesulphonic acid was prepared from the monohydrate by azeotropic distillation with benzene and vacuum-dried over phosphorus(V) oxide [12].

RESULTS

The electrochemical study of the vanadium(V)/(IV) couple in non-aqueous solvents is rendered more difficult by its relatively high redox potential (the thermodynamic value is given as 1.0 V [13]). Thus, solvents as DMSO, ethanol or hexamethylphosphoric acid triamide (HMPA) are ruled out because they are more easily oxidized than vanadium(IV). Acetonitrile was the most suitable solvent for these studies. Furthermore, the investigations had to be carried out with solid electrodes. Of those tested (Pt, Au, SnO_2 and C) only a carbon electrode could be used. A typical cyclic voltammogram of the quasi-reversible vanadium(V)/(IV) couple in acetonitrile in the presence of the internal reference redox system is shown in Fig. 1a. Compared to the single systems (Figs. 1b,c) both redox couples are somewhat affected by the presence of each other because of chemical side reactions of the electrochemically generated species and because reduction to vanadium(III) occurs at potentials lower than 0.4 V vs. SCE. For that reason the ferrocene/ferricinium reference system had to be measured separately. The formal potential $(E_a + E_c)/2$ of the vanadium couple ranged from 0.514 to 0.829 V vs. the reference redox system, depending on the *p*-toluenesulphonic acid concentration (Table 1).

In order to characterize the electrode processes in more detail, the dependences of the peak current (i_p) upon the square root of the scan rate (v) and on the vanadium concentration (C_o) [14] were studied for *p*-toluenesulphonic acid concentrations of 0.0, 0.01, 0.1 and 0.5 M. The equation relating these parameters is

$$i_p = k(n_\alpha \alpha)^{1/2} n A D^{1/2} C_o v^{1/2}$$

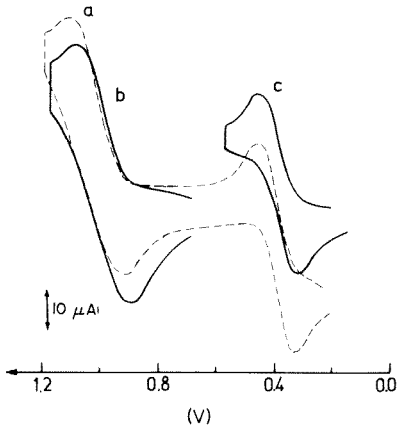

Fig. 1. Cyclic voltammograms of V(IV)/V(V) (a) in the presence of ferrocene and (b) alone; (c) ferrocene/ferricinium alone in acetonitrile vs. aqueous SCE (0.1 M TEAP, scan rate 20 mV s^{-1}, 0.1 M *p*-toluenesulphonic acid).

TABLE 1

Influence of *p*-toluenesulphonic acid (TS) on the vanadium(V)/(IV) redox potential in solutions of 0.1 M TEAP in acetonitrile (reference redox system: ferrocene/ferricinium)

[TS] (M)	$(E_a + E_c)/2$ (V)	ΔE_p^a (mV)
0.00	0.514	310
0.01	0.510	280
0.1	0.593	190
0.5[b]	0.738	150
1.0[b]	0.829	120

[a]Difference between anodic E_a and cathodic E_c peak potentials; scan rate 40 mV s^{-1}; 10^{-3} M V(IV) solution. [b]Without TEAP.

where k is the Randles-Sevčik constant, n is the number of transferred electrons, A is the electrode area (cm^2), D is the diffusion coefficient ($cm^2\ s^{-1}$) and α is the transfer coefficient. From the straight lines obtained it may be concluded that both the oxidation of vanadium(IV) and the reduction of vanadium(V) are diffusion-controlled processes. Because, also, the ratio of anodic to cathodic peak current was always unity, it is evident that no side reactions occur under the experimental conditions. This also followed from plots of $i_p v^{-1/2}$ vs. $v^{1/2}$ [14], varying the scan rate from 10 mV s^{-1} to 100 mV s^{-1}, which were all lines parallel to the abscissa.

The reversibility of the vanadium(IV)/(V) couple can be estimated from the differences in the anodic and cathodic potentials which correlate with the heterogeneous rate constant k_s [15]. As is seen in Table 1, the reversibility increases with increasing *p*-toluenesulphonic acid concentration. Attempts to determine k_s from the peak potentials by use of the supplementary ψ-function [14] as well as the electron transfer coefficient according to Nicholson and Shain [16] did not give reliable results for the following reasons. Firstly, the necessary determination of the diffusion coefficient by chronopotentiometry failed in the solvent studied, a difficulty already found by others [14] in solvents of low viscosity such as acetonitrile. Secondly, the reversibility of the system is too low to study the electrode processes over a wide range of scan rates, which complicates the evaluation of k_s and makes the determination of α nearly impossible. As mentioned above, the influence of solvents on the vanadium redox potential could not be studied by a complete change of the solvent because representative cyclic voltammograms were not obtained from the few applicable solvents. For that reason the solvent influence was investigated in acetonitrile as a reference system by adding small amounts of other solvents to the measuring solution. The change in the formal potential in the presence of methylene chloride, water, DMSO and HMPA is illustrated in Fig. 2. In the concentration ranges tested, the solvents did not affect the reversibility (ΔE_p values) or the magnitude of the anodic and cathodic currents.

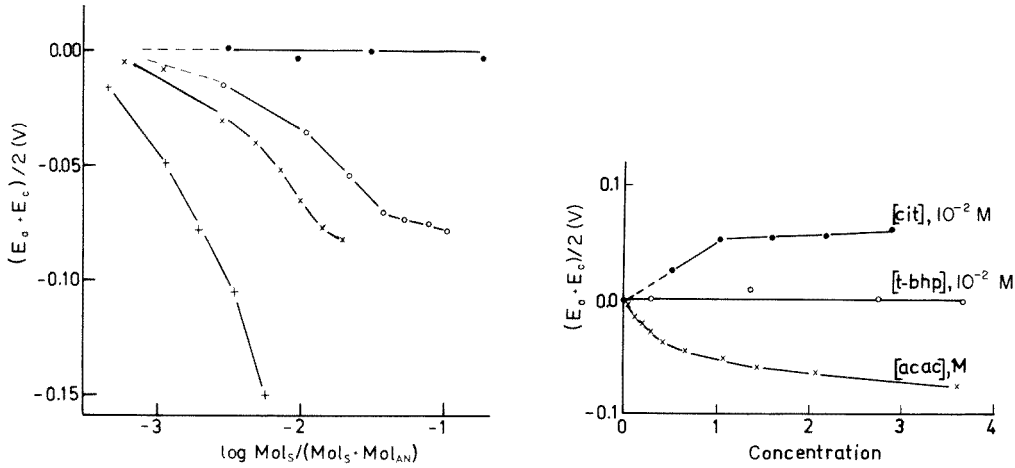

Fig. 2. Solvent influence on the V(V)/V(IV) redox potential in acetonitrile as reference solvent (0.1 M TEAP, 0.1 M *p*-toluenesulphonic acid, 2×10^{-3} M V(IV), 20 mV s^{-1}, reference redox system ferrocene/ferricinium). Solvents: (•) methylene chloride; (○) water; (×) DMSO; (+) HMPA.

Fig. 3. Influence of (•) citrate, (○) *t*-butyl hydroperoxide, (×) acetylacetonate on the formal potential of the V(V)/V(IV) couple in acetonitrile solution. Conditions as in Fig. 2.

In the same way the effect of some ligands of interest as activators in vanadium-catalyzed homogeneous redox reactions was tested. From the selected ligands only citrate and acetylacetone could be applied because other known activators such as 8-quinolinol and 1,10-phenanthroline are oxidized at $\geqslant$0.7 and $\geqslant$1.0 V vs. SCE, respectively. The influence of citrate and acetylacetone is shown in Fig. 3. Again, the ligands do not affect the reversibility of the system, but change the formal potential of the vanadium couple. An additional effect was observed in the presence of the oxidant in the catalytic reaction [4], *t*-butyl hydroperoxide, because the ratio of anodic to cathodic peak currents decreased with increasing peroxide concentration. The solution turned from green through yellow to red; this is caused by the reaction of vanadium(IV) with the peroxide to give the yellow vanadium(V) species and a red vanadium(V) peroxo complex [17].

DISCUSSION

The great catalytic activity of vanadium in homogeneously catalyzed reactions in aqueous solutions is related to its capability of changing between two oxidation states in a one-electron step, i.e. V(V) $\leftrightarrow$ V(IV) [1—3]. This behaviour seems to be a necessary basis for efficient redox catalysis even in non-aqueous solutions. From the cyclic voltammetric study it became evident

that vanadium changes between oxidation states (IV) and (V) without any side reactions. When the substrate and the oxidizing agent were replaced by suitable voltage sweeps, the vanadium oscillated between the two oxidation states as often as was wished. Thus the vanadium couple is very promising as a redox catalyst in non-aqueous solvents.

The shift in the formal potential (as a measure of the conditional redox potential of vanadium(V)/(IV)) with *p*-toluenesulphonic acid concentration shows an increase in the oxidizing power of the catalyst with increasing acid concentration. In a similar way the redox potential can be changed by suitable choice of solvent or mixed solvent. From Fig. 2 a general tendency can be deduced. The formal potential is decreased with increasing donor strength of the mixed solvents as is seen by comparison with Gutmann's donor numbers [18]: HMPA (38.8) > DMSO (29.8) > water (18.0) > acetonitrile (14.1) > methylene chloride (<2). The mixing of solvents affected the vanadium redox potential by the same order of magnitude as in the presence of organic ligands (Fig. 3) which have already been applied in kinetic-catalytic analysis as activators for the metal ion catalyst.

Interestingly, the effect of acetylacetone is to be classified between that of DMSO and water; this correlates with the estimate of the donor number of 20 for acetylacetone [19]. The effect of citric acid cannot be interpreted because no equilibrium data for vanadium complexes are available. From the fact that the redox potential of the vanadium(V)/(IV) couple is changed by solvents at similar concentrations as it is by ligands, it can be concluded that for activation of catalytic reactions, mixed solvents will have the same importance in non-aqueous systems as do organic ligands in aqueous solutions.

REFERENCES

1 P. R. Bontchev, Talanta, 19 (1972) 675.
2 H. A. Mottola, in B. H. Campbell (Ed.), C.R.C. Crit. Rev. Anal. Chem., Vol. 4, Cleveland, OH, 1975, p. 229.
3 H. Müller, M. Otto and G. Werner, Katalytische Methoden in der Spurenanalyse, Reihe: Moderne Spurenanalytik, Vol. 4, Akadem. Verl. Ges., Leipzig, 1980.
4 M. Otto and G. Werner, Abstracts Analytiktreffen, Neubrandenburg (G.D.R.), 1979.
5 M. Michlmayr and V. Gutmann, Inorg. Chim. Acta, 1 (1967) 471.
6 G. Gritzner, H. Murauer and V. Gutmann, J. Electroanal. Chem., 101 (1979) 177.
7 I. F. Abdullin, A. I. Kostromin and P. K. Agasyan, Zh. Anal. Khim., 33 (1978) 236.
8 H. M. Koepp, H. Wendt and H. Strehlow, Z. Elektrochem., 64 (1960) 483.
9 J. Cave, P. R. Dixon and K. R. Seddon, Inorg. Chim. Acta, 30 (1978) L349.
10 V. Gutmann and H. Laussegger, Mh. Chemie, 98 (1967) 439.
11 J. F. Coetzee, G. P. Cunningham, D. K. Guire and G. R. Padmanabhan, Anal. Chem., 34 (1962) 1139.
12 A. J. Libbey and J. T. Stock, Anal. Chem., 42 (1970) 526.
13 A. B. Hart and J. R. Partington, J. Chem. Soc., 66 (1944) 1563.
14 R. N. Adams, Electrochemistry at Solid Electrodes, M. Dekker, New York, 1969.
15 R. S. Nicholson, Anal. Chem., 37 (1965) 1351.
16 R. S. Nicholson and I. Shain, Anal. Chem., 36 (1964) 706.
17 M. Otto, J. Stach and R. Kirmse, Inorg. Chem., submitted for publication.
18 V. Gutmann, Coordination Chemistry in Nonaqueous Solutions, Springer-Verlag, Vienna, 1968.
19 M. Nishizawa and K. Saito, Bull. Chem. Soc. Jpn., 51 (1978) 483.

Analytica Chimica Acta, 126 (1981) 71—93
Elsevier Scientific Publishing Company, Amsterdam — Printed in The Netherlands

POLAROGRAPHIC REDUCTION OF ALDEHYDES AND KETONES
Part 19[a]. Hydration-Dehydration Equilibria and their Effect on Reduction of α,α,α-Trifluoroacetophenone

W. JAMES SCOTT[b] and PETR ZUMAN*

Department of Chemistry, Clarkson College of Technology, Potsdam, NY 13676 (U.S.A.)

(Received 29th September 1980)

SUMMARY

In acidic media, at pH <5, the carbonyl group of α,α,α-trifluoroacetophenone (I) is reduced in the protonated form to give alcohol and pinacol, whereas at pH >7 the first reduction step involves hydrogenolysis of the trifluoromethyl group of the unprotonated form of I to yield acetophenone, which can undergo further reduction at more negative potentials. Reduction of both the carbonyl group at lower pH and of the C—F bonds in the unprotonated form are accompanied by hydration-dehydration equilibria. At pH >7 these reactions involve addition of water and of hydroxide ions. The increase of current at pH >8 is due to a shift of the equilibria in favor of the geminal diol anion of I; the decrease at pH >10 is due to an increase in the rate of the addition of hydroxide ions with increasing pH. Spectrophotometric measurements at μ = 0.1 gave the following values for the acid dissociation constant of the geminal diol of I: $K_2 = 6.4 \times 10^{-11}$ in 2% ethanol and 5×10^{-12} in 40% ethanol. Formation of the hemiketal results in an increase of the absorbance of the free carbonyl form with increasing ethanol concentration. Formation of the hydrate and hemiketal of I in dimethylformamide is compared.

Analytically important 1,3-diketones bearing one or more trifluoromethyl groups adjacent to the carbonyl group are subject, in aqueous and water-containing solutions, to complex equilibria involving hydration-dehydration of carbonyl groups and to keto—enol and acid—base equilibria resulting in formation of both geminal diol anions and carbanion-enolates. The identification of species present at various pH values and in various solvents is too complex to be solved with a single model compound. Methodology for study of acid—base and keto—enol equilibria was developed using non-halogenated 1,3-diketones [1—3]. To study hydration-dehydration and acid—base equilibria involving the geminal diol group $-C(OH)_2CF_3$ by spectrophotometric and electrochemical methods, α,α,α-trifluoroacetophenone ($C_6H_5COCF_3$), referred to subsequently as trifluoroacetophenone or (I) was chosen as a model compound. Conjugation of the benzene and carbonyl groups shifts the reduction to more positive potentials, increases the intensity of the $n \rightarrow \pi^*$ band and shifts the $\pi \rightarrow \pi^*$ absorption band to longer wavelengths.

[a]Part 18. L. Deshler and P. Zuman, Anal. Chim. Acta, 73 (1974) 337.
[b]Present address: Technicon, Tarrytown, NY 10591, U.S.A.

0003—2670/81/0000—0000/$02.50

The literature contains little information on the electrochemical behavior of trifluoroacetophenone. Formation of radical anions between −40° and −50°C by controlled potential electrolysis in acetonitrile solutions containing tetraethylammonium perchlorate has been demonstrated [4] by e.s.r. measurements. Failure to obtain pinacols was attributed [5] to carbon—fluorine bond fission preceding the attack on the carbonyl group. Products and their yields from controlled potential electrolysis of I at a large mercury pool cathode and a single pH have been briefly described [6]. The choice of 1.5 M acetic acid containing 1 M lithium chloride in aqueous 80% ethanol as the reaction medium was based on experience with electroreductions of other acetophenones [7]. However, while acetic acid is a suitable medium for a study of pinacol formation, it is less suitable for study of carbon—fluorine bond fission, as proved in the present study. In the pH region used, two competing processes result in a mixture of products. At more positive potentials acetophenone formation predominates, whereas at more negative potentials the reduction proceeds further and yields pinacol. At both potentials during the initial stages of electrolysis, where less than 60% of I had been converted, formation of α-fluoroacetophenone was reported [6].

Electrolytic cleavage of a carbon—fluorine bond was first reported [8] in the reduction of phenacyl fluoride. Such reduction has been also assumed to occur in aliphatic compounds bearing fluorine adjacent to a carbonyl group or to a double bond of α,β-unsaturated ketones [9—12]. Reports [13, 14] of the reduction of C—F bonds in compounds bearing both a trifluoromethyl and a sulfamido group on a benzene ring have not been confirmed for reduction at the dropping mercury electrode, where reductive cleavage of the $-SO_2NH_2$ group has been proved [15]. Lund has, nevertheless, observed [16] a hydrogenolysis of the CF_3 group in these compounds when electrolysis was carried out on a preparative scale at a mercury pool cathode.

Comparison of half-wave potentials, wave-heights and their pH-dependence reported for trifluorothenoylacetone [17, 18] with those for 2-acetylthiophene and thenoylacetone seems to indicate that the CF_3 group undergoes electrolytic hydrogenolysis in the first reduction step rather than the reduction of the γ-carbonyl group assumed by the authors [17, 18]. The reduction is evidently complicated by hydration-dehydration in addition to keto—enol and acid—base equilibria. Results reported [18] for the controlled potential electrolysis at the limiting current of the first wave of trifluorothenoylacetone do not exclude the possibility of thenoylacetone formation.

The carbonyl group adjacent to the trifluoromethyl is hydrated in aqueous solutions. Reported values [19, 20] for the equilibrium constant $K_d = [C_6H_5COCF_3]/[C_6H_5C(OH)_2CF_3]$ are of the order of 10^{-2}, and the dissociation constant [21] of the geminal diol is $pK_2 = 10.0$. These values indicate that at pH <9 only about 1% of compound I is present in the unhydrated, free carbonyl form, with geminal diol predominating.

The present authors indicated [20] that electrochemical methods yield

values of K_d smaller by a factor of four than do optical methods. The mechanism of electroreduction of trifluoroacetophenone, the role of accompanying acid—base and hydration-dehydration equilibria, and conditions for evaluating equilibrium constants are dealt with in the present study.

EXPERIMENTAL

Apparatus

D.c. polarographic current—voltage curves were recorded by means of a Sargent Mark XVI polarograph. Current—voltage curves using a.c., pulse and derivative pulse techniques were obtained by means of a PAR Model 170 Polarographic Analyzer and recorder (Princeton Applied Research, Princeton, NJ). Linear voltage sweep and cyclic voltammograms were obtained by means of a voltage sweep source constructed for us by courtesy of R. N. Adams (University of Kansas, Lawrence) with scan rates from 0.25 to 2×10^3 V min^{-1}; a Tektronix type 564B storage oscilloscope equipped with type 3A9 and 2A63 differential amplifier units was used for recording. Current—voltage curves with rectangular voltage polarization were recorded with a commutator constructed according to the principle suggested by Kalousek [22] and built to the design proposed by Němec and Holub [23]. The auxiliary potential was held constant at a potential corresponding to the limiting current of the wave to be studied with a Bipolar Potentiostat Model 100A (MI Associates, Cambridge, MA), which was also employed for preparative controlled-potential electrolyses.

Aqueous solutions were placed in a 10-ml Kalousek cell, generally with a saturated calomel electrode (s.c.e.) as reference. On occasion, a mercury—mercury(I) sulfate (m.s.e.) reference was used. Temperature-controlled experiments were carried out in a water-jacketed vessel with the reference electrode separated by a sintered glass disc and an agar plug. Non-aqueous solutions were polarographed in a single compartment cell fitted with a silver—silver chloride reference employing 0.1 M lithium chloride as supporting electrolyte.

Preparative controlled-potential electrolysis at a dropping mercury electrode (d.m.e.) was carried out in small volumes (1—2 ml) of electrolyzed solution stirred by the falling mercury drop, in a cell designed by Manoušek [24], equipped with a separated saturated calomel reference electrode.

The pH values of the solutions were measured with a Sargent digital pH meter (model DR) and a Sargent combined glass electrode (type S-30072-15). For solutions containing 30 or 40% ethanol, the electrode was standardized with ethanol-containing buffers.

Electronic absorption spectra were recorded with a Pye-Unicam SP800A spectrophotometer (Cambridge, England) using a matched pair of 1-cm fused quartz cells, and a Cary 14 spectrophotometer using a matched pair of 10-cm cells. The temperature of the cells was kept constant by circulating water from a Haake FJ water-bath (Germany) at 25.00 ± 0.03°C. Water or alcohols

were added to non-aqueous solvents with a Manostat Digi-pet with a full load capacity of 1.0 ml.

The g.l.c. traces were recorded on a Varian Aerograph Model 1200 gas chromatograph equipped with a hydrogen flame ionization detector. The stationary phase employed was 3% SE-30 silicone gum rubber on Varaport 30, 100—120 mesh. The column was 5 feet long (1/8 in. i.d.).

Substances and solutions

α,α,α-Trifluoroacetophenone (Aldrich, 99% pure) was used as received; stock solutions, usually 0.01 M, were prepared by dissolving weighed amounts in absolute ethanol and were stored at 4°C in the dark for a maximum of a week. For measurements in non-aqueous solvents, the stock solution was prepared in the particular solvent. Reagent-grade acetophenone was distilled prior to use (b.p. 202.0°C).

Acetonitrile, benzene, carbon tetrachloride, chloroform and dimethylformamide (DMF) were Eastman spectral grade and were used as received. Baker reagent-grade dioxane was freed from peroxides by filtration through a column of activated alumina.

Chemicals for the preparation of buffers and other supporting electrolytes were of analytical-reagent grade. Preliminary experiments were carried out in five supporting electrolytes: 0.1 M sulfuric acid, acetate buffer pH 4.7, phosphate buffer pH 6.9, borate buffer pH 9.2, and 0.1 M sodium hydroxide. For more detailed investigations, Britton—Robinson universal buffer (pH 2—12) was employed. Values of pH below 2 and above 12 were obtained by the use of sulfuric acid and sodium hydroxide solutions, respectively. The effect of buffer concentration was examined in borate and in acetate buffers. Ammonium chloride and ethylammonium chloride buffers were obtained by titration of the pure base with hydrochloric acid.

Procedures

For polarographic experiments, the supporting electrolyte (9.9—9.5 ml) was deaerated for 5 min with a vigorous stream of nitrogen; the required amount of stock solution (0.1—0.5 ml) was then added and deaeration continued for a further 30 s prior to the recording of the *i—E* curves. Single sweep and cyclic voltammograms were measured at the end of the drop life. Deaeration of non-aqueous solvents required 10—15 min.

Preparative controlled-potential electrolysis was carried out in a 2-ml sample of 1×10^{-3} M solution. Long periods of time (40—60 h) were required for the electrolyses as the current was kinetically controlled. At the end of the electrolysis, aliquots of the electrolyzed solution were examined by u.v. spectrophotometry and gas chromatography. Fluoride was determined by the lanthanum—alizarin fluorine blue method [25] at 620 nm.

For spectrophotometric measurements, aqueous solutions of the required concentration were prepared by addition of ethanolic stock solution to individual buffers. Measurements were made against blanks containing the

same concentrations of ethanol. Non-aqueous solutions were prepared in spectral-grade solvents from stock solutions in the same medium. When mixed solvents were used, the second solvent was added directly to the cells. Spectra were recorded within 2 min of preparation of the solution. Any spectral time-dependence was checked at 10-min intervals.

To exclude the role of ketal formation when ethanol was used as solvent for the stock solution, spectra in various buffers were compared when an ethanolic stock solution of trifluoroacetophenone was added to the buffer (resulting in a 2.5% ethanol content) and when the neat compound was added. No differences in the spectra were found and no changes with time were observed when the pH was lower than about 12 (at 25°C).

In sodium hydroxide solutions at 25°C, measurable irreversible changes were observed during the first two hours. Absorption increased in the 230—250-nm region and a new absorption band was formed at 275 nm. In more dilute (1×10^{-4}—3×10^{-4} M) sodium hydroxide solutions these changes were proved to be affected by the presence of oxygen. All spectra in alkaline media were therefore investigated with the use of stoppered cells after de-aeration of solutions by a stream of nitrogen.

RESULTS

Electrochemical studies

Aqueous solutions. Current—voltage curves for aqueous solutions of α,α,α-trifluoroacetophenone (I) containing 2.5% ethanol or less were recorded by means of d.c., a.c. and pulse polarography, linear sweep voltammetry and rectangular voltage polarization (Kalousek commutator). Two processes are involved in the reduction of I at the dropping mercury electrode over the pH range 0—14. The process observed in acidic media results in the formation of a wave i_{HA}, that at pH >7 is characterized by a wave i_A. The latter is accompanied at more negative potentials by the acetophenone reduction wave i_p.

The height of wave i_{HA} between pH 0 and 4 remains practically constant with all techniques used (Figs. 1, 2, Table 1) and decreases with increasing pH in the shape of a dissociation curve with inflexion point at pK' about 5.5. In the region of decrease, wave i_{HA} is not well separated from wave i_A, unless the concentration of I is below 3×10^{-4} M in media which contain less than 2.5% ethanol. Characteristic potentials of waves ($E_{1/2}$), summits (E_s) or peaks (E_p) are shifted with increasing pH to more negative values by about 50 mV/pH (Fig. 3).

The height of wave i_A that replaces wave i_{HA} reaches a limiting value at pH about 6 and remains pH-independent up to pH about 7 (Figs. 1, 2). With further increase in pH, the height of this wave increases to a maximum value and then shows a decrease in the shape of part of a dissociation curve with a pK' value of about 11 (Fig. 4). The shape of the increase at pH >7 depends on the technique used (Figs. 1, 2), the greatest differences being for cyclic voltammetry at high scanning rate (Fig. 2). For a.c. polarograms, the half-

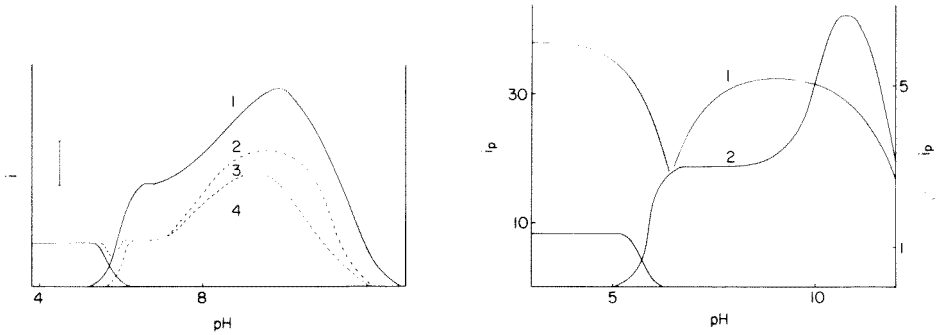

Fig. 1. Dependence of currents of α,α,α-trifluoroacetophenone on pH in Britton—Robinson buffers for (1) d.c. polarography (1×10^{-3} M ketone, 5% ethanol); (2) a.c. polarography (2.5×10^{-3} M, 2.5% ethanol); (3) pulse polarography (2.5×10^{-4} M, 2.5% ethanol); (4) derivative pulse polarography (2.5×10^{-4} M, 2.5% ethanol). Current scale (on the left): (1) 0.20 μA; (2) 0.22 μA; (3), (4) 0.15 μA.

Fig. 2. Dependence of currents for 4×10^{-3} M α,α,α-trifluoroacetophenone on pH obtained by linear sweep voltammetry in Britton—Robinson buffers containing 2% ethanol. Scanning rates: (1) left current scale 33 V s^{-1}; (2) right hand scale 0.066 V s^{-1}.

width of peak i_A increases at pH >5, reaches a limiting value at pH 6.5 and remains constant up to pH 7.5.

The growth of wave i_A at pH >8 is accompanied by an increase of an acetophenone wave i_p observed at more negative potentials. The characteristic potentials of this wave were found to be practically identical with those of an authentic sample of acetophenone. The ratio $i_A : i_p$ is independent of pH up to pH 10. In linear sweep voltammetry, peak i_p appeared only at scanning rates higher than about 20 V s^{-1}.

The change in the measured current signals with pH is accompanied by a variation in the character of the current. The d.c. polarographic curves of trifluoroacetophenone are kinetically controlled over the entire pH range, i.e. their height is governed by the rate of a chemical reaction. This is shown by the independence of the limiting current of both waves i_{HA} and i_A on the height of the mercury reservoir, by the large (ca. 10% deg^{-1}) temperature coefficient and by the fact that observed currents were less than 10% of the corresponding theoretical diffusion current. The latter deduction was based on a comparison of the wave-height of trifluoroacetophenone with that of an equimolar solution of acetophenone obtained under identical conditions.

With rapid voltage scanning techniques the current is limited by the rate of chemical reaction only when the scanning rate is slower than about 20 V s^{-1}. Under such conditions the current i_{HA} or i_A is independent of the scanning rate (Fig. 5). At scanning rates above about 20 V s^{-1}, the current is diffusion-controlled, as is shown by the linear dependence on the square root of the scanning rate (Fig. 5). These results resemble those reported for formaldehyde [26], pyridine carboxaldehydes [27, 28], and glyoxalic acid

[29]. Further, only at scanning rates above 20 V s^{-1} are the i—E curves peak shaped, as observed for diffusion currents, whereas at lower scanning rates steps are formed. The dependence of the current (Fig. 5) and the shape of the i—E curves follow a similar pattern even at pH 12, where the peak i_A is less than 10% of the peak current at pH 10 (Fig. 4). The current at scanning rates above 20 V s^{-1} is thus diffusion-controlled, but even then shows decrease with increasing pH. This indicates that the decrease of current i_A with increasing pH at pH >10 is due to a shift in the position of an acid—base equilibrium rather than to a change in the rate of generation of the acid form. The shape of the i—E curve for the more negative reduction of acetophenone (i_p) was more a wave than a peak even at 30 V s^{-1}, indicating that the current i_p is governed by the rate of a chemical reaction transforming the electroinactive product of the electrode reaction i_A to acetophenone, the reduction of which produces current i_p.

The increase of current i_A at pH >8 in d.c. polarography is independent of buffer concentration, buffer composition, presence of boric acid and ionic strength varied by addition of sodium chloride. The chemical reaction governing this increase thus does not involve participation of bases other than hydroxide.

Temperature coefficients of waves i_{HA} and i_A between 25 and 45°C are large and vary between 7.2 and 14.5% deg^{-1}. Between 45 and 55°C the temperature coefficient of wave i_{HA} at pH 4.1 remains high (10% deg^{-1}), resulting in a doubling of the wave height over a 10°C interval, whereas the temperature coefficients of wave i_A at pH 6.8 and 9.3 decrease (2.5 and 2.9% deg^{-1}, respectively) and tend towards the theoretical value for diffusion currents (1.8% deg^{-1}). This indicates that with increasing temperature the rate of the chemical reaction increases so much that it becomes comparable with the rate of transport by diffusion.

No changes of wave-heights of trifluoroacetophenone with time were observed over the first hour at 25°C up to pH 12. When alkaline solutions were acidified, the same wave was obtained as for solutions prepared by direct addition of trifluoroacetophenone to the corresponding acidic media. The decrease in wave-height at pH 10—12 at 25°C is thus not caused by cleavage of the trifluoroacetophenone.

The absence of anodic peaks in cyclic voltammetry even at 50 V s^{-1} indicates the irreversibility of the process. Logarithmic analysis gave linear log $i/(i_d - i)$ vs. E plots with the following values for trifluoroacetophenone (values for acetophenone in brackets): at pH 4, αn_a = 1.93 (0.44); at pH 8, αn_a = 0.78 (0.58); and at pH 10, αn_a = 0.48 (0.72). Results with rectangular voltage polarization, where the auxiliary voltage in the Kalousek commutator [22, 23] was adjusted to correspond to the limiting currents of waves i_{HA} or i_A, showed no anodic wave over the whole pH range, confirming the irreversibility of the reduction process.

Ethanolic solutions. The limiting current of wave i_{HA} in 0.1 M hydrochloric acid and in acetate buffer pH 4.7 decreases markedly with increasing

TABLE 1

Comparison of characteristic potentials (V vs. s.c.e.) and currents obtained by various electrochemical techniques for currents i_{HA} and i_A of the reduction of α,α,α-trifluoroacetophenone and i_p for the reduction of electrogenerated acetophenone at 25°C

D.c. polarography[a]							A.c. polarography[b]						
pH	$-E_{1/2}$			i (μA)			pH	$-E_s$			i (μA)		
	HA	A	P	HA	A	P		HA	A	P	HA	A	P
2.3[f]	0.72			0.26			4.1[g]	0.76			0.15		
3.1[f]	0.74			0.24			4.6[g]	0.78			0.22		
4.0[f]	0.79			0.23			5.4[g]	0.82			0.24		
5.1[f]	0.85	1.0		0.21	0.06		5.7[h]	0.89			0.10		
6.3[f]		0.94			0.50		5.8_5^h		0.95			0.10	
7.1[f]		1.01			0.60		6.6[h]		0.99			0.17	
7.6[f]		1.05	1.50		0.70	0.05	6.9[h]		1.02	1.51		0.15	0.02
8.1[f]		1.06	1.52		0.77	0.07	7.6_5^h		1.05	1.53		0.25	0.05
8.5[f]		1.04	1.50		0.87	0.10	10.1[f]		1.11	1.59		0.35	0.16
8.9[f]		1.05	1.50		0.91	0.12	10.8[f]		1.11	1.62		0.26	0.14
9.3[f]		1.06	1.52		1.07	0.12	11.2[f]		1.14	1.63		0.10	0.08
9.8[f]		1.08	1.55		1.27	0.10	11.8[f]		1.16	1.65		0.03	0.03
10.2[f]		1.08	1.55		1.08	0.12							
10.6[f]		1.09	1.55		0.94	0.13							
11.1[f]		1.11	1.57		0.73	0.16							
11.6[f]		1.10	1.58		0.42	0.10							

[a]5% ethanol, 1×10^{-3} M compound I. [b]2.5% ethanol, 2.5×10^{-3} M compound I; 100 Hz, 10 mV peak-to-peak amplitude. [c]Derivative pulse polarography, scan to −1.6 V, 2.5% ethanol, 2.5×10^{-4} M compound I. [d]2% ethanol, 4×10^{-3} M compound I, 33 V s^{-1}. [e]Ratio of peak currents i_{HA} and i_A at 33 V s^{-1} and 0.066 V s^{-1}. [f]Britton—Robinson buffer. [g]Acetate buffer. [h]Phosphate buffer. [j]Small.

ethanol concentration up to about 30% ethanol and shows a slight increase at higher concentrations (Fig. 6).

In Britton—Robinson buffers containing 30% ethanol, the pH dependence of the limiting current had a shape similar to that observed in the presence of 2.5% ethanol (Fig. 7), but the current i_{HA} (and wave i_A at pH 6—8) is about half that for 2.5% ethanolic solutions. Separation of waves i_{HA} and i_A at pH 5—7 in the presence of 30% ethanol was poor and the presence of two waves could be proved only by logarithmic analysis. The relative increase of wave i_A at pH >8 is more pronounced in the presence of 30% ethanol (Fig. 7) and the maximum value reaches about 10% of the theoretical diffusion current. The more negative acetophenone wave i_p shows a dip resulting from a decrease in the limiting current with increasingly negative potentials, and its height increases with increasing ethanol concentration at pH >10.

Non-aqueous media. Trifluoroacetophenone is reduced in dimethylsulfoxide (DMSO) at −0.83 V, in dimethylformamide (DMF) at −0.78 V and in acetonitrile at −1.07 V (all vs. Ag/AgCl) in freshly prepared solutions. With

Derivative pulse[c]					Cyclic voltammetry[d]							Ratio
pH	$-E_s$		i_p (μA)		pH	$-Ep$			i_p (μA)			$i_{33}/i_{0.066}$[e]
	HA	A	HA	A		HA	A	P	HA	A	P	
4.1[g]	0.74	0.96	3.5	1.7_5	2.0[f]	0.84			6.5			8.0
4.6[g]	0.76	0.98	3.8_5	2.1	4.0[f]	0.96			6.2			7.8
5.1[g]	0.77	0.99	3.0	2.7	4.9_5[f]	1.02			5.5			8.5
5.5[g]	0.80	—	3.3	—	6.0[f]	0.82	1.14		5.5			7.6
6.1[h]	0.85	1.07	4.4	j	6.8_5[f]	0.84	1.22		5.0			7.6
6.6[h]	0.94		9.9		8.0[f]		1.24	1.72	4.5		4.5	8.3
7.4[h]	0.97		10.4		10.0[f]		1.24	1.74	5.0		5.0	5.4
7.7[f]	0.98		10.1		11.1[f]		1.24	1.76	4.3		4.0	3.2
9.8[f]	1.09		9.5		11.5[f]		1.24	1.72	3.2		3.5	—
10.3[f]	1.09		8.2									
11.2[f]	1.11		6.0									
11.5[f]	1.14		3.0									

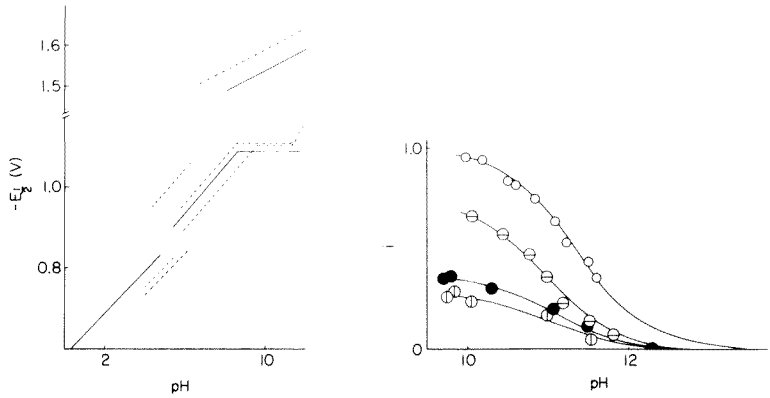

Fig. 3. Dependence of characteristic potentials (vs. s.c.e.) on pH (conditions as in Fig. 1): (—) $E_{1/2}$, d.c. polarography; (—·—) E_s, a.c. polarography; (-----) E_s derivative pulse polarography.

Fig. 4. Dependence on relative currents of α,α,α-trifluoroacetophenone on pH in alkaline solutions. Experimental conditions as in Fig. 1. (○) D.c. polarography; (⊖) pulse polarography; (●) a.c. polarography; (⊕) derivative pulse polarography.

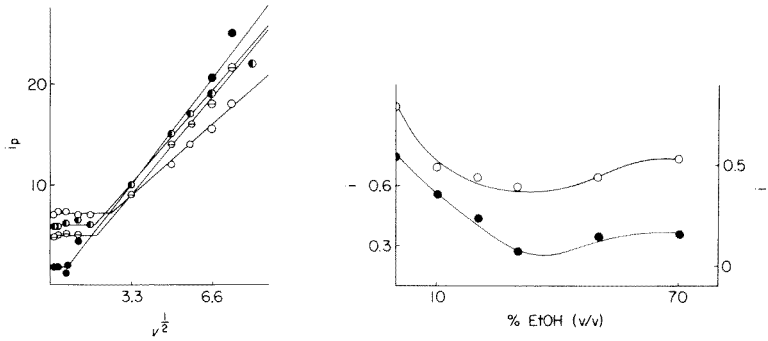

Fig. 5. Dependence of peak current (in μA) of α,α,α-trifluoroacetophenone on the square root of scanning rate (in V s^{-1}). Britton—Robinson buffers; (•) pH 4.0; (⊖) pH 8.1; (◐) pH 9.8; (○) 0.01 M sodium hydroxide.

Fig. 6. D.c. polarographic currents (in μA) of 2×10^{-3} M α,α,α-trifluoroacetophenone as a function of ethanol concentrations (% v/v). (○) Acetate buffer pH 4.8, right-hand current scale; (•) 0.1 M hydrochloric acid, left-hand current scale.

time the wave decreases and is replaced by another wave in the potential region where acetophenone is reduced (−1.4 to −1.5 V).

As the total height of the original wave is similar to the final wave-height and practically equal to the height of a wave in an equimolar acetophenone solution, it can be assumed that the process corresponds to a one-electron reduction [30]. As the wave-height and potential are little affected by addition of an acid (sulfuric) or base (tributylamine), it is possible to assume that the trifluoromethyl group rather than the carbonyl group is involved in this reduction process.

The height of the wave in DMF solution decreases in the presence of water (Fig. 8). Dependence of the wave-height on the logarithm of the water concentration has the shape of a dissociation curve with an inflexion point at about 0.1 M water.

Anodic waves. An anodic, diffusion-controlled wave i_a is observed at pH >8. The height of the wave at pH <10 is about a fifth of the reduction wave i_A. The height increases somewhat at pH >9, reaches a maximum value at pH 10.5, but shows no marked decrease at pH >10 where wave i_A decreases. The height of the wave is a linear function of concentration. Its half-wave potential shows a linear shift to more negative values by about 60 mV/pH.

Controlled-potential electrolysis. Experiments in controlled-potential electrolysis with the d.m.e. were complicated by the fact that kinetic currents of trifluoroacetophenone are less than 10% of the theoretical diffusion currents. In order to make 4×10^{-3} M solutions, 10% ethanol had to be used. To obtain at least 50% conversion, it was necessary to carry out electrolysis for 40—60 h. Electrolysis at pH 3 resulted in a decrease of wave i_{HA}. Samples of the electrolyzed solution transferred to a buffer at pH 8 did not exhibit

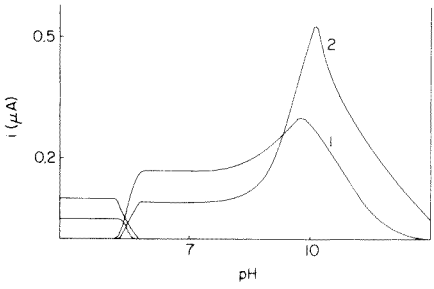

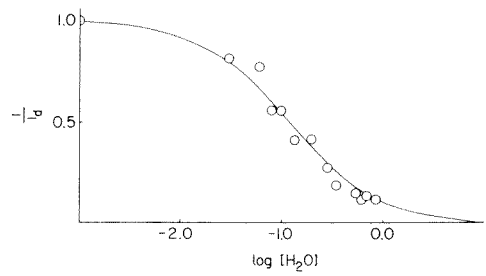

Fig. 7. Dependence of d.c. polarographic limiting currents of 2.5×10^{-4} M α,α,α-trifluoroacetophenone on pH in Britton—Robinson buffers, containing: (1) 2.5%, (2) 30% (v/v) ethanol.

Fig. 8. D.c. polarographic currents of 1×10^{-3} M α,α,α-trifluoroacetophenone in DMF containing 0.1 M sodium perchlorate as a function of logarithm of water concentration; experimental points are shown with the theoretical dissociation curve for a monobasic acid.

acetophenone waves. The absence of acetophenone in the electrolysis product was proved by spectrophotometry and gas chromatography. Less than 4% of the theoretical fluoride concentration was found in this product, probably resulting from hydrolysis.

In contrast, electrolysis at pH 11 at —1.30 V corresponding to the limiting current of wave i_A resulted in an increase in the more negative acetophenone wave i_p (Fig. 9). Absorption spectra showed acetophenone bands ($n \rightarrow \pi^*$ at 210 nm, broad benzenoid at 230—255 nm, $n \rightarrow \pi^*$ at 280 nm) indicating practically 100% yield. Similarly, electrolysis at the limiting current of wave i_A at pH 9.8 produced fluoride ions quantitatively.

Spectrophotometric studies

Aqueous solutions. In solutions containing 0.5—2.5% ethanol over the pH range 1—9, trifluoroacetophenone shows a strong $\pi \rightarrow \pi^*$ absorption band at 205 nm, a medium-intensity benzenoid band between 240 and 275 nm and a weak band corresponding to $n \rightarrow \pi^*$ transition at 290 nm (Table 2). At pH >9 the band at 290 nm increases and simultaneously the benzenoid band at 270 nm decreases. Measurement at 290 nm gave a value of $pK_2 = 10.2$ at $\mu = 0.1$; this is in good agreement with the reported value of 10.0 [21]. Addition of sodium chloride solutions up to 0.5 M has practically no effect on spectra at pH 4.7, 6.8, or 9.2.

For comparison, spectra of acetophenone were recorded: the strong $\pi \rightarrow \pi^*$ absorption appears at about 200 nm, the benzenoid absorption, showing little fine structure, gives a broad band between 220 and 270 nm, and a weak $n \rightarrow \pi^*$ band is observed at 278 nm (Table 2).

Ethanol—water mixtures. The absorption spectra in water—ethanol mixtures show the same pattern and maxima as those in aqueous 0.5% ethanol. Only the ratios of the absorbances at some of the fine structure peaks in the

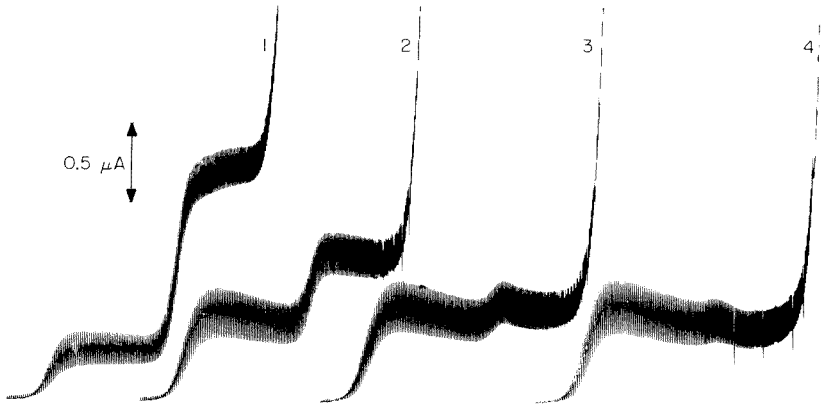

Fig. 9. Controlled-potential electrolysis: 1.2 ml of 4×10^{-3} M α,α,α-trifluoroacetophenone in Britton—Robinson buffer pH 11 electrolyzed at −1.30 V. D.c. polarographic curves recorded after (1) 36 h; (2) 11 h; (3) 3 h; (4) start of electrolysis.

250—270-nm region differ somewhat in absolute ethanol from those in aqueous solutions. With increasing ethanol concentration, the absorbances at 260 nm and 290 nm remain practically unchanged up to about 20% ethanol ($\log[C_2H_5OH] \approx 0.55$ M) and then increase, the plot (Fig. 10) resembling part of a dissociation curve. Dilution with water restores the original absorbance; the spectra are time-independent.

In 3×10^{-3} M solutions of trifluoroacetophenone containing 40% ethanol, the spectra are unchanged up to pH 10. With further increase in pH the benzenoid absorption at 250—270 nm decreases, the band at 290 nm increases (reaching $\epsilon = 1 \times 10^2$ l mol^{-1} cm^{-1}) at pH >12 and a new band at 235 nm ($\epsilon \approx 10^3$ l mol^{-1} cm^{-1}) is formed. The increase of absorbance at 290 nm and 235 nm with increasing pH follows the shape of a dissociation curve of a monobasic acid, with a pK value of 11.6 in borate buffers and 11.24 in dilute sodium hydroxide solutions. In solutions of pH >12.5 hydrolysis occurs, resulting in an increase of a band at 277 nm and strong increase of absorbance at 235 nm with an isosbestic point at 240 nm.

Mixtures of ethanol with organic solvents. Addition of 2% ethanol to hexane (Fig. 11) results in a decrease of the bands at 252 and 286 nm observed in pure hexane, and in the appearance of bands with fine structure in the 240—270 nm range, characteristic of unconjugated benzene rings. At low ethanol concentrations (0—3%) it takes several hours for the equilibrium to become established. A gradual decrease of the bands at 252 and 286 nm was also observed with increasing methanol concentration. The rate of decrease is faster than in the presence of ethanol and increases in the presence of tributylamine or toluenesulfonic acid.

Similarly, the absorbance at 300 nm (with cut-off at lower wavelengths) decreases after addition of 2% ethanol to solutions of trifluoroacetophenone in dioxane, chloroform, carbon tetrachloride and benzene.

TABLE 2

Absorption properties of α,α,α-trifluoroacetophenone and acetophenone
(λ_{max} is given in nm, and ϵ as l mol^{-1} cm^{-1})

Solvent	α,α,α-Trifluoroacetophenone						Acetophenone					
	π → π*		Benzenoid		n → π*		π → π*		Benzenoid		n → π*	
	λ_{max}	ϵ	λ_{max}	ϵ	λ_{max}	ϵ	λ_{max}	ϵ	λ_{max}	ϵ	λ_{max}	ϵ
99.5% H_2O— 0.5% C_2H_5OH	205	1×10^4	250	3.5×10^3	290	10	200	2×10^4	242	6.1×10^3	278	1.1×10^3
			256	4.5×10^3					and several other bands			
			260	5×10^3								
			266	4×10^3								
50% H_2O— 50% C_2H_5OH			250	6×10^3	290	30						
			256	7.5×10^3								
			260	8×10^3								
			266	6×10^3								
4% H_2O— 96% C_2H_5OH			250	6.5×10^3	290	40						
			256	7.5×10^3								
			260	8×10^3								
CH_3CN	<225[c]	>2×10^4	255	1.4×10^4	290	2×10^3	c	c	244	1.2×10^4	278	1.0×10^3
$HCON(CH_3)_2$	c	c	<260[c]	>5×10^3	290	1×10^3	c	c	c	c	279	1.0×10^3
$(CH_3)_2SO$	c	c	<260[c]	>1×10^4	290	4×10^3						
$CH_3(CH_2)_4CH_3$	<205[c]	>1.2×10^4	252	1.3×10^4	286	1.8×10^3						
C_6H_6	c	c	c	c	290	1.7×10^3						
Dioxan	c	c	c	c	290	1.6×10^3						
$CHCl_3$	c	c	257	1.3×10^4	290	1.7×10^3						
CCl_4			<260[c]	7.1×10^4	290	1.5×10^3						

[c]Cut off.

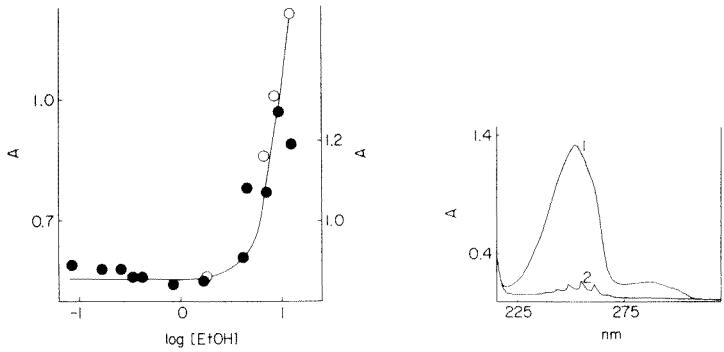

Fig. 10. Absorbance of α,α,α-trifluoroacetophenone as a function of the logarithm of ethanol concentration: (•) 1.86×10^{-3} M ketone, absorbance at 260 nm, right-hand scale; (○) 2×10^{-2} M ketone, absorbance at 290 nm, left-hand scale.

Fig. 11. Absorption spectra of 1×10^{-4} M α,α,α-trifluoroacetophenone in (1) hexane; (2) hexane containing 2% ethanol (v/v).

When acetonitrile is used, the absorption bands at 260 nm and at 290 nm decrease in the presence of ethanol over a period of several hours or within 5 min when heated to 70°C. Fine structure of benzenoid bands appears when the ethanol concentration exceeds 50%. The rate of the decrease increases with increasing ethanol concentration.

When spectra were recorded in dimethylformamide solutions immediately after mixing with ethanol, the band at 290 nm decreased with increasing ethanol concentration. The dependence of the absorbance on the logarithm of the ethanol concentration has the shape of a dissociation curve with an inflexion point at $[C_2H_5OH] = 0.025$ M. Measurements in dimethylformamide solutions were complicated by the fact that the absorption spectrum of trifluoroacetophenone in the pure solvent changed slowly with time. In dimethylsulfoxide this decrease was so fast that it prevented any study of the role of ethanol.

Non-aqueous media. The $\pi \rightarrow \pi^*$ absorption band occurs for most of the solvents used in the spectral region where the solvent is not transparent, but the benzenoid band at 250—260 nm was observed in most of the solvents and its molar absorptivity varied around 1.3×10^4 l mol^{-1} cm^{-1}. Similarly the $n \rightarrow \pi^*$ absorption band of the carbonyl group showed small variations around 1.7×10^3 l mol^{-1} cm^{-1} (Table 2).

Strong acids or bases, or ethyl orthoformate [31], do not affect the u.v. spectra. Whereas spectra in acetonitrile show little variation with time, the band at 300 nm increases with time in dimethylformamide and even more rapidly in dimethylsulfoxide.

Mixtures of organic solvents with water. Addition of water to a solution of trifluoroacetophenone in acetonitrile results in an immediate decrease in absorbance both at 260 and 290 nm, followed by a slow increase. For

example, the molar absorptivity at 256 nm in acetonitrile (1.4×10^4 l mol^{-1} cm^{-1}) decreases immediately after addition of 2% water to 2.1×10^3, but then increases over a period of 24 h to an equilibrium value of 6.6×10^3 l mol^{-1} cm^{-1}. The increase in the absorbance at 256 nm is accompanied by an increase of the band at 290 nm.

When the absorption spectra of freshly prepared solutions were recorded, the plot of absorbance at 256 and 285 nm as a function of the logarithm of concentration of water has the shape of a dissociation curve with inflexion point at about 0.8 M water (Fig. 12).

A similar change in spectra was observed in freshly prepared dimethylformamide solutions. The absorbance vs. log[H_2O] plot has the shape of a dissociation curve with inflexion point at about 1.0 M water.

DISCUSSION

Electrode processes

Determination of the number of electrons transferred in the reduction of α,α,α-trifluoroacetophenone and identification of the product formed was complicated by the kinetic nature of waves i_{HA} and i_A over the whole pH range and by the slow cleavage of the trifluoroacetophenone. This kinetic character made it impossible to compare wave-heights with waves of known model substances, and caused the limiting current to be, at most, less than 10% of the theoretical diffusion current. Nevertheless, wave i_{HA} was always considerably smaller than i_A, while wave i_A was larger (3 times larger under optimum conditions) than the two-electron acetophenone wave i_p. Furthermore, whereas the presence of the acetophenone wave indicated that acetophenone is formed in the reduction wave i_A, its absence at lower pH values showed that acetophenone is not formed in wave i_{HA}. Finally, controlled-potential electrolysis gave no proof of acetophenone and fluoride ion formation when carried out at a potential corresponding to the limiting current of wave i_{HA}, but gave positive proof of both in the case of electrolysis at the potential corresponding to the limiting current of wave i_A.

Hence at pH <6, trifluoroacetophenone in the unhydrated form is reduced

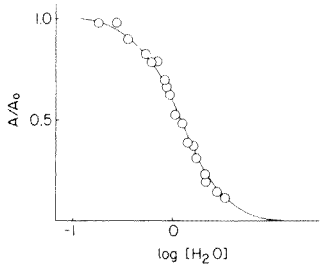

Fig. 12. Relative absorbance of 1×10^{-4} M α,α,α-trifluoroacetophenone at 256 nm in acetonitrile as a function of the logarithm of water concentration; experimental points are shown with the theoretical dissociation curve of a dibasic acid.

in a two-electron step to the alcohol, whereas at pH >7 the reduction takes place in a six-electron step and acetophenone is formed. This system represents another example [32] of compounds (like *p*-cyanoacetophenone [33], *p*-diacetylbenzene [34] and 4,4′-diacetyldiphenylmethane [35]) which are reduced by different mechanisms and give different products according to the media (especially pH) used.

The mixture of products obtained in the controlled-potential electrolysis at a mercury pool electrode [6], where the control of pH at the electrode surface is more difficult to achieve than at the d.m.e., probably resulted from competitive processes.

Identification of electrolysis products, presence of the acetophenone wave at pH >7 and the pH-dependence of currents and potentials in all the electrochemical techniques employed make it possible to deduce the following overall reduction scheme

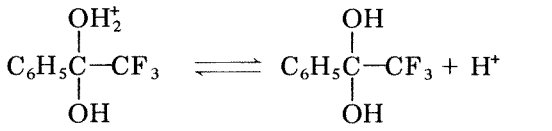

(1)

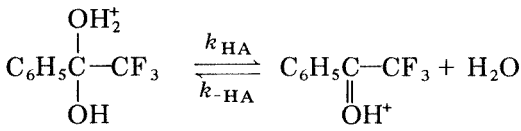

(2)

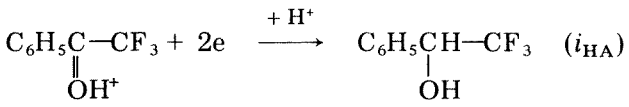

(3)

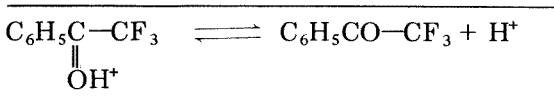

(4)

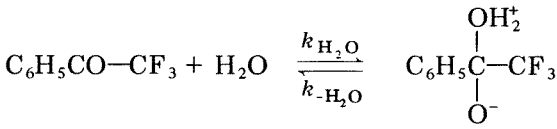

(5)

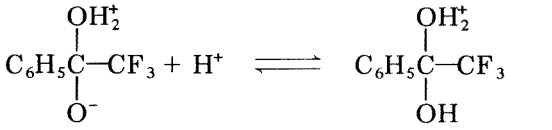

(6)

followed by (1)

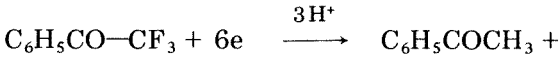

(7)

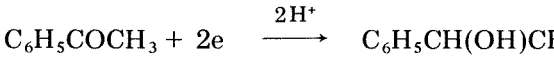

(8)

$$C_6H_5COCF_3 + OH^- \underset{k_{-1}}{\overset{k_1}{\rightleftharpoons}} C_6H_5\underset{\displaystyle O^-}{\overset{\displaystyle OH}{\underset{|}{\overset{|}{C}}}}-CF_3 \quad (K_1) \tag{9}$$

$$C_6H_5\underset{\displaystyle OH}{\overset{\displaystyle OH}{\underset{|}{\overset{|}{C}}}}-CF_3 \underset{k_{-2}}{\overset{k_2}{\rightleftharpoons}} C_6H_5\underset{\displaystyle O^-}{\overset{\displaystyle OH}{\underset{|}{\overset{|}{C}}}}-CF_3 + H^+ \quad (K_2) \tag{10}$$

The height of wave i_{HA} in acidic media is governed by the rate of dehydration in reaction sequence (1)—(3). The pH-independence of i_{HA} indicates that the hydration involves reaction with water in step (2) rather than with hydroxonium ions. The decrease of the wave-height at pH >5, observed even with rapid scanning when the current at pH <4 was diffusion-controlled, indicates that the protonation reaction involves the free carbonyl compound, as in step (4), rather than the geminal diol, as in step (1). Hence wave i_{HA} is attributed to reduction of the protonated form in step (3). This conclusion is supported by the observed pH-dependence of half-wave and other characteristic potentials (Fig. 3). The decrease of current in the shape of a dissociation curve even with rapid potential scanning indicates that establishment of equilibrium (4) is rapid. As for other protonation reactions of aryl alkyl ketones [36], it is possible to assume that protonation takes place as a surface reaction. The possibility of step (3) proceeding in two one-electron processes to yield a pinacol cannot be excluded.

In the region between pH 6 and about 8 the height of the reduction wave of the unprotonated ketone in a six-electron step (7) is governed by the pH-independent rate of dehydration. This is attributed to the reaction (5) involving loss of a water molecule in the rate-determining step with rate constant k_{-H_2O}.

These experimental results do not allow formation of difluoro- and monofluoro-acetophenone as intermediates to be excluded. Some indications of consecutive reduction can be drawn from the formation of two waves in pulse polarography in this pH range (Table 1). Yet preparative electrolysis with the d.m.e. gave no indication of such products being formed; moreover, reports on the preparative reduction of the trifluoromethyl groups [6] indicate simultaneous cleavage of all three C—F bonds at the same potential.

There is no indication (e.g., decrease in wave-height of i_A at higher pH values to one half of its initial value) that protonation of intermediate electrolysis products takes place between electron transfers. The shape of the i—E curves and their pH-dependence shows no resemblance to curves of aryl alkyl ketones [37]. This can be considered as further circumstantial evidence that reduction of the trifluoromethyl group rather than that of carbonyl takes place in wave i_A.

However, the protonation of the carbanions formed in reduction of the trifluoromethyl group is only a moderately rapid reaction: the rate of pro-

tonation (probably one of the proton transfers) governs the amount of acetophenone available for further reduction in step (8) and thus the height of wave i_p. The height of wave i_p is frequently smaller than it would be if all the product of the first reduction step i_A were quantitatively and rapidly converted to acetophenone. The role of conversion of an electro-inactive primary product to acetophenone was confirmed by electrolysis at a controlled potential corresponding to the limiting current of wave i_A. Increase of the wave i_p in the course of electrolysis (Fig. 9) indicated that more conversion to acetophenone can take place during longer times. The shape of the wave i_p indicates a surface reaction.

Increase in i_A at pH >8.5 is interpreted as due to the shift in equilibrium (10) to the right-hand side, which increases the dehydration rate (9) with constant k_{-1}. Decrease in i_A at pH >10 is ascribed to the increase in rate of reaction (9) with the rate constant k_1, which decreases the concentration of the electroactive free carbonyl form and increases that of electroinactive geminal diol anion.

Considering reaction (5) with rate constant $k_{H_2O} + k_{-H_2O}$ and reaction (9) with rate constant k_{-1} to be competitive reactions producing the electroactive free carbonyl form $C_6H_5COCF_3$, the latter in eqn. (9) accompanied by a rapidly established equilibrium (10) with equilibrium constant K_2, it is possible to interpret the pH-dependence of the current over the pH range 7—12. In buffered solution the competitive reactions producing the electroactive unhydrated species follow first-order kinetics with overall rate constant $k_{overall}$ which is related to rate constants $(k_{H_2O} + k_{-H_2O})$, k_1, k_{-1} and the dissociation constant K_2 by

$$k_{overall} = (k_{H_2O} + k_{-H_2O}) + \{k_{-1}/(1 + [H^+]/K_2)\} - k_1 [OH^-] \quad (11)$$

A rigorous treatment of polarographic currents governed by rates of competitive reactions has been applied [38, 39] to reduction of the aldehydic form of glucose, formed from the α- and β-forms of glucose. Such a treatment was possible because the rate of mutarotation and changes in properties of glucose solutions with time after preparation were experimentally accessible. No such kinetic information was available in the present case. Moreover, for any calculation of the rate constants $k_{H_2O} + k_{-H_2O}$, it would be necessary to know the value of the equilibrium constant of reaction (5), K_{H_2O}, which is not accessible to measurement. [The value of K_{H_2O} is related to K_d by an equation involving the accessible value of K_2, but also the unknown dissociation constant of $C_6H_5C(OH_2^+)(O^-)CF_3 \rightleftharpoons C_6H_5C(OH)(O^-)CF_3 + H^+$.] On the assumption that polarographic kinetic currents are a linear function of the rate constant of the reaction governing the formation of the electroactive species, it is possible to estimate relative values of $(k_{H_2O} + k_{-H_2O})$, k_1 and k_{-1}.

The set of rate constants must satisfy eqn. (11) so as to give values for $k_{overall}$ reaching a maximum value at pH 10 which is about 1.5 times higher than the value at pH 7—8. The value of K_2 used in the calculation was 6.35×10^{-10}. The dependence of $k_{overall}$ on pH is very sensitive to the ratio of the

values of k_{-1} to $(k_{H_2O} + k_{-H_2O})$ (Fig. 13), but somewhat less to $k_{-1}:k_1$. The best fit with the experimental points shows a set where $(k_{H_2O} + k_{-H_2O}):k_{-1}$ is 1:1.2 and $k_{-1}:k_1$, about $1:1 \times 10^3$ (Fig. 14). This ratio of values of k_{H_2O} and k_1 ($1:1.2 \times 10^3$) exemplifies the predominance of the addition of hydroxide ions (step 9) over that of water (step 5) in alkaline media. A similar ratio has been observed for the addition of water and hydroxide ions to pyridinecarboxaldehydes [40].

The pH-dependence of the half-wave potentials (Fig. 3) is in agreement with the suggested reaction scheme. The shift of wave i_{HA} with increasing pH to more negative values is due to acid—base equilibrium (step 1) preceding the electron transfer (step 3). The half-wave potentials of wave i_{HA} could not be measured (because of the close proximity of wave i_A) in the pH range pH 5—6.5, where a break at pH about 5.5 (pK') would be expected, corresponding to the surface reaction.

The shift of wave i_A to more negative potentials at pH 6—8.5 is probably due to establishment of equilibria (4)—(6) preceding reduction in step (7). Even though reduction of the carbon—halogen bond is usually pH-independent, the present system corresponds to halogen derivatives which contain an acidic group as well as the C—X bond [41]. The independence of half-wave potentials at pH greater than about 9 indicates that the predominating ionized state of the unhydrated species present in the bulk of the solution undergoes electrolysis, and if acid—base equilibria are operating they are shifted in favor of the electroactive form, i.e. reactions (4) and (6) go to the right.

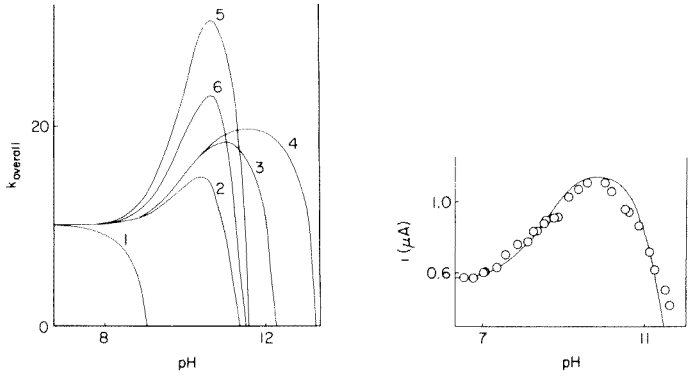

Fig. 13. Sensitivity of the pH-dependence of the value $k_{overall}$ calculated according to eqn. (11) to values of $(k_{H_2O} + k_{-H_2O})$, k_1 and k_{-1}. Theoretical curves calculated for $(k_{H_2O} + k_{-H_2O}) = 10\ s^{-1}$, $K_2 = 1 \times 10^{-10}$ and: (1) $k_{-1} = 10\ l\ mol^{-1}\ s^{-1}$, $k_1 = 1 \times 10^6\ l\ mol^{-1}\ s^{-1}$; (2) $k_{-1} = 10$, $k_1 = 1 \times 10^4$; (3) $k_{-1} = 10$, $k_1 = 1 \times 10^3$; (4) $k_{-1} = 10$, $k_1 = 1 \times 10^2$; (5) $k_{-1} = 30$, $k_1 = 1 \times 10^4$; (6) $k_{-1} = 20$, $k_1 = 1 \times 10^4$.

Fig. 14. pH-Dependence of d.c. polarographic currents of 1×10^{-3} M α,α,α-trifluoroacetophenone in Britton—Robinson buffers containing 5% ethanol (v/v); experimental points are shown with the theoretical curve calculated on the assumption that the current is governed by the rate of a first-order reaction with rate constant $k_{overall}$ following eqn. (11) for $K_2 = 6.35 \times 10^{-10}$ and $(k_{H_2O} + k_{-H_2O})$: $k_{-1}:k_1$ in the ratio $1:1.2:1 \times 10^3$.

The nature of the anodic waves observed at pH 8 was not investigated. These waves may correspond to oxidation or mercury salt formation. The process seems, nevertheless, different from that observed [42] for dialkyl and some aryl alkyl ketones, as the current is a linear function of concentration. Nor does trifluoroacetophenone contain an α-hydrogen which is considered to be essential for the proposed reaction [42].

Some quantitative differences (between the ratio of signals at pH 7 and 10 and in the range of pH over which the increase of wave i_A occurs) observed when different electrochemical techniques were used may be due to differences in the time intervals over which the current was measured as well as to adsorption phenomena involved in the reduction of the unprotonated form $C_6H_5COCF_3$. The ratio of the signal caused by adsorption to that caused by a faradaic process is higher for the techniques based on periodically changed voltage than for d.c. polarography.

The initial information about the electrode process was deduced from data obtained by d.c. polarography. This was rather fortunate as the interpretation of the results obtained by the other techniques used would have been more difficult. In addition to the more pronounced adsorption phenomena mentioned above, the current signals for a.c. and derivative pulse polarography, as well as linear sweep methods, depend on αn_a, and hence the relative height of individual current signals does not offer information on the relative number of electrons transferred in individual steps. Moreover, the waves arising from acetophenone reduction were invariably less clearly shown than in the d.c. technique. The present investigation supports the recommendation [43] that initial investigations of an unknown system should be done by d.c. polarography.

Spectral properties

The intensive absorption band at 205 nm can be ascribed to $\pi \rightarrow \pi^*$ transitions. The group of fine structure bands at 240—270 nm observed in aqueous and ethanolic solutions corresponds to overlap of two bands: the benzene absorption (with fine structure) of the unconjugated benzene ring in the geminal diol $C_6H_5C(OH)_2CF_3$ and hemiketal $C_6H_5C(OH)(C_2H_5)CF_3$ and the wide band (without fine structure) corresponding to the benzenoid absorption of the grouping C_6H_5CO of the unhydrated molecule $C_6H_5COCF_3$. The band at 290 nm corresponds to the forbidden transition $n \rightarrow \pi^*$ of the carbonyl group of the unhydrated molecule $C_6H_5COCF_3$.

The change in the spectra from a group of fine structure bands to a wide round maximum, makes the bands in the 240—270 nm region suitable for an estimate of the degree of solvation in aqueous or ethanolic solvents, but insufficient for quantitative measurement of the concentration of the free carbonyl form for which the band at 290 nm is best suited. At this wavelength the absorption of the solvated molecule is negligible. Unfortunately, the band is broad and of low intensity so that its measurement in solutions containing low concentrations of the free carbonyl form is rather inaccurate.

In organic solvents, the similarity of wavelength and molar absorptivity at both the 250—260-nm and 290-nm regions to those of acetophenone indicates that even when trifluoroacetophenone exists in the solid form as a hydrate and is transferred to an organic solvent as such, the equilibrium is practically completely shifted in favor of the unhydrated form.

Addition of water or ethanol to a nonhydroxylic solvent results not only in a marked decrease in absorbance but also in the appearance of fine structure (Fig. 11). Disappearance of the fine structure of the benzenoid band because of conjugation of a carbonyl group can be used as a diagnostic tool for the presence of such conjugation.

Reactions in solutions

Evaluation of the hydration-dehydration equilibrium constant [20] and of the reaction with ammonia [44] are discussed elsewhere, hence only hydrolysis and hemiketal formation will be discussed here.

Hydrolysis occurs in aqueous solutions and in the presence of 40% ethanol at pH >12 (at 25°C) and yields a species containing the C_6H_5CO group, as indicated by the increase in absorbance at 260 and 290 nm and in the wave in the potential region where the acetophenone wave i_p is observed. This indicates the possibility of a mechanism different from cleavage of aldehydes with a $COCX_3$ grouping [45, 46]. The hydrolysis was found to be slow in acetonitrile, faster in dimethylformamide and fastest in dimethylsulfoxide solutions, and to be affected by the presence of strong acids or bases.

Polarographic currents depend on ethanol concentration (Fig. 6) partly because of a change in viscosity, and partly because of hemiketal formation. Hence information about hemiketal formation is better obtained from absorption spectra, from the increases in the benzenoid bands at 250—260 nm and the carbonyl band at 290 nm, observed with increasing methanol or ethanol concentration (Fig. 10).

In the system described formally by the following overall equations

$$C_6H_5C(OH)_2CF_3 \overset{K_{deh}}{\rightleftharpoons} C_6H_5COCF_3 + H_2O \tag{12}$$

$$C_6H_5C(OC_2H_5)(OH)CF_3 \overset{K_{ket}}{\rightleftharpoons} C_6H_5COCF_3 + C_2H_5OH \tag{13}$$

the concentration of the free carbonyl form can be expressed by

$$[CO] = S_{CO} \Big/ \left(1 + \frac{H_2O}{K_{deh}} + \frac{[C_2H_5OH]}{K_{ket}}\right) \tag{14}$$

For an analytical concentration S_{CO}, expression (14) indicates an increase in concentration of the free carbonyl form with increasing ethanol concentration, provided that $K_{ket} \ll K_{deh}$. K_{deh} can be taken equal to $K_d\,[H_2O] = K_d \times 55$ and is approximately equal [20] to 1.0. K_{ket} can be obtained from $K_{ket} = K_d/K_4$; a K_4 value of 3.5 has been reported [47] from n.m.r. studies,

yielding a value of $K_{ket} = 0.018/3.5 = 5 \times 10^{-3}$, and the above condition for increase in the free carbonyl form in the presence of ethanol is fulfilled. Changes in u.v. spectra (Fig. 10) indicate the possibility of determining K_4 independently. A smaller value $K_{ket} = 0.025$ than $K_{deh} = 0.14$ was also obtained for reactions of α,α,α-trifluoroacetophenone with ethanol and water in dimethylformamide as solvent.

REFERENCES

1 G. Nisli, D. Barnes and P. Zuman, J. Chem. Soc. (B), (1970) 764.
2 G. Nisli, D. Barnes and P. Zuman, J. Chem. Soc. (B), (1970) 771.
3 G. Nisli, D. Barnes and P. Zuman, J. Chem. Soc. (B), (1970) 778.
4 V. V. Bukhtiyarov and N. N. Bubnov, Teor. Eksp. Khim., 4 (3) (1968) 413.
5 J. H. Stocker, R. M. Jenevein and D. H. Kern, J. Org. Chem., 34 (10) (1969) 2810.
6 J. H. Stocker and R. M. Jenevein, Chem. Commun., 16 (1968) 934.
7 J. H. Stocker and R. M. Jenevein, J. Org. Chem., 33 (1968) 294.
8 P. J. Elving and J. T. Leone, J. Am. Chem. Soc., 79 (1957) 1546.
9 A. M. Wilson and N. L. Allinger, J. Am. Chem. Soc., 83 (1961) 1999.
10 R. Kabasakalian and J. McGlotten, Anal. Chem., 34 (1962) 1440.
11 O. Hrdý, Collect. Czech. Chem. Commun., 27 (1962) 2447.
11a H. S. de Boer, W. J. van Oort and P. Zuman, Anal. Chim. Acta, 120 (1980) 31.
12 A. I. Cohen, Anal. Chem., 35 (1963) 128.
13 H. Lund, Acta Chem. Scand., 13 (1959) 192.
14 A. I. Cohen, B. T. Keeler, N. H. Coy and H. L. Yale, Anal. Chem., 34 (1962) 216.
15 O. Manoušek, O. Exner and P. Zuman, Collect. Czech. Chem. Commun., 33 (1968) 4000.
16 H. Lund, private communication, Aarhus, 1966.
17 P. J. Elving and C. M. Callahan, J. Am. Chem. Soc., 77 (1955) 2077.
18 P. J. Elving and P. G. Grodzka, Anal. Chem., 33 (1961) 2.
19 R. Stewart and J. D. Van Dyke, Can. J. Chem., 48 (1970) 3961.
20 W. J. Scott and P. Zuman, J. Chem. Soc. Faraday Trans. I, 72 (1976) 1192.
21 R. Stewart and R. van der Linden, Can. J. Chem., 38 (1960) 399.
22 M. Kalousek, Collect. Czech., Chem. Commun., 13 (1948) 105.
23 L. Němec and I. Holub, unpublished results, Prague, 1965.
24 O. Manoušek, unpublished results, Prague, 1965.
25 A. M. G. Macdonald, in O. Eichler, H. Farah, M. Herken and A. D. Welch (Eds.), Handbook of Experimental Pathology, Springer Verlag, Berlin, Vol. XX/2, 1970, p. 23.
26 P. Valenta, Collect. Czech. Chem. Commun., 25 (3) (1960) 853.
27 E. Laviron, Bull. Soc. Chim. France, (1961) 2325.
28 J. Volke and P. Valenta, Collect. Czech. Chem. Commun., 25 (1960) 1580.
29 J. Kůta and P. Valenta, Collect. Czech. Chem. Commun., 28 (1963) 1593.
30 P. H. Given and M. E. Peover, J. Chem. Soc., (1958) 2674.
31 G. Kesslin and R. Bradshaw, Ind. Eng. Chem., Prod. Res. Develop., 5 (1) (1966) 27.
32 P. Zuman, Fresenius Z. Anal. Chem., 224 (1967) 374.
33 P. Zuman and O. Manoušek, Collect. Czech. Chem. Commun., 34 (1969) 1580.
34 Yu. Kargin, O. Manoušek and P. Zuman, J. Electroanal. Chem., 12 (1966) 443.
35 A. Ryvolová-Kejharová and P. Zuman, Collect. Czech. Chem. Commun., 35 (1970) 22.
36 P. Zuman, Collect. Czech. Chem. Commun., 33 (1968) 2548.
37 P. Zuman, D. Barnes and A. Ryvolová-Kejharová, Disc. Faraday Soc., 45 (1968) 202.
38 J. M. Los and K. Wiesner, J. Am. Chem. Soc., 75 (1953) 6346.
39 J. M. Los, L. B. Simpson and K. Wiesner, J. Am. Chem. Soc., 78 (1956) 1564.
40 S. Cabani, P. Gianni and E. Matteoli, J. Phys. Chem., 76 (1972) 2959.

41 P. Zuman, Chem. Listy., 56 (1962) 219; and references therein.
42 M. Heyrovský, Collect. Czech. Chem. Commun., 28 (1963) 26.
43 G. Cauquis and V. D. Parker, in M. Baizer (Ed.), Organic Electrochemistry, M. Dekker, New York, 1973, p. 139.
44 W. J. Scott and P. Zuman, Anal. Chim. Acta, 126 (1981) 259.
45 J. Hine and G. F. Koser, J. Org. Chem., 36 (1970) 1348.
46 P. Zuman, W. Szafranski and D. Visioli, unpublished results.
47 J. P. Guthrie, Can. J. Chem., 53 (1975) 898.

Analytica Chimica Acta, 126 (1981) 95—104
Elsevier Scientific Publishing Company, Amsterdam — Printed in The Netherlands

SEMIDIFFERENTIAL ELECTROANALYSIS WITH A SOLID WORKING ELECTRODE

MASASHI GOTO*, MASAO KATO and DAIDO ISHII

Department of Applied Chemistry, Faculty of Engineering, Nagoya University, Chikusa-ku, Nagoya (Japan)

(Received 22nd September 1980)

SUMMARY

Semidifferential electroanalysis is described for hexacyanoferrate(III), dichromate, copper(II), *p*-aminophenol, *p*-benzoquinone, *m*-dinitrobenzene, guanine, guanosine, adenine, and adenosine at a stationary solid working electrode. Nearly symmetrical, peaked curves are obtained for the electrode processes of all the samples investigated. The predicted dependence of peak height and peak potential on concentration, electrode area, and potential scan rate are confirmed experimentally for the glassy carbon disk electrode. It is demonstrated that the technique with the solid working electrode provides higher sensitivity and better resolution than ordinary linear sweep voltammetry. The sensitivity is somewhat worse than in differential pulse voltammetry, but the technique has the advantage of speed.

In recent years, a new voltammetric technique, semidifferential electroanalysis, has been investigated in attempts to improve the speed and sensitivity of voltammetry [1—5]. The technique measures the semiderivative, e, of the current, i, with respect to time, t, as a function of the electrode potential, E, under the experimental conditions of ordinary linear sweep voltammetry. The method provides higher sensitivity and better resolution than ordinary linear sweep voltammetry, and the time required for measurement is generally shorter than that for differential pulse voltammetry at a hanging mercury drop or a mercury film working electrode. In the present paper, the theoretical relationships at a stationary solid working electrode are compared with experimental data obtained by using the glassy carbon disk electrode, to extend the applicability of the technique.

In semidifferential electroanalysis with a planar working electrode, the shape of the e vs. E curves, derivative neopolarograms, observed for reversible electrode reductions is a symmetrical peak as described [1, 2] by

$$e = n^2F^2AvD^{1/2}C\,(4RT)^{-1}\,\mathrm{sech}^2\,\{nF\,(2RT)^{-1}\,(E - E_{1/2})\} \qquad (1)$$

where n is the electron transfer number, F the Faraday constant, A the electrode area, v the potential scan rate, D the diffusion coefficient of oxidant, C the concentration of oxidant, R the gas constant, T the absolute temperature, and $E_{1/2}$ the d.c. polarographic half-wave potential. The peak height, e_p, the

0003—2670/81/0000—0000/$02.50

peak potential, E_p, and the peak width at half-height, W_p, in the derivative neopolarograms are given by $e_p = n^2F^2AvD^{1/2}C\ (4RT)^{-1}$, $E_p = E_{1/2}$, $W_p = 3.53RT\ (nF)^{-1}$, respectively. For irreversible electrode reductions, the following equations apply [2]:

$$e = -n^2\alpha AF^2vD^{1/2}C\ (RT)^{-1} \sum_{j=1}^{\infty} (-1)^j\, j \exp\{jz(j!)^{1/2}\} \qquad (2)$$

where z is defined by

$$z = n\alpha F\ (RT)^{-1}\ (E_s - E) + 1/2 \ln\ \{RTk_s^2\,(n\alpha FvD)^{-1}\} = n\alpha F\,(RT)^{-1}\,(E_* - E) \qquad (3)$$

and $e_p = \alpha n^2F^2AvD^{1/2}C\ (3.367RT)^{-1}$, $E_p = E_* + 0.055RT\ (n\alpha F)^{-1}$, and $W_p = 2.94RT\ (\alpha nF)^{-1}$. In these equations, α represents the transfer coefficient, E_s the standard potential, k_s the heterogeneous rate constant at E_s, and E_* the characteristic potential defined by eqn. (3).

It should be noted that the peak height of the derivative neopolarogram for both reversible and irreversible processes is predicted to be proportional to the concentration of the reducible species, to the electrode area, and to the potential scan rate. The peak potential for a reversible process is a constant equal to the d.c. polarographic half-wave potential, but that for an irreversible process shifts with the potential scan rate. The peak width is very dependent on the electron transfer number for both processes. Though the above equations are couched in terms of reduction processes, it is evident that the conclusions are easily widened to cover oxidation processes.

EXPERIMENTAL

Apparatus

A block diagram of the apparatus used is shown in Fig. 1. A potential sweeper (Nikko Keisoku Co., model NPS-2) or a function generator (NF Co., model FG-121B) was used for potential sweeping. The analog semidifferential circuits with current follower [1, 6] were used for the current-to-voltage converter and the semidifferentiation of current. An X-Y recorder (Yokogawa Co., model 3077) was used for recording the i vs. E and e vs. E curves.

Glassy carbon disks (5.00, 3.00, or 0.85 mm diameter, ca. 5 mm thick) sealed into 15 cm of glass tubing with epoxy resin, were used as the station-

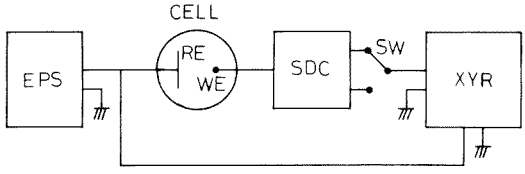

Fig. 1. Block diagram of apparatus for semidifferential electroanalysis. (EPS) electrode potential sweeper; (RE) reference electrode; (WE) working electrode; (SDC) semidifferential circuit; (SW) switches for i and e measurements; (XYR) X-Y recorder.

ary solid working electrode. The exposed surface of the disks was polished with emery paper, and then to a mirror finish with wet alumina powder (0.05 μm) on an acrylic plate. The electrode was cleaned with distilled and deionized water before use, and the polishing with alumina powder was repeated between each run. The Ag/AgCl electrode was made from a silver sheet (4 × 4 cm) coated with silver chloride immersed in a saturated KCl solution and separated from the sample solution by an agar salt bridge. This large electrode served as both the counter and the reference electrode. The electrolytic cell (capacity 25 ml) was made from a glass weighing vessel. The uncompensated resistance of the cell was about 750 Ω.

Reagents and solutions

Potassium hexacyanoferrate(III), potassium dichromate and copper sulfate pentahydrate were used for inorganic samples, and *p*-aminophenol, *p*-benzoquinone, *m*-dinitrobenzene, guanine, guanosine, adenine, and adenosine as organic samples. Supporting electrolytes were either KCl or H_2SO_4 solutions for inorganic samples and Britton—Robinson buffers at different pH for organic samples. Solutions were prepared by direct weighing of the appropriate quantities of special-grade (Japanese Industrial Standard) reagents without further purification. For samples where electrolysis occurred at potentials more negative than that of the silver—silver chloride electrode, solutions were deoxygenated by passage of nitrogen. Measurements were made at room temperature.

RESULTS AND DISCUSSION

Shapes of e vs. E curve

Figures 2—4 show the cyclic derivative neopolarograms (*e* vs. *E* curves), compared with the corresponding voltammograms (*i* vs. *E* curves), for typical inorganic samples. Figure 2 represents the curves for the reversible electrode reaction $Fe(CN)_6^{3-} + e^- \rightleftarrows Fe(CN)_6^{4-}$ in 0.1 M KCl at a potential scan rate of 100 mV s^{-1}. In this case, sharp and virtually symmetrical peaks were observed in the *e* vs. *E* curve for the reduction and re-oxidation processes while broad and asymmetrical peaks were observed in the ordinary *i* vs. *E* curve. There was a small peak potential difference between the reduction and re-oxidation wave in the *e* vs. *E* curve; this is mainly due to the presence of uncompensated resistance in the cell. Figure 3 represents for the curves for a totally irreversible electrode reaction $Cr_2O_7^{2-} + 14\ H^+ + 6\ e^- \rightarrow 2\ Cr^{3+} + 7\ H_2O$ in 0.5 M H_2SO_4. In this case, no re-oxidation wave was observed and the shape of the *e* vs. *E* curve for the reduction process was a rather broad but almost symmetrical peak as predicted from the theory. Figure 4 shows the case of a stepwise electrode reaction, which involves two successive reductions and in which the final reduction product deposits on the electrode. In Fig. 4, the first reduction wave corresponds to $Cu(II) + e^- \rightleftarrows Cu(I)$, and the second reduction wave to $Cu(I) + e^- \rightleftarrows Cu$ in 0.5 M KCl. The second reduction

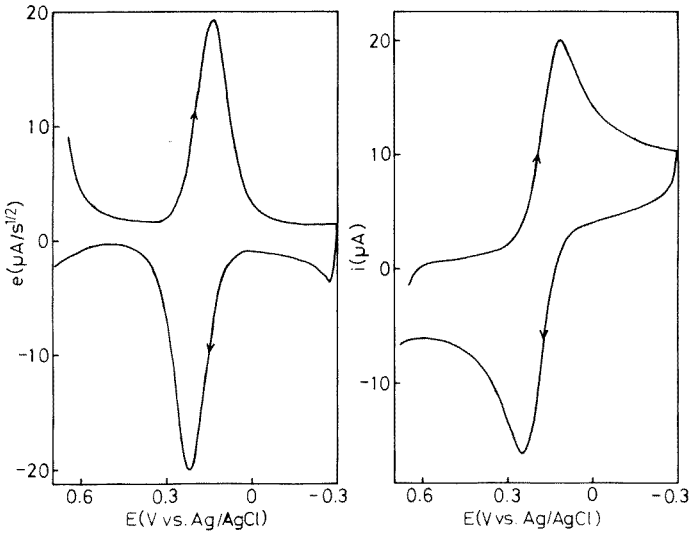

Fig. 2. Comparison between e vs. E and i vs. E curve for 400 μM $Fe(CN)_6^{3-}$ in 0.1 M KCl. Scan rate 100 mV s^{-1}; electrode area 19.6 mm^2; temperature 29°C.

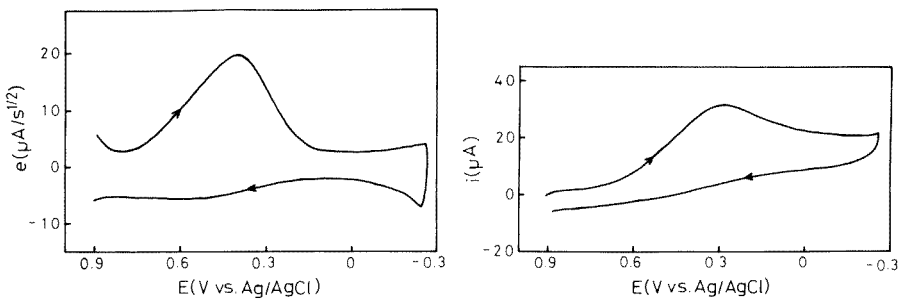

Fig. 3. Comparison between e vs. E and i vs. E curve for 100 μM $Cr_2O_7^{2-}$ in 0.5 M H_2SO_4. Temperature 31°C; other conditions as in Fig. 2.

wave in the e vs. E curve showed a sharp but asymmetrical peak; a similar peak was observed in the reduction process of Pb^{2+} in 0.1 M KCl. The first re-dissolution peak (3) and the second re-dissolution peak (4) in Fig. 4 correspond to the re-oxidation reactions of copper and copper(I), respectively. For the first re-dissolution process, a sharp minimum and maximum were observed in the e vs. E curve, while a sharp but asymmetrical peak was observed in the i vs. E curve. This phenomenon is similar to that observed in the re-dissolution process of amalgamated metal from a mercury film electrode [5]. It should be noted that the current is not zero in the ranges —0.6 to —0.9 V and —0.9 to —0.15 V, because the reduction of Cu(II) and/or Cu(I) continues to some extent.

Figures 5—7 show cyclic derivative neopolarograms with the corresponding cyclic voltammograms for typical organic systems. Figure 5 shows the

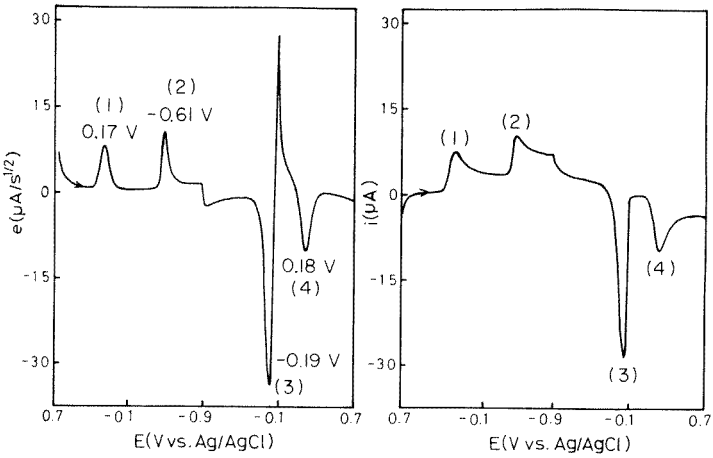

Fig. 4. Comparison between e vs. E and i vs. E curve for 400 μM Cu(II) in 0.5 M KCl. Scan rate 100 mV s^{-1}; electrode area 7.07 mm^2; temperature 34°C; peak (1) 1st reduction, (2) 2nd reduction, (3) 1st re-dissolution, (4) 2nd re-dissolution.

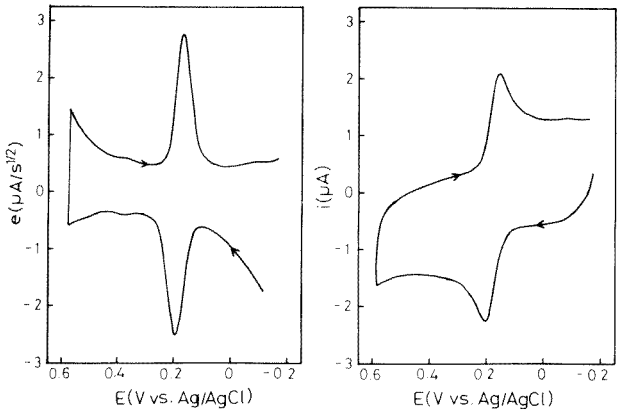

Fig. 5. Comparison between e vs. E and i vs. E curve for 8 μM p-aminophenol in Britton—Robinson buffer of pH 6.3. Temperature 20°C, other conditions as in Fig. 2.

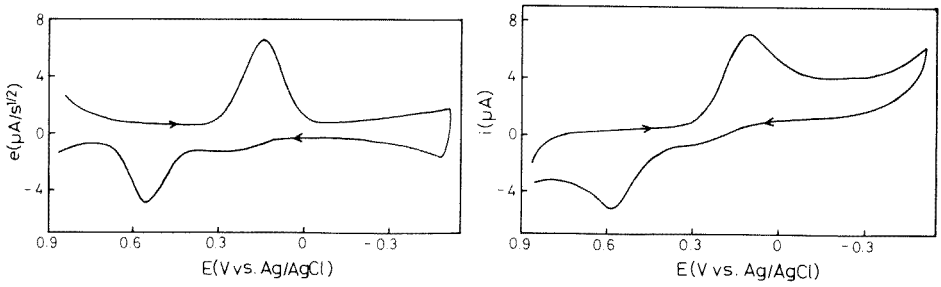

Fig. 6. Comparison between e vs. E and i vs. E curve for 300 μM p-benzoquinone in Britton—Robinson buffer pH 2.8 (50% ethanolic solution). Scan rate 100 mV s^{-1}; electrode area 7.07 mm^2; temperature 20°C.

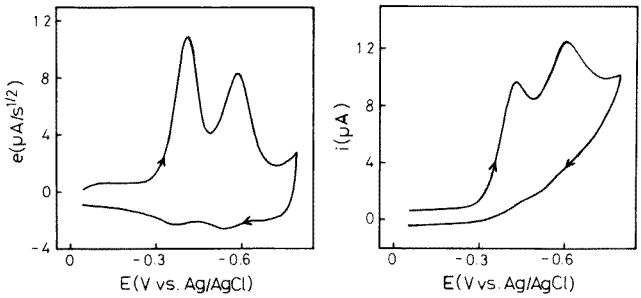

Fig. 7. Comparison between e vs. E and i vs. E curve for 100 μM m-dinitrobenzene in Britton—Robinson buffer pH 4.1 (10% ethanolic solution). Conditions as in Fig. 6.

curves for the reversible 2-electron oxidation of p-aminophenol in Britton—Robinson (B—R) buffer pH 6.3; Fig. 6 shows curves for the quasi-reversible 2-electron reduction of p-benzoquinone in B—R buffer pH 2.8 (50% ethanolic solution). Figure 7 shows curves for the totally irreversible reduction of m-dinitrobenzene in B—R buffer pH 4.1 (10% ethanolic solution), which occurs in two 4-electron steps first to the dinitroso derivative and then to the hydroxylamine derivative. As expected from theory, sharp symmetrical peaks were observed in the e vs. E curve for the oxidation and re-reduction of p-aminophenol. In the case of p-benzoquinone, a large difference in peak potential between the reduction and re-oxidation wave was observed and both peaks in the e vs. E curve were somewhat broad, but virtually symmetrical. Benzoquinone forms a reversible system at pH 2.8 at the DME, and the different behavior with the two techniques is mainly due to the difference in potential scan rate between semidifferential electroanalysis (100 mV s^{-1}) and d.c. polarography (2 mV s^{-1}). Two successive reduction peaks were clearly observed for m-dinitrobenzene but the re-oxidation waves were almost negligible. In this case, the derivative neopolarogram showed relatively sharp peaks despite the irreversibility of the electrode reaction, because each reduction process involves a 4-electron transfer.

It is evident from Figs. 2—7 that the derivative neopolarograms have very attractive analytical features such as a smooth base line, good peak symmetry, and good resolution compared to ordinary voltammograms.

Peak potentials and peak widths of e vs. E curves

Tables 1 and 2 show the derivative neopolarographic peak potentials at different concentrations for the reduction or oxidation processes of inorganic and organic samples, respectively. The peak potentials for all the species investigated excluding dichromate were found to be roughly independent of concentration, and to average the potential values shown in the bottom lines of Tables 1 and 2. The peak potentials for the reduction processes of dichromate and m-dinitrobenzene tended to shift to more negative potentials with increase in the potential scan rate (Table 3). This phenomenon is predictable

TABLE 1

Peak potentials (given in V vs. Ag/AgCl) of e vs. E curves for the reductions of hexacyanoferrate(III) in 0.1 M KCl, copper(II) in 0.5 M KCl, and dichromate in 0.5 M H_2SO_4 at different concentrations
[Potential scan rate and temperature: 100 mV s^{-1} and 30°C for $Fe(CN)_6^{3-}$, 100 mV s^{-1} and 31°C for $Cr_2O_7^{2-}$, and 50 mV s^{-1} and 34°C for Cu(II)]

$C(\mu M)$	$Fe(CN)_6^{3-}$	Cu(II)		$Cr_2O_7^{2-}$
		1st	2nd	
10				0.355
20	0.192	0.173	−0.610	0.316
30				0.391
40	0.189	0.165	−0.606	0.365
50				0.387
60	0.189	0.161	−0.614	
80	0.187	0.160	−0.609	
100	0.190	0.183	−0.590	
	Av. 0.189	0.168	−0.606	

TABLE 2

Peak potentials (given in V vs. Ag/AgCl) of e vs. E curves for p-aminophenol, p-benzoquinone, and m-dinitrobenzene in Britton—Robinson buffer solution at different concentrations
(Potential scan rate: 100 mV s^{-1}, temperature: 20°C)

$C(\mu M)$	p-Aminophenol oxidation at pH 6.3	p-Benzoquinone reduction at pH 2.8	m-Dinitrobenzene reduction at pH 4.1	
			1st	2nd
2	0.184			
4	0.194			
6	0.194			
8	0.196			
10	0.194			
20	0.192	0.199	−0.412	−0.591
40	0.198	0.190	−0.422	−0.598
60	0.202	0.183	−0.435	−0.618
80	0.207	0.183	−0.427	−0.609
100	0.211		−0.423	−0.603
	Av. 0.197	0.189	−0.424	−0.604

from eqn. (3) and from the expression $E_p = E_* + 0.055RT(n\alpha F)^{-1}$, in the case of irreversible electrode processes.

The peak widths for the reduction of hexacyanoferrate(III), the first reduction of copper(II), and the oxidation of p-aminophenol were 130 mV, 104 mV, and 62 mV under the experimental conditions shown in Figs. 2, 4,

TABLE 3

Peak potentials (given in V vs. Ag/AgCl) of e vs. E curves for the reductions of dichromate in 0.5 M H_2SO_4 and m-dinitrobenzene in Britton—Robinson buffer (pH 4.1, 10% ethanol) at different potential scan rates

v (mV s^{-1})	$Cr_2O_7^{2-}$	m-Dinitrobenzene	
		1st	2nd
25	0.450		
33	0.426		
50	0.424	—0.388	—0.563
70		—0.400	—0.574
100	0.399	—0.423	—0.603
125	0.369		

and 5, respectively. These experimental values have to be compared with the respective theoretical values for reversible electrode processes of 92 mV, 93 mV, and 45 mV, calculated from $W_p = 3.53RT\,(nF)^{-1}$. In all these cases, the experimental peak widths are larger than the theoretical ones for reversible processes. This is largely due to the presence of uncompensated resistance in the cell, and indicates that the glassy carbon surface is not completely clean.

Dependence of peak height on concentration, potential scan rate, and electrode area

Peak heights of the e vs. E curves were plotted against concentrations for the inorganic and organic systems. In all cases, the plots were linear and passed through the origin; the slopes are given in Table 4. The relative standard deviations were less than ±5% excluding the cases of dichromate and m-dinitrobenzene. The detection limits of the investigated species were found to be 1×10^{-5}—5×10^{-7} M, depending on the reversibility of the electrode processes concerned and the electron transfer number involved.

TABLE 4

Slopes of the plots between peak heights of e vs. E curves and concentrations

Species	Process	Supporting electrolyte	v (mV s^{-1})	A (mm^2)	T' (°C)	n	de_p/dC ($mA \cdot s^{-1/2} \cdot M^{-1}$)
$Fe(CN)_6^{3-}$	Reduction	0.1 M KCl	100	19.6	30	1	49.0
$Cr_2O_7^{2-}$	Reduction	0.5 M H_2SO_4	100	19.6	31	6	90.2
Cu(II)	1st Reduction	0.5 M KCl	50	19.6	34	1	36.2
p-Aminophenol	Oxidation	B—R (pH 6.3)	100	19.6	20	2	—260
p-Benzoquinone	Reduction	B—R (pH 2.9)[a]	100	19.6	20	2	48.8
m-Dinitrobenzene	1st Reduction	B—R (pH 4.1)[b]	100	7.07	20	4	74.8
	2nd Reduction					4	56.8

[a] 50% ethanol. [b] 10% ethanol.

The best and worst detection limits were observed in the determination of *p*-aminophenol and dichromate, respectively.

Figures 8 and 9 show the relationship between peak height and potential scan rate, and electrode area in the case of inorganic samples. In all cases, linearity was satisfactory and the lines passed through the origin. Similar results were also observed for organic samples. It is, therefore, clear that the peak height is proportional to both potential scan rate and electrode area, as predicted from the theory.

Analytical application

The proposed semidifferential electroanalytical technique was tested for the simultaneous determination of the purine bases and their nucleosides. Figure 10 shows the anodic derivative neopolarogram for a mixture of adenine, adenosine, guanine, and guanosine recorded in Britton—Robinson buffer of pH 2.6. Four successive well-defined oxidation peaks were observed and it seems to be readily possible to determine simultaneously each component in the mixtures, particularly when Fig. 10 is compared with the ordinary linear sweep voltammograms reported in the literature for these compounds [7]. The detection limits with the present technique (10^{-5}—5×10^{-6} M) were about ten times better than those obtained in ordinary linear sweep voltammetry [7]. The detection limits are worse than those available by differential pulse voltammetry, the principal advantage of the proposed technique being its rapidity.

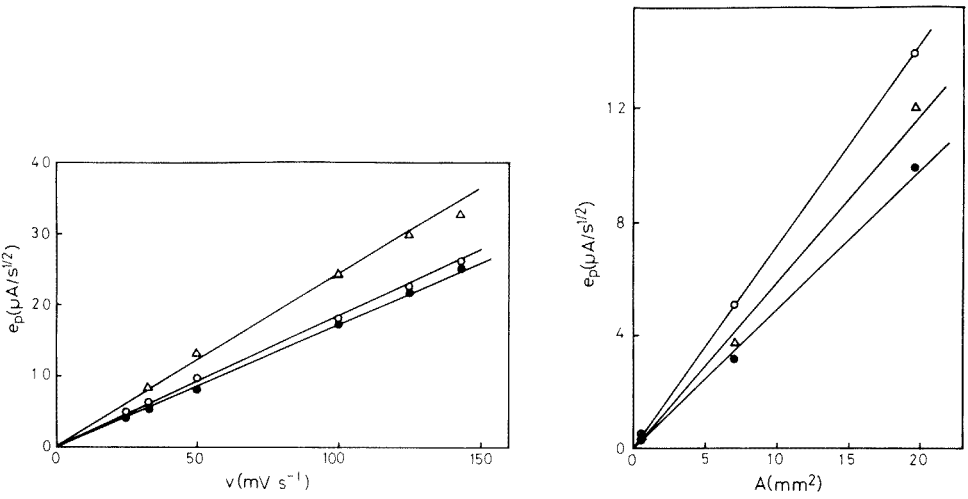

Fig. 8. Relationship between peak height of e vs. E curve and scan rate. Electrode area 19.6 mm^2. (○) 400 μM $Fe(CN)_6^{3-}$ in 0.1 M KCl at 29°C; (●) 100 μM $Cr_2O_7^{2-}$ in 0.5 M H_2SO_4 at 31°C; (△) 400 μM Cu(II) in 0.5 M KCl at 34°C.

Fig. 9. Relationship between peak height of e vs. E curve and electrode area. Scan rate 100 mV s^{-1}. (○) 300 μM $Fe(CN)_6^{3-}$ in 0.1 M KCl at 32°C; (△) 200 μM Cu(II) in 0.5 M KCl at 33°C; (●) 50 μM $Cr_2O_7^{2-}$ in 0.5 M H_2SO_4 at 25°C.

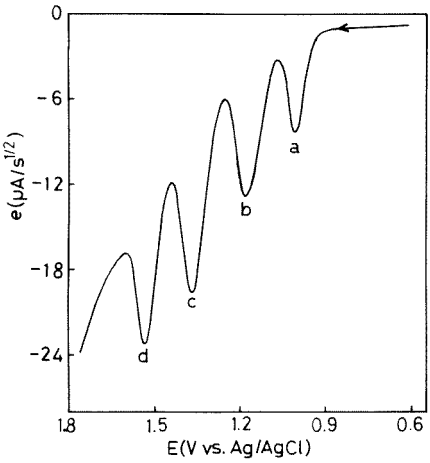

Fig. 10. Typical e vs. E curve for a mixture of 200 μM each of adenine, adenosine, guanine, and guanosine in Britton—Robinson buffer pH 2.6. Scan rate 100 mV s^{-1}; electrode area 7.07 mm^2; temperature 23°C. (a) Guanine; (b) guanosine; (c) adenine; (d) adenosine.

Conclusions

The theoretical predictions (except for W_p) concerning semidifferential electroanalysis with a planar electrode have been roughly confirmed with a stationary solid working electrode.

It is evident that semidifferential electroanalysis with a solid working electrode provides an attractive and efficient method for the identification and assay of electroactive species. The proposed technique provides better sensitivity (about one order of magnitude) and better resolution than ordinary linear sweep voltammetry, because of the symmetrical peak shape and relatively small interference of the electrical double layer, resulting from semidifferentiation of voltammograms. The time required for measurement in the technique is shorter than for differential pulse voltammetry. This is an important feature in achieving accurate results without significant change of the electrode surface state when solid working electrodes are used.

REFERENCES

1 M. Goto and D. Ishii, J. Electroanal. Chem., 61 (1975) 361.
2 P. Dalrymple-Alford, M. Goto and K. B. Oldham, J. Electroanal. Chem., 85 (1977) 1.
3 P. Dalrymple-Alford, M. Goto and K. B. Oldham, Anal. Chem., 49 (1977) 1390.
4 M. Goto, K. Ikenoya, M. Kajihara and D. Ishii, Anal. Chim. Acta, 101 (1978) 131.
5 M. Goto, K. Ikenoya and D. Ishii, Anal. Chem., 51 (1979) 110.
6 M. Goto, T. Hirano and D. Ishii, Bull. Chem. Soc. Jpn., 51 (1978) 470.
7 T. Yao, T. Wasa and S. Musha, Bull. Chem. Soc. Jpn., 50 (1977) 2917.

Analytica Chimica Acta, 126 (1981) 105—116
Elsevier Scientific Publishing Company, Amsterdam — Printed in The Netherlands

PHASE SOLUBILITY ANALYSIS OF MIXTURES OF TWO IONIC COMPOUNDS

Part 1. Completely or Nearly Completely Dissociated Electrolytes. A Novel Technique for Studying Ion-Pair Formation

SHYAM SHUKLA and LOUIS MEITES*

Department of Chemistry, Clarkson College of Technology, Potsdam, NY 13676 (U.S.A.)

(Received 17th December 1980)

SUMMARY

Curves having shapes that are unusual and difficult to interpret quantitatively are obtained in phase solubility analyses of samples containing two ionic substances that have an ion in common and that are extensively dissociated in the solvent employed. Procedures are described for the interpretation of such curves. They are based on non-linear regression, and their application is illustrated with the aid of data for a mixture of sodium and potassium iodates. They also yield information about ion-pair formation by the electrolytes involved.

Phase solubility analysis is a technique that has found many applications in analyzing mixtures of very closely related substances, such as geometrical or optical isomers or closely homologous compounds. The sample considered here contains two substances, A and B, whose properties are so similar that they cannot conveniently be separated or distinguished. By virtue of that similarity it is possible to determine the sum of their concentrations in a solution containing both. Different weights w of the sample are combined with appropriate volumes of a solvent in which the solubilities of both compounds are limited, and the mixtures are allowed to stand at constant temperature until dissolution is complete or until solubility equilibrium is attained. A portion of each clear supernatant solution is analyzed to determine the sum c of the concentrations of A and B in each, and the values of c are plotted against those of w/V, where V is the volume of the solution.

If the dissolved A and B do not interact, the plot consists of three linear segments, each having a slope smaller than the preceding one, as shown schematically in Fig. 1. At the lowest values of w/V there is a region, which is here called "region 1", in which the solid dissolves completely and the solutions are unsaturated with both A and B. At some point the solution will just be saturated with one component, say A, while it is still not saturated with the other. As w/V increases beyond that point, c continues to increase, but does so less rapidly than in region 1 because only the concentration of B increases while that of A remains constant. This portion of the plot is here

0003—2670/81/0000—0000/$02.50

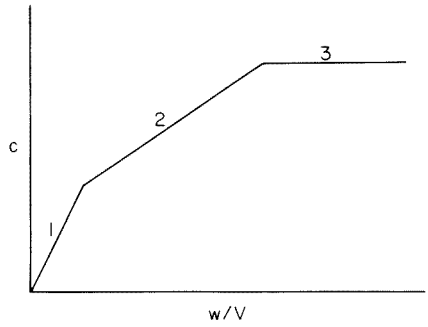

Fig. 1. Schematic curve obtained in the phase solubility analysis of a mixture of two compounds that do not interact.

called "region 2". As w/V increases further, the solution eventually becomes saturated with B as well as with A, and then c becomes independent of w/V. This final horizontal segment of the plot is here called "region 3".

The number of points of intersection of the linear segments is equal to the number of components of the sample. The ratios of the values of w/V at the points of intersection give the ratios of the weight fractions of the components. Reviews by Mader [1, 2] give detailed information about the interpretation of the data and about the complications that may arise.

Though this simple technique has been much used, especially in the pharmaceutical industry, for analyzing mixtures of non-ionic materials, there seems to be no mention in the literature of any attempt to apply it to mixtures of ionic substances that have an ion in common. The practical importance of such an attempt arises from the facts that amine hydrochlorides and many other ionic substances are common pharmaceutical materials, and that techniques for assaying them are often needed. The difficulty is obvious: if a mixture of A^+X^- and B^+X^- is analyzed in the fashion described above, the concentration of the common ion X^- increases as w/V increases in region 2, and its increase represses the solubility of A^+X^-. In addition, the ionic strength of the solution varies with the concentration of dissolved B^+X^-, and the solubility of A^+X^- is altered by the resulting variation of its mean ionic activity coefficient. For both these reasons, the concentration of A^+ is not independent of w/V, and therefore the variation of c with w/V is non-linear, in region 2. It is difficult to locate the points of intersection of the segments of the plot, and uncertainties in the composition of the sample result.

This paper describes a procedure for interpreting the data obtained in phase solubility analyses of such mixtures, and examines the results obtained by applying it to data secured with a mixture of sodium and potassium iodates. Special attention is paid to the problems that may arise from ionic association resulting from the chemical natures of the constituents of the sample and the limited value of the dielectric constant of the solvent employed.

THEORY

The sample considered contains the two ionic constituents A^+X^- and B^+X^-, and A^+X^- is identified as the one that does not dissolve completely in region 2. M_{AX} is defined as the gram-formula weight of A^+X^-, f_{AX} as the weight fraction of A^+X^- in the sample, K_{AX} as its thermodynamic solubility product in the solvent and at the temperature employed, $y_{\pm,AX}$ as its mean ionic molarity activity coefficient, and $\mathring{a}_{AX}$ as its Debye—Hückel distance of closest approach. The experimental variables c and w/V were defined above. In this section, it is assumed that both A^+X^- and B^+X^- are completely dissociated in all the solutions.

Neglecting hydrolysis and other possible side reactions, the electroneutrality principle requires that

$$c = [X^-] = [A^+] + [B^-] \tag{1}$$

in every region of the curve. This general equation takes different forms in different regions. In region 1, where both compounds dissolve completely, eqn. (1) becomes

$$c = [(f_{AX}/M_{AX}) + (1 - f_{AX})/M_{BX}] \; [w/V] \tag{2}$$

where M_{BX} represents the gram-formula weight of B^+X^-. It is assumed that c is expressed in mol dm^{-3}, w in g, and V in dm^3. In region 2, where the solutions are saturated with A^+X^- and the equation for its solubility product must be obeyed, eqn. (1) becomes

$$c = [(K_{AX}/y^2_{\pm,AX}\, c) + (1 - f_{AX})/M_{BX}] \; [w/V] \tag{3}$$

In region 3, where the solutions are saturated with both A^+X^- and B^+X^-, c has some constant value, which is here set equal to a new parameter S

$$c = S \tag{4}$$

It is required to find the value of f_{AX} that is most consistent with these equations and the experimental data.

Computations

That value can be found with the aid of non-linear regression, whose utility in such situations has become increasingly obvious during the last few years. For this purpose a general program [3], which had been written locally and used in applications of many different kinds, was employed. To it there had to be added a subroutine that would solve the above set of discontinuous equations to yield, for each of the experimental values of w/V, the value of c corresponding to the values of the parameters furnished to the subroutine by the main portion of the program. The main portion of the program compares these values of c with the measured ones, computes the sum of the squares of the deviations, and adjusts the values of the parameters so as to minimize this sum.

Of the quantities that appear in eqns. (2—4), w/V is the independent variable and c the dependent one; the value of M_{AX} will always be known a priori; and the quantity $y_{\pm,AX}$ varies with ionic strength in a way that may be represented by the Debye—Hückel equation, which for aqueous solutions at 25°C may be written

$$y^2_{\pm,AX} = \exp\,[-2.3532\, c^{1/2}/(1 + 0.3286\, \mathring{a}_{AX}\, c^{1/2})] \qquad (5)$$

in which c represents the ionic strength, as is appropriate for a 1:1 electrolyte. The gram-formula weight of the impurity, M_{BX}, which appears in eqns. (2) and (3), may be identical with M_{AX} and in any event will often be known. Computation time is minimized when the value of M_{BX} is known and when an estimate of $\mathring{a}_{AX}$ can be obtained from the apparent ionic diameters given by Kielland [4], using one of the approximations

$$\mathring{a}_{AX} \cong (\mathring{a}_{A^+} + \mathring{a}_{X^-})/2 \cong (a_{A^+}a_{X^-})^{1/2} \qquad (6)$$

For potassium and iodate ions Kielland gave $\mathring{a}_{K^+} = 3$ Å and $\mathring{a}_{IO_3^-} = 4$ Å, so that the expected value of $\mathring{a}_{KIO_3}$ is close to 3.5 Å. The effects of errors in M_{BX} and $\mathring{a}_{AX}$ are discussed below. Unless values can be assigned to both with reasonable certainty, both should be taken as adjustable parameters, and a five-parameter (f_{AX}, S, M_{BX}, K_{AX} and $\mathring{a}_{AX}$) fit is then involved. Both because more parameters have to be evaluated and because their interrelationships are much more intricate, this leads to a substantial increase of execution time.

In the simpler case there are consequently three adjustable parameters (f_{AX}, K_{AX}, and S) and three others whose values are unaltered during execution (M_{AX}, M_{BX}, and $\mathring{a}_{AX}$). The known or estimated values of all six are obtained in a short interactive dialogue at the start of execution. The initial value of S is obtained by asking for the number of points believed to lie in region 3 of the curve and averaging the values of c for those points. Very crude estimates of the other adjustable parameters suffice.

The heart of the program is the subroutine that computes the value of c corresponding to these values of the parameters, or to the values resulting from their subsequent adjustment, and one of the experimental values of w/V furnished to it by the main body of the program. The first step is to examine whether the preceding point was assigned to region 3. If so, the current point is assigned to region 3 as well; if not, it is tentatively assigned to region 1, a value of c is computed from eqn. (2), and the corresponding value of $y^2_{\pm,AX}$ is computed from eqn. (5). The inequality

$$K_{AX}/(y^2_{\pm,AX}\, c) > f_{AX}\, w/(M_{AX}\, V) \qquad (7)$$

whose significance is easy to deduce by comparing eqns. (2) and (3), is then examined. If it is satisfied, the value of c is consistent with the assumption — which was that the point belongs in region 1 — used to obtain it, and is accordingly returned to the main body of the program and used to calculate the square of its deviation from the experimental value at the point being examined.

If the inequality given by expression (7) is not satisfied, the solution must be saturated with AX according to the current values of the adjustable parameters, and consequently the point is tentatively assigned to region 2. New values of c and $y^2_{\pm,AX}$ are computed by solving eqns. (3) and (5) by successive approximation, and are used to examine the inequality

$$w/V < [M_{BX}/(1 - f_{AX})]\ [S - (K_{AX}/(y^2_{\pm,AX}\, S))] \qquad (8)$$

whose right-hand side is obtained by combining eqns. (3) and (4) and corresponds to the value of w/V at the point of intersection of regions 2 and 3.

If this inequality is satisfied, the value of c is consistent with the assumption that the point lies in region 2, and accordingly it is returned to the main body of the program. If it is not satisfied, or if the preceding point was assigned to region 3 by this process, c is assigned the value of S. In either event the square of the deviation from the experimental value of c is computed and summed, and the next value of w/V is supplied to the subroutine until all of the points have been examined.

EXPERIMENTAL

Ordinary reagent-grade chemicals, calibrated weights and glassware, and standard volumetric techniques were used throughout. The "samples" corresponded to mixtures containing 90.0% of potassium iodate and 10.0% of sodium iodate by weight ($f_{KIO_3} = 0.900$), but to avoid possible uncertainties resulting from incomplete mixing of the two solids each sample was prepared by weighing $0.9000w$ g of potassium iodate and $0.1000w$ g of sodium iodate into a 100-cm^3 volumetric flask. Exactly 100 cm^3 of water was added to each flask, and the flasks were placed in a water thermostat at 25.00 ± 0.01°C. After standing, with frequent shaking, until all of the solid had dissolved or until equilibrium had been attained, the flasks were left undisturbed until the supernatant solutions appeared to be completely clear, and an appropriate aliquot of each solution was removed with a pipet to whose tip a small tygon tube tightly packed with cotton was attached to ensure that no suspended solid would be taken. After removing the tygon tube the level of the solution in the pipet was adjusted to the mark, and the solution was discharged into an Erlenmeyer flask and analyzed by titration with a solution of sodium thiosulfate that had been standardized against the potassium iodate employed.

If the solubilities of all the components of the sample were small, all the values of w/V could be made so small that the volumes of undissolved material could be neglected, and then V could be taken to be equal to the total volume of the mixture. Sodium and potassium iodates are too soluble in water at 25°C to permit making that approximation. Consequently, the values of V for the points in regions 2 and 3 were calculated from the equation

$$V = (w + 100\, d_0 - u)/d \qquad (9)$$

where w, as defined above, is the total weight of sample combined with 100 cm^3 of water having a density equal to d_0 and weighing 100 d_0 g; u is the weight of material remaining undissolved after equilibrium has been reached; and d is the density of the solution. Values of u were determined (except in region 1, where of course $u = 0$) by filtering the entire amount of each mixture remaining from analysis of the supernatant liquid through a sintered-glass filtering crucible, applying prolonged suction to remove as much of the mother liquor as possible, and drying to constant weight at 110°C. Values of d were obtained with the aid of a Mettler/Parr model DMA 60 densitometer equipped with a model DMA 601 density-measuring cell.

There are two different statistical assumptions that can be made conveniently in processing the data: they correspond to two different ways of preparing the samples for analysis. One assumption is that the standard error of a single experimental value of the measured quantity (which in this work was a volume of a standard solution of thiosulfate, but which might equally well be an absorbance, a voltammetric limiting current, or any other quantity appropriate to the nature of the sample) is independent of w/V. When this assumption is to be made, equal volumes of the equilibrated solutions should be taken, and should be diluted to the same extent if dilution is needed to bring the measured quantity into a convenient range. The other assumption, which was adopted here, is that the relative standard error of measurement is independent of w/V. To justify this assumption, all the values of the measured quantity should be approximately equal, and the extent to which the equilibrated solutions are diluted, and the volumes of the diluted solutions taken for analysis must be chosen with a view to this end.

A procedure has been described [5] for deciding which of the experimental points have the greatest influence on the value of any particular parameter when several parameters are being evaluated simultaneously by non-linear regression. In the present situation, the points that have the greatest weight in computing f_{AX} are those in region 1. If the experiments are designed in such a way that the absolute standard error of measurement is independent of w/V, the relative standard error will generally be smallest for the points in region 3, will increase as c decreases, and may be unacceptably large for the most crucial points. It is therefore better to adopt the second of the alternatives described in the preceding paragraph.

RESULTS AND DISCUSSION

The data are shown in Fig. 2, which yields $f_{KIO_3} = 0.879$ when analyzed in the customary way. It may be noted that a generally similar plot, in which the curvature in region 2 arose from a different kind of interaction between the dissolved components, was observed and discussed by Bacher [6].

Analysis in the fashion described above, using the literature values of M_{NaIO_3} (197.89 g mol^{-1}) and $\mathring{a}_{KIO_3}$ (3.5 Å), gave $f_{KIO_3} = 0.8819$, $K_{KIO_3} =$

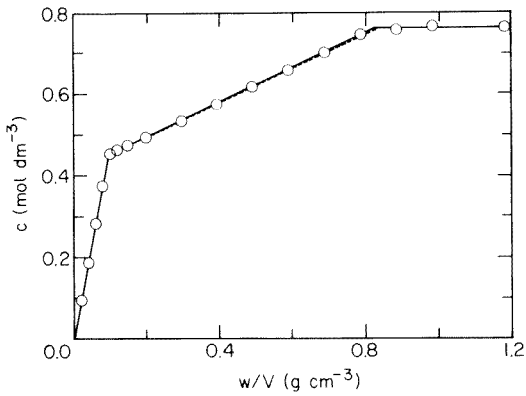

Fig. 2. The dependence of c on w/V for samples containing 90.0% of potassium iodate and 10.0% of sodium iodate by weight. The dashed straight line is drawn to aid in discerning the curvature in region 2.

7.52×10^{-2} mol^{2}dm^{-6}, and $S = 0.7589$ mol dm^{-3} with a relative standard deviation from regression of 2.89×10^{-3}.

The first of these values is slightly less erroneous than the one obtained from the traditional graphical treatment. It corresponds to the value $f_{NaIO_3} = 0.118$ for the weight fraction of the impurity, and the relative error in this value is generally similar to the relative errors expected in practical phase solubility analyses of simple systems that do not involve interactions of the dissolved constituents. The source of the error, and the way in which it can be eliminated, are discussed in a later section.

The value obtained for K_{KIO_3} may be assessed by combining it with eqn. (5) and with the assumed value of 3.5 Å for $\mathring{a}_{KIO_3}$ to compute the solubility s of potassium iodate in pure water at 25°C

$$K_{KIO_3} = s^2 \exp[-2.3532\, s^{1/2}/(1 + 0.3286\, \mathring{a}_{KIO_3}\, s^{1/2})] \qquad (10)$$

whose solution is $s = 0.4252$ mol dm^{-3} = 91.0 g dm^{-3}. The literature value [7, 8] is 90.6 ± 0.1 g dm^{-3}. The agreement between these figures shows that the value obtained for K_{KIO_3} is closely consonant with the truth if the assumption that $\mathring{a}_{KIO_3} = 3.5$ Å is correct.

The value of S would be equal to the mean of the experimental values of c in region 3 if there were no random errors in the data, and consequently no possible uncertainty in deciding whether any point belonged in region 2 or region 3. No value of S differing appreciably from that mean was ever obtained.

What has been discussed so far is the ideal situation, in which the identity of BX (and hence the correct value of M_{BX}) is known, and in which an a priori value can also be assigned to $\mathring{a}_{AX}$. In practice there will be many situations in which one or the other is unknown. Table 1 shows the penalties that ignorance of M_{BX} will exact. The value obtained for K_{KIO_3} hardly changes, as

TABLE 1

Effects of errors in M_{BX}
(It is assumed that the identity of BX is unkown, and that M_{BX} is accordingly assigned an incorrect value, which is given in the first column. The second and fourth columns give the values obtained for f_{KIO_3} and K_{KIO_3} by assuming that M_{KIO_3} = 214.00 and $\mathring{a}_{KIO_3}$ = 3.5 Å. Slight irregularities in these values arise from the arbitrary natures of the criteria that terminate execution.)

M_{NaIO_3} (g mol^{-1})	f_{KIO_3}	Mole % of KIO_3	K_{KIO_3}, ($\times 10^{-2}$ mol^{2}dm^{-6})	Relative standard deviation from regression ($\times 10^{-3}$)
175	0.8958	87.55	7.53	7.19
185	0.8897	87.46	7.53	4.67
190	0.8867	87.42	7.53	3.64
195	0.8836	87.37	7.52	2.98
200	0.8806	87.33	7.52	2.99
205	0.8775	87.28	7.52	3.65
210	0.8745	87.24	7.52	4.71
220	0.8692	87.23	7.55	7.21
230	0.8634	87.17	7.55	10.6
		87.34 ± 0.12[a]	7.53 ± 0.01[a]	

[a]Mean and standard deviation.

is to be expected, but that obtained for f_{KIO_3} varies considerably. Almost all of the variation results from defining f_{KIO_3} as the weight fraction of potassium iodate, for the corresponding values of the mole fraction of potassium iodate have a relative standard deviation of only 0.1%.

Table 2 shows the consequences of ignorance of $\mathring{a}_{AX}$. Here the value obtained for K_{KIO_3} varies considerably because it depends on $\mathring{a}_{KIO_3}$ as shown by eqn. (10). Of course, this variation scarcely affects the value of s obtained by combining the calculated value of K_{KIO_3} and the assumed one of $\mathring{a}_{KIO_3}$ with eqn. (10). There is also a variation of f_{KIO_3}; it is smaller than that in Table 1 but is still too large to be acceptable for many purposes.

Detailed analyses of the error surfaces involved in such calculations show that the values of M_{BX} and $\mathring{a}_{AX}$ are interrelated in such a way that both of these should be included among the adjustable parameters if the value of either is uncertain. There are then five parameters to be evaluated, and their values were found to be f_{KIO_3} = 0.8844, K_{KIO_3} = 7.08 × 10^{-2} mol^{2}dm^{-6}, S = 0.7589 mol dm^{-3}, M_{NaIO_3} = 195.98 g mol^{-1}, and $\mathring{a}_{KIO_3}$ = 2.99 Å. This value of f_{KIO_3} is slightly, but only very slightly, better than that obtained from the literature values of M_{NaIO_3} and $\mathring{a}_{KIO_3}$. The values of K_{KIO_3} and $\mathring{a}_{KIO_3}$ together give the solubility of potassium iodate in pure water as 90.0 g dm^{-3}, which is again within a few tenths of a percent of the literature value. It seems unnecessary to comment on the agreement between the value of M_{NaIO_3} obtained from this calculation and the literature value of 197.89.

TABLE 2

Effects of errors in $\hat{a}_{AX}$
(It is assumed that the properties of AX are so little known that $\hat{a}_{AX}$ is assigned an incorrect value, which is given in the first column. The second and third columns give the values obtained for f_{KIO_3} and K_{KIO_3} by assuming that M_{KIO_3} = 214.00 g mol^{-1} and M_{NaIO_3} = 197.89 g mol^{-1}.)

$\hat{a}_{KIO_3}$ (Å)	f_{KIO_3}	K_{KIO_3}, ($\times 10^{-2}$ mol^{2}dm^{-6})	Relative standard deviation from regression ($\times 10^{-3}$)
2.0	0.8877	6.15	2.57
2.5	0.8851	6.63	2.68
3.0	0.8833	7.09	2.80
3.25	0.8825	7.31	2.84
3.5	0.8819	7.52	2.89
3.75	0.8811	7.72	2.94
4.0	0.8807	7.92	2.99
4.5	0.8797	8.29	3.08
5.0	0.8788	8.64	3.15
	0.8823 ± 0.0028[a]		

[a]Mean and standard deviation.

Ion-pair formation

It was said above that mixtures of potassium and sodium iodates provide a severe test of the applicability of this procedure. In the foregoing sections, it has been assumed that potassium iodate is completely dissociated in aqueous solutions at 25°C, and this is known to be untrue. The formation of ion pairs in such solutions has been studied by several authors [9–12], and Smith and Martell [13] chose the value $K_d = a_{K^+} a_{IO_3^-} / a_{K^+IO_3^-} = 1.8_2 \pm 0.1_7$ mol dm^{-3} for the thermodynamic dissociation constant K_d.

To take the formation of A^+X^- ion pairs into account, eqn. (1) must be replaced by

$$c = [A^+] + [B^+] + [A^+X^-] \tag{11}$$

As before, c denotes the total concentration of dissolved material, which in the present case is the total concentration of iodate found by titration. Equations (2) and (4) are applicable in regions 1 and 3, respectively, regardless of whether dissociation is complete or not, but eqn. (3) must be replaced by

$$c = [K_{AX}/(y^2_{\pm,AX}\,(c - K_{AX}/K_d))] + [(1 - f_{AX})/M_{BX}]\;[w/V] + K_{AX}/K_d \tag{12}$$

in region 2. Consequently the criteria given by expressions (7) and (8) must be reformulated: if

$$[K_{AX}/(y^2_{\pm,AX}\,(c - K_{AX}/K_d))] + K_{AX}/K_d > f_{AX}\,w/M_{AX}\,V \tag{13}$$

the point belongs in region 1, but if

$$w/V < [M_{BX}/(1 - f_{AX})]\ \{S - [K_{AX}/(y^2_{\pm,AX}\,(c - K_{AX}/K_d))] - K_{AX}/K_d\} \quad (14)$$

the point belongs in region 3.

Assuming, as in the simple three-parameter fit described above, that M_{AX}, $\mathring{a}_{AX}$, and M_{BX} are all known (and are equal to 214.00 g mol^{-1}, 3.5 Å, and 197.89 g mol^{-1}, respectively, for a mixture of potassium and sodium iodates) gave $f_{KIO_3} = 0.8830$, $K_{KIO_3} = 6.42 \times 10^{-2}$ mol^{2}dm^{-6}, $K_{KIO_3}/K_d = 3.69 \times 10^{-2}$ mol dm^{-3}, and $S = 0.7589$ mol dm^{-3}, with a relative standard deviation from regression of 3.16×10^{-3}. These values of K_{KIO_3} and K_{KIO_3}/K_d correspond to $K_d = 1.74$ mol dm^{-3}, which is well within the range given by Smith and Martell [13]. According to eqn. (10), the values of K_{KIO_3} and $\mathring{a}_{KIO_3}$ correspond to $[K^+] = [IO_3^-] = 0.3884$ mol dm^{-3} in a saturated solution of potassium iodate in pure water; in addition, the concentration of the ion pair in such a solution is equal to $K_{KIO_3}/K_d = 0.0369$ mol dm^{-3}, so that the total solubility is 0.4253 mol dm^{-3} or 91.0 g dm^{-3}, again in close agreement with the known value.

However, even this treatment misrepresents the facts, for sodium iodate is also known to form ion pairs of appreciable stability [10, 13]; the single value in the literature corresponds to $K_{d,NaIO_3} = a_{Na^+}a_{IO_3^-}/a_{Na^+IO_3^-} = 3.0$ mol dm^{-3}. Equations (2) and (4) are still applicable in their respective regions, but region 2 must be described by writing

$$c = [A^+] + [B^+] + [A^+X^-] + [B^+X^-] \quad (15)$$

in place of eqns. (1) and (11). Since $[X^-] = [A^+] + [B^+]$, while the concentrations of free A^+ and B^+ ions are given by

$$[A^+] = f_{AX}\,w/(M_{AX}\,V) - [A^+X^-]$$

$$= f_{AX}\,w/(M_{AX}\,V) - (y^2_{\pm,AX}\,[A^+][X^-]/K_{d,AX}) \quad (16)$$

and, similarly,

$$[B^+] = [(1 - f_{AX})\,w/(M_{BX}\,V)] - (y^2_{\pm,BX}\,[B^+][X^-]/K_{d,BX}) \quad (17)$$

eqns. (15—17) may be combined to yield the cubic equation

$$(y^2_{\pm,BX}\,y^2_{\pm,AX}/K_{d,BX})\,[X^-]^3 + y^2_{\pm,BX}\,[X^-]^2 - \{[y^2_{\pm,BX}\,K_{AX}/K_{d,BX}] + [(1 - f_{AX})\,w/(M_{BX}\,V)]\}[X^-] - K_{AX} = 0 \quad (18)$$

which is solved by the Newton—Raphson method. Then $[A^+]$ and $[B^+]$ are evaluated by solving eqns. (16) and (17), respectively, and $[A^+X^-]$ and $[B^+X^-]$ are computed from the equation

$$[A^+X^-] = y^2_{\pm,AX}\,[A^+][X^-]/K_{d,AX}$$

and a similar equation for $[B^+X^-]$. Assignment of the point to the appropriate region is made by means of two criteria. If the inequality

$$[K_{AX}/(y_{\pm,AX}^2\,[X^-])] + K_{AX}/K_{d,AX} > f_{AX}\,w/(M_{AX}\,V)$$

is satisfied, the point belongs in region 1, and the value of c computed from eqn. (15) is discarded in favor of that computed from eqn. (2) before comparison with the experimental value of c. If the inequality

$$[(1-f_{AX})\,w/(M_{BX}\,V)] < [1+(y_{\pm,BX}^2\,[X^-]/K_{d,BX})]\,[S-(K_{AX}/(y_{\pm,AX}^2\,[X^-])) - (K_{AX}/K_{d,AX}) - [B^+X^-]]$$

is satisfied, the point belongs in region 2 and the value of c obtained from eqn. (15) is retained; otherwise it is discarded and replaced by the one ($c = S$) appropriate to region 3.

Values of $y_\pm$ were again obtained from eqn. (5), using $\mathring{a}_{AX}$ ($\mathring{a}_{KIO_3}$) = 3.5 Å and $\mathring{a}_{BX}$ ($\mathring{a}_{NaIO_3}$) = 4.0 Å on the basis of Kielland's compilation [4]. Taking M_{AX}, M_{BX}, and $K_{d,AX}$ (1.74 mol dm^{-3} according to the last fit described) as known, the results were f_{KIO_3} = 0.8923, K_{KIO_3} = 6.17 × 10^{-2} mol^{2}dm^{-6}, $K_{d,NaIO_3}$ = 0.31 mol dm^{-3}, and S = 0.7567 mol dm^{-3}. The value of $K_{d,NaIO_3}$ is much too low, and even the solubility of potassium iodate in water is underestimated by these figures [which give S = 0.4149 mol dm^{-3} = 88.9 g dm^{-3} on combining them with eqn. (10)], but the analytical result is greatly improved. The discrepancy between the literature value of $K_{d,NaIO_3}$ and the value obtained from this fit suggests that association of sodium and iodate is more extensive in the presence of potassium iodate (which is in large excess throughout much of region 2) than it is in solutions containing sodium iodate alone. This may reflect the formation of ion triplets such as $K^+IO_3^-Na^+$ and $Na(IO_3)_2^-$ under these conditions.

A similar fit, in which both $K_{d,NaIO_3}$ and K_{d,KIO_3} were taken as adjustable parameters, gave f_{KIO_3} = 0.8994, in nearly exact agreement with the expected value, but also gave clearly erroneous values for the dissociation constants of the two ion pairs. Such errors are to be expected if appreciable concentrations of either ion triplet are formed, for the description based only on the existence of ion pairs then misrepresents the concentrations of the dissolved species and the ways in which they depend on w/V.

Such problems are unlikely to arise in dealing with amine hydrochlorides and other substances of relatively high molecular weight, which are of most concern in applications of phase solubility analysis in the pharmaceutical industry. In general these substances are less soluble, and also contain larger ions, than potassium and sodium iodates, and for both these reasons are much less prone to ionic association. It is to be expected that the simple three-parameter fit based on eqns. (2–8) will give adequate analytical results with any of the mixtures to which the technique is likely to be applied in practice [14].

REFERENCES

1 W. J. Mader, Phase Solubility Analysis, in J. Mitchell, Jr., I. M. Kolthoff, E. S. Proskauer and A. Weissberger (Eds.), Organic Analysis, Interscience, New York, Vol. II, 1954, pp. 253–267.
2 W. J. Mader, Crit. Revs. Anal. Chem., 1 (1970/71) 193.
3 L. Meites, The General Multiparametric Curve-Fitting Program CFT4, Computing Laboratory of the Department of Chemistry, Clarkson College of Technology, Potsdam, NY, 1976.
4 J. Kielland, J. Am. Chem. Soc., 59 (1937) 1675.
5 L. Meites, Anal. Chim. Acta, 74 (1975) 177.
6 F. A. Bacher, unpublished work, cited in Ref. 1.
7 J. E. Ricci, J. Am. Chem. Soc., 56 (1934) 290.
8 A. E. Hill and S. F. Brown, J. Am. Chem. Soc., 53 (1931) 4316.
9 C. W. Davies, Trans. Faraday Soc., 26 (1930) 592.
10 W. H. Banks, E. C. Righellato and C. W. Davies, Trans. Faraday Soc., 27 (1931) 621.
11 C. B. Monk, J. Am. Chem. Soc., 70 (1948) 3281.
12 M. Spiro, Trans. Faraday Soc., 55 (1959) 1746.
13 R. M. Smith and A. E. Martell, Critical Stability Constants, Plenum, New York, 1976, Vol. 4, p. 126.
14 A copy of a computer program PHASOL effecting this fit, together with one of the general non-linear regression program CFT4 on which it is based, may be obtained by remitting $95.00 to the Computing Laboratory, Department of Chemistry, Clarkson College of Technology, Potsdam, NY 13676, U.S.A. Prior purchasers of CFT4 or its predecessors may obtain PHASOL alone by remitting $25.00 to the same address.

Analytica Chimica Acta, 126 (1981) 117—124
Elsevier Scientific Publishing Company, Amsterdam — Printed in The Netherlands

SEPARATION OF URANIUM FROM MOLYBDENUM USING A DIAMINE FUNCTIONAL GROUP BONDED TO CONTROLLED-PORE GLASS

S. E. NORTHCOTT and D. E. LEYDEN*
Department of Chemistry, University of Denver, Denver, CO 80208 (U.S.A.)
(Received 8th December 1980)

SUMMARY

A method for selective extraction of uranium from carbonate solutions containing molybdate is reported. A liquid chromatography column, packed with N-β-aminoethyl-γ-aminopropyltrimethoxysilane immobilized on a glass substrate, was utilized in a continuous flow system. The selective retention of the uranyl carbonate species $[UO_2(CO_3)_2 \cdot 2H_2O]^{2-}$ and $UO_2(CO_3)_3^{4-}$ on protonated immobilized diamine is the basis for this separation. Recoveries of uranium and molybdenum from synthetic samples ranged from 96.7 to 113.4% for uranium and from 96.7 to 110.5% for molybdate for a range of recommended conditions.

The rapid separation of uranium from molybdenum and other elements and its subsequent recovery is of continuing interest to the mining industry as well as chemical analysts. Uranium and molybdenum are often concomitant elements in natural ore samples. A variety of methods for uranium detection and recovery have been previously reported [1—9]. Ion-exchange chromatography has enjoyed widespread use as a separation and preconcentration tool for metal ions [10, 11] and uranium extraction by ion-exchange chromatography has been reported [5—8]. Chemically bonded immobilized chelates have been shown to be useful for metal ion recovery and preconcentration [12—17].

Specifically, N-β-aminoethyl-γ-aminopropyltrimethoxysilane immobilized on controlled-pore glass, has been used to preconcentrate several cations and anions prior to quantification by x-ray fluorescence [18—20]. Previous studies of uranium and molybdenum extraction using immobilized diamine [19—21] have shown a pH-dependence for the extraction of both metals. Figure 1 is a composite of these pH data. Distribution coefficients were not published, but the possibility of chromatographic separation of uranium and molybdenum is suggested by the shapes of the plots and relative positions of the extraction maxima.

This paper describes a continuous-flow separation of uranium from molybdenum based on the complexation of uranyl carbonate with an immobilized diamine functionality. Step gradient chromatography is used to control the pH of the mobile phase, and, hence, the chemistry of selective

0003—2670/81/0000—0000/$02.50

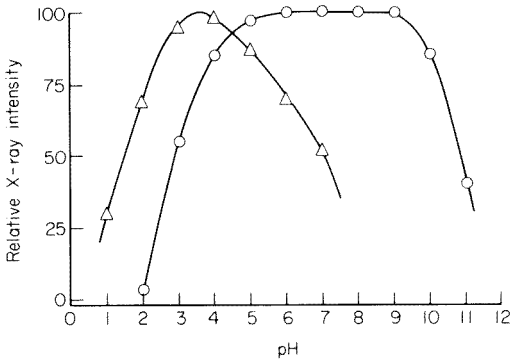

Fig. 1. Dependence of extraction upon pH for $UO_2(CO_3)_3^{4-}$ [21] and MoO_4^{2-} [19]: (△) MoO_4^{2-}; (○) $UO_2(CO_3)_3^{4-}$.

uranium extraction. The stationary phase in the column is N-β-aminoethyl-γ-aminopropyltrimethoxysilane bonded to controlled-pore glass particles.

EXPERIMENTAL

Apparatus

The flow system consisted of a glass liquid chromatography column, 25.0 cm × 0.6 cm diameter, an Altex pump (Model 110A) and a six-way solvent selection valve (Rheodyne 5012). All connections were made with teflon tubing (1.5 mm i.d. × 3.0 mm o.d.) or stainless steel tubing (0.25 mm i.d. × 1.5 mm o.d.). A spectrophotometer (Bausch-Lomb Spectronic 20) and an atomic absorption spectrophotometer (Perkin-Elmer Model 2380) were used to detect and quantify the uranyl and molybdate ions, respectively in the effluent samples from the column.

Reagents

The silylated controlled-pore glass was prepared by stirring 6 g of controlled-pore glass (120—200 mesh; Electronucleonics, Inc.) in 0.1 l of a 1% (v/v) toluene solution of N-β-aminoethyl-γ-aminopropyltrimethoxysilane (Dow Corning Z6020). The reaction time was 30 min. The silylated glass was collected in a Büchner funnel on Whatman filter paper, washed with toluene, then washed with isopropanol. Finally, the glass was dried in a vacuum oven for 12 h at 80°C. The resultant immobilized diamine had a capacity of 0.35 mmol of UO_2^{2+} per gram of glass as measured by a breakthrough experiment.

All reagents were Baker Analyzed Reagents except for the 4-(2-pyridylazo)-resorcinol (Eastman Kodak). The buffer solutions were 0.1 mol l^{-1} potassium hydrogenphthalate (pH 3.0) and 0.1 mol l^{-1} potassium dihydrogenphosphate (pH 8.0). The colorimetric reagent used in the spectrophotometric determination of uranium was 3.0×10^{-5} mol l^{-1} 4-(2-pyridylazo)resorcinol (pH 9.0). The buffer solution (pH 9.0) used with this reagent was 1.0 mol l^{-1}

triethanolamine [4]. Stock solutions containing uranium and molybdenum were prepared from uranyl acetate dihydrate and ammonium paramolybdate and ammonium carbonate. The stock solutions were divided into two sets. Set 1 contained a series of four solutions in which $C_U < C_{Mo}$; the uranium concentration in each solution was 8.8 mg l^{-1}, and the molybdenum concentrations were 60, 600, 3000, and 6000 mg l^{-1} in the series, each solution being 0.01 mol l^{-1} in ammonium carbonate (pH 8.0). Set II contained four solutions in which $C_{Mo} < C_U$; the molybdenum concentration in each solution was 6.0 mg l^{-1}, and the uranium concentrations were 88, 882, 4410 and 6300 mg l^{-1}, each solution being at pH 3.0 with no ammonium carbonate present.

Capacity study of silylated controlled-pore glass

The chromatography column was dry-packed with 2.1 g of the silylated controlled-pore glass. The support bed was 8.0 cm × 0.6 cm diameter. Capacity for retention of uranium was measured in a breakthrough experiment. The column was adjusted to pH 8.0 with 0.1 mol l^{-1} potassium dihydrogenphosphate buffer solution. A solution containing 882 mg U l^{-1} and 0.01 mol l^{-1} ammonium carbonate was administered to the column until uranium breakthrough was detected. All of the bed material was bright yellow, and remained so until dilute nitric acid was used to elute the extracted uranium. The uranium effluent was collected and volumetrically diluted, and uranium was determined by the spectrophotometric method [4].

Flow rate studies

A working range was established for the flow rate of the column system. Extractions of uranyl carbonate were conducted at flow rates between 0.44 and 4.42 cm min^{-1}. For each extraction, the composition of the mobile phase in the column was sequentially changed using a 6-way solvent switching valve. The solvent cycle was: 25 ml of water, 25 ml of buffer, 200 ml of uranium/molybdenum stock solution, 25 ml of buffer, 25 ml of water, 25 ml of 0.1 mol l^{-1} HNO_3, 25 ml of water. The buffer solution was potassium dihydrogenphosphate (pH 8.0). The stock solution contained 8.8 mg U l^{-1}, 600 mg Mo l^{-1} and 0.01 mol l^{-1} ammonium carbonate. Column effluent was collected in two steps. Sample A contained all the effluent generated before switching to nitric acid in the solvent cycle. Sample B contained the effluent generated during the interval of nitric acid elution. Uranium and molybdenum contents were determined in these samples.

Molybdenum concentration and extraction studies

Extractions of uranyl carbonate from solutions containing different amounts of molybdate were conducted. The column bed was employed, and the flow rate was 2.65 cm min^{-1} for each experiment. Again, a solvent cycle was employed analogous to the one described above. The buffer was potassium dihydrogenphosphate (pH 8.0). Stock solutions of uranyl and molybdate

ions were those enumerated in Set I under Reagents. The column effluent was collected in two steps as above, and the uranium and molybdenum contents were determined.

For the extraction studies, the same column bed of silylated controlled-pore glass was used. The composition of the mobile phase was changed by use of the solvent cycle described above. The buffer was 0.1 mol l^{-1} potassium hydrogenphthalate, and the uranium and molybdenum stock solutions were those given in Set II under Reagents. The flow rate was 2.65 cm min^{-1}, and the column effluent was collected into one sample. Uranium and molybdenum were determined in this sample later.

Uranium and molybdenum determinations

The spectrophotometric determination of the uranium content of the effluent samples employed 4-(2-pyridylazo)resorcinol (PAR) [4]. For each determination, 5 ml of triethanolamine buffer and 25 ml of 3×10^{-5} mol l^{-1} PAR solution were placed into a 50-ml volumetric flask. An aliquot of effluent sample was added to the flask and the solution was diluted to volume. The absorbances of this solution and a similar set of uranium standards (0.0—1.3 mg l^{-1}) were measured at 530 nm.

The molybdenum content of each effluent sample was determined after volumetric dilution by atomic absorption spectrometry. The absorption of a solution containing an aliquot of effluent sample was measured at 313 nm. Absorptions of a set of standard molybdenum solutions (0.0—42.0 mg l^{-1}) were measured for calibration.

DISCUSSION

The use of silylated glass and silica surfaces in metal ion extraction from aqueous solution is well known [18–23], and the chemistry of N-β-aminoethyl-γ-aminopropyltrimethoxysilane (AEPTS) immobilized on silica is thought to be analogous to that of ethylenediamine [18]. Evidence showing that separation of uranium from molybdenum is possible by complexation of a uranyl carbonate anion with protonated AEPTS substrate is presented below.

The complexation of the uranyl carbonate and molybdate anions with AEPTS immobilized on silica or glass particles has been shown to be pH-dependent [19—21]. The nature of this pH-dependence, plotted in Fig. 1, can be understood by examining the acid—base chemistry of surface-bound AEPTS and the acid—base chemistry of the uranyl carbonate and molybdate anions.

The plot of pH/extraction data for uranyl carbonate shows a plateau (pH 5.0—9.0) corresponding to maximum interaction between the AEPTS substrate and the uranyl carbonate anion. The extraction of uranyl carbonate by complexation with an immobilized diamine depends on two factors: the stability of the uranyl carbonate anion in solution is one factor, and the pro-

tonation of the diamine functionality is the other. Two uranyl carbonate anions are formed by UO_2^{2+} in carbonate solution [24]

$$UO_2^{2+} + 2CO_3^{2-} \rightleftharpoons [UO_2(CO_3)_2 \cdot 2H_2O]^{2-} \quad (\beta_2 = 4 \times 10^{14}) \tag{1}$$

$$UO_2^{2+} + 3CO_3^{2-} \rightleftharpoons UO_2(CO_3)_3^{4-} \quad (\beta_3 = 2 \times 10^{18}) \tag{2}$$

These anions are stable between pH 5.0 and 11.0 [25]. No distinction will be made between these two anions in their ability to form ion pairs with the protonated AEPTS substrate. Evidence that the diamine functionality is protonated can be drawn from the acid—base solution chemistry of ethylenediamine, a model compound for the immobilized AEPTS. The pK_{b1} and pK_{b2} for ethylenediamine (en) are 4.07 and 7.15, respectively.

Calculation of the ratio of diprotonated to monoprotonated ethylenediamine at pH 5.0 gives $[enH_2^{2+}]$: $[enH^+]$ = 71:1. At pH 9.0, $[enH^+]$: [en] = 8.5:1. The fact that ethylenediamine is protonated between pH 5.0 and 9.0 suggests that the immobilized diamine is also protonated in this pH range. Above pH 9.0, the extraction/pH plot for the uranyl carbonate anion decreases sharply as does the ratio of protonated to unprotonated diamine. The extraction/pH plot for uranyl carbonate anion also decreases dramatically below pH 5.0, even though the AEPTS substrate is diprotonated. This large decrease in extraction in acidic solution is due to the dissociation of the uranyl carbonate anion to yield UO_2^{2+} as the major uranium species in solution. No ion pair is formed between UO_2^{2+} and the positively charged diprotonated AEPTS substrate. At pH 8.0, the pH of the mobile phase used in these extraction experiments, the uranyl carbonate anion is complexed with the protonated AEPTS immobilized on the surface of the column packing.

The absence of molybdate complexation with immobilized AEPTS at pH 8.0 allows for recovery of the molybdenum in the effluent from the column while the uranium is retained on the bed. A discussion of the pH-dependence of the molybdate interaction with the silylated surface is warranted. Figure 1 shows a plot of molybdenum extraction as a function of pH for AEPTS immobilized on controlled-pore glass. At pH 3.0, the molybdate extraction curve shows a maximum, with a large decrease on either side. Molybdenum complexed with the immobilized AEPTS has been shown to be monomeric MoO_4^{2-} [20], and the diamine functionality of the AEPTS is diprotonated at pH 3.0. (The ethylenediamine model compound has a pK_{b2} = 7.15.) The ability of the immobilized AEPTS to extract molybdate decreases on either side of pH 3.0. This appears to be a combination of two effects. The equilibria of molybdate ions in acidic solution favor the formation of polymeric molybdate anions [26], so less monomeric MoO_4^{2-} is available for complexation below pH 3.0. The decrease in molybdate extraction above pH 3.0 follows the decrease in the ratio of diprotonated to monoprotonated AEPTS substrate as pH increases. At pH 8.0, monoprotonation of the AEPTS substrate predominates, and little complexation of molybdate occurs.

TABLE 1

Flow rates employed during uranium extraction and corresponding recovery values for uranium and molybdenum

Flow rate (cm min^{-1})	U recovery[a] (%)	Mo recovery[b] (%)
0.44	113.4	100.0
0.88	96.7	96.7
1.77	104.9	110.5
2.65	107.8	97.0
3.54	99.6	97.1
4.42	32.0	100.0
4.42	32.5	96.9

[a]Uranium concentration 8.8 mg l^{-1}. [b]Molybdenum concentration 600 mg l^{-1}.

In order to establish a working range for this flow separation technique, the flow rate of the mobile phase and the concentration of molybdate in the analyte solution were varied in extraction experiments using the column bed. The column effluent was collected in two samples, as described in Procedure, and the molybdenum and uranium content of each sample was determined for comparison with the starting amount taken. The percentage recovery of uranium and molybdenum and the set of flow rates employed are given in Table 1. The recovery of uranium and molybdenum was independent of the flow rate employed over a range of 0.44 to 3.54 cm min^{-1}. The mean recovery of uranium for this range was 104.5 ± 6.6%, and the mean molybdenum recovery was 100.3 ± 5.9%. A large decrease in uranium recovery was observed at 4.42 cm min^{-1}, probably resulting from incomplete elution of the uranyl carbonate from the column bed. Flow rates greater than 4.42 cm min^{-1} were not used, to avoid excessive pressure inside the glass column.

A series of four molybdenum concentration variation experiments were conducted at 2.65 cm min^{-1}, a flow rate inside the established working range. Separation and recovery of uranium and molybdenum was observed to be independent of molybdenum concentration for solutions containing 60—6000 mg Mo l^{-1}. The mean recovery of uranium was 99.3 ± 6.9% and the mean recovery of molybdenum was 94.7 ± 1.6% in this study.

The observation of selective extraction of uranium from molybdenum at pH 8.0 using a column bed of AEPTS on controlled-pore glass led to a complementary study. The selective extraction of molybdenum at pH 3.0 (the pH of maximum molybdate complexation with immobilized AEPTS) was attempted. A series of four experiments was conducted. The molybdenum concentration was held constant and the uranium concentration was varied. Table 2 shows the uranium concentration range and the molybdenum and uranium recovery data. Uranium and molybdenum occur together in the column effluent. A separation was not obtained at pH 3.0.

TABLE 2

Concentration of uranium in the stock solution and corresponding recovery values for uranium and molybdenum

U concentration (mg l^{-1})	U recovery (%)	Mo recovery (%)
88	84.4	13.8
882	81.2	58.5
4410	104.6	61.8
6300	79.6	142.1[a]

[a]Molybdate from a previous experiment was present in this effluent.

The absence of the uranyl carbonate complex at pH 3 allows for ion pairing between uranyl and molybdate ions in solution. This interaction between the uranium and molybdenum species prevents 100% extraction of the molybdate by positively charged AEPTS on controlled-pore glass. The effect of increasing the uranium concentration in the analyte solution appears to be an increase in the percentage of molybdate that is not extracted.

This work was supported in part by Research Grant CHE 78-23123 from the National Science Foundation and by the AMAX Foundation.

REFERENCES

1 C. J. Rodden (Ed.), Analytical Chemistry of the Manhattan Project, McGraw-Hill, New York, 1950, p. 14.
2 J. J. Katz and E. Rabinowitch, The Chemistry of Uranium, Vol. 1, McGraw-Hill, New York, 1951, p. 111.
3 A. R. Main, Anal. Chem., 26 (1954) 1507.
4 T. M. Florence and Y. Farrar, Anal. Chem., 35 (1963) 1613.
5 K. A. Kraus, F. Nelson and G. E. Moore, J. Am. Chem. Soc., 77 (1955) 3972.
6 J. Korkisch and L. Godl, Anal. Chim. Acta, 71 (1974) 113.
7 E. S. Gladney, J. W. Owens and J. W. Starner, Anal. Chem., 48 (1976) 973.
8 L. R. Hathaway and G. W. Jones, Anal. Chem., 47 (1975) 2035.
9 B. B. Jablonski and D. E. Leyden, Anal. Chem., 51 (1979) 681.
10 F. Helfferich, Adv. Chromatogr., 1 (1965) 3.
11 H. F. Walton (Ed.), Ion Exchange Chromatography, Dowden, Hutchinson and Ross, Stroudsburg, PA, 1950.
12 K. F. Sugaware, H. H. Weetall and D. G. Schucker, Anal. Chem., 46 (1974) 489.
13 E. Gruska, Bonded Stationary Phases in Chromatography, Ann Arbor Science Publishers, Ann Arbor, MI, 1974.
14 D. M. Hercules, L. E. Cox, S. Onisick, G. D. Nichols and J. C. Carver, Anal. Chem., 45 (1973) 1973.
15 J. M. Hill, J. Chromatogr., 76 (1973) 455.
16 J. R. Parrish, Lab. Pract., 24 (1975) 399.
17 D. C. Locke, J. Chromatogr. Sci., 11 (1973) 120.
18 D. E. Leyden and G. H. Luttrell, Anal. Chem., 47 (1975) 1612.
19 D. E. Leyden, G. H. Luttrell, W. K. Nonidez and D. B. Werho, Anal. Chem., 48 (1976) 67.

20 D. E. Leyden, M. L. Steele, B. B. Jablonski and R. B. Somoano, Anal. Chim. Acta, 100 (1978) 545.
21 B. B. Jablonski and D. E. Leyden, in C. S. Barrett, D. E. Leyden, J. B. Newkirk and C. O. Ruud (Eds.), Advances in X-Ray Analysis, Vol. 21, Plenum, New York, 1978, p. 59.
22 J. R. Jezorek and H. Freiser, Anal. Chem., 51 (1979) 366.
23 T. Seshadri and A. Kettrup, Fresenius Z. Anal. Chem., 296 (1979) 247.
24 L. A. Maclaine, Proc. Int. Conf. Peaceful Uses At. Energy, 8 (1956) 30.
25 F. Habashi, Principles of Hydrometallurgy, Vol. 2, Gordon and Breach, New York, 1970, p. 217.
26 D. H. Killeffer and A. Linz, Molybdenum Compounds, Interscience, New York, 1952, p. 81.

Analytica Chimica Acta, 126 (1981) 125—133
Elsevier Scientific Publishing Company, Amsterdam — Printed in The Netherlands

THE USE OF AN INEXPENSIVE ELECTRONIC FILTER FOR IMPROVING DETECTION LIMITS IN THE GAS CHROMATOGRAPHIC—CHEMILUMINESCENT DETERMINATION OF NITROSAMINES

MARTIN E. B. BROWN[a], DIGBY L. JAMES* and JOHN WARREN

Department of Industry, Laboratory of the Government Chemist, Cornwall House, Stamford Street, London SE1 9NQ (Gt. Britain)

(Received 6th December 1980)

SUMMARY

The construction and use of an electronic noise filter is described. It is evaluated by use with a laboratory-built selective chemiluminescent detector used for the gas chromatographic analysis of mixtures of volatile *N*-nitrosamines. A ten-fold reduction in the noise level was achieved with a corresponding decrease in detection limit to 4 nl l^{-1}.

This study is concerned with the construction of a simple and inexpensive electronic filter to reduce the noise associated with a selective chemiluminescent detector [1] (Fig. 1) for the gas chromatographic analysis of volatile *N*-nitrosamines. The principle of operation of the detector is based on the catalytic cleavage of the N—NO bond of any nitrosamines eluting from the gas chromatograph into the catalytic pyrolyzer, liberating nitric dioxide. This passes through a U-tube at —136°C to freeze out any organic fragments of the pyrolysis which may interfere with the chemiluminescent reaction. The gases remaining flow into the reaction chamber and react with ozone to form electronically excited nitrogen dioxide. This rapidly returns to its ground state with the emission of radiation in the range 600—2000 nm (λ_{max} = 1200 nm). This emission is detected by a photomultiplier tube with extended red sensitivity behind a 610-nm cut-off filter to eliminate emissions of shorter wavelength caused by other reactions such as those of carbon monoxide or ethylenic compounds with ozone. Photomultiplier sensitivity falls off very rapidly in the red/infra-red region, so that the photomultiplier only sees a small proportion of the emission (Fig. 2). This is, nonetheless, a sensitive technique and a commercial instrument [2] based on the same principles has a detection limit of 10 nl l^{-1}.

Nitrosamines have been found to be carcinogenic toward many animal species and they are strongly suspected of also being carcinogenic to humans [3]. Most nitrosamine determinations are concerned with samples from the

[a]Present address: Plasma-Therm Ltd., 6 Station Road, Penge, London, SE20 7BZ, Gt. Britain.

0003—2670/81/0000—0000/$02.50

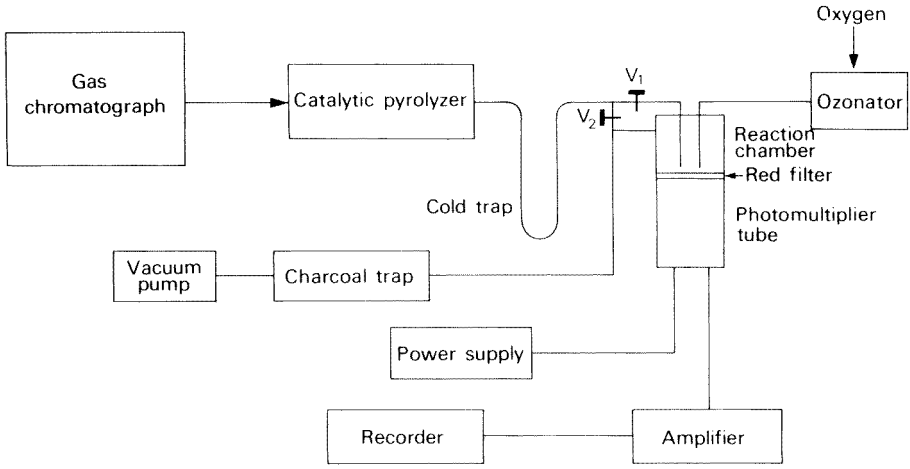

Fig. 1. Schematic diagram of the selective chemiluminescence detector system.

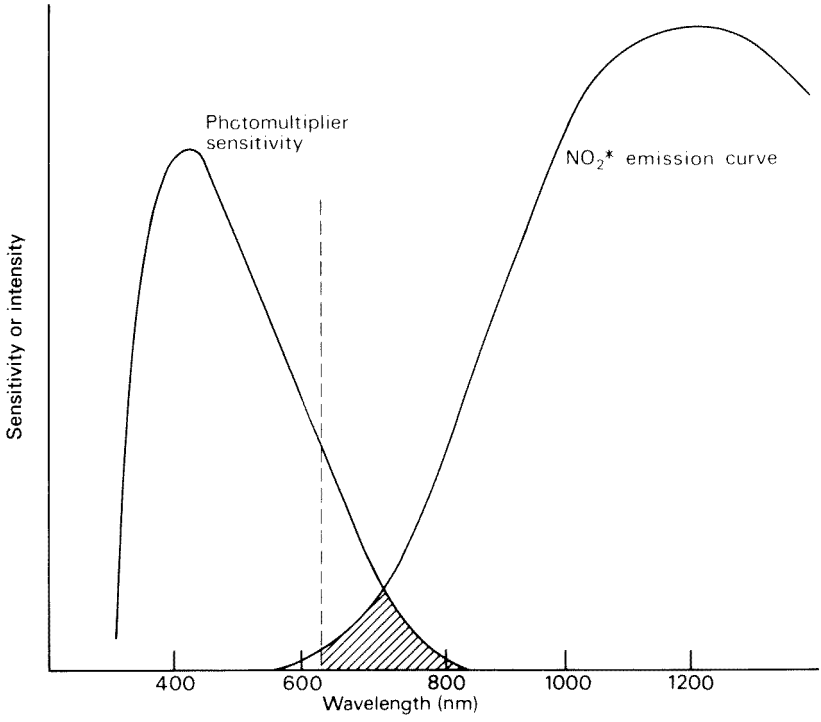

Fig. 2. Photomultiplier tube sensitivity compared with the emission from the reaction between NO and O_3.

human environment and these often have nitrosamines in the nl or sub-nl l^{-1} range. Extraction and preconcentration can bring samples into the $\mu l\ l^{-1}$ or sub-$\mu l\ l^{-1}$ range so that the analytical instrumentation must be capable of measuring such levels.

The instrument used in the present study was previously reported [1] to have a detection limit of 0.1 $\mu l\ l^{-1}$ and so could be used only for the screening of fairly concentrated samples. In this Laboratory, however, analyses of samples in the sub-$\mu l\ l^{-1}$ range are required regularly, and so efforts were made to improve the detection limit by the optimisation of each instrumental variable. Several changes were made in instrumentation and operation (which are detailed in the Experimental section). The major effort was put into the reduction of photomultiplier noise. Placing the photomultiplier tube inside a refrigerated water-cooled housing to minimise dark current noise gave a reduction in the dark current but achieved only a small reduction in the noise. Several resistive/capacitive circuits were used to damp out the noise, but these seriously affected sensitivity and caused peak broadening. The sum of all these efforts failed to achieve a lower detection limit, and so the use of an active electronic filter was considered.

Theory of electronic filters

Analytical devices and their associated detectors contribute electrical noise to the output signal. This noise is usually at a frequency higher (i.e., of shorter period) than that of the output analytical signal. The unwanted noise can be removed by a low-pass filter. This essentially allows all signals below its cut-off frequency F_c to pass through the filter to the output, and frequencies above the cut-off frequency to be eliminated. The characteristics of an ideal low-pass filter are shown in Fig. 3a. The cut-off frequency is chosen so that the frequency of the noise is above the cut-off frequency and the

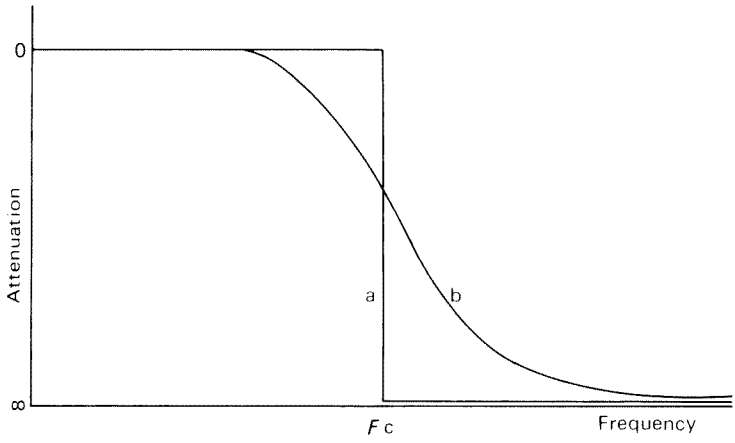

Fig. 3. (a) Ideal and (b) actual attenuation rates for noise filters.

required signal placed below the cut-off frequency, enabling the latter to be passed through the filter unattenuated.

In practice, the ideal response shown in Fig. 3a can never be achieved. The main problem lies in obtaining an infinite cut-off slope or attenuation rate (a sharp cut-off point) at the cut-off frequency. The response generally obtained is shown in Fig. 3b.

Another problem associated with electronic filters is insertion loss. This is the loss of signal response caused by the presence of the capacitors and resistors of a filter, and represents the amount of attenuation within the pass band of the filter. Both of these practical disadvantages occur in the simple resistive/capacitive (RC) type filter where a resistor is in series with the signal output and a capacitor is in parallel with it.

If it is assumed that the input resistance, R_L, of the device to which the filter output is connected is finite, there will be an insertion loss equal to $R_L/[R_1(1 + j\omega CR_L) + R_L]$. This is usually significant. Also, the cut-off slope is usually shallow, which is inadequate for effective filtering and is represented by an output response that halves the output voltage for every octave of frequency above F_c.

The analytical signals from most general analytical instruments such as gas chromatographs and spectrophotometers usually have very low periods. This creates another problem for the RC circuit referred to above. To achieve the correct value of F_c, very large capacitors and resistors would have to be used, which could create very high insertion losses. More complicated passive filter networks can be devised which can improve the cut-off slope and insertion loss parameters. However, trade-offs are always necessary and compromises can be considerable.

A better method of filtering is possible by using active filter technology. This involves passive elements (resistors and capacitors) connected around an electronic amplifier. There are several configurations of such filters, and an example utilising an operational amplifier is shown in Fig. 4. Active filters can be cascaded (connected in series) to produce very high attenuation rates

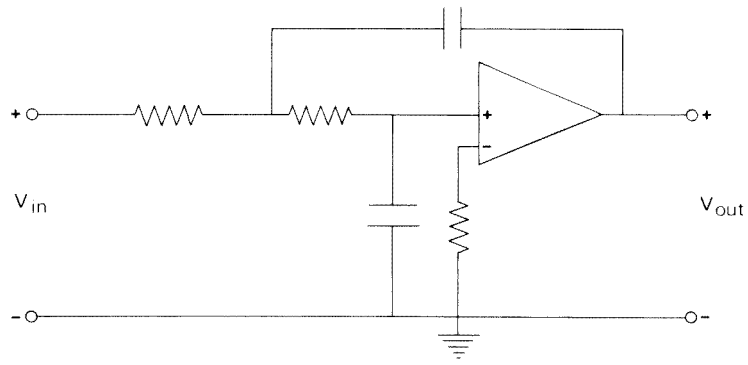

Fig. 4. Circuit diagram of a second-order low-pass active filter.

with a minimum insertion loss and can be designed to have cut-off frequencies as low as 0.01 Hz. Another advantage is that the active filter can be designed to achieve an extremely high attenuation rate immediately above the cut-off frequency, which is not possible with simple passive networks. This facility allows noise very close in frequency or period to the desired signal to be attenuated.

It is possible to purchase active filters in modular form that only require the external connection of a few resistors to establish the required parameters of cut-off frequency and response. The modules have a size of only a few centimetres and are relatively easy to implement and inexpensive to purchase. A typical circuit diagram is shown in Fig. 5. This arrangement utilises two filter modules in cascade, which produces a reduction in output signal above the cut-off frequency of about 16 times per octave. The input voltage of these two modules must not exceed certain levels, depending on the type of module, and so the first amplifier has a gain chosen to meet this criterion for a specific input. The gain of the amplifier is calculated from $(R_1 + R_2)/R_2$. The output amplifier acts as a buffer or isolation amplifier, and by adjustment of the preset potentiometer, any d.c. offset voltage produced up to this stage can be eliminated. The remaining resistor values are calculated from manufacturers' data sheets and are easily derived once the cut-off frequency, type of response and order of the filter are known.

The cut-off frequency. This can be estimated as long as there is an instrument for visually displaying the analytical signal, such as a chart recorder or storage oscilloscope. Because the analytical signal does not have, usually, a periodic waveform, it is more correct to estimate the frequency from the rise time of this signal and the associated noise. For example, if the desired analytical signal takes approximately 2 s to reach 90% of its peak height, this would correspond to an approximate frequency of $1/(2 \times 4) = 0.125$ Hz if the waveform is periodic. If the slowest component of the noise has an approximate rise time of 0.5 s, then the associated frequency for a periodic waveform would be $2/4 = 0.5$ Hz. Thus, the cut-off frequency should be chosen to be between these two values, preferably as close as possible to 0.125 Hz without causing degradation to the required output signal.

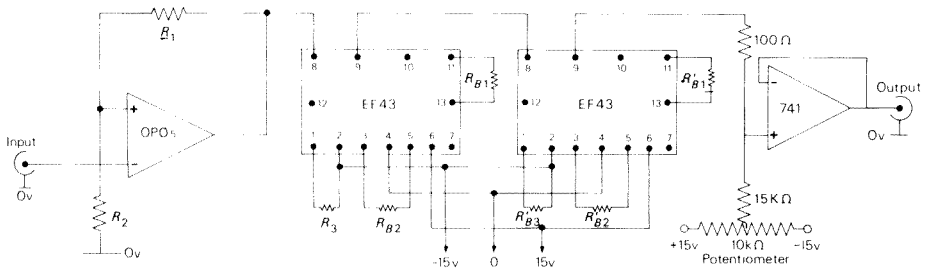

Fig. 5. Circuit diagram of an active electronic filter.

Types of response. There are essentially three main types of response, Bessel, Butterworth and Chebychev [4]. The essential differences between these responses is that Chebychev has an extremely high attenuation rate immediately after the cut-off frequency, but contains a ripple attenuation within the pass band. The Butterworth has the flattest response within the pass band and a reasonably good attenuation rate, whereas the Bessel shows the best phase response with the flattest delay characteristics. This response allows more exact copying of the analytical signal with a slight degradation of the attenuation rate. The response chosen is selected by different combinations and values of resistors and capacitors and the way that they are grouped around the active filter units.

Order of filter. This essentially relates to the final attenuation rate. A single-order filter will have a response that will halve its output for every octave in frequency after the cut-off frequency. A second-order filter will quarter its output per octave, a fourth-order filter will divide its output by a factor of sixteen, and so on.

EXPERIMENTAL

Preparation of standards

Standard nitrosamine solutions containing three volatile nitrosamines, nitrosodimethylamine (NDMA), nitrosodiethylamine (NDEA) and nitrosodipropylamine (NDPA) were prepared at 100 μl l^{-1}, 10 μl l^{-1}, 1 μl l^{-1} and 0.1 μl l^{-1} concentrations. These were prepared from a 1000-μl l^{-1} stock solution of the three nitrosamines which had been prepared from the individual pure compounds (Eastman Kodak Chemicals). All standards were made up in hexane (Koch-Light, puriss).

Apparatus

The apparatus was similar to that used by Gough et al. [1], but with several changes. The gas chromatograph was a Pye 104 containing a 4 m (1.8-mm i.d.) stainless steel column packed with 15% Carbowax 20M on Diatomite C AW DMCS. The carrier gas was argon at 11 ml min^{-1}. The column temperature of 190°C was selected to give a retention time of ca. 5 min for NDMA to obtain a good chromatographic separation from the solvent peak. The eluant flowed through a heated (150°C) transfer line into a catalytic pyrolyzer operated at 550°C. The pyrolyzer outflow passed through 2-mm i.d. teflon tubing to a U-shaped stainless steel (4-mm i.d.) trap which was immersed in frozen pentane at −136°C. The outlet from the trap passed via 2-mm i.d. teflon tubing to the reaction chamber. The reaction chamber was connected to a water-cooled thermoelectric refrigerated chamber (Products for Research, Danvers, MA; model TE104) containing the photomultiplier tube (EMI 9658A) operated at a cathode potential of 1500 V (Brandenburg model 472R). The reaction chamber was separated from the photomultiplier by a 610-nm cut-off filter (Corning 2-60) held in place by O-rings. This signal

from the photomultiplier tube was fed to a picoammeter (Keithley Instruments model 414S) and then, via the active filter, to be displayed on a chart recorder (Bryans Southern model 28000).

Construction of the electronic filter. The circuit chosen is shown in Fig. 5. The filter was constructed around two modular active filters (Barr and Stroud Ltd., model EF43). These have a maximum input voltage of 5 V, and the gain of the first amplifier (Precision Megalithics model OP05) was adjusted to allow for this. The values of R_1 and R_2 were set to 15 kΩ and 10 kΩ respectively to achieve compatibility with the output of the Keithley 414S amplifier which has an output of 1 V. The 10-kΩ potentiometer was set so that the output of the second amplifier (model 741) was 2.5 V.

Setting up of the electronic filter

A 5-μl sample of a 1-μl l^{-1} nitrosamine standard was injected onto the column and the rise time of 90% of the peak value was measured from the chart recorder running at high speed. The corresponding frequency was calculated as described in the theory section, giving a frequency of 0.0585 Hz. The frequency of the noise was measured in a similar manner from the same recorder trace. The minimum frequency was found to be 1.75 Hz. From these two values a cut-off frequency of 0.06 Hz was selected, and obtained in the filter unit by setting the resistances to the following values (kΩ): $R_1 = 15$, $R_2 = 10$, $R_{B1} = 102.2$, $R_{B2} = 115.6$, $R_{B3} = 70$, $R'_{B1} = 115.1$, $R'_{B2} = 102$, $R'_{B3} = 176$.

The EF43 filter units are capable of any of the three filter responses described earlier. A Bessel response was selected and by having the two filter modules cascaded together, a fourth-order response was obtained.

Evaluation of the performance of the electronic filter

In order to evaluate the effectiveness of the filter, the analytical signal and the associated noise produced on the injection of 5 μl of a 1-μl l^{-1} nitrosamine standard was monitored both with and without the use of the filter. Experiments were also carried out using a RC filter for comparative purposes. The values of the resistance and capacitance (115 kΩ and 250 μF) were chosen to give a degree of noise reduction similar to that for the active filter.

A series of ten replicate injections of the 0.1-μl l^{-1} standard were run with the filter in circuit and ten replicate injections of the 1-μl l^{-1} standard were run without the filter to provide information for statistical analysis.

RESULTS AND DISCUSSION

The results of the study of the electronic filter are shown in Fig. 6. The effectiveness of the filter for the analysis of the 1-μl l^{-1} standard solution can be clearly seen in Fig. 6 which shows the traces obtained without and with the filter. Although a slight loss of sensitivity occurred when using the filter, a visual estimate of the reduction in baseline noise shows an improve-

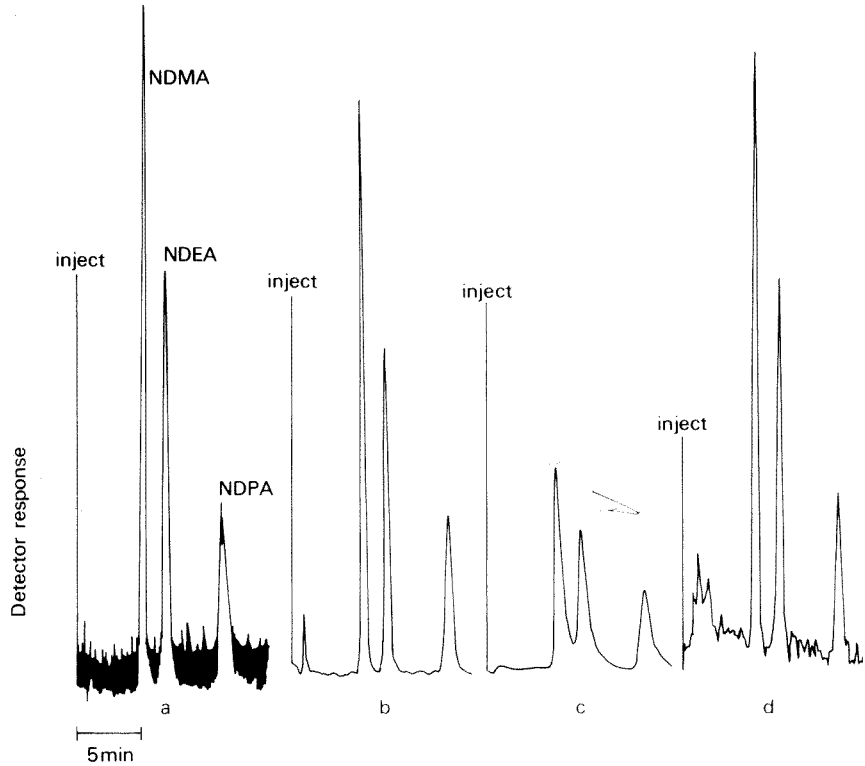

Fig. 6. Chemiluminescent detector response to a 5-μl injection of a 1-μl l^{-1} *N*-nitrosamine solution (a) without a filter in the circuit; (b) with the filter in the circuit; (c) with an RC filter in the circuit; (d) is the response to 5 μl of a 0.1-μl l^{-1} *N*-nitrosamine solution with the filter in the circuit at greater (10×) scale expansion.

ment of an order of magnitude. The effect of the alternative, an RC filter, is also shown in Fig. 6. It can be seen that a marked loss of sensitivity occurs coupled with an apparent degradation of the chromatography; this is due to peak broadening caused by the excessive response time associated with such filters.

It can be seen from Fig. 6a that the determination limit (twice the noise level) for NDMA without using the filter is approximately 0.1 μl l^{-1}. In order to obtain an estimate of the new determination limit for NDMA with the electronic filter, it was decided to repeat the experiment reported in Fig. 6b using a standard of ten times lower concentration. The results are shown in Fig. 6d. This trace was obtained at a ten-fold increase in scale expansion in order to facilitate the visual estimation of the signal-to-noise ratio. It can be seen that a determination limit of 10 nl l^{-1} for NDMA can easily be attained. This is a marked improvement over the limit obtained without the filter.

The limit of detection both without and with the filter was determined by measuring the peak heights of NDMA for ten replicate injections at the

1- and 0.1-μl l^{-1} levels, respectively, and calculating the standard deviation. The 2σ values obtained were 90 and 4 nl l^{-1}, respectively. Thus the use of the electronic filter improves the detection limit more than 20 times.

Conclusion

The electronic noise filter greatly reduced the noise with only a small loss in signal sensitivity and no degradation of the response. Because of this, the detection limit was improved by more than an order of magnitude. Such filters are relatively simple to construct and are inexpensive; the one used here cost about £60. They clearly have the potential for wider applications since the cut-off frequency of the filter can be tuned to cope with noise peculiar to any chemiluminescence detector, and, in fact, they can be used with any analytical detector which generates noise of a much higher frequency than the desired signal. Particularly, active noise filters could be applied to the output of other analytical devices employing photomultiplier tubes as detectors.

REFERENCES

1 T. A. Gough, K. S. Webb and R. F. Eaton, J. Chromatogr., 137 (1977) 293.
2 D. H. Fine, F. Rufeh, D. Lieb and D. P. Rounbehler, Anal. Chem., 47 (1975) 1188.
3 P. N. Magee and J. M. Barnes, Adv. Cancer Res., 10 (1967) 163.
4 J. L. Hilburn and D. E. Johnson, Manual of Active Filter Design, McGraw-Hill, London, 1973, pp. 8, 10, 162.

Analytica Chimica Acta, 126 (1981) 135—145
Elsevier Scientific Publishing Company, Amsterdam — Printed in The Netherlands

THE APPLICATION OF ATOMIC ABSORPTION SPECTROMETRY IN THE ANALYSIS OF METALLIC SODIUM
Part 1. Volatilization Characteristics of Sodium Salts During Electrothermal Atomization

K. GARBETT, G. I. GOODFELLOW and G. B. MARSHALL*

Chemistry Division, Central Electricity Research Laboratories, Kelvin Avenue, Leatherhead KT22 7SE (Gt. Britain)

(Received 5th January 1981)

SUMMARY

The volatilization characteristics of six common sodium salts from the graphite rod of an electrothermal atomizer are described. Most of the salts have a relatively simple volatilization behaviour and can be completely removed from the graphite rod during a 20 s heating stage at temperatures 200—300°C above their melting points. This predictable and controllable vaporization behaviour shows the potentiality of the graphite rod atomizer for selectively volatilizing a sodium salt matrix and leaving behind less volatile trace metals for subsequent high temperature volatilization and measurement by atomic absorption spectrometry.

Liquid sodium is widely used as a coolant in fast reactors. Regular measurement of trace constituents, such as iron, chromium and nickel, in cooled, abstracted samples is necessary in order to monitor the degree of corrosion occurring within the alloy-steel containment systems [1].

There are two principal pre-treatment techniques used for the analysis of cooled samples [2—5]: (a) removal of metallic sodium by vacuum distillation, leaving a residue of non-volatile trace impurities for determination, and (b) dissolution of the sodium in a suitable solvent, such as ethanol, removal of the solvent by evaporation and conversion of the residue to a suitable sodium salt by addition of an acid. The latter technique is simpler and more rapid but does not incorporate a sodium separation stage. The residue from the first procedure, or the salt solution from the second, can be conventionally analysed by a number of techniques, including spectrophotometry and atomic absorption spectrometry (a.a.s.).

The problem of using a.a.s., in particular with electrothermal atomization (e.t.a.), in direct measurement of the solutions of sodium salts is that the sodium matrix can seriously interfere with the determination of the trace metals. However, e.t.a. has the attraction that its high absolute sensitivity (10^{-11}—10^{-13} g) permits good concentrational sensitivity using very small samples [6].

This paper presents a study of the volatilization characteristics of various sodium salts from a graphite rod used in e.t.a. In Part 2 [7] a procedure is described for determining iron, chromium and nickel by a.a.s., based on the differential volatilization techniques described here.

The rapidity of the programmed heating sequences of the graphite rod prevents the establishment of an overall thermal equilibrium. It was impossible, therefore, to judge beforehand whether the vapour pressure at rod temperatures between the melting and boiling points of the various sodium salts would be sufficient for complete volatilization of a specified quantity of salt or whether the rod temperature had to be high enough to exceed the boiling point and so reach saturation vapour pressure. This paper includes a detailed examination of this problem.

The graphite rod was chosen in preference to a tube furnace, because the sodium salts, vapourized from the surface, would be more readily dispersed by the surrounding inert gas stream and thus not cause interference with subsequent heating sequences.

EXPERIMENTAL

Chemicals and instrumentation

All chemicals were analytical-reagent grade (British Drug Houses Ltd.) and solutions were prepared in deionized distilled water.

Measurements were made using a Shandon-Southern atomic absorption spectrometer (Model A3000) fitted with a graphite rod atomizer (Model A3472) and a Model A3370 controller (modified to be equivalent to the later Model A3470). Compressed air was used for cooling the graphite rod assembly and high-purity argon for providing an inert atmosphere around the rod. For most of the work 2-μl capacity graphite rods (Type 1, Part No. A3475) were used but larger capacity rods (5 μl, Type 2, Part No. A3476) were used for a few experiments.

The Shandon-Southern instrument allows the absorbance to be measured continuously from start to finish of the "dry-ashing" and atomization stages. By making measurements under similar conditions with a sodium hollow-cathode lamp and a hydrogen continuum lamp at the same wavelength, it is possible to distinguish largely whether a volatilized species is present in the atomic or non-atomic state. The absorbance of the samples was recorded on a Servoscribe two-pen recorder (Model 2S).

Procedures

By measuring the absorbance maximum during the atomization stage, when the temperature is high enough to volatilize the alkali metal salts completely, a direct measurement can be made related to the mass of sodium salt remaining on the rod at the end of the dry-ashing stage. A graph can then be constructed of absorbance vs. dry-ashing temperature, which is essentially a volatilization curve of the alkali metal salt under examination.

Additionally, continuous absorbance measurement during the dry-ashing and atomization stages provides information on the manner in which salts are volatilized during any one heating cycle, whereas a.a.s. measurement at the atomization stage (of the salt remaining after dry ashing) provides a simple way of evaluating the volatilization characteristics over a range of temperatures.

Because of the restricted size of the heated cavity in the graphite rod, it was not possible to use any directly attached thermocouple to monitor temperature during the heating cycle. Optical pyrometry was therefore chosen to measure the temperature, although it was recognized that this technique would only provide temperatures at one instant during the heating cycle and that it would be of lesser accuracy. A Leeds and Northrup (Model 8622-C) optical pyrometer was focussed from above onto the centre of the cavity of the rod and the temperature was measured at the end of the time period for the particular stage being monitored. It was found that the temperatures during the final few seconds of the dry-ashing stage were approximately constant and could be measured with a variation of ±20°C. During these measurements it was necessary to remove the glass funnel which normally covered the furnace and because of this the argon flow was increased to 3.5 l min^{-1} to ensure a satisfactory inert atmosphere around the graphite rod.

The heating cycles used were: solvent evaporation stage (channel 1), 2.2—2.5 V (ca. 90°C) for 40 s, set to give a smooth solvent evaporation within 40 s; dry-ashing stage (channel 2), variable voltages for 20 s, this time being chosen to give selective volatilization within a convenient heating period; atomization stage (channel 4), 6.9—7.4 V (ca. 2600°C) for 1.5 s, set to give the maximum atomization temperature without volatilizing carbon from the graphite rod. Gas flow rates were 2.5 l min^{-1} for argon and 8 l min^{-1} for compressed air.

Because of the relatively large quantities of salt present (e.g., 2 μl of a 5% solution is equivalent to 100 μg of dry salt), absorption measurements with the sodium hollow-cathode lamp had to be made at a wavelength of low sensitivity, i.e., the sodium line at 330.3 nm. Absorptions were also measured at the same wavelength using the hydrogen continuum lamp. Six different sodium salts were examined at concentrations such that at the atomization stage an acceptable absorbance was observed when dry-ashing temperatures were sufficiently low that volatilization did not occur at that stage. These concentrations were 5% (w/v) for NaCl, NaBr, and NaI; 1% (w/v) for NaF and 0.25% (w/v) for $NaNO_3$ and Na_2SO_4. Replicate measurements (4—6) of absorbance at the atomization stage were made for each dry-ashing temperature. The absorbance was plotted as a function of the dry-ashing stage temperature; representative examples of the temperature plots are illustrated later. The dry-ashing temperature was estimated from frequent calibrations of the graphite rods in the absence of any added salt.

RESULTS

Temperature calibration of the graphite rod furnace

Dry-ashing temperatures. Data were obtained from 20 Type 1 graphite rods taken from six batches. For all calibrations, the temperature attained at the end of the dry-ashing stage was approximately linearly related to the final applied voltage across the rod. A typical calibration curve is shown in Fig. 1. On repeated use the average temperature of the graphite furnace assembly increased by 20—30°C, and although this did not affect the applied voltage/temperature relationship it limited the maximum temperature attainable by approximately 100°C. It was assumed that these variations occurred as a result of changes in the resistance of the rod assembly, in particular at the contact areas between the supports at each end of the graphite rod.

With the optical pyrometer, only limited measurements could be made of the variation in temperature within the graphite rod cavity or of the rate of change in temperature during dry ashing. The results suggested, however, that the edges of the cavity were approximately 50°C cooler than the centre, that after 4—5 s the cavity reached within 100°C of its final temperature and then reached within 50°C after 7 to 8 s; thereafter the temperature increased only slowly.

A considerable rod-to-rod variation in temperature calibration was found. Overall, a variation of up to 350°C was observed at any specific applied voltage, although this range was less for rods of the same batch (ca. 100°C variation). On repeated use, a small (ca. 50°C maximum) increase in temperature was observed in the calibration for each graphite rod.

Atomization stage temperatures. It was difficult to measure the final atomization temperature by optical pyrometry because of the short atomization times of 1—2 s and the fact that the rod temperature changed rapidly within this time. The best estimate that could be made was by repeating the measurements a number of times and taking the mean value. Accurate values of the atomization temperature were not too important provided that the temperature was sufficient to volatilize the residual salt on the rod completely after dry ashing. The results (Fig. 2) showed that the temperatures reached were not only dependent on the applied atomization stage voltage and the time of atomization, but also on the temperature reached at the end of the preceding dry-ashing stage.

At temperatures in excess of 2700°C, particles of carbon were lost from the graphite rods, and led to a measurable absorbance and the appearance of a black vapour. This temperature was therefore the effective maximum.

Volatilization of sodium salts

When a sodium hollow-cathode lamp is used, the absorbance at atomization can arise from a combination of atomic absorption, non-specific molecular absorption and losses of light by particle scattering. Similar measurements at the same wavelength using a hydrogen lamp give absorbance values

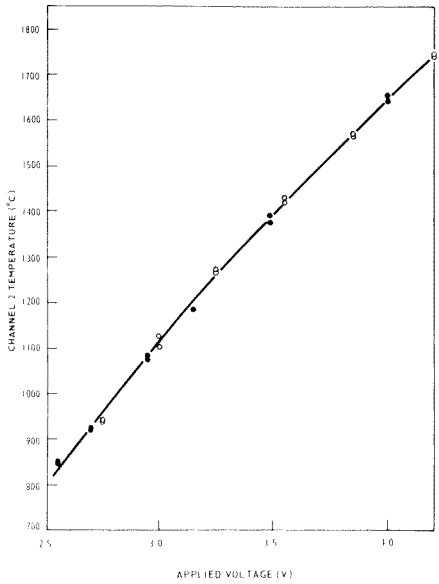

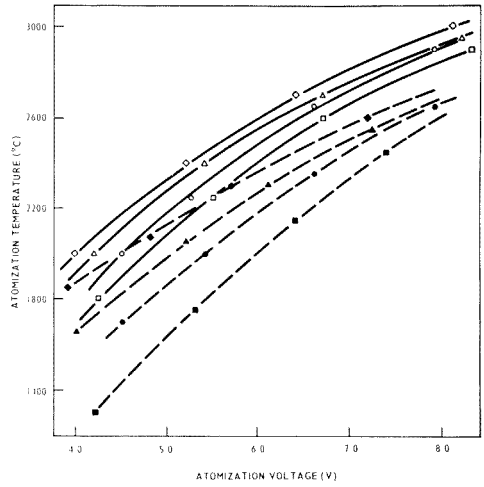

Fig. 1. Typical temperature calibration for a Type 1 graphite rod using channel 2 (dry ashing, Stage 1) measured after 20 s: (○) cold furnace assembly; (●) hot furnace assembly.

Fig. 2. Temperature calibration for a Type 1 graphite rod for atomization times of (---) 1 s and (—) 2 s and at final dry-ashing temperatures of (■□) 600°C, (●○) 900°C, (▲△) 1300°C, (◆◇) 1500°C.

which arise essentially from the latter two factors. Therefore the difference between the two sets of readings, either displayed or calculated, is that arising from the sodium atomic absorption.

Sodium halides. The volatilization of the sodium halides as observed with a hydrogen lamp followed a simple pattern. In each case (see for example Figs. 3—5 and Table 1) the onset of volatilization occurred at temperatures just above the melting point and was complete at temperatures 200—300°C above that. Only in the case of sodium chloride was the apparent volatilization behaviour similar when measured with the hydrogen and hollow-cathode sources; this is illustrated in Fig. 3. With sodium bromide, sodium iodide and sodium fluoride, a more complex behaviour was found with the sodium hollow-cathode lamp. With sodium bromide and sodium iodide, another species with different volatilization characteristics was formed during the dry-ashing stage, whereas with sodium fluoride a large difference was observed in the magnitudes of absorbances between the two lamp sources. These characteristics are shown in Figs. 4 and 5 and are summarized in Table 1.

The occurrence of two types of volatilizable species was more readily observed with sodium iodide (Fig. 4). For example, in Fig. 4(B) at 640°C (i.e., below the melting point of 651°C) no volatilization occurred during

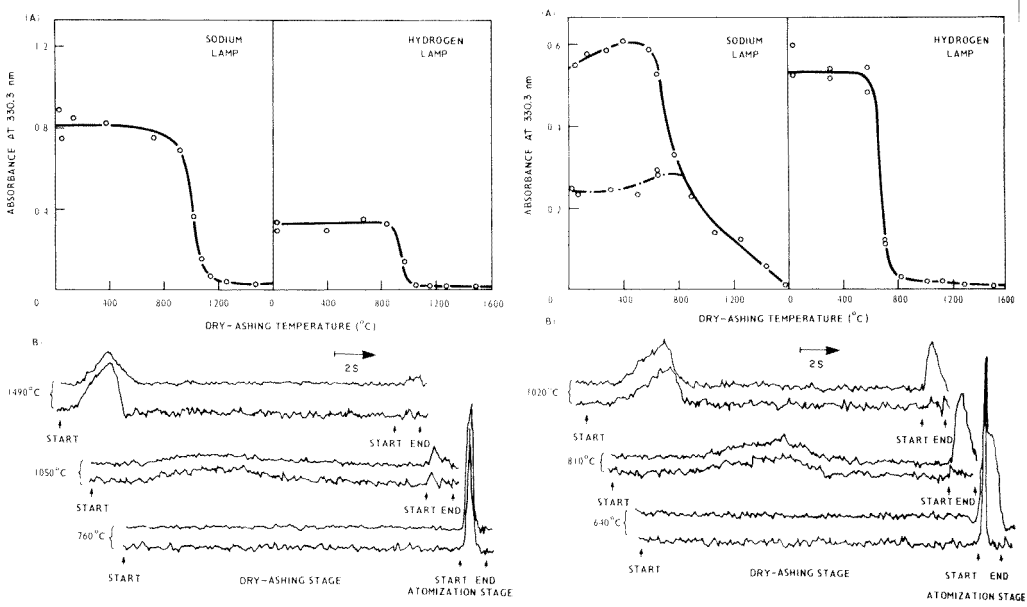

Fig. 3. The volatilization behaviour of sodium chloride. (A) The variation of mean maximum absorbance during atomization with dry-ashing temperature. (B) Typical continuous absorbance measurement using a sodium hollow-cathode lamp (upper traces) or a hydrogen lamp (lower traces), at the indicated dry-ashing temperatures.

Fig. 4. The volatilization behaviour of sodium iodide. (A) The variation of mean maximum absorbance during atomization with dry-ashing temperature (continuous line); absorbance of the second "unresolved peak" during atomization (dotted line). (B) as Fig. 3B.

dry ashing, but a species which exhibited essentially non-specific absorption was volatilized rapidly during the first 0.5 s of atomization, followed by a species which was more slowly volatilized and which exhibited atomic absorption alone. At temperatures somewhat above the melting point (e.g., at 810°C), the first of these two species was volatilized during dry ashing (as indicated by the similarity of dry-ashing absorbance signals for both light sources) whereas the atomic absorbing species persisted until the atomization stage. Even at 1020°C, the atomic absorbing species still remained unvolatilized until the atomization stage. One possible explanation for the presence of an atomic absorbing species during the atomization stage could be that even at temperatures considerably in excess of its melting point there was a residual amount of sodium iodide on the rod after dry ashing because the 20-s dry-ashing period was insufficient. However, this was unlikely because the same mass of sodium chloride was completely volatilized during dry ashing (as shown by both the hollow-cathode lamp and hydrogen lamp profiles in Fig. 3(A) even though its melting point (801°C) was some 150°C higher than that of sodium iodide.

The volatilization profiles for sodium fluoride were similar (Fig. 5) when

TABLE 1

Volatilization behaviour of sodium salts

Salt		M.p./b.p. (°C)	Dry-ashing temperature range over which volatilization is observed (°C)	
			Measured by sodium hollow-cathode lamp[a]	Measured by hydrogen lamp[a]
NaF		988/1695	1020—1600	1000—1200
NaCl		808/1465	870—1150	870—1150
NaBr	First peak	755/1390	800—960	780—970
	Second peak (unresolved)		900—1600	—
NaI	First peak	651/1304	660—800	640—820
	Second peak (unresolved)		750—1600	—
Na_2SO_4		884[b]	1000—1300	1000—1260
$NaNO_3$		308[c]	750—1350	800—1050

[a]At 330.3 nm. [b]Volatilizes without decomposition. [c]Decomposes to sodium nitrite at 380°C; above 800°C decomposes rapidly to sodium oxide m.p. 920°C, sublimes at 1275°C.

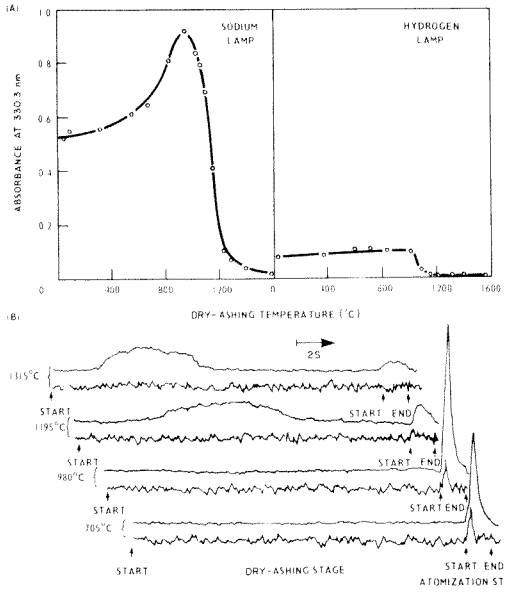

Fig. 5. The volatilization behaviour of sodium fluoride. (A) The variation of mean maximum absorbance during atomization; with dry-ashing temperature. (B) as Fig. 3B.

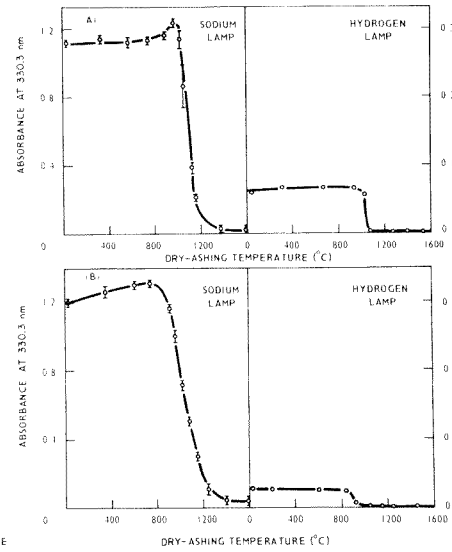

Fig. 6. The volatilization behaviour of (A) sodium sulphate; (B) sodium nitrate.

measured with either lamp. However, compared with other halides the mean value of absorbance at the atomization stage for dry-ashing temperatures below the melting point was much greater with the sodium lamp than with the hydrogen lamp, reflecting a greater contribution from atomic absorption. An unusual feature was the marked increase in absorbance as the dry-ashing temperature approached the melting point.

Sodium sulphate and sodium nitrate. Sodium sulphate and sodium nitrate showed the same effect as sodium fluoride, i.e., enhanced higher mean absorbance signals with the hollow-cathode lamp at temperatures below their melting points. The volatilization behaviour of sodium sulphate (Fig. 6A) was similar to those of sodium chloride and sodium fluoride. Thus only a single absorbance signal was observed in both the dry-ashing and atomization stages of the heating cycle. Volatilization occurred over a temperature range of 0—300°C above the melting point (see also Table 1).

The volatilization of sodium nitrate, as measured with a sodium hollow-cathode lamp, is shown in Figs. 6 and 7 and Table 1. At high dry-ashing temperatures, e.g. 1600°C, a two stage volatilization was detected (Fig. 7). An initial intense atomic absorption over the first 1—3 s was followed by a weak unresolved atomic absorption peak observed as a prolonged "tail" lasting a further 3 s. This behaviour is also shown by the volatilization profile (Fig. 6B) where the salt is seen to vaporize over a much wider temperature range (600°C) than salts with simple volatilization characteristics such as sodium chloride (300°C). This behaviour resembles that of sodium iodide.

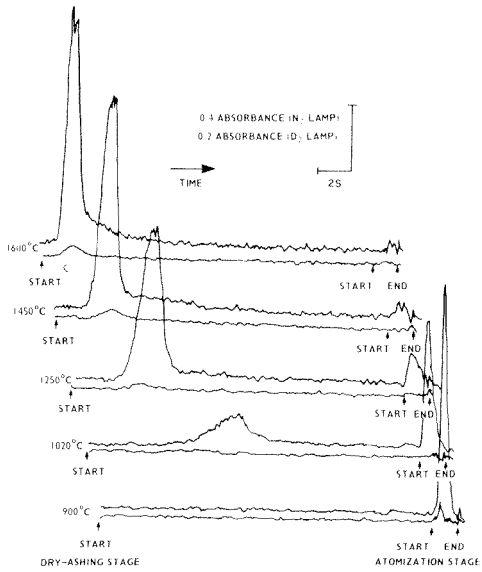

Fig. 7. Continuous absorbance measurements of the volatilization of sodium nitrate throughout the dry-ashing and atomization stages at the dry-ashing temperatures indicated (upper traces, sodium hollow-cathode lamp; lower traces, hydrogen lamp).

The complex behaviour of sodium nitrate during the dry ashing was confirmed visually by volatilizing larger amounts of the salt. The intense absorption was caused by a flame, tinged yellow at its edges, which burnt above the graphite rod. This flame was seen first at a dry-ashing temperature of 980°C but could also be seen momentarily at temperatures up to 1300°C. Above 1200°C, the flame was rapidly masked by a plume of white vapour, which became the only observable feature above 1300°C.

Effect of salts on the graphite rod

It is important for analytical purposes that the sodium salt should not adversely affect the graphite rod on repeated volatilization; only the sodium halides satisfied this requirement. With sodium sulphate or sodium nitrate, at the highest concentration used (a 4% (w/w) solution), rapid attack on the rod caused pitting or breakage after 50—60 heating cycles. This compares with 200—300 cycles for a 5% solution of sodium chloride. In addition, sodium nitrate caused rod fracture very rapidly (ca. 10 cycles) if the rod was allowed to cool completely and to stand in air for 1—2 h before re-use. The rate of attack was considerably reduced at lower concentrations of the sulphate or nitrate, and no serious attack was observed for 0.25% solutions. It is presumed that these effects are caused by oxidation of the rod by oxy-anions.

DISCUSSION

Volatilization of sodium salts

When only the non-specific absorbance was monitored with the hydrogen lamp, all the salts had a similar simple behaviour. Except for sodium nitrate, which decomposes on melting, no volatilization appeared to occur until the melting point was exceeded. Then, within a temperature range 200—300°C above this, all the salts were volatilized. Volatilization was accompanied by a plume of white vapour and was complete at temperatures well below the boiling point (Table 1).

Sodium nitrate decomposes at temperatures above its melting point (Table 1) and it is probable that its volatilization characteristics are determined by its decomposition products, presumably sodium nitrite and, above 800°C, sodium oxide.

When the combined non-specific and atomic absorbance were monitored with a sodium hollow-cathode lamp, the observed volatilization characteristics were usually more complex than those found with the hydrogen lamp. With sodium bromide, iodide and nitrate, a second atomic absorbing species was detected. Because atomic absorption measurements are very sensitive, these second species may have been present in only small amounts. The species responsible for these effects could not be identified. Possibly a reaction occurred to a small extent during the relatively brief heating time of the dry-ashing or atomization stages in that portion of the salt in contact with the graphite, forming a sodium species with a significantly higher melting

point than the original salt. This may have been a carbide or an alkali metal—graphite compound [8].

A two-stage volatilization behaviour was observed with sodium nitrate. With large amounts of sodium nitrate at dry-ashing temperatures above 1000°C, a flame was observed above the rod and it is reasonable to infer that a similar combustion occurred with the smaller amounts of sodium nitrate used during the volatilization studies. This behaviour could be attributable to the decomposition of molten sodium nitrate [8] (Table 1) where above 800°C a rapid decomposition to sodium oxide, nitrogen and oxygen takes place. It is believed that the oxygen produced in this decomposition reacted with the graphite rod to form the flame observed during the dry-ashing stage. The visible yellow colour in this flame indicated that thermally emitting sodium vapour was present which would correlate with the strong atomic absorption signal (Fig. 7) at dry-ashing temperatures as low as 1020°C. The residue of sodium oxide presumably determines the volatilization behaviour at higher temperatures.

Application to the determination of trace metals in sodium

This study shows that the melting point of the sodium salts is a far better indicator of the expected volatilization behaviour than the boiling point and, provided that the dry-ashing temperature is some 200—300°C above the melting point, complete volatilization will occur. These temperatures are at least 300°C below that at which compounds of the trace metals of interest in liquid sodium coolant systems (i.e., iron, chromium and nickel) would be expected to volatilize themselves. The removal of the matrix by selective volatilization during the dry-ashing stage is therefore practicable.

Other factors which have a bearing on the successful application of e.t.a. in the analysis of sodium are the degradation effect of some sodium salts on the graphite rod and the establishment of a controlled dry-ashing temperature. Sodium nitrate and sodium sulphate, in comparison with sodium halides, are not suitable matrices for e.t.a. because they attack the rod and markedly reduce its lifetime.

The measurement of actual rod temperature with an optical pyrometer is time-consuming and therefore not suitable for routine analysis. However, in practice, only the heating conditions necessary to attain complete matrix volatilization need be characterized. The minimum applied voltage for the dry-ashing stage at which complete volatilization occurs will define the correct conditions for selective volatilization. This method has proved satisfactory and has been tested in the practical application of the selective volatilization technique described in Part 2 [7].

The work was carried out at the Central Electricity Research Laboratories and is published by permission of the Central Electricity Generating Board.

REFERENCES

1 L. Silverman, The Determination of Impurities in Nuclear Grade Sodium Metal, Pergamon, Oxford, 1971.
2 E. A. Trevillion, CEGB Report No. RD/B/N 3031, 1974.
3 J. M. Scarborough, C. D. Bingham and P. F. DeVries, Anal. Chem., 39 (1967) 1394.
4 D. B. Ratcliffe and C. S. Byford, CEGB Report No. RD/M/N 1083, 1979.
5 I. Huber, I. Schreinlechner and F. Benischek, At. Absorpt. Newsl., 16 (1977) 64.
6 C. W. Fuller, Electrothermal Atomization for Atomic Absorption Spectrometry, The Chemical Society, London, 1977.
7 K. Garbett, G. I. Goodfellow and G. B. Marshall, Anal. Chim. Acta, 126 (1981) 147.
8 J. C. Bailar, Jr., H. J. Emeleus, R. Nyholm and A. F. Trotman-Dickinson (Eds.), Comprehensive Inorganic Chemistry, Vol. 1, Pergamon, Oxford, 1973.

Analytica Chimica Acta, 126 (1981) 147—156
Elsevier Scientific Publishing Company, Amsterdam — Printed in The Netherlands

THE APPLICATION OF ATOMIC ABSORPTION TECHNIQUES IN THE ANALYSIS OF METALLIC SODIUM
Part 2. Determination of Iron, Nickel and Chromium in Sodium Salt Solutions by Electrothermal Atomization

K. GARBETT, G. I. GOODFELLOW and G. B. MARSHALL*

Chemistry Division, Central Electricity Research Laboratories, Kelvin Ave., Leatherhead KT22 7SE (Gt. Britain)

(Received 5th January 1981)

SUMMARY

Sodium chloride is selectively volatilized at 1100°C before subsequent atomization of the trace metals for determination by atomic absorption spectrometry. Ammonia can be added to prevent loss of trace metals during NaCl removal. The procedure is applicable to iron, nickel and chromium up to 50 mg kg^{-1} of sodium metal, with standard deviations of 0.5—2.8 mg kg^{-1}, and is potentially applicable to segregation analysis of sodium billets.

In Part 1 [1] the volatilization behaviour of sodium salts from a graphite rod atomizer was described. It was shown that the salts produced a high absorbance signal from molecular species at the atomization stage, but that this could be eliminated by volatilizing the salts during the preceding dry-ashing stages at temperatures 200—300°C above their melting points. It was further shown that sodium halides did not adversely affect the graphite rods, but sodium sulphate, and in particular sodium nitrate, attacked the graphite, severely reducing its working lifetime.

In this paper the determination of iron, chromium and nickel in sodium chloride solutions is described, together with a limited study of sodium sulphate solutions. These metals are amongst the most important of those which participate in the corrosion and mass transfer processes of liquid sodium systems. The dry-ashing stages can be used to volatilize the sodium salts selectively leaving behind only the trace metals for subsequent volatilization and determination by atomic absorption spectrometry (a.a.s.) during the atomization stage. This in situ separation eliminates any interference from the sodium matrix and permits the direct measurement of sodium salt solutions containing relatively nonvolatile trace metals.

EXPERIMENTAL

Reagents

All chemicals were obtained from British Drug Houses Ltd. Sodium chloride, sodium sulphate, ammonium iron(III) sulphate, nickel sulphate and

disodium-EDTA were analytical-reagent grade; chromium(III) sulphate was laboratory-reagent grade; iron(III) chloride, nickel chloride and chromium(III) chloride standard solutions for a.a.s. were used. Ammonia, sulphuric acid and hydrochloric acid were obtained as concentrated volumetric solutions. All solutions were prepared in deionized distilled water.

Apparatus

The apparatus used was as described previously [1]. The furnace was cooled with compressed air (8 l min^{-1}) and was fitted with graphite rods capable of holding either 2 μl (Type 1, A3475) or 5 μl (Type 2, A3476) of sample. During measurements, the rods were surrounded by a flow of high-purity argon (2.5 l min^{-1}).

Procedure

Measurements were made at 232.0, 248.3 and 357.9 nm for nickel, iron and chromium, respectively, using the appropriate hollow-cathode lamp. The heating cycle of the electrothermal atomizer was: solvent evaporation (channel 1), 2.0—2.4 V ($\approx$90°C) for 40 s; dry-ashing (channels 2 or 3), various voltages and temperatures for 20 s (type 1 rods) or 60 s (type 2 rods); atomization (channel 4), 6.9—7.4 V (2400—2600°C) for 1.5 s.

Frequent "temperature versus applied voltage" calibrations were made during the dry-ashing stages for each graphite rod, in the absence of any salt, by optical pyrometry as described previously [1]. From these, estimates were made of the dry-ashing temperatures attained when sample salts were present. Direct temperature measurements in the presence of salts were impracticable as they obscured the graphite surface and also because the surface luminescence of the salt could indicate a temperature significantly different from that of the graphite.

To define the instrumental conditions required for the trace metal analysis, the volatilization behaviour of the following solutions was determined: (a) trace metal (1 mg l^{-1}, as the chloride or sulphate) in 0.01 M hydrochloric or 0.005 M sulphuric acid; (b) aqueous 5% w/w sodium chloride or sodium sulphate solutions; (c) trace metal (1 mg l^{-1}, as chloride or sulphate) in aqueous 5% sodium chloride or sodium sulphate solutions. In general, type 1 (2 μl) graphite rods were used and normally four replicate measurements of absorbance at the atomization stage were made at each dry-ashing temperature. The absorbance during the atomization stage provided an indirect measure of the volatilization behaviour during the preceding dry-ashing stage. Graphs were prepared showing the volatilization behaviour as a function of the dry-ashing temperature. EDTA and ammonia additions were made to some solutions to modify the volatilization characteristics of the trace metals. An identical procedure was used for solutions containing EDTA but a modified procedure was followed with ammonia. Here the heating cycle was halted on completion of the solvent evaporation stage, 2 μl of ammonia solution was added, the solvent evaporation stage was then repeated and the heating cycle completed.

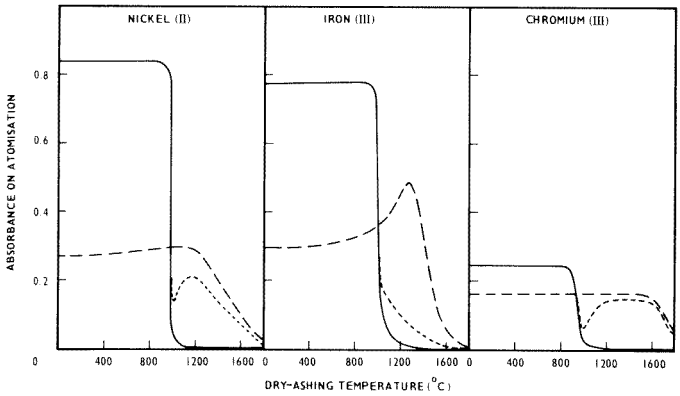

Fig. 1. Volatilization behaviour of trace metal chlorides in 5% (w/w) sodium chloride solution. (—) 5% (w/w) sodium chloride solution; (- - -) trace metal chloride, 1 mg l^{-1}, in 0.01 M HCl; (----) trace metal chloride in 5% sodium chloride. The curves are coincident with 5% sodium chloride below 1000°C.

RESULTS

Volatilization behaviour in 5% sodium chloride solutions

The volatilization behaviour of 5% (w/w) sodium chloride solutions and of chloride solutions of iron(III), nickel(II) and chromium(III) with and without the presence of 5% sodium chloride is shown in Fig. 1. At each wavelength the sodium chloride (in the absence of any trace metal) was volatilized during the dry-ashing stage over the range 900—1200°C, i.e., at temperatures above its melting point of 808°C but below its boiling point. (Although the same weight of sodium chloride was added to the graphite rod in every case, the absorbance at the atomization stage from salt remaining after low temperature dry-ashing depends on the wavelength of measurement. This is because the molecular absorption of sodium chloride varies with wavelength, and light losses by particle scattering from the vapour also depend on wavelength.)

In the absence of sodium chloride, volatilization of each trace metal chloride occurred at a temperature in excess of 1400°C. There was a marked enhancement in the iron atomic absorption at dry-ashing temperatures approaching 1300°C.

When trace metal and sodium chloride were both present, volatilization was more complex. At dry-ashing temperatures up to about 1050°C, the results were identical to those obtained for sodium chloride alone. An absorbance by the trace metal vapour was only observed when dry-ashing temperatures were high enough to volatilize all the sodium chloride during the preceding dry-ashing stage. However, even in this temperature region all the trace metals showed some change in volatilization and in sensitivity compared with their volatilization in the absence of sodium salt. This effect was particularly severe with iron(III).

Volatilization behaviour in sodium chloride solutions in the presence of ammonia or EDTA

The results described above show, especially for iron(III), a marked decrease in the absorbances of the trace metals in the presence of sodium chloride. This was thought to be caused by the large excess of sodium chloride suppressing the hydrolysis of the relatively volatile transition metal chlorides. In the absence of sodium chloride, these trace metal chlorides hydrolyse at the solvent evaporation stage to form hydrated oxides which have a much higher volatilization temperature than those of the chlorides, particularly iron(III) chloride.

To prevent the loss of the required metal halide at the dry-ashing stage, additions of either EDTA or ammonia were made. EDTA was added to the bulk test solutions to form preferentially the stable transition metal complexes so that decomposition to the metal oxides occurred at the dry-ashing stage. The addition of ammonia to the bulk solution was impracticable, because of precipitation of the hydrated oxides. Therefore, an in situ hydrolysis was carried out on the graphite rod by adding a small volume of ammonia solution to the solid residue remaining on completion of the solvent evaporation stage.

The effect of EDTA was examined at bulk solution concentrations of 10^{-1} M, 10^{-2} M and 10^{-3} M EDTA for iron(III) and at 10^{-2} M EDTA for nickel(II) and chromium(III). The effect of ammonia was tested by adding to the residue after the solvent evaporation stage 2 μl of 1 M ammonia solution, and for iron(III) alone, 10^{-1} M solution. These reagents introduced no contamination, except for iron(III) with EDTA, where significant contamination was found at the highest EDTA concentration. The results for EDTA and 1 M ammonia solution addition are shown in Figs. 2 and 3.

Ammonia (1 M) was found to increase the absorbance and to change the volatilization behaviour of both iron(III) and chromium(III) from that of

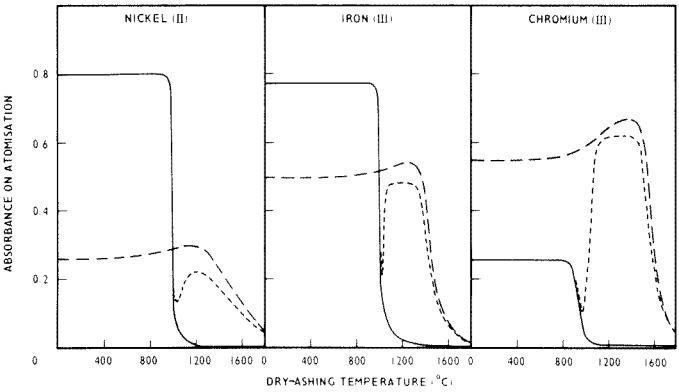

Fig. 2. Volatilization behaviour of trace metal chlorides in 5% (w/w) sodium chloride solution after in-situ hydrolysis with 1 M ammonia solution. Key as Fig. 1. Ammonia (2 μl of 1 M) added to each sample after evaporation to dryness.

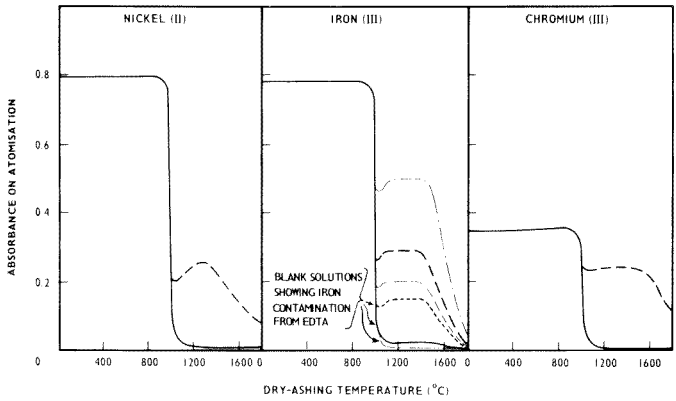

Fig. 3. Volatilization behaviour of trace metal chlorides in 5% (w/w) sodium chloride solutions containing EDTA. Sodium chloride (5%) with: (---) 10^{-1} M EDTA; (——) 10^{-2} M EDTA; (—·—) 10^{-3} M EDTA. Metal chloride (1 mg l^{-1}) in 5% sodium chloride with: (—·—) 10^{-1} M EDTA; (- - -) 10^{-2} M EDTA; (- - -) 10^{-3} M EDTA. All curves coincide below 1000°C.

these elements in the presence of sodium chloride alone; little change in the behaviour of nickel(II) was observed. The measured absorbance was lower with iron(III) after 0.1 M ammonia addition (not shown) presumably because the degree of hydrolysis was less than with the 1 M solution. Some losses of residual volatile metal chloride therefore occurred at the dry-ashing stage.

At all concentrations, EDTA was found to minimize the formation of volatile chloride and enhance the absorbance in a similar way to ammonia. Representative results for iron(III) with different concentrations of EDTA are shown in Fig. 3. At the concentrations examined, EDTA did not influence the volatilization behaviour of either iron(III) or chromium(III) to the same extent as 1 M ammonia.

Determination of trace metals in 5% sodium chloride solutions

The results in the previous two sections show that determination of trace metals in sodium chloride solutions is practicable provided that sodium chloride is removed at the dry-ashing stage. The dry-ashing temperatures should be between 1050°C and 1400°C, i.e., temperatures in excess of that required to volatilize the sodium chloride but less than that needed to volatilize the trace metals.

The technique was tested at concentrations up to 1 mg l^{-1} for each trace metal in solutions containing either 5% (w/w) sodium chloride alone or 5% sodium chloride and ammonia or EDTA. In each case the procedure as previously described was followed but at a fixed dry-ashing temperature of 1150°C (channel 2, 3.0—3.2 V, 20 s) and using 2-μl samples (type 1 graphite rods). The results are summarized in Table 1.

As expected, EDTA and ammonia enhanced the sensitivity for both iron(III) and chromium(III) but decreased the precision compared with

TABLE 1

Absorbances measured for trace metals dissolved in 5% (w/w) sodium chloride solutions[a]

Concentration (mg l^{-1})	Nickel (232.0 nm)	Iron (248.3 nm)			Chromium (357.9 nm)		
	No addition[b]	No addition	+ 1 M NH_3	+ 10^{-2} M EDTA	No addition	+ 1 M NH_3	+ 10^{-2} M EDTA
0	0.026 (0.005)	0.019 (0.002)	0.023 (0.005)	0.061 (0.008)	0.009 (0.003)	0.025 (0.013)	0.011 (0.008)
0.2	0.076 (0.005)	0.043 (0.017)	0.107 (0.016)	0.128 (0.010)	0.042 (0.005)	0.195 (0.024)	0.066 (0.005)
0.4	0.118 (0.007)	0.066 (0.007)	0.207 (0.005)	0.186 (0.013)	0.066 (0.005)	0.324 (0.034)	0.132 (0.012)
0.6	0.169 (0.013)	0.088 (0.009)	0.277 (0.023)	0.241 (0.009)	0.119 (0.003)	0.490 (0.024)	0.173 (0.013)
0.8	0.235 (0.013)	0.108 (0.012)	0.352 (0.024)	0.288 (0.007)	0.145 (0.009)	0.615 (0.029)	0.232 (0.011)
1.0	0.255 (0.018)	0.143 (0.021)	0.446 (0.017)	0.348 (0.003)	0.195 (0.008)	0.739 (0.033)	0.291 (0.014)
Sensitivity (absorbance per mg l^{-1})	0.23	0.12	0.42	0.29	0.18	0.72	0.28
Range of standard deviation (mg l^{-1})	0.02—0.08	0.01—0.17	0.01—0.06	0.01—0.04	0.01—0.05	0.02—0.05	0.02—0.05
Limit of detection (mg l^{-1})[c]	0.096	0.056	0.050	0.126	0.062	0.082	0.124

[a] 2-μl samples, type 1 graphite rods; dry-ashing stage (1150°C), 20 s; atomization stage (ca. 2500°C), 1.5 s. Each absorbance given is the mean of four results with the standard deviation for a single result in parenthesis. [b] Results in the presence of ammonia or EDTA were identical so are not quoted. [c] Limit of detection is defined as 4.652 S_B, where S_B is the standard deviation of the blank.

sodium chloride alone, resulting in a similar overall precision, expressed in concentration terms. At a higher dry-ashing temperature of 1300°C, the precision was similar to those in Table 1 in terms of measured absorbance but, as expected, there was a decrease in sensitivity (Figs. 1—3). The overall precision at this higher dry-ashing temperature therefore decreased, this being particularly severe for iron(III) in 5% sodium chloride solutions alone [sensitivity, 0.061 absorbance per mg l^{-1}, range of standard deviations 0.08—0.32 mg l^{-1}, limit of detection 0.38 mg l^{-1}].

In an attempt to obtain greater sensitivity, type 2 graphite rods were examined. These rods accommodate a 5-μl sample in a cavity of similar diameter but of greater depth, to that in a type 1 rod. Satisfactory results were not obtained because of the poor evaporation characteristics of the viscous sodium chloride solutions, which either sputtered during evaporation or formed a ring of solid salt around the cavity. This ring was incompletely removed at the dry-ashing temperature used previously (1150°C) and was only removed at temperatures in excess of 1300°C. This resulted in decreased sensitivity and poorer precision, offsetting any gain in sensitivity from greater sample volumes. No overall improvement in precision resulted, and similar results to those given in Table 1 for the type 1 rods were obtained.

With chromium(III), the residual sodium chloride did not give a high non-specific absorbance at the wavelength of measurement and accordingly the measurements could be carried out in the larger cavity at the lower dry-ashing temperature of 1150°C. A greater sensitivity and a better overall precision were therefore obtained; for example 5% sodium chloride solutions with in situ hydrolysis by 5 μl of 1 M ammonia gave a sensitivity, limit of detection and range of standard deviations of 0.66 absorbance per mg Cr l^{-1}, 0.030 mg Cr l^{-1} and 0.008—0.019 mg Cr l^{-1}, respectively.

Volatilization behaviour in 5% (w/w) sodium sulphate solutions

Although it was known from previous work that sodium sulphate caused more rapid deterioration of graphite rods than sodium chloride [1], it was examined to see whether it had any advantage as a matrix over sodium chloride. The procedure as previously described was followed, and the results are shown in Fig. 4.

The volatilization behaviour was very similar to that of sodium chloride solutions, but a higher dry-ashing temperature ($\lessapprox$1400°C) was required for complete volatilization. The dry-ashing temperature range was therefore more restricted than with sodium chloride solutions.

Analytical measurements in 5% sodium sulphate solutions were made with the same conditions as 5% sodium chloride (Table 1) but at a dry-ashing temperature of 1400°C. The results are summarized in Table 2.

There was no improvement in either precision or sensitivity compared with a sodium chloride medium. Therefore, since sodium sulphate solutions attack graphite more rapidly than sodium chloride solutions there is no advantage in using a sulphate medium.

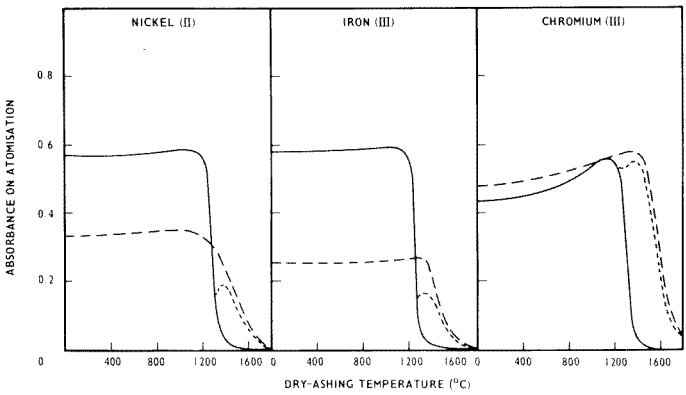

Fig. 4. Volatilization behaviour of trace metal sulphate in 5% (w/w) sodium sulphate solution. (——) 5% (w/w) sodium sulphate; (- - -) trace metal sulphate, 1 mg l^{-1}, in 0.005 M sulphuric acid; (---) trace metal sulphate in 5% sodium sulphate. The curves coincide with 5% sodium sulphate below about 1200°C.

DISCUSSION

This paper has demonstrated that any viable electrothermal a.a.s. technique for the determination of trace elements in a sodium salt matrix should first involve an in situ removal of the matrix. It has been shown that at the relatively slow heating rates of the dry-ashing stage, the sodium salt matrix may be removed with only small and acceptable losses of the less volatile trace metal salts.

The necessity of carrying out an in situ separation limits the minimum dry-ashing temperature to approximately 1100°C for sodium chloride or to 1400°C for sodium sulphate. Volatilization of the trace metal salts themselves imposes a maximum dry-ashing temperature, varying from 1300°C to 1500°C. These limits define the dry-ashing temperature range for the analytical determination.

At dry-ashing temperatures between 1100°C and 1400°C, only relatively small changes in sensitivity were found for both nickel(II) and chromium(III) in the presence of sodium chloride (Fig. 1). However, for iron(III) there was a marked reduction in sensitivity, probably because of a reduction in the degree of hydrolysis to hydrated iron(III) oxide, and hence the vaporization loss of the more volatile iron(III) chloride. To reduce this loss, ammonia and EDTA were added to convert the iron(III) chloride to less volatile iron(III) oxide during the dry-ashing stage. This approach was successful in minimizing the loss of iron(III), and both reagents markedly improved the overall sensitivity for both iron(III) and chromium(III), although not for nickel(II). A 1 M ammonia solution was found to give the greatest enhancement in sensitivity; EDTA was less effective and introduced significant contamination of iron(III).

TABLE 2

Analytical data for trace metals dissolved in 5% (w/w) sodium sulphate[a]

	Iron(III)	Nickel(II)	Chromium(III)
Sensitivity (absorbance per mg l^{-1})	0.15	0.19	0.52
Range of standard deviations (absorbance)	0.011—0.018	0.010—0.019	0.010—0.038
Range of standard deviations (mg l^{-1})	0.07—0.12	0.05—0.10	0.02—0.07
Limit of detection (mg l^{-1})	0.28	0.20	0.08

[a]2-μl samples; type 1 graphite rods; dry-ashing stage, 1400°C, 20 s; atomization stage, ~2500°C, 1.5 s.

Precision measurements in sodium chloride matrices, either with or without the addition of ammonia and EDTA, were made. These showed that although an increased sensitivity could be obtained with EDTA or ammonia, this was accompanied by a decrease in precision which offset any gain in sensitivity. A similar overall precision expressed in concentration terms was therefore found for each chemical condition examined. Attempts to improve sensitivity and precision by using the larger capacity 5-μl graphite rods were unsuccessful except for chromium. This was because of the poor evaporation characteristics from the deeper sample cavity of these rods.

Although it was possible to carry out the determinations with sodium sulphate solutions at dry-ashing temperatures between about 1300°C and 1500°C there was no improvement in precision. Also, as sodium sulphate solutions attack the graphite rod, there is no advantage in using this medium.

The results in Table 1 indicate that with a sodium chloride matrix, each of the trace metals may be determined in a 5% sodium chloride solution within the range 0.03—1 mg l^{-1}, with limits of detection of 0.050—0.096 mg l^{-1} and standard deviations of 0.01—0.06 mg l^{-1}. Converted into trace metal concentrations in samples of sodium metal these correspond to a range of about 2—50 mg kg^{-1}, limits of detection of 2.6—4.8 mg kg^{-1} and standard deviations of 0.56—2.8 mg kg^{-1}.

In principle, the selective volatilization technique should also be applicable to the tubular graphite furnace electrothermal atomizer commercially available with other atomic absorption spectrometers. For example, Ediger et al. [2] have reported the determination of trace metals (Cu, Cr, Fe, Pb and Zn) in sea water (about 3% sodium chloride) with such a system. It is considered, however, that the open graphite rod system may have advantages over the graphite tube system for the volatilization of gross amounts of salts, because re-deposition cannot occur in an open rod system whereas it could occur on the cooler parts of the tube system. This could cause accumulation of deposits which may re-volatilize during the atomization stage with significant interference effects.

One particular advantage of electrothermal atomization is its high absolute sensitivity. If it is assumed that semi-micro manipulation will allow 50 mg of

sodium metal to be dissolved in ethanol and subsequently converted to sodium chloride, this will provide approximately 2 ml of solution (≡5% NaCl). This volume will be vastly in excess of that needed for triplicate measurements for each of the three metals ($9 \times 2\ \mu l$). The technique therefore has potential application to segregation analyses where a series of small samples may be taken across a solidified sodium metal sample and each analysed for trace metals.

While the technique of electrothermal atomization with a graphite rod furnace has been shown capable of application to iron, chromium and nickel in sodium, it should also be applicable to the determination of other trace elements provided that they can be volatilized at a temperature >300°C above the melting point of sodium chloride.

The work was carried out at the Central Electricity Research Laboratories and is published by permission of the Central Electricity Generating Board.

REFERENCES

1 K. Garbett, G. I. Goodfellow and G. B. Marshall, Anal Acta, 126 (1981) 135.
2 R. D. Ediger, G. E. Peterson and J. D. Kerber, At. Absorpt. Newsl., 13 (1974) 61.

Analytica Chimica Acta, 126 (1981) 157—165
Elsevier Scientific Publishing Company, Amsterdam — Printed in The Netherlands

DETERMINATION OF INORGANIC AND METHYLATED ARSENIC SPECIES IN MARINE ORGANISMS AND SEDIMENTS

W. A. MAHER

Department of Oceanography, The University of Southampton (Gt. Britain)

(Received 26th November 1980)

SUMMARY

The determination of inorganic arsenic, monomethylarsenic and dimethylarsenic in marine organisms and estuarine sediments is described. The arsenic species are isolated by solvent extraction, separated by ion-exchange chromatography and selectively determined by arsine generation. Recoveries of spikes of 5 and 10 μg of arsenic taken through the whole procedure were 92—96%. Typical results obtained in a study of the forms of arsenic in several species of macroalgae, tissues of *Mercenaria mercenaria* and estuarine sediments are given.

The chemical form of arsenic in marine environmental samples is of interest from several standpoints. Marine organisms show widely varying concentrations of arsenic [1—3] and knowledge of the chemical forms in which the element occurs in tissues is relevant to the interpretation of these variable degrees of bioaccumulation and to an understanding of the biochemical mechanisms involved. Different arsenic species have different levels of toxicity [4] and bioavailability [5] and this is important in food chain processes, while physicochemical behaviour in processes such as adsorption onto sediments also varies with the species involved [6]. It has been shown that inorganic arsenic(III and V), monomethylarsenic (MMA) and dimethylarsenic (DMA) acids are present in natural waters [7], biological material [8] and sediments [9]. Thus analytical methods for the separation and measurement of these species are necessary for the study of pathways of accumulation and deposition in marine organisms.

Several methods for separating these arsenic species have been reported, including paper chromatography [10], electrophoresis [11], gas—liquid chromatography [7] and ion-exchange chromatography [9]. Modifications of the procedure developed by Braman et al. [12], in which inorganic and methylated species are isolated as volatile arsines and separated by sequential volatilization, are extensively used [13—15]. Arsine generation, however, suffers from severe metal ion interferences [16], and molecular rearrangements of the arsines during generation have been reported [13], although they can be made of negligible significance by appropriate choice of experimental conditions.

0003—2670/81/0000—0000/$02.50

This paper gives an account of a method which has been applied to the determination of inorganic arsenic, monomethylarsenic and dimethylarsenic in marine organisms and estuarine sediments, where sample pretreatment and interferences present greater problems than those met in earlier papers.

EXPERIMENTAL

Reagents

All reagents were of analytical grade. Stock solutions of arsenic(V) and arsenic(III) (1000 μg ml^{-1}) were prepared by dissolving As_2O_5 and As_2O_3, respectively, in 0.1 M sodium hydroxide solution. MMA and DMA stock solutions were prepared by dissolving their sodium salts in 1 M hydrochloric acid. Working standards were prepared by dilution of the stock solutions with 1 M hydrochloric acid. Other organic arsenic standards were prepared by dissolving *o*-arsanilic acid and arsenazo-I in 1 M HCl.

A reducing solution, consisting of a 1 M potassium iodide solution saturated with ascorbic acid, was prepared; it was discarded when it became yellow.

Apparatus

A Varian-Techtron AA5 atomic absorption spectrometer fitted with a Perkin-Elmer HGA 72 carbon furnace was used for the determination of arsenic, after arsine generation by injection of a small volume of acidified sample through a zinc reductor column. The column consisted of a glass tube (8 × 1.5 cm i.d.) packed with untreated zinc (2.5-mm mesh) and fitted with an injection port at the top and a stopcock at the bottom. Gas inlet and outlet holes were positioned such that a continuous stream of gas flowed through the column when it was connected into the inert gas line between the HGA 72 control module and the inlet to the furnace. A small column of calcium chloride (8—16 mesh) was also inserted into the inert gas line (between the zinc column and furnace) to prevent water vapour from entering the carbon furnace.

Sample storage and preparation

Samples were stored frozen to minimize possible changes by bacterial action. Samples of macroalgae were washed with distilled water to remove salts, dried at 60—80°C, and ground to pass a 340-μm sieve.

Molluscs were separated into their component tissues (mantle, visceral mass, gills, foot and abductors). Samples of each tissue were homogenized and a sub-sample taken for analysis.

Sediments were also dried at 60—80°C and ground to pass a 340-μm sieve.

Initial extraction

Biological material, dry (0.5—1 g) or wet (1—4 g), was refluxed in a 100-ml round-bottomed flask with 50 ml of 0.1 M sodium hydroxide solution for 24 h. The extract was filtered through Whatman No. 41 filter paper and

the solution evaporated to dryness under vacuum in a rotary evaporator. The residue was dissolved in 15 ml of 8.5 M hydrochloric acid.

Dried sediments (1 g) were shaken with 2 × 10 ml of 6 M hydrochloric acid for 5—6 h in a 50-ml polyethylene centrifuge tube, centrifuged and the supernatant solution retained. The residue was further extracted with 20 ml of a solution 0.1 M in sodium hydroxide and 1 M in sodium chloride. This extraction was repeated. The combined alkaline extracts were refluxed for 6 h and evaporated to dryness in a rotary evaporator. The residue was dissolved in 15 ml of 8.5 M hydrochloric acid. This solution, and the supernatant solution from the initial leaching, were analysed separately for arsenic compounds.

Isolation of inorganic and methylarsenic compounds

An aliquot (10 ml) of acid concentrate was transferred to a 50-ml glass centrifuge tube, and 1 ml of the reducing solution added. After 30 min, the arsenic species were extracted into 5 ml of toluene, using a vortex stirrer. Centrifugation was required to separate the organic phase which was transferred to a 100-ml separating funnel with a Pasteur pipette. The extraction was repeated with a further 5 ml of toluene. The arsenic species were back-extracted from the combined toluene extracts into water (2 × 4 ml) and after the addition of 1 ml of concentrated hydrochloric acid and 50 μl of a 5% potassium dichromate solution, the solution was made up to exactly 10 ml.

Chromatographic separation of the arsenic species

The arsenic species were separated on a 18 × 1.25-cm column of Dowex 50AG—X8 (100—200 mesh) which was washed initially with 50 ml of 0.5 M HCl. The extract (<1.5 ml) was added to the column and eluted sequentially with 0.5 M hydrochloric acid (10 ml), water (16 ml) and 1.5 M ammonia (25 ml). The fractions contained inorganic arsenic, MMA and DMA, respectively.

Determination of arsenic

The arsenic in each fraction was determined by reduction to the corresponding arsine in the zinc reductor column, decomposition of the arsine evolved in a heated carbon tube furnace, and by measurement of atomic absorption of the arsenic at 193.7 nm. The principal advantages of using the zinc reductor column are its rapidity and freedom from interferences by other elements.

Initial reduction of inorganic arsenic(V), MMA and DMA to the trivalent oxidation state was required for quantitative reduction to the corresponding arsine on the column. Conversion of the first of the above eluates was achieved by the addition of 1.5 ml of concentrated hydrochloric acid and 0.5 ml of reducing agent. The other eluates were evaporated to dryness after the addition of 2 ml of concentrated nitric acid to the monomethylarsenic fractions. The residues were dissolved in 2 ml of concentrated hydrochloric

acid and 1 ml of reducing agent added. After 30 min (to allow complete reduction) the solutions were diluted to 10 ml.

Before injection of 0.5—1 ml of solution into the zinc column, the inert gas flow rate was adjusted to 0.7 l min^{-1}, and the furnace (1700°C) and recorder were turned on and allowed to establish a stable baseline (approximately 10 s). The solution was injected as quickly as possible using a syringe and the furnace turned off when the recorder signal had returned to the previously established baseline (approximately 20 s).

Blanks for the entire procedure were typically less than 4 ng ml^{-1} and derived mainly from the hydrochloric acid.

RESULTS AND DISCUSSION

Cation exchangers have been used by several workers to separate inorganic and methylated arsenic species [9, 17, 18]. However, because of the presence of large quantities of inorganic and organic material in extracts of biological samples, the efficiency of the ion-exchange process may be impaired. Solvent extraction was used to avoid this difficulty.

Preconcentration of inorganic arsenic and methylarsenic compounds by extraction from acidic solution into toluene has been reported [19, 20]. Experiments were done to check if these species could be extracted selectively and quantitatively into toluene. The extraction was found to depend critically on the acid concentration (Figs. 1 and 2) and the presence of the reducing agent. When potassium iodide was not present, less than 5% of arsenic(V), monomethylarsenic acid (MMAA) and dimethylarsenic acid (DMAA) was extracted from 8 M hydrochloric acid. Potassium iodide reduces the arsenic species to the trivalent forms which are readily extracted into toluene. When

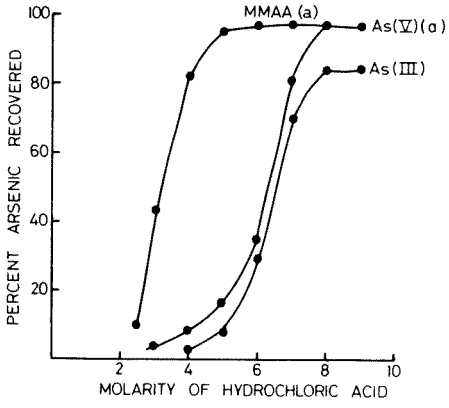

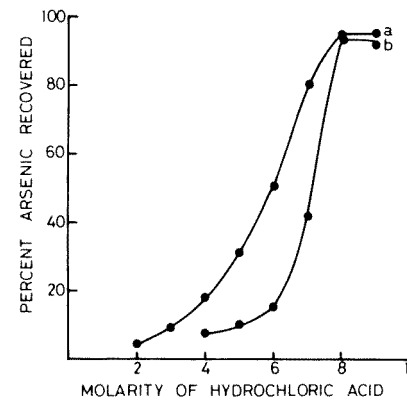

Fig. 1. Effect of acid concentration on the extraction of inorganic arsenic and MMAA into toluene: (a) acidic solution 0.1 M in KI; reduction time 1 h.

Fig. 2. Effect of acid concentration on the extraction of DMAA into toluene: acidic solution (a) 0.1 M in KI and ascorbic acid; (b) 0.1 M in KI only; reduction time 1 h.

ascorbic acid was added, in order partially to prevent the formation of iodine in the acidic solution, the percentage of extracted DMAA increased considerably over most of the acidity range (Fig. 2). Other organic arsenic compounds such as *o*-arsanilic acid and arsenazo-I were not extracted into toluene under any of the conditions investigated.

Inorganic arsenic(III) can be selectively extracted into toluene in the presence of inorganic arsenic(V), MMAA and DMAA, by carrying out the extraction without addition of the reducing agent. However, if any reducing species is present, e.g. iodide, the other arsenic species will be reduced and coextracted. Thus, in the analysis of most natural materials, inorganic arsenic(III) cannot be determined with any certainty and procedures were developed to measure only the total inorganic arsenic.

In the presence of the reducing agent, quantitative recoveries of the three arsenic species were obtained by extraction from hydrochloric acid (>7.5 M) with two 5-ml portions of toluene, followed by back-extraction into two 4-ml portions of water. Washing of the organic phase with acid was not employed as losses of DMA occurred.

Experiments with individual arsenic species (50 μg As) showed that DMAA was reduced more slowly than the other forms; a reduction time of 20—30 min was required for complete recovery of this species. In some of the development work, reduction times of up to 1 h were employed. The recoveries for the overall extraction procedure are given in Table 1.

Attempts to concentrate the aqueous solution after back-extraction, by boiling with and without oxidizing agents (nitric acid or hydrogen peroxide) to prevent losses of arsenic(III) species, led to variable recoveries of inorganic arsenic and MMA.

A modification of the elution scheme used by Tam et al. [17], described in the experimental section, was used to separate the arsenic species by cation exchange (Fig. 3). Recoveries were quantitative for arsenic(V), MMA and DMA, but not for arsenic(III) (Table 2). The aqueous extract was therefore oxidized by the addition of a 5% solution of potassium dichromate and concentrated hydrochloric acid, before the ion-exchange separation. This ensured that the species were present as arsenic(V).

TABLE 1

Percentage recoveries[a] of arsenic species in the solvent extraction procedure

Form	Arsenic added (μg)		
	1	5	10
As(V)	96.3 ± 1.0	97.2 ± 0.4	98.3 ± 0.6
MMA	95.6 ± 0.7	98.2 ± 0.5	99.0 ± 0.3
DMA	96.1 ± 1.5	97.9 ± 0.9	96.2 ± 1.0

[a] Values are means of two determinations.

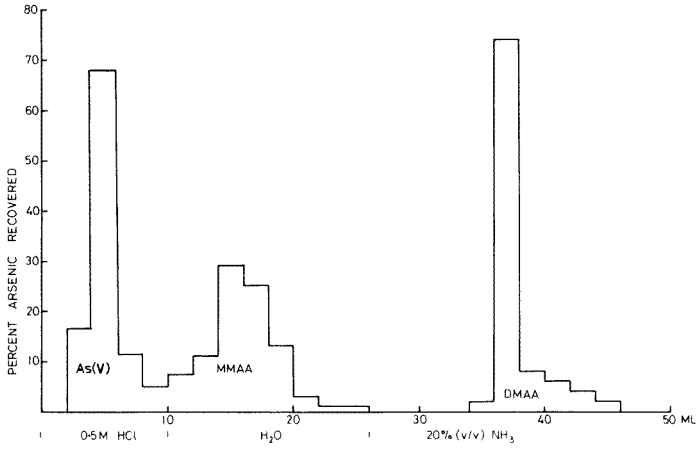

Fig. 3. Elution of arsenic compounds from Dowex 50AG-X8 (100—200 mesh) resin (50 μg As for each species).

The capacity of different reagents to remove arsenic from tissues was examined with macroalgae. The results (Table 3) showed that sodium hydroxide solutions or hot water generally gave the most effective extraction of arsenic. When arsenic in the extracts of *Laminaria digitata* was measured by the recommended procedure, it was found that much of the arsenic in the extracts was not accounted for by the forms determined (Table 4). Refluxing with 0.1 M sodium hydroxide solution gave the greatest recovery in the total characterized fraction. This refluxing was also found not to degrade MMAA or DMAA to inorganic arsenic and thus was used in all further studies of organic materials.

The recoveries of known additions of arsenic in various forms taken through the entire recommended procedure are shown in Table 5. With additions in the range 5—10 μg of arsenic, recoveries of 92—97% were obtained and in all cases recoveries were better than 90%. The chromatographic behaviour of each species when carried through the entire procedure

TABLE 2

Percentage recoveries[a] of arsenic species in the ion-exchange separation

Form	Arsenic added (μg)		
	0.1	0.5	1.0
As(III)	94.0 ± 1.8	—	92.3 ± 0.7
As(V)	96.0 ± 1.6	98.5 ± 0.8	98.0 ± 0.5
MMA	97.0 ± 0.8	96.5 ± 0.5	97.2 ± 0.3
DMA	97.1 ± 1.1	95.2 ± 0.2	96.1 ± 1.3

[a] Values are means of two determinations.

TABLE 3

Extraction of arsenic from macroalgae by various reagents

Alga	Total As[a] ($\mu g\ g^{-1}$)	Amount of arsenic ($\mu g\ g^{-1}$) extracted by			
		Water[b]	NaOH (0.1 M)[b]	NaOH (1 M)[c]	HCl (7.5 M)[c]
Laminaria digitata	56.1	48.9	53.8	55.0	55.0
Laminaria saccharina	49.0	47.6	39.7	41.9	35.8
Cystoseira tamariscifolia	28.6	24.8	28.1	28.5	19.0
Halidrys siliquosa	20.0	19.8	19.6	18.2	17.9

[a]Determined after decomposition with a mixture of nitric, sulphuric and perchloric acids. [b]Refluxed for 24 h with 30 ml. [c]Leached at room temperature for 5 h with 3 × 10 ml.

TABLE 4

Characterized forms of arsenic in extracts of *Laminaria digitata*

Extraction reagent[a]	Amount of arsenic ($\mu g\ g^{-1}$)				Characterized As / Extracted As[b]
	As	MMA	DMA	Total characterized	
Water	13.4	1.1	1.7	16.2	0.33
7.5 M HCl	7.9	0.8	—	8.7	0.16
1 M NaOH	7.2	—	—	7.2	0.13
0.1 M NaOH	12.8	2.9	14.6	30.3	0.56

[a]For conditions of extraction, see Table 3. [b]From Table 3.

TABLE 5

Percentage recoveries[a] of known amounts of arsenic in the recommended procedure

Form	Amount added (μg)		
	1	5	10
As(V)	91 ± 2	95 ± 1	94 ± 1
MMA	91 ± 1	94 ± 1	96.5 ± 0.5
DMA	90 ± 2	93 ± 2	92 ± 1

[a]Values are means of three determinations.

was identical with that when added directly to the column, indicating that the methylated species had not been degraded to inorganic arsenic.

Typical results obtained in a study of the forms of arsenic in several species of macro algae, tissues of *Mercenaria mercenaria* and estuarine sediments collected from the southern coast of England are given in Table 6.

TABLE 6

Forms of arsenic in selected marine organisms and sediments

Sample		Arsenic ($\mu g\ g^{-1}$) as			
			MMA	DMA	Total
Algae					
Laminaria saccharina		3.2	0.6	11.8	49.0
Cystoseira tamariscifolia		0.5	0.2	15.6	28.1
Halidrys siliquosa		0.1	—	7.6	20.0
Mollusc tissues (*Mercenaria mercenaria*)					
Mantle		1.1	0.8	1.5	8.4
Gills		—	0.2	2.0	3.4
Foot		—	—	0.8	2.0
Abductors		1.0	0.7	1.7	6.7
Visceral mass		2.4	9.9	6.4	23.2
Estuarine sediments					
Sample 1	HCl extract	10.6	0.7	0.3	12.3
	NaOH extract	0.8	1.9	4.1	6.1
Sample 2	HCl extract	5.2	0.8	0.1	6.4
	NaOH extract	1.4	5.0	2.6	8.5

In the extraction procedure for sediments an initial leach with 6 M hydrochloric acid was used in order to remove the bulk of carbonate and hydrated oxide phases before extraction with sodium hydroxide solution. This procedure gave a recovery of ca. 70% of the total arsenic in the sediment as determined following total decomposition.

The results for organisms show that a major part of the characterized arsenic in the algae occurred as DMA or as one or more compounds which become degraded to this form during oxidation or hydrolysis. A recent report [21] on algae from a region with unusually high concentrations of arsenic reached a similar conclusion. Significant fractions of DMA were found in the clam tissues, with a notable occurrence of MMA in the visceral mass. In sediments, significant amounts of the methylated forms were found in the sodium hydroxide extracts, indicating their importance in the organic material associated with these deposits.

I am grateful to Dr. J. D. Burton for critically reading the manuscript. This work was supported by a grant from the Dafydd Lewis Trust.

REFERENCES

1 T. M. Leatherland and J. D. Burton, J. Mar. Biol. Assoc. U.K., 54 (1974) 457.
2 G. Lunde, Environ. Health Perspect., 19 (1977) 47.
3 R. A. Grieg, D. R. Wenzloff and J. B. Pearce, Marine Pollut. Bull., 7 (1976) 185.
4 M. Dean Luh, R. A. Baker and D. E. Henley, J. Sci. Tot. Environ., 2 (1973) 1.
5 E. J. Coulson, R. E. Remington and K. M. Lynch, J. Nutr., 19 (1935) 255.

6 L. W. Jacobs, J. K. Syers and D. R. Keeney, Soil Sci. Soc. Am. Proc., 34 (1970) 750.
7 M. O. Andreae, Anal. Chem., 49 (1977) 820.
8 D. L. Johnson and R. S. Braman, Deep Sea Res., 22 (1975) 503.
9 D. G. Inverson, M. A. Anderson, T. R. Holm and R. R. Stanforth, Environ. Sci. Technol., 13 (1979) 1491.
10 G. K. H. Tam, S. M. Charbonneau, G. Lacroix and F. Bryce, Bull. Environ. Contam. Toxicol., 21 (1979) 371.
11 T. Edwards, H. L. Merilees and B. C. McBride, J. Chromatogr., 106 (1975) 210.
12 R. Braman, D. Johnson, C. Foreback, J. Ammons and F. Bricker, Anal. Chem., 49 (1977) 621.
13 Y. Talmi and D. T. Bostick, Anal. Chem., 47 (1975) 2145.
14 A. U. Shaikh and D. E. Tallman, Anal. Chim. Acta, 98 (1978) 251.
15 E. A. Crecelius, Anal. Chem., 50 (1978) 826.
16 A. E. Smith, Analyst, 100 (1975) 300.
17 G. K. H. Tam, S. M. Charbonneau, F. Bryce and G. Lacroix, Anal. Biochem., 86 (1978) 505.
18 F. T. Henry and T. M. Thorpe, Anal. Chem., 52 (1980) 80.
19 E. H. Daughtrey, A. W. Fitchett and P. Mushak, Anal. Chim. Acta, 79 (1975) 199.
20 A. Yasui, C. Tsutsumi and S. Toda, Agric. Biol. Chem., 42 (1978) 2139.
21 D. W. Klumpp and P. J. Peterson, Environ. Pollut., 19 (1979) 13.

Analytica Chimica Acta, 126 (1981) 167—174
Elsevier Scientific Publishing Company, Amsterdam — Printed in The Netherlands

A NOVEL DEVICE FOR THE ACCURATE DISPENSING OF SMALL VOLUMES OF LIQUID SAMPLES

J. G. SHABUSHNIG and G. M. HIEFTJE*
Department of Chemistry, Indiana University, Bloomington, IN 47405 (U.S.A.)
(Received 4th December 1980)

SUMMARY

A sample dispenser with electronic control of delivered volume has been designed and evaluated. With this device, liquid samples are dispensed in the form of uniform droplets less than 4 nl in volume; total volumes as small as 40 nl can be delivered with 1.5% precision. Important features of the microdroplet formation process have been studied and the effect of sample solution concentration and viscosity have been examined. The dispenser is expected to find application in several areas, including electrothermal atomization atomic absorption spectrometry, automated titrimetry, and high-precision, low-volume solution sampling.

Many analytical techniques require the accurate and precise application or delivery of small volumes of liquid samples. In order to meet these needs, various syringe-based dispensers have been designed [1—3]. However, these devices are generally limited to delivering volumes of 1 μl or larger and are not amenable to rapid, electronic control of the volume dispensed. They often suffer also from irreproducible transfer of the sample to a surface, such as that of an electrothermal atomizer [4].

Tiny samples in the form of microdroplets, typically 50—100 μm in diameter, have been used by several researchers in the study of atomization processes in chemical flames [5—7], and as a means of sample introduction in quantitative analysis [8]. Microdroplets have also been employed for titrant delivery in micro-titrations [9, 10].

The use of a microdroplet generator for sample delivery is attractive primarily because of the wide range of volumes which can be accurately dispensed and the ease with which this volume can be controlled by varying the number of droplets generated. Unfortunately, most devices used to generate microdroplets are not convenient to use and require substantial bulk volumes from which the droplets are extracted. Such devices form droplets by forcing the desired solution through a vibrating capillary or orifice and sonically decomposing the resulting jet into a stream of droplets. This method requires relatively large amounts of sample solution, is prone to failure from capillary clogging, and expels microdroplets with considerable velocity, making them hard to control and encouraging droplet splashing or shattering.

0003—2670/81/0000—0000/$02.50

In order to overcome these difficulties, a new kind of droplet-generator-based sample dispenser has been designed after the method described by Abbott and Cannon [11]. This system, shown in operation in Fig. 1, generates microdroplets by rapidly withdrawing a glass stylus from an aliquot of sample solution contained in a suitable reservoir. As the stylus is withdrawn, it pulls with it a filament of solution from the reservoir. Upon further withdrawal of the stylus, the filament detaches itself first from the stylus, and then from the bulk of solution remaining in the reservoir. This filament then collapses upon itself, forming a microdroplet which falls freely from the apparatus. The microdroplets fall in a reproducible trajectory and are easily collected on a surface or in a container.

In this paper, the utility of this device for sample dispensing and application is evaluated. It is demonstrated that sample volumes as small as 40 nl can be reliably dispensed, and sample delivery rates can range from the application of a single 40-nl volume in 0.7 s to sample flows of 36 μl min^{-1}. At present, sample delivery precision is known to be at least as good as 1.5% relative standard deviation (r.s.d.) for volumes greater than 40 nl. Unfortunately, measurement uncertainty currently precludes a better estimate of precision. Potential areas of application of the new apparatus are considered and its limitations discussed; the system is expected to be especially useful where small total volumes of sample material are available and where sample delivery precision is critical.

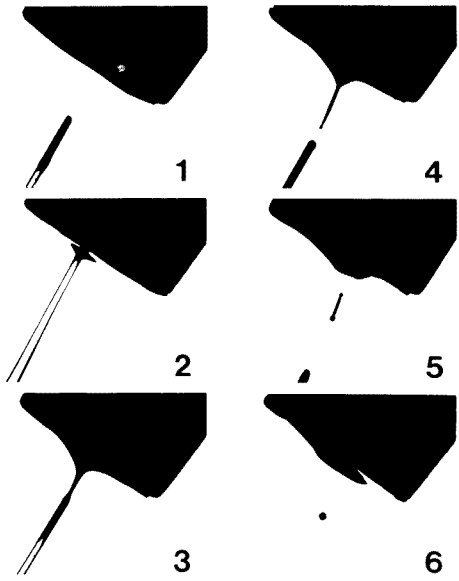

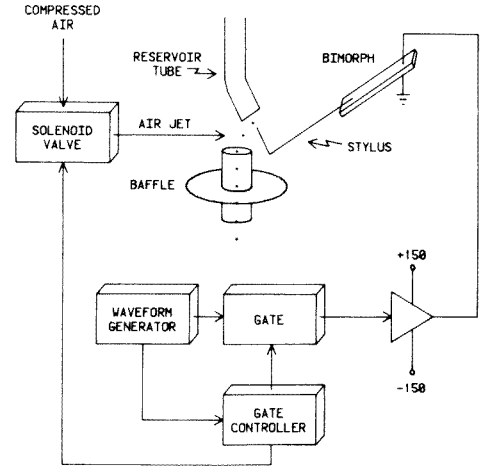

Fig. 1. Microdroplet formation sequence: (1—3) filament formation; (4) filament detaches from stylus; (5) filament collapse; (6) microdroplet.

Fig. 2. Schematic diagram of sample dispenser based on a microdroplet generator.

EXPERIMENTAL

Instrument description

A schematic diagram of the new sample dispenser is shown in Fig. 2, with the specific components listed in Table 1. The stylus is solid, drawn borosilicate glass with a main shaft 0.5 mm in diameter × 30 mm long and a tip 120 μm in diameter × 10 mm long. These specific dimensions are not critical, but have proven convenient in routine use. The stylus is driven by a ceramic piezoelectric bimorph mounted in a cantilever configuration. The stylus is affixed to the bimorph with epoxy cement and can be accurately positioned with respect to the reservoir by means of a vertical screw translator.

The bimorph itself is driven by an amplifier supplying a 100 V peak-to-peak sine wave at 157 Hz, the resonant frequency of the bimorph–stylus combination. It is necessary to operate this system at resonance in order to produce sufficient deflection of the stylus for microdroplet formation. The influence of operating frequency on stylus deflection is clearly shown in Fig. 3.

TABLE 1

Instrumental components (see Fig. 1)

Bimorph	PZT-5H 1.75 × 0.5 × 0.021 in. (Vernitron Piezoelectric Division, Bedford, OH)
Waveform generator	Built in-house, based on an EXAR XR-2206 CP integrated circuit
Gate	1H-5022 FET gate used in conjunction with a 741 operational amplifier
Gate controller	Built in-house, based on 7490 decade counters and 7485 4-bit comparators.
Amplifier	Built in-house, 2-stage push-pull amplifier capable of delivering 300 V peak-to-peak, approximate gain of 75.
Solenoid valve	Model 339-V-12-5 12-V solenoid valve (Angar Scientific, East Hanover, NJ)

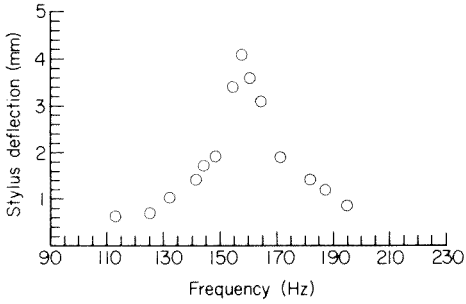

Fig. 3. Stylus deflection as a function of bimorph driving frequency (100 V peak-to-peak voltage applied to bimorph).

The reservoir tube used in the present study is a 4-cm long section of 2-mm i.d. glass tubing which holds the sample solution by capillary action. If a large sample volume is to be employed or many repetitive volumes of the same solution are to be dispensed, the reservoir tube can be coupled to a larger vessel through a siphon.

The baffle is a 25-mm section of 6-mm i.d. glass tubing placed through the center of a 40-mm diameter aluminum disk. This combination serves to shield the falling microdroplets from air currents about the apparatus, making their trajectory and therefore the location of sample deposition more reproducible.

An electronic gate allows the operator to select the exact number of microdroplets which are dispensed. Each cycle of the bimorph driving wave produces a single microdroplet. In turn, the number of driving wave cycles is controlled by a preset value in the gate controller, which opens the gate between the wave form generator and amplifier for the requisite number of cycles. In routine use, the volume which is dispensed is related to the number of bimorph driving cycles through a calibration curve or measured droplet volume. This hardware scheme could easily be duplicated under software control with a small laboratory computer or microprocessor.

The ceramic bimorph exhibits a significant level of hysteresis upon start up, causing the initial 100 droplets (200—400 nl total volume) to be formed with unacceptable reproducibility. Fortunately, acceptable precision (ca. 1%) and accuracy (±1.5%) can be restored by discarding the microdroplets formed in the first 100 cycles. The microdroplets are discarded by a jet of air which blows them into a trap. After the initial 100 cycles the air jet is terminated, allowing the remainder of the microdroplets to be dispensed. The air jet is synchronized with the gate controller and requires approximately 1 psig of air pressure to operate reliably.

Assessment of precision and accuracy

Several methods were employed to determine the volume of a single microdroplet, in order to assess the reproducibility of droplet volume, and to examine the effect of experimental variables on droplet size.

Droplet volume and its reproducibility were initially measured indirectly from the diameter of the impression formed by a falling microdroplet in a bed of fine-grain magnesium oxide [12]. Such a bed is easily prepared by burning a strip of magnesium ribbon in air and collecting the resulting oxide smoke on a microscope slide. The slide thus prepared was passed through the stream of falling microdroplets, with the resulting impressions viewed under a microscope. The diameters of these impressions were then quantified by comparison with a standard stage micrometer. To obtain the true droplet diameter, the values so obtained were multiplied by an empirically determined factor of 0.85 [13], to correct for distortion of the microdroplet on impact. This method allows droplet diameters to be determined with an accuracy of ±0.5 μm and a precision of 1.9% r.s.d.

A second method was employed to evaluate the accuracy and precision with which aggregates of microdroplets could be dispensed. For these measurements, the reservoir of the microdroplet generator was filled with a solution containing 10 mg Mg ml^{-1}. The dispenser was then used to deliver selected amounts of this "sample" into vials containing 3 ml of deionized water. The concentration of the resulting magnesium solution was determined by atomic absorption spectrometry. With this technique, accuracy of sample dispensing was evaluated by comparing measured magnesium concentrations with those calculated from the known microdroplet size, number of microdroplets dispensed, concentration of original magnesium solution, and the volume into which the sample was delivered.

The major uncertainty in this latter method is in the microdroplet volume measured from magnesium oxide impressions. A ± 0.5 μm uncertainty in diameter generates an approximately 2% uncertainty in volume for the range of microdroplet diameters examined. Other sources of error, propagated through the measurement procedure, raise the overall uncertainty to 3%.

Precision of sample delivery was determined by dispensing 5 replicate samples into measured volumes of water and comparing the resulting magnesium concentrations. Measurement of 5 aliquots of the same sample produced 1.0—1.5% r.s.d., indicating the limit of this method. Of course, these precision values are actually a result of errors in both the dispensing and measurement procedures. The precision of sample delivery might actually be better than the values reported.

RESULTS AND DISCUSSION

Single droplet studies

The size of individual microdroplets is governed by both the stylus diameter and the depth to which it penetrates the bulk liquid in the sample reservoir. Penetration depth is conveniently measured under stroboscopic illumination with a microscope containing a calibrated reticle. The range over which microdroplet size can be tuned with a 120-μm diameter stylus is indicated in Fig. 4. As shown, increasing penetration depth results in the production of microdroplets of a larger diameter. Increasing or decreasing the stylus diameter shifts this entire range up or down.

In the present study, microdroplets between 175—200 μm are preferred; they are large enough to fall along a reproducible trajectory but still possess a small individual volume for fine resolution in total sample volumes.

Solution viscosity and surface tension strongly affect the size of generated microdroplets. Although no exact relationship between these parameters has yet been deduced, Fig. 5 clearly shows an increase in microdroplet diameter with increasing solution viscosity. This behavior arises, presumably, from the formation of a longer, more stable filament from the higher viscosity solution (cf. Fig. 1, frame 4). This longer filament produces a larger microdroplet upon collapse. Also, surface tension influences microdroplet size by altering

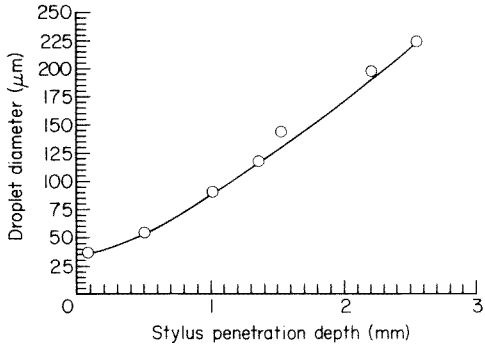

Fig. 4. Droplet diameter as a function of depth to which stylus penetrates bulk solution.

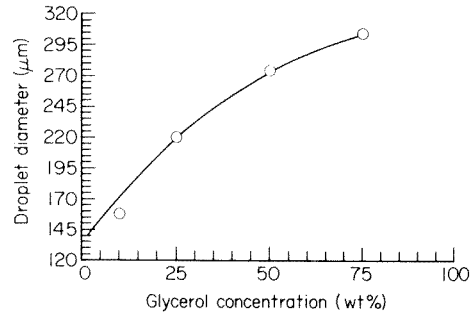

Fig. 5. Droplet diameter as a function of glycerol concentration in aqueous solution. Range of viscosities across curve is from 1 to 1000 cP (approximately).

the "grip" the stylus has on the solution filament. This "grip" affects the moment of detachment of the filament, and therefore influences the size of the resulting microdroplet. Importantly, although these factors affect the size of microdroplets dispensed, and therefore necessitate calibration, a wide range of solution viscosities as well as organic solvents can be conveniently dispensed.

From the magnesium oxide impression measurements, single microdroplets can be produced with a precision in diameter of 3.3% r.s.d. However, this error propagates to a relative standard deviation of 10% in terms of volume.

Aggregate sample studies

Calibration curves for the sample dispenser operating over the volume range 0—200 nl are shown in Fig. 6. Comparison with calculated values indicates an accuracy of approximately ±1.5% over these ranges. Typical values for precision, indicated in Table 2, suggest a usable lower limit for volumes dispensed of about 40 nl (with use of air jet).

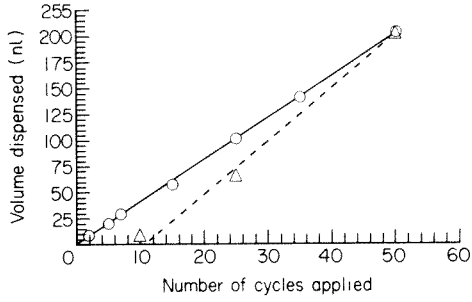

Fig. 6. Calibration curve for sample dispenser showing effect of the air jet on small volume samples (○) Experimental values after air jet turned off giving the fit $V_{nl} = (2.50 \pm 0.05)\ N + 2.5 \pm 1.5$ with S.E. = 1.7 nl and r = 0.998; (△) experimental values without air jet.

TABLE 2

Precision as a function of volume dispensed (without and with air jet deflection)

Volume dispensed (nl)		R.s.d. (%)[a]	
Without air jet	With air jet[b]	Without air jet	With air jet[b]
7.8	8.4	32.5	35.7
65	19.5	6.0	17.3
204	28.5	3.4	6.3
431	38.0	0.6	1.6
830	213	0.4	0.3
2,600		1.06	
3,900		0.4	
7,300		1.5	
10,100		1.1	
24,600		1.2	

[a]Based on a minimum of 5 measurements. [b]Air jet used to deflect initial 100 droplets.

Figure 6 indicates the importance of using the air-jet droplet deflection system to improve accuracy and precision for sample volumes below 200 nl. The use of the air-jet eliminates roll-off in the calibration curve, restoring an intercept at the origin. The improvement in precision is indicated by data in Table 2. For sample volumes greater than 200 nl, the air jet system is not required. Above the point of convergence of the two plots in Fig. 6, the data sets with and without the air stream are superimposed. Other data not included in Fig. 6 demonstrated linear behavior to 25 μl (V_{nl} = (2.53 ± 0.07) N + 2.51 ± 1.3 with S.E. = 5.1 nl). The only limits to larger volumes are reservoir capacity and the maximum count compatible with the gate controller. In the present instrument, both factors can be easily modified to accommodate a larger range of sample volumes if desired.

Droplet charge

In the course of this study on microdroplet formation, it was noticed that the microdroplets possess a small inherent charge. The charge was determined by passing the microdroplet stream between a set of planar copper electrodes held at 13.5 kV and measuring the resulting deflection. This method yields a value for the inherent charge on each microdroplet of 10^{-13} coulombs or approximately 10^6 electrons.

Conclusion

A sample dispenser based on a microdroplet generator can provide a wide range of sample volumes, nanoliter to microliter, under convenient electronic control. The device is reliable, inexpensive to build, and simple to operate. This device is currently being employed to improve precision in sample application to an electrothermal atomizer, but should also be useful in

microtitration or other applications where small, reproducible sample aliquots are needed.

This paper was presented in part at the Pittsburgh Conference on Analytical Chemistry and Applied Spectroscopy, Atlantic City, NJ, March, 1980. The work was supported in part by the Office of Naval Research, by the National Institutes of Health through grant PHS GM17904, and by the National Science Foundation through grant CHE 79-18073.

REFERENCES

1 K. R. Millar, F. Cookson and F. M. Gibb, Lab. Pract., 28 (1979) 752.
2 E. H. Pals, D. N. Baxter, E. R. Johnson and S. R. Crouch, Chem., Biomed., and Environ. Instrum., 9 (1979) 71.
3 V. Sacchetti, G. Tessari and G. Torsi, Anal. Chem., 48 (1976) 1175.
4 F. J. M. J. Maessen, F. D. Posma and J. Balke, Anal. Chem., 46 (1974) 1445.
5 G. M. Hieftje and H. V. Malmstadt, Anal. Chem., 40 (1968) 1860.
6 G. M. Hieftje and H. V. Malmstadt, Anal. Chem., 41 (1969) 1735.
7 B. M. Joshi and R. D. Sacks, Anal. Chem., 51 (1979) 1781.
8 G. J. Bastiaans and G. M. Hieftje, Anal. Chem., 45 (1973) 1994.
9 G. M. Hieftje and B. M. Mandarano, Anal. Chem., 44 (1972) 1616.
10 T. W. Hunter, J. T. Sinnamon and G. M. Hieftje, Anal. Chem., 47 (1975) 497.
11 C. E. Abbott and T. W. Cannon, Rev. Sci. Instrum., 43 (1972) 1313.
12 K. R. May, J. Sci. Instrum., 22 (1945) 187.
13 K. R. May, J. Sci. Instrum., 27 (1950) 128.

Analytica Chimica Acta, 126 (1981) 175—183
Elsevier Scientific Publishing Company, Amsterdam — Printed in The Netherlands

ADSORPTION OF CALCIUM AND MAGNESIUM IONS ON SURFACES

J. R. MAJER* and S. E. A. KHALIL

Chemistry Department, University of Birmingham, P.O. Box 363, Edgbaston, Birmingham B15 2TT (Gt. Britain)

(Received 10th December 1980)

SUMMARY

The adsorption of calcium and magnesium ions at trace levels in solution on borosilicate glass and polypropylene is described. The rate and extent of adsorption increases with increasing pH and the process is not completely reversible. The apparent energies of activation for the adsorption of calcium and magnesium ions on borosilicate glass are 17.5 and 10.5 kJ mol^{-1}, respectively. The corresponding half-lives are 568 and 127 h. For polypropylene the half-lives increase to 5775 and 537 h, respectively.

Because it is not always possible to analyse samples immediately after collection, it is necessary to ensure that samples can be stored without their composition changing. It is therefore important that there be no adsorption onto the surface of the container. The practice of freezing liquid samples so as to avoid adsorption is one solution to this problem. The stability of very dilute solutions with respect to adsorption and desorption must be determined before long-term storage is carried out. Loss of traces of ions by adsorption on laboratory glassware has long been recognized as a problem in radiochemistry [1]. The adsorption of fission products [2—4] and chromate [5] on glass has been studied to establish the efficiency of cleaning procedures. A comprehensive treatment of the adsorption of ions from nitric acid solutions and a discussion of associated analytical problems have been given by Starik [6].

The determination of trace concentrations of calcium and magnesium in water and in clinical samples, mainly in blood and urine, is widely required and of great importance, but little information has been published on the adsorption of calcium and magnesium on glass and plastic surfaces. The present work was confined to container adsorption of low concentrations of calcium and magnesium ions in order to develop a method for studying trace quantities of these ions.

EXPERIMENTAL

Apparatus, reagents and stock solutions

A Varian-Techtron model AA5 atomic absorption spectrometer, with air—acetylene flame was used. The instrument settings, slit width, wavelength,

0003—2670/81/0000—0000/$02.50

TABLE 1

Conditions used for determining calcium and magnesium by atomic absorption spectrometry

Parameter	Calcium	Magnesium
Wavelength, nm	422.7	285.2
Slit width, μm	100	100
Lamp current, mA	5	3
Flame height, cm	10	5
Acetylene flow rate, l h^{-1}	3	3
Air flow rate, l h^{-1}	15	15
Calibration, ppm	0—4	0—3

flame type and conditions are given in Table 1. The pH values were measured on an EIL Model 7030 pH meter fitted with Pye-Ingold pH electrodes.

Analytical-grade chemicals were used without further purification. Deionised water was used throughout (see below).

A 1000 ppm calcium stock solution was prepared by dissolving 1.2485 g of calcium carbonate in a minimum amount (5 ml) of concentrated nitric acid in a 500-ml volumetric flask and diluting to volume with water. From this solution, standard solutions of either 0.2, 0.4, 0.5, 1.0, 1.5 and 2 ppm or 2, 2.5, 3 and 4 ppm calcium were prepared immediately before use by suitable dilution (1 + 24) with 0.75% EDTA solution. The 0.75% (w/v) EDTA solution was prepared by dissolving 3.75 g of disodium-EDTA in water in a 500-ml volumetric flask.

A 1000 ppm magnesium stock solution was prepared by dissolving 0.5000 g of magnesium ribbon in 10 ml of concentrated nitric acid in a 500-ml volumetric flask and diluting to volume with water. From this solution, standard solutions of either 0.2, 0.4, 0.6, 0.8 and 1.0 ppm or 0.5, 1.0, 1.5, 2.0, 2.5 and 3.0 ppm magnesium were prepared immediately before use as required, by suitable dilution (1 + 24) with the above EDTA solution.

Deionized water was prepared by passing distilled water through an ion-exchange column containing 2 beds of cation (Amberlite IRC-50, analytical grade) and anion (Amberlite LR-4B, analytical grade) exchange resins.

Procedures for studying adsorption

Only new containers were used; they were 100-ml volumetric flasks made of polypropylene or borosilicate glass.

Cleaning procedure. The new containers were cleaned by immersing in 10% Decon 90 overnight, followed by rinsing in tap water and immersing in concentrated sulphuric acid—nitric acid (1 + 1) for 12 h (borosilicate glass) or 3 h (polypropylene). Polypropylene develops a yellow colour after >3 h. The containers were rinsed with distilled water, immersed in concentrated nitric acid for 3 h, rinsed with distilled water and finally with deionised water. If any container blank solutions were found to have detectable back-

grounds of calcium or magnesium after the cleaning process, the containers were discarded.

Solutions examined. The experiments were carried out on solutions of pH 1.5, 5, 7, 8 and 11 in the presence of 0.75% EDTA solution, and at two different concentration levels of each metal ion (0.5 and 2 ppm), in both types of flask. Into the cleaned flasks (10 borosilicate glass and 10 polypropylene) were pipetted 0.05 ml (to prepare 0.5 ppm Ca^{2+} or Mg^{2+} solutions) or 0.2 ml (to prepare 2 ppm Ca^{2+} or Mg^{2+} solutions) of 1000 ppm calcium or magnesium stock solution. A 0.75% solution of disodium-EDTA (4 ml) was added to each flask and the solutions were diluted to about 90 ml. The solutions were adjusted to pH 1.5, 5, 7, 8 or 11 with dilute sodium hydroxide or dilute nitric acid, and the volumes made up to 100 ml. The pH of each was checked and if necessary adjusted to within ±0.1 of the required pH. All test solutions were aged in the light at room temperature.

The solutions were shaken in the containers for a few seconds before aliquots were taken for the analysis. Fresh standards were used to compare adsorption losses. The test solutions were analysed at daily intervals. Compensation for small day-to-day changes in the working curves was made by running standards in acidic medium at approximately 15-min intervals during the analytical run.

Effect of temperature. Twenty solutions, 10 of each concentration level, were prepared in both borosilicate glass and polypropylene containers at pH 1.5, 5, 7, 8 and 11. The flasks were put in a thermostatted bath and the temperature controlled to within ±0.01°C. Five temperatures were investigated (40, 50, 60, 65 and 70°C).

Investigation of reversibility of adsorption. This was done by filling the volumetric flasks which had adsorbed calcium or magnesium ions with 0.1 M nitric acid (pH 1). The amount of desorbed ions was determined at daily intervals (for 5 days), and was calculated from the increase in the original concentration of calcium and magnesium in the borosilicate glass and polypropylene containers.

The per cent adsorption was calculated from $\%_{ads} = 100\ (C_0 - C_t)/C_0$, where C_0 is the original calcium or magnesium concentration (2 or 0.5 ppm), and C_t is the calcium or magnesium concentration at time t after the introduction of the solution into the test container. Thus $C_0 - C_t$ represents the amount of calcium or magnesium removed from solution by adsorption.

RESULTS AND DISCUSSION

The analysis of dilute aqueous solutions and clinical samples

While a study of the losses of calcium and magnesium ions from dilute aqueous solutions to container surfaces during analysis is of general interest, it is of particular significance in clinical studies of the concentrations of these two elements in serum because of the low levels involved.

The elements routinely determined in serum, plasma, blood cells and urine are the electrolyte metals calcium, magnesium, sodium and potassium, and iron, copper and zinc. The normal levels in serum are 92—104 ppm for calcium and 21.5 ppm for magnesium. These elements can be determined by atomic absorption spectrometry in the air—acetylene flame. Cooke and Price [7] have published methods for determining both elements in clinical and biological samples. Reproducible results are obtained only when EDTA is added to the sample solution before measurement.

In some recent studies it was noticed that the results obtained for calcium in serum were affected by prior treatment of the glassware used. If the glass surface had previously been exposed to solutions containing calcium then unsatisfactory results were obtained [8]. In the work described here, disodium-EDTA solution was used as a releasing agent for both calcium and magnesium.

Figures 1 and 2 show the results of experiments designed to measure adsorption with 0.5 ppm and 2 ppm of calcium and magnesium in aqueous solutions at different pH values stored in borosilicate and polypropylene containers. The percentage adsorption was calculated as shown above for a period of up to 30 days. Polypropylene containers showed slower rates for the adsorption of calcium and magnesium than the glass containers, as is shown by the data in Table 2 and by examination of Figs. 1 and 2.

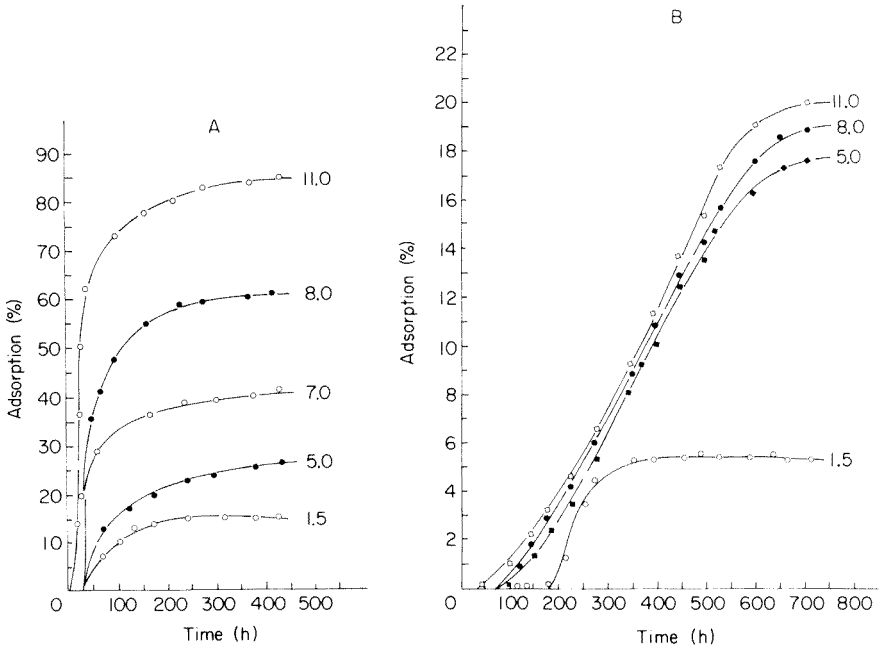

Fig. 1. Plots of % adsorption at different pH values against time. (A) 0.5 ppm Ca^{2+} on borosilicate glass; (B) 2 ppm Ca^{2+} on polypropylene. The numbers on the curves indicate pH.

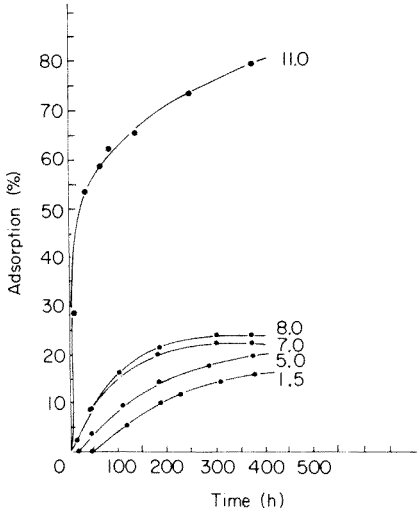

Fig. 2. Plot of % adsorption of 0.5 ppm Mg^{2+} in aqueous solutions on borosilicate glass at different pH values against time.

Adsorption of calcium and magnesium from aqueous solutions during storage appeared to depend on at least three parameters: container material, pH of solution and concentration of calcium and magnesium. The fact that there was greater adsorption of calcium and magnesium on glass surfaces seemed to suggest that these ions may become an integral part of the silicate lattice by an ion-exchange mechanism, while the interaction on the polymer surfaces is that of physical adsorption. Calcium loss in both glass and polypropylene containers was found in general to be slow compared with magnesium loss (Table 2 and Figs. 1 and 2). The rate and extent of adsorption of both calcium and magnesium is highly dependent on pH, the final amount adsorbed being <5% at pH 1, and >70% at pH 11.

The fact that the adsorption of magnesium was greater than that of calcium on both surfaces is related to the size of the ions. Magnesium has the smaller ionic size and therefore has a stronger interaction with surfaces.

TABLE 2

Adsorption of magnesium and calcium from aqueous solutions of initial concentrations 0.5 and 2 ppm at pH 7.0 in borosilicate glass and polypropylene containers

Conc. (ppm)	Container	Adsorption (%)			
		Calcium		Magnesium	
		72 h	336 h	72 h	336 h
2	Borosilicate glass	2.5	13	12.5	20
2	Polypropylene	1.5	8	2.5	12.5
0.5	Borosilicate glass	30	40	32.5	43
0.5	Polypropylene	6	10	8.1	28

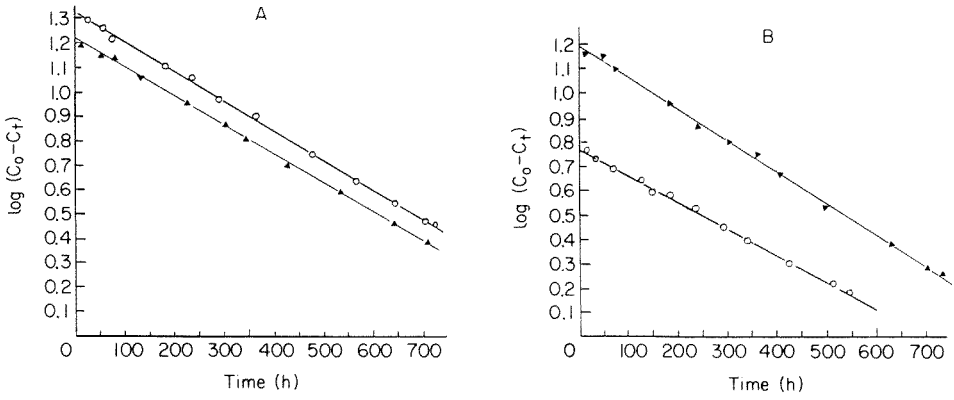

Fig. 3. Plots of log $(C_0 - C_t)$ against time for polypropylene (▲) and borosilicate glass (○) at pH 7.0, with (A) 2 ppm Ca^{2+}, and (B) 2 ppm Mg^{2+}.

Adsorption curves for 0.5 and 2 ppm calcium or magnesium in both borosilicate glass and polypropylene are similar, except that the degree of adsorption is less pronounced for the higher concentration.

Figure 3 shows plots of log $(C_0 - C_t)$ against time for calcium and magnesium losses from aqueous solutions at pH 7 in borosilicate glass and polypropylene containers. A linear relationship is observed between log $(C_0 - C_t)$ and time, suggesting first-order kinetics for the loss of calcium and magnesium from solutions under these experimental conditions. The rate constants for the loss of calcium and magnesium in borosilicate glass and polypropylene containers were determined from the slope of the line by the least squares method and are given in Table 3. The corresponding half-lives of calcium and magnesium losses in solution calculated from $t_{1/2} = 0.693/k$ are also given. The half-lives of calcium and magnesium losses in aqueous solutions depend on the nature of the container and are greater for polypropylene than for borosilicate glass, i.e., the borosilicate glass containers showed a faster rate for the adsorption than did polypropylene. The half-lives also show that the rate of loss of magnesium is greater than that of calcium on both surfaces.

TABLE 3

Rate constants and half-lives for losses of Ca^{2+} and Mg^{2+} from 2 ppm aqueous solutions at pH 7.0

	Calcium		Magnesium	
	$k(h^{-1})$	$t_{1/2}(h)$	$k(h^{-1})$	$t_{1/2}(h)$
Glass	1.22×10^{-3}	568	0.545×10^{-2}	127
Polypropylene	1.20×10^{-4}	5775	0.129×10^{-2}	537

TABLE 4

Saturation values of 0.5 and 2 ppm Ca^{2+} and Mg^{2+} solutions at different pH after 30 days

Conc. (ppm)	Container	Ca^{2+} adsorbed (%)					Mg^{2+} adsorbed (%)				
		pH 1.5	5.0	7.0	8.0	11.0	pH 1.5	5.0	7.0	8.0	11.0
2	Glass	3.5	10	14	17.5	85	15	20	35	50	80
	Polypropylene	5.2	10.5	14.5	20	22.5	6.5	7.5	20	25	27.5
0.5	Glass	14	25	40	60	86	16	30	43	66	87
	Polypropylene	8.3	12	20	25	30	10	20.5	24	28	30.5

In both polypropylene and glass containers the percentage loss of calcium and magnesium from 2 ppm solutions was much lower than that found from 0.5 ppm solutions at the same pH. The results for the saturation values of 0.5 ppm and 2 ppm calcium and magnesium after 30 days storage are given in Table 4.

It was found that during a 30-day ageing period, little calcium or magnesium was adsorbed on borosilicate glass or polypropylene container surfaces when the test solutions were maintained at pH 1.5. However, if the test solutions were maintained at pH >1.5, both borosilicate glass and polypropylene surfaces adsorbed the metal ions. Adsorption increases slowly at first then rapidly and linearly above pH 7 (Fig. 4). The effect of acidity on the adsorption of calcium or magnesium on borosilicate glass may be attributed to the increasing ionic dissociation of silicic acid in the glass with increasing pH.

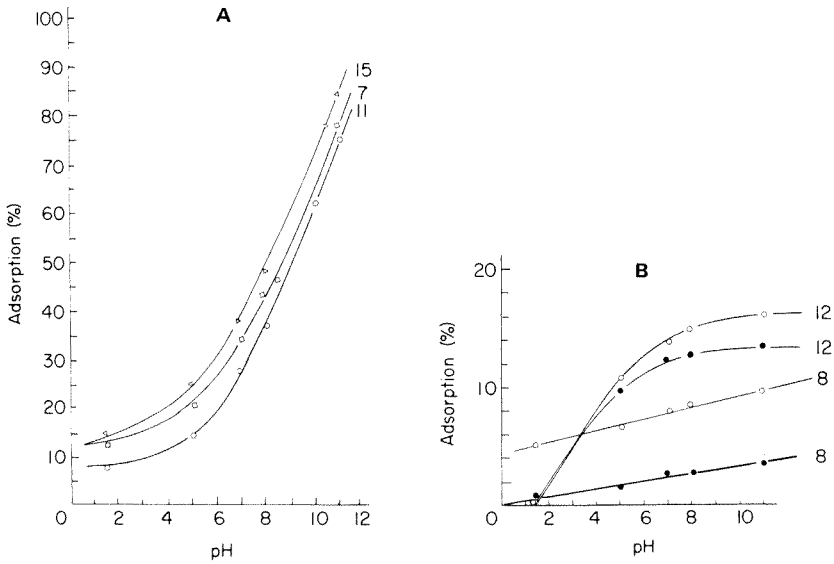

Fig. 4. Graph of % adsorption after different periods of time (days given on curves) against pH: (A) 0.5 ppm Ca^{2+} on borosilicate glass; (B) 2 ppm Ca^{2+} (•) and 2 ppm Mg^{2+} (○) on polypropylene.

Temperature effect

Borosilicate glass shows a positive temperature coefficient for adsorption of calcium and magnesium from solution. Increase of temperature was found to have no effect on the adsorption of calcium and magnesium onto polypropylene surfaces.

The temperature sensitivity of the adsorption process on borosilicate glass may be due to reaction of calcium and magnesium with the surfaces, or to some other steps in the adsorption process, e.g., the diffusion of calcium or magnesium ions through the liquid film at the solid surface, or a reduction in the degree of hydration of the ions. The data in support of the fact that the adsorption process depends on the reaction of calcium or magnesium on or at the borosilicate glass surface are given in Fig. 5, where the temperature dependence of the rate of adsorption of calcium and magnesium ions on borosilicate glass surfaces is shown by plotting the logarithm of the rate of adsorption against the reciprocal of the absolute temperature. The temperature dependences of the adsorption reactions are indicated by the slopes of the lines in Fig. 5. The apparent activation energies may be calculated from these slopes using the Arrhenius equation. The values obtained are 10.5 kJ mol^{-1} for magnesium and 17.5 kJ mol^{-1} for calcium. The greater rate of loss of magnesium is due to the lower activation energy required for the reaction of magnesium ions at the surface of borosilicate glass.

Desorption and reversibility

When borosilicate glass and polypropylene which had adsorbed calcium or magnesium were acidified with nitric acid (pH 1), the adsorption of the cal-

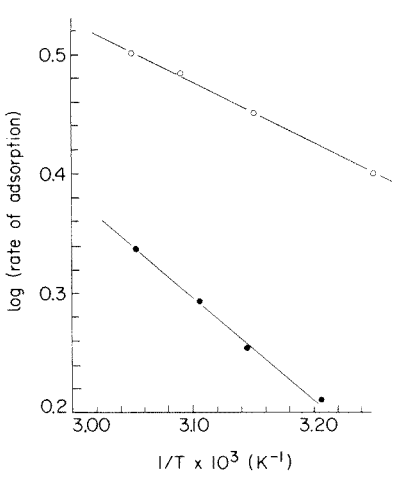

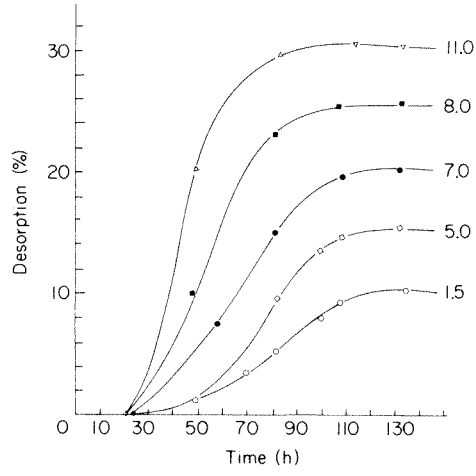

Fig. 5. Plot of log (rate of adsorption) of (•) Ca^{2+} and (○) Mg^{2+} against reciprocal of absolute temperature at pH 7.0.

Fig. 6. Graph of % desorption of Ca^{2+} at different pH values from borosilicate glass against time.

cium ions showed partial irreversibility for both containers, whereas magnesium adsorption was completely irreversible. This is attributed to the small size of magnesium ions which causes strong bonding between magnesium and container surfaces. Figure 6 shows the variation of the percentage of calcium desorbed ($C_t'/C_0 - C_t$), where C_t' is the concentration of calcium appearing in solution after time t when a surface loaded with an initial concentration $C_0 - C_t$ is exposed to nitric acid.

REFERENCES

1 J. Belloni, M. Haissinsky and H. N. Salama, J. Phys. Chem., 63 (1959) 881.
2 J. W. Hensley, A. O. Long and J. E. Willard, Ind. Eng. Chem., 41 (1949) 1415.
3 A. O. Long and J. E. Willard, Ind. Eng. Chem., 44 (1952) 916.
4 G. K. Schweitzer and W. M. Jackson, J. Am. Chem. Soc., 74 (1952) 4178.
5 E. P. Laug, Ind. Eng. Chem., 6 (1934) 111.
6 I. E. Starik, U.S. Atomic Energy Commission Report AEC tr-6314, 1964.
7 P. A. Cooke and W. J. Price, Spectrovision, 16 (1966) 7.
8 D. Cotterell, private communication, 1979.

Analytica Chimica Acta, 126 (1981) 185—190
Elsevier Scientific Publishing Company, Amsterdam — Printed in The Netherlands

SPECTROPHOTOMETRIC DETERMINATION OF SODIUM BY ION-PAIR EXTRACTION WITH CROWN ETHER COMPLEXES AND MONOANIONIC DYES†

MAKOTO TAKAGI, HIROSHI NAKAMURA, YUMIKO SANUI and KEIHEI UENO*

Department of Organic Synthesis, Faculty of Engineering, Kyushu University, Higashi-ku, Fukuoka 812 (Japan)

(Received 9th July 1980)

SUMMARY

A highly selective photometric procedure for the determination of sodium in blood serum is proposed, based on the ion-pair extraction of a sodium—cryptand complex. A comparative study of cryptands with various cavity sizes, different pairing anions and extraction solvents is described. The use of cryptand 211, picrate and toluene, as ligand, pairing anion and extraction solvent, respectively, allows sodium to be determined at the $\mu g\ ml^{-1}$ level. A 350-fold amount of potassium (by weight) does not interfere, nor do other alkali metals. Possible interferences by multivalent cations are masked by EDTA.

A selective photometric determination of potassium with 18-crown-6 and bromocresol green has already been described [1]; the potassium complex of the crown ether was extracted into benzene as an ion-pair with the dye anion. In the study reported here, a bicyclic cryptand was used instead of the crown ether to extract sodium selectively, making it possible to determine sodium in the presence of other alkali metal ions. A comparative study of cryptands with various cavity sizes with different pairing anions and extraction solvents allowed the optimal conditions to be established for the selective determination of sodium, and the procedure was applied to the determination of sodium in blood serum.

EXPERIMENTAL

Reagents

Picric acid and resazurin. Picric acid was recrystallized from ethanol. Resazurin was prepared by precipitation from an aqueous methanolic solution of the commercial sodium salt with excess of hydrochloric acid. The blackish-brown crystalline powder gave the correct elemental analysis for the anhydrous free acid. These dyes were stored as aqueous 2.5×10^{-3} M solutions in the form of their tetramethylammonium salts.

†Contribution No. 586 from the Department of Organic Synthesis, Faculty of Engineering, Kyushu University, Japan.

Cryptands. Commercial products (E. Merck, under the trade name Kryptofix) were used as received. The cryptands 2B22, 222, 221 and 211 were stored as aqueous 2.5×10^{-3} M solution.

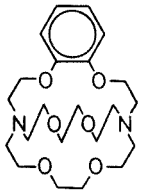
222B

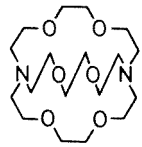
222

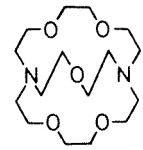
221

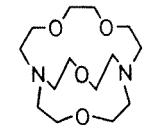
211

Tetramethylammonium hydroxide solution (alkali metal-free). An aqueous solution of tetramethylammonium bromide was treated with silver oxide and the clear filtrate was diluted to 0.2 M and stored in a plastic container.

Standard solutions. The standard or stock solutions of alkali metal chlorides ($1—5 \times 10^{-3}$ M) were acidified to 1×10^{-3} M with sulfuric acid.

Other reagents were of analytical grade and were used without further purification.

Solvent extraction

In a typical run, the aqueous solution was prepared by mixing 2.0 ml of picrate solution, 2.0 ml of cryptand solution, 0.5—4 ml of alkali chloride solution and enough water to give a total volume of 10 ml. This solution was shaken with 10 ml of toluene in a stoppered centrifuge tube for 10 min, and then centrifuged for 10 min at 3000 rpm. The absorbance of the organic phase was measured at 358—370 nm against a reagent blank on a Hitachi UV 200-20 double-beam spectrophotometer. When resazurin was used as the anionic dye, 1,2-dichloroethane was employed as the extraction solvent, and the absorbance was measured at 630 nm. The temperature was kept at 25 ± 2°C throughout the extraction study.

All the glassware (pyrex or similar grade) was soaked in nitric acid after conventional cleaning. This procedure was essential to obtain reproducible results when solutions with low alkali metal concentration were handled.

Recommended procedure for the determination of sodium in blood serum

Place 1.0 ml of serum and 3.0 ml of 0.1 M trichloroacetic acid solution in a centrifuge tube, mix well and then centrifuge for 10 min at 3000 rpm. Dilute a 0.50-ml aliquot of the supernatant liquid to 10.0 ml with water.

Transfer a 2.0-ml aliquot of the sample solution to a stoppered centrifuge tube, to which add 1.0 ml of aqueous 0.05 M EDTA (tetramethylammonium salt) solution, 1.0 ml of aqueous 0.2 M tetramethylammonium hydroxide solution, 2.0 ml of picrate solution, 1.0 ml of cryptand 211 solution and enough water to give a total volume of 10 ml. Mix well, shake with 10.0 ml of toluene for 10 min, and then centrifuge for 10 min at 3000 rpm. After

phase separation, measure the absorbance of the organic phase at 358 nm against a reagent blank using standard quartz cells.

RESULTS AND DISCUSSION

Ion-pair extraction of sodium—cryptand complexes

In a previous investigation [1], it proved impossible to establish conditions for the selective determination of sodium with the use of monocyclic crown ethers, because most of these crown ethers form more stable complexes with potassium than with sodium. However, it was expected that a selective procedure for sodium could be developed by taking advantage of the more selective nature of alkali metal complexation by bicyclic polyethers (cryptands) [2].

The ion-pair extraction of alkali metal—cryptand complexes can be shown schematically as

$$M^+ + CR + A^- \rightleftharpoons (M \cdot CR)^+ A^-$$

where M^+, CR and A^- represent alkali metal ion, cryptand and dye anion, respectively. M^+ and A^- are present in the aqueous phase, whereas the cryptand can be used in the aqueous or organic phase; the ion pair $(M \cdot CR)^+ A^-$, is in the organic phase. Thus, the original alkali metal concentration in the aqueous phase can be determined by measuring the absorbance of the organic phase after extraction.

In contrast to the monocyclic crown ethers, the ion-pair extraction of the alkali metal—cryptand complex takes place in a pH-dependent manner, because of the basic nature of the cryptands. However, at pH above 10.5, where the protonation of cryptands can be neglected, the extraction becomes pH-independent. Lower pH caused some extraction of the protonated cryptand (CRH^+), which made the extraction pattern of the metal ion complicated. Accordingly, the absorbance of the organic phase was measured after extraction at pH >10.5.

A comparative extraction study was carried out on Li^+, Na^+, K^+, Rb^+ and Cs^+ using the cryptands with various cavity sizes listed above, and different anionic dyes and solvents, to establish the optimal conditions for the selective determination of sodium ion.

Some typical results are illustrated in Figs. 1 and 2. The plots in these figures are generally not linear, because the extraction is not quantitative. For example, in the extraction of potassium as illustrated in Figs. 1 and 2, only about 92% and 67%, respectively, of potassium ion was extracted. The slopes of the plots in these figures define the apparent molar absorptivities of the complexed alkali metal ion-pairs. For the non-linear plots, the lower metal concentration portion was approximated by a straight line, although the procedure proved to be rather arbitrary for the less well extracted metal ions.

When 1,2-dichloroethane was used as the extraction solvent, picrate in

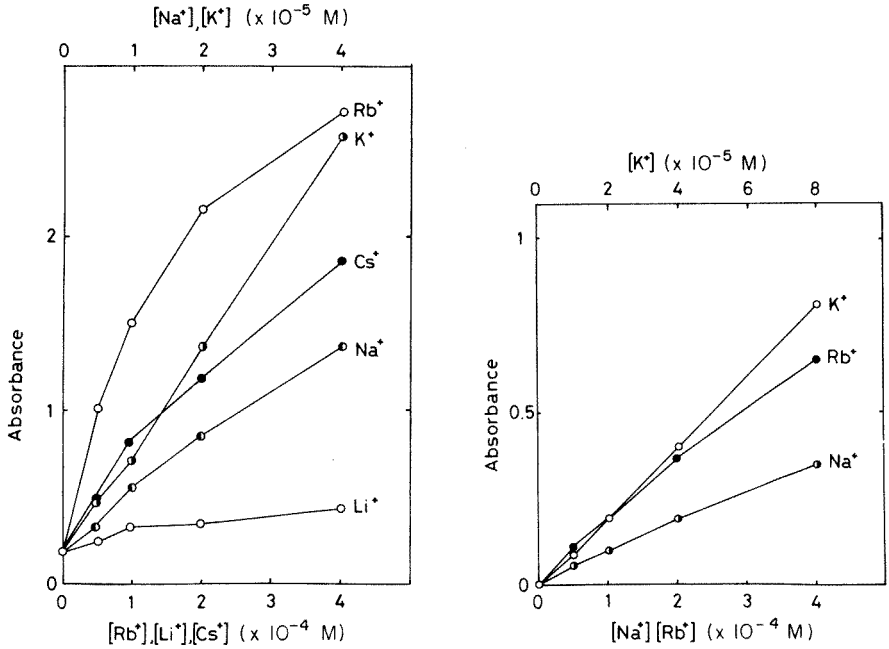

Fig. 1. Extraction of alkali metal ions into 1,2-dichloroethane by cryptand 2B22 with resazurin (λ_{max} 630 nm). Initial concentrations, [2B22] (aqueous) = [resazurin] (aqueous) = 5×10^{-4} M; pH >10.5 (Me_4NOH).

Fig. 2. Extraction of alkali metal ions into toluene by cryptand 221 with picrate (λ_{max} 360 nm). Initial concentrations, [221] (aqueous) = [picric acid] (aqueous) = 5×10^{-4} M; pH >10.5 (Me_4NOH).

TABLE 1

Apparent molar absorptivities of the alkali metal cryptate ion-pair after extraction

Cryptand	Anion	Extraction solvent	Li	Na	K	Rb	Cs
			"ϵ" ($\times 10^3$) at 630 nm				
222	Resazurin	1,2-Dichloroethane	1	35	55	47	6
2B22	Resazurin	1,2-Dichloroethane	1	30	61	21	9
221	Resazurin	1,2-Dichloroethane	1.4	45	16	3	5
211	Resazurin	1,2-Dichloroethane	18	1	—[a]	—	—
			"ϵ" ($\times 10^3$) at 360 nm				
222	Picrate	Toluene	—	—	2.3	1.6	—
2B22	Picrate	Toluene	—	1.8	13	2.9	—
221	Picrate	Toluene	—	0.9	10	1.9	—
211	Picrate	Toluene	—	2.3	0.01	—	—

[a] Dashes indicate no extraction.

the aqueous phase (pH 10.5) was partly extracted, giving a high blank value in the final measurement. Therefore, only resazurin was used as the pairing anion in the 1,2-dichloroethane extraction. In contrast, the resazurin ion-pair cannot be extracted into toluene, so that only picrate was employed in the toluene extraction. These results suggest that picrate is more hydrophobic than resazurin in the ion-pair extraction of cryptand complexes. The results are summarized in Table 1.

Resazurin surpasses picrate in photometric sensitivity, but picrate provides better selectivity among the neighboring metals. The higher photometric sensitivity in the resazurin ion-pair extraction may be partly due to the higher molar absorptivity of resazurin (ϵ = 6.7 × 10^4 l mol^{-1} cm^{-1} at λ_{max} 630 nm) compared to picrate ion (ϵ = 1.6 × 10^4 l mol^{-1} cm^{-1} at λ_{max} 360 nm), and partly due to the higher extraction ratio in the resazurin—1,2-dichloroethane system than in the picrate—toluene system. It should be noted that the selectivity of cryptand 221 to sodium and potassium is completely reversed by changing both the dye and the extraction solvent. This proves that the selectivity of metal extraction is not governed solely by the relative ease of complexation of the metal ion with the cryptand in the aqueous phase, and indicates the importance of the ion-pairing interaction in the extraction step.

It can be concluded from Table 1 that sodium ion can be determined most selectively with the use of cryptand 211, picrate and toluene as ligand, pairing anion and extraction solvent, respectively.

Extraction spectrophotometry of sodium in blood serum

Since spectrophotometry is the most practical routine technique among the instrumental methods for trace element determinations, the proposed method was applied to the determination of sodium in blood serum. A

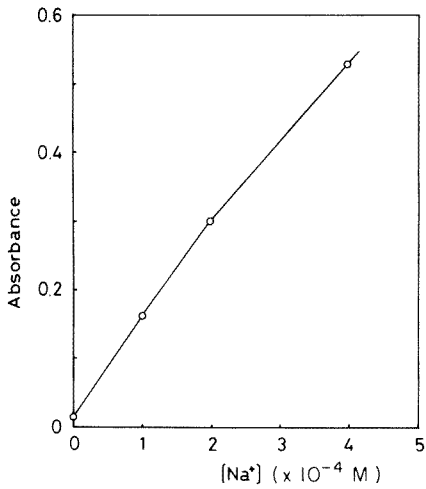

Fig. 3. Calibration curve for sodium in blood serum obtained with the cryptand 211—picrate—toluene system at 358 nm. The sodium ion concentrations given relate to the final solution.

TABLE 2

Determination of sodium in blood serum

Sample	Sodium ion concentration (meq l^{-1})	
	This method	Atomic absorption
A	146	142
B	143	141
C	137	140
D	138	137

calibration curve was prepared according to the procedure described in the Experimental part using a standard sodium chloride solution instead of serum. The calibration curve (Fig. 3) is almost linear over the range $0—4 \times 10^{-4}$ M sodium ion. The proposed method is fairly sensitive, so that serum samples must be diluted 400-fold.

The selectivity for sodium over potassium is about 350:1 (by weight). Lithium, rubidium and cesium, although they are not usually found in blood, do not interfere at all. Any possible interferences by multivalent cations can be masked with EDTA (tetramethylammonium salt) [3]. Contamination by lipophilic ions, e.g., surfactants, must be strictly eliminated. As shown in Table 2, the results by the proposed method are in good agreement with those obtained by the atomic absorption method.

This method is sensitive (Sandel sensitivity, 0.017 μg Na cm^{-2}) so that sodium in various samples can be determined down to the μg ml^{-1} level without difficulty.

The authors are grateful for a Grant-in-Aid for Scientific Research from the Ministry of Education, Science and Culture of Japan.

REFERENCES

1 H. Sumiyoshi, K. Nakahara and K. Ueno, Talanta, 24 (1977) 763.
2 J. M. Lehn and J. P. Sauvage, J. Am. Chem. Soc., 97 (1975) 6700.
3 H. Nakamura, M. Takagi and K. Ueno, Anal. Chem., 52 (1980) 1668.

Analytica Chimica Acta, 126 (1981) 191—197
Elsevier Scientific Publishing Company, Amsterdam — Printed in The Netherlands

DETERMINATION OF THE EXTRACTION CONSTANT OF GOLD DIETHYLDITHIOCARBAMATE DICHLORIDE BY SUBSTOICHIOMETRIC EXTRACTION

J. M. LO*, C. L. TSENG and S. J. YEH

Institute of Nuclear Science, National Tsing Hua University, Hsinchu, Taiwan 300 (Republic of China)

(Received 1st September 1980)

SUMMARY

Radioactive gold(III) with radioactive palladium(II) as reference ion in a chloride medium was substoichiometrically extracted with zinc diethyldithiocarbamate in chloroform. A formula for calculation of the extraction constant of the gold(III) complex was derived, for which only the values of distribution ratios of gold and palladium between the two phases had to be measured experimentally. The extraction constant was found to be log K = 68.9 ± 0.4.

More than thirty metals form chelates with diethyldithiocarbamate (DDC) [1]. The extraction constant of gold(III) diethyldithiocarbamate is one of the highest involving that ligand [2, 3]. Kukula et al. [4, 5] found that the gold chloride diethyldithiocarbamates $Au(DDC)_2Cl$ and $Au(DDC)Cl_2$ could exist if gold(III) were extracted from a chloride medium with diethyldithiocarbamate. The absolute values of the extraction constants of these chelates are very high, and their determination is difficult and complicated [6—8]. The present study is a new approach in the determination of the extraction constants of gold diethyldithiocarbamates using a fairly simple and reliable experimental technique.

THEORY

To an aqueous solution containing equivalent amounts of gold(III) and palladium(II) in a chloride ion medium, a substoichiometric amount of extractant, $Zn(DDC)_2$ in chloroform, is added. The mixture is shaken to reach equilibrium. In this extraction system, palladium(II) functions as a reference ion and its extraction constants, $K_{Pd(DDC)_2}$ and $K_{Pd(DDC)Cl}$, are used as reference values in the estimation of the extraction constants of gold(III). Both the gold and palladium are labelled with radioisotopes, whereas $Zn(DDC)_2$ is not radioactive. From previous work [9], the following equations can be written for the above substoichiometric extraction scheme

$$2/3\ Au^{3+} + Zn(DDC)_{2(o)} \rightleftharpoons 2/3\ Au(DDC)_{3(o)} + Zn^{2+}$$

$$Pd^{2+} + Zn(DDC)_{2(o)} \rightleftharpoons Pd(DDC)_{2(o)} + Zn^{2+}$$

The equilibrium constants for these reactions are

$$K_1 = [Au(DDC)_3]_o^{2/3}\,[Zn^{2+}]/[Au^{3+}]^{2/3}\,[Zn(DDC)_2]_o$$

$$K_2 = [Pd(DDC)_2]_o\,[Zn^{2+}]/[Pd^{2+}]\,[Zn(DDC)_2]_o$$

so that

$$[Au(DDC)_3]_o^{2/3}\,[Pd^{2+}]/[Au^{3+}]^{2/3}\,[Pd(DDC)_2]_o$$
$$= (K_{Au(DDC)_3})^{2/3}/K_{Pd(DDC)_2} = K_1/K_2 = K$$

The definitions of the terms and the symbols used are summarized in Table 1. This equation can be converted to

$$\frac{(\alpha_{Pd(DDC)_2})^{3/2}\,(r_{*Au})}{(r_{*Pd})^{3/2}} = \frac{(\alpha_{Pd^{2+}})^{3/2}}{(K_{Pd(DDC)_2})^{3/2}\,(\alpha_{Au^{3+}})} \times K_{Au(DDC)_3}\left\{1 + \frac{K_{Au(DDC)_2Cl}[Cl^-]}{K_{Au(DDC)_3}[DDC^-]} + \frac{K_{Au(DDC)Cl_2}[Cl^-]^2}{K_{Au(DDC)_3}[DDC^-]^2}\right\} \quad (1)$$

TABLE 1

Definitions and constant values used

Symbol	Definition[a]	Value	Ref.
1. Extraction constants			
$K_{Pd(DDC)_2}$	$[Pd(DDC)_2]_o/[Pd^{2+}][DDC^-]^2$	$10^{69.8}$	[13]
$K_{Pd(DDC)Cl}$	$[Pd(DDC)Cl]_o/[Pd^{2+}][DDC^-][Cl^-]$	$10^{47.2}$	[13]
$K_{Au(DDC)_3}$	$[Au(DDC)_3]_o/[Au^{3+}][DDC^-]^3$		
$K_{Au(DDC)_2Cl}$	$[Au(DDC)_2Cl]_o/[Au^{3+}][DDC^-]^2[Cl^-]$	$10^{81.5}$	[7]
$K_{Au(DDC)Cl_2}$	$[Au(DDC)Cl_2]_o/[Au^{3+}][DDC^-][Cl^-]^2$	$10^{68.2}$	[6]
2. Total concentration of the metal involved			
$C_{Pd(w)}$	$[Pd^{2+}] + [PdCl^+] + [PdCl_2] + \cdots\cdots\cdots$		
$C_{Pd(o)}$	$[Pd(DDC)_2]_o + [Pd(DDC)Cl]_o$		
$C_{Au(w)}$	$[Au^{3+}] + [AuCl^{2+}] + [AuCl_2^+] + \cdots\cdots$		
$C_{Au(o)}$	$[Au(DDC)_3]_o + [Au(DDC)_2Cl]_o + [Au(DDC)Cl_2]_o$		
3. Ringbom coefficients[b]			
$\alpha_{Pd^{2+}}$	$C_{Pd(w)}/[Pd^{2+}]$	$10^{6.59}$	[10—12]
$\alpha_{Au^{3+}}$	$C_{Au(w)}/[Au^{3+}]$	$10^{26.35}$	[10—12]
$\alpha_{Pd(DDC)_2}$	$C_{Pd(o)}/[Pd(DDC)_2]_o$		
$\alpha_{Au(DDC)_3}$	$C_{Au(o)}/[Au(DDC)_3]_o$		
4. Distribution ratios[c]			
r_{*Pd}	$C_{Pd(o)}/C_{Pd(w)}$		
r_{*Au}	$C_{Au(o)}/C_{Au(w)}$		

[a]The subscript "o" represents the organic phase and no subscript or "w" represents the aqueous phase. [b]The values of $\alpha_{Pd^{2+}}$ and $\alpha_{Au^{3+}}$ are calculated for $[Cl^-] = 0.1$ M. $\alpha_{Au(DDC)_3}$ is equal to the term bracketed { } in eqn. (1). [c]The asterisks indicate that the values were determined by radioactivity measurement in the present study.

Here, $\alpha_{Pd^{2+}}$ and $\alpha_{Au^{3+}}$ are the constants which can be calculated from the overall stability constants of the metal—chloride complexes in the chloride medium [10—12]. Values for $K_{Pd(DDC)_2}$ and $K_{Pd(DDC)Cl}$ are available in the literature [13] (Table 1). Usually the experimental condition can be adjusted so as to maintain $[Cl^-] = 0.1$ M and $[Cl^-] \gg [M^{m+}]$.

Let $Y = (\alpha_{Pd(DDC)_2})^{3/2} (r_{*Au})/(r_{*Pd})^{3/2}$ and $X = 1/[DDC^-]$. Then eqn. (1) becomes

$$Y = A K_{Au(DDC)_3} + B K_{Au(DDC)_2Cl} X + C K_{Au(DDC)Cl_2} X^2 \quad (2)$$

where $A = (\alpha_{Pd^{2+}})^{3/2}/(K_{Pd(DDC)_2})^{3/2} (\alpha_{Au^{3+}})$, $B = (\alpha_{Pd^{2+}})^{3/2} |Cl^-|/(K_{Pd(DDC)_2})^{3/2} (\alpha_{Au^{3+}})$, and $C = (\alpha_{Pd^{2+}})^{3/2} [Cl^-]^2/(K_{Pd(DDC)_2})^{3/2} (\alpha_{Au^{3+}})$. The values of A, B, and C can be regarded as constants in eqn. (2), which can easily be evaluated from the data given in Table 1.

Both Y and X can be obtained from the experimental data as follows. From the definitions in Table 1

$$\begin{aligned} \alpha_{Pd(DDC)_2} &= C_{Pd(o)}/[Pd(DDC)_2]_o = 1 + [Pd(DDC)Cl]_o/[Pd(DDC)_2]_o \\ &= 1 + K_{Pd(DDC)Cl}[Cl^-]/K_{Pd(DDC)_2}[DDC^-] \end{aligned} \quad (3)$$

and $K_{Pd(DDC)_2} = [Pd(DDC)_2]_o/[Pd^{2+}][DDC^-]^2 = \alpha_{Pd^{2+}} r_{*Pd}/\alpha_{Pd(DDC)_2}[DDC^-]$

By combining these two equations,

$$K_{Pd(DDC)_2} = \alpha_{Pd^{2+}} r_{*Pd}/[DDC^-]^2 \{1 + K_{Pd(DDC)Cl}[Cl^-]/K_{Pd(DDC)_2}[DDC^-]\}$$

and $K_{Pd(DDC)_2}[DDC^-]^2 + K_{Pd(DDC)Cl}[Cl^-][DDC^-] - \alpha_{Pd^{2+}} r_{*Pd} = 0$

From the latter equation,

$$[DDC^-] = \{-K_{Pd(DDC)Cl}[Cl^-] + \{(K_{Pd(DDC)Cl}[Cl^-])^2 + 4\alpha_{Pd^{2+}} K_{Pd(DDC)_2} r_{*Pd}\}^{1/2}\}/2 K_{Pd(DDC)_2}$$

From the values given in Table 1, $(K_{Pd(DDC)Cl}[Cl^-])^2 \gg 4\alpha_{Pd^{2+}} K_{Pd(DDC)_2} r_{*Pd}$. Hence

$$[DDC^-] = \alpha_{Pd^{2+}} (K_{Pd(DDC)Cl}[Cl^-])^{-1} r_{*Pd} \quad (4)$$

From the initial definitions of X and Y and from eqns. (3) and (4), Y and X can be converted to functions of the experimentally measured distribution ratios r_{*Au} and/or r_{*Pd} only. That means that Y and X in eqn. (2) can be measured experimentally. In accordance with eqn. (2), $K_{Au(DDC)_3}$, $K_{Au(DDC)Cl}$, and $K_{Au(DDC)Cl_2}$ can be obtained simultaneously be plotting Y vs. X.

EXPERIMENTAL

Reagents

The substoichiometric extraction agent, $Zn(DDC)_2$, was prepared by the method suggested by Wyttenbach and Bajo [14]. The radiotracer ^{198}Au was produced by irradiating gold metal (99.999%, Koch-Light, Colnbrook,

England) in the Tsing Hua Open Pool Reactor at the University (neutron flux $\simeq 2 \times 10^{12}$ n cm^{-2} s^{-1}) for 12 h. The gold was dissolved in aqua regia, the solution repeatedly evaporated on a water bath to near dryness to remove nitric acid (adding water to avoid drying out), and finally diluted with 0.1 M hydrochloric acid. The gold(III) solution and the ^{198}Au solution were prepared in this way. Palladium chloride (extra pure grade, Wako Co., Japan) was irradiated under the same conditions as above for 6 h to form ^{109}Pd. The irradiated compound was allowed to cool for one day until ^{38}Cl had decayed, and was then dissolved in 0.1 M hydrochloric acid. Un-irradiated palladium chloride was also dissolved in 0.1 M hydrochloric acid. All the other reagents were pro analysi grade (Merck). Sub-boiling redistilled water (ca. 92°C) was used throughout.

Extractions

Glass-stoppered Erlenmeyer flasks (50 ml) were used as extraction vessels. The volume of aqueous and organic phases was 10.0 ml. The concentrations of gold(III) and palladium(II) were adjusted to $(1/m) \times 10^{-4}$ M 0.1 M hydrochloric acid (where m is the oxidation number of the metal ions). In each extraction, either gold(III) or palladium(II) was used with the labelled solution. Several different concentrations of the extractant, $Zn(DDC)_2$, were prepared and used in a series of substoichiometric extractions of the gold—palladium solutions. All the extractions had reached equilibrium after shaking mechanically for 2 h at 25 ± 0.1°C [6—8, 13].

Radioactivity measurements

Aliquots (5 ml) of the organic and aqueous phases were taken from the flasks for radioactivity counting after the extractions were completed. A Ge(Li) detector was used. The 412-keV γ-ray was detected for ^{198}Au, whereas the 88-keV γ-radiation (from ^{109m}Ag, the daughter of ^{109}Pd) was detected for ^{109}Pd. The detector was connected to a 4096-channel pulse-height analyzer, with a high resolution of 2.2 keV (f.w.h.m.) for the 1332-keV ^{60}Co γ-radiation and a peak-to-Compton ratio of 27. The peak analysis was carried out with the Hewlett-Packard 2116 C computer program.

RESULTS AND DISCUSSION

The substoichiometric extraction technique combined with radiometry has been successfully used to determine the equilibrium constants for the extractions of Bi(III), Hg(II), Cd(II), As(III), and Fe(II) from chloride media with diethyldithiocarbamate [9]. In these experiments, copper(II) and zinc(II) were the cations chosen as reference ions and their extraction constants were used as reference values. They were chosen because the extraction constants $K_{Cu(DDC)_2}$ and $K_{Zn(DDC)_2}$ are within the same intermediate order of magnitude (10^{15}—10^{40}), and no mixed chloride compound was observed during extractions from chloride media with diethyldithiocarbamate.

However, this procedure cannot profitably be applied to the determination of the extraction constants of gold diethyldithiocarbamates, because of their extremely high values [2—5]. In order to provide more reliable experimental data, another reference cation which has a very large, known extraction constant must be used. Palladium(II) is a good choice for this purpose. Two extraction constants, $K_{Pd(DDC)_2}$ and $K_{Pd(DDC)Cl}$, are known [13] and can be used for the estimation of extraction constants of gold(III) diethyldithiocarbamates.

In accordance with the theoretical considerations given above, only the distribution ratios of gold and palladium between the two phases need be measured, and this can be done simply and reliably by substoichiometric extraction combined with radiometry [9]. A measurable radioactivity will always remain in both phases if the concentration ratios of metal to extractant are adjusted suitably. In the present experiments, r_{*Au} increased from 3.2 to 27.0 with an increase of concentration of $Zn(DDC)_2$ from 2.6×10^{-5} M to 6.2×10^{-5} M. The corresponding values of r_{*Pd} increased from 0.3 to 3.5. In the substoichiometric extractions, the molar ratios of DDC to gold added to react are all less than 1. From the experimental values of r_{*Au} and r_{*Pd}, the corresponding values of Y and X were calculated as outlined in the Theory section. By plotting Y vs. X, a parabolic curve which passes through the origin is obtained, as shown in Fig. 1. It should be noted that $Au(DDC)_3$ does not exist in the extraction system in accordance with eqn. (2) because the intercept of the curve in Fig. 1 is zero. Equation (2) is then transformed to

$$Y/X = B\,K_{Au(DDC)_2Cl} + C\,K_{Au(DDC)Cl_2}\,X \qquad (5)$$

By plotting Y/X vs. X, a straight line is obtained, as shown in Fig. 1. The zero intercept of the straight line indicates that $Au(DDC)_2Cl$ also does not exist in the extraction system. However, the positive slope of the straight line reveals that $K_{Au(DDC)Cl_2}$ does exist. It is concluded, therefore, that $Au(DDC)Cl_2$ is the only complex present in the substoichiometric extraction system. This was confirmed by a separate experiment carried out as follows. The organic phase of one of the above extractions which did not involve ^{198}Au was transferred to a small quartz ampoule, the chloroform was completely evaporated at room temperature, and the ampoule was sealed and irradiated in the reactor for 1 min. The ^{38}Cl (1.64 and 2.17 MeV γ-radiation, $t_{1/2}$ = 37.29 min) was counted for 1 min immediately after irradiation and the ^{198}Au (0.412 MeV γ-radiation, $t_{1/2}$ = 2.697 d) was counted for 1 min three days later. Then the ratio of the disintegration rates of ^{38}Cl and ^{198}Au at the end of the irradiation (denoted by R in eqn. 6) could be obtained. This value was calculated from the above counting rates through half-life corrections and counting-efficiency calibrations. The calibrations were done against an efficiency vs. energy curve obtained by counting several different standard sources under the same conditions as above. From the ratio of the disintegration rates, R, the molar ratio of gold to chlorine in the sample

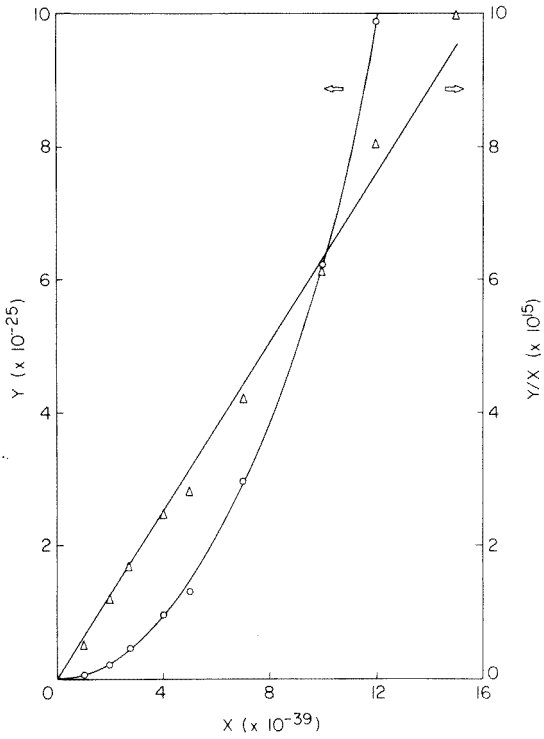

Fig. 1. Substoichiometric extraction of the Au(III)—Pd(II) pair with $Zn(DDC)_2$. For explanation of X and Y see text.

(denoted by M in eqn. 6) was calculated in accordance with the following equations [15]

$A_1 = n_1 f_1 \sigma_1 \phi (1 - e^{-\lambda_1 t})$ and $A_2 = n_2 f_2 \sigma_2 \phi (1 - e^{-\lambda_2 t})$

so $A_1/A_2 = n_1 f_1 \sigma_1 (1 - e^{-\lambda_1 t})/n_2 f_2 \sigma_2 (1 - e^{-\lambda_2 t})$

and

$$R = M f_1 \sigma_1 (1 - e^{-\lambda_1 t})/f_2 \sigma_2 (1 - e^{-\lambda_2 t}) \quad (6)$$

where the subscripts 1 and 2 represent gold and chlorine, respectively; A is the disintegration rate at the end of the irradiation; n is the number of atoms of gold or chlorine; f is the isotopic abundance of ^{197}Au or ^{37}Cl; ϕ is the neutron flux, σ the cross section, λ the decay constant and t the irradiation time. The molar ratios of gold to chlorine obtained from several runs were all very close to 1:2. So the empirical formula $Au(DDC)Cl_2$ was established.

The substoichiometric extraction described above is limited to the case where the molar ratio of DDC/Au added to react is less than 1. When more concentrated chloroform solutions of $Zn(DDC)_2$ ($>8.0 \times 10^{-5}$ M) were added for the extraction of the same Au(III)—Pd(II) solution (so that DDC/Au > 1),

it was found that r_{*Au} decreased with increasing amounts of $Zn(DDC)_2$ added. This abnormal behaviour was also reported by Chermette et al. [7], who suggested that an ionic complex, $Au(DDC)_2^+Cl^-$, is formed which is not suitable for extraction. This situation is beyond the scope of the present study.

The extraction constant of $Au(DDC)Cl_2$ can be obtained from the slope of the straight line in Fig. 1, in accordance with eqn. (5), and was found to be $\log K = 68.9 \pm 0.4$. This value is very close to that found by Chermette et al. [6] with their complicated method (Table 1).

J. M. Lo thanks the Chinese National Science Council for financial support.

REFERENCES

1 A. Hulanicki, Talanta, 14 (1967) 1371.
2 J. Růžička and J. Starý, Substoichiometry in Radiochemical Analysis, Pergamon, Oxford, 1968.
3 J. Starý and K. Kratzer, Anal. Chim. Acta, 40 (1968) 93.
4 F. Kukula, M. Krivánek and M. Kyrs, J. Radioanal. Chem., 3 (1969) 43.
5 F. Kukula and M. Simkova, J. Radioanal. Chem., 4 (1970) 271.
6 H. Chermette, J. F. Colonat and J. Tousset, Anal. Chim. Acta, 80 (1975) 335.
7 H. Chermette, J. F. Colonat and J. Tousset, Anal. Chim. Acta, 88 (1977) 331.
8 H. Chermette, J. F. Colonat, H. Montes and J. Tousset, Anal. Chim. Acta, 88 (1977) 339.
9 S. J. Yeh, J. M. Lo and L. H. Shen, Anal. Chem., 52 (1980) 528.
10 A. Ringbom, Complexation in Analytical Chemistry, Wiley—Interscience, New York, 1963.
11 L. G. Sillen and A. E. Martell, Stability Constants of Metal—ion Complexes, The Chemical Society, London, 1971.
12 K. Burger and D. Dyrssen, Acta Chem. Scand., 17 (1963) 1489.
13 G. B. Briscoe and S. Humphries, Talanta, 16 (1969) 1403.
14 A. Wyttenbach and S. Bajo, Anal. Chem., 47 (1975) 2.
15 P. Kruger, Principles of Activation Analysis, Wiley—Interscience, New York, 1971.

Analytica Chimica Acta, 126 (1981) 199—205
Elsevier Scientific Publishing Company, Amsterdam — Printed in The Netherlands

SUBSTOICHIOMETRIC DETERMINATION OF INORGANIC TIN IN ORGANOTIN COMPOUNDS

HISANORI IMURA and NOBUO SUZUKI*
Department of Chemistry, Faculty of Science, Tohoku University, Sendai, 980 (Japan)
(Received 3rd December 1980)

SUMMARY

Inorganic tin(IV) present in organotin compounds is determined substoichiometrically by complexation with salicylideneamino-2-thiophenol in a non-aqueous medium, after isolation of the tin(IV) by iodide extraction. The method is applied to the degradation products in commercial chemicals and those formed by u.v.-irradiation.

Organotin compounds are widely used in industry and agriculture, e.g., tributyltin compounds as antifouling paints for ships, triphenyltin compounds in wood preservatives, and dioctyltin compounds as stabilizers for synthetic polymers, and one would expect that information would be available as to the exact chemical composition of organotin compounds, their biochemical effects and metabolic fate in nature. Such is not the case, however, largely because of failure to develop analytical procedures for particular species including inorganic tin.

In the present paper, the substoichiometric determination of inorganic tin in various organotin chemicals is described. Substoichiometric determination of tin(IV) via complex formation with salicylideneamino-2-thiophenol (SATP) in a non-aqueous medium has been successfully applied to coal fly-ash [1]. The method, however, cannot be directly employed for tin in the presence of butyltin compounds, because SATP also reacts with butyltin compounds. Various separation methods have been suggested; these involve solvent extraction [2—4] or laminar [4—10], column [11], and gas chromatography [12, 13]. However, various sources of error, such as decomposition and evaporation loss, may occur in these procedures.

It is known that inorganic tin(IV) can readily be extracted from sulfuric acid containing iodide into an organic solvent [14, 15], but data on the partition behavior of butyltin compounds in this system are not available. In this paper a rapid and simple separation of tin(IV) and butyltin compounds by solvent extraction in the presence of iodide is combined with the substoichiometric method involving SATP, and is applied to various commercial organotin chemicals.

0003—2670/81/0000—0000/$02.50

EXPERIMENTAL

Reagents and apparatus

Organotin compounds. Tributyltin chloride (Bu_3SnCl) and butyltin trichloride ($BuSnCl_3$) were purified by distillation under reduced pressure. Dibutyltin dichloride (Bu_2SnCl_2, 99.98% pure), dibutyltin bis(isooctylthioglycolate) ($Bu_2Sn(OTG)_2$, >95%), dioctyltin dichloride (Oc_2SnCl_2), and octyltin trichloride ($OcSnCl_3$) were obtained from Kyodoyakuhin Chemicals Co. Bis(tributyltin) oxide ($(Bu_3Sn)_2O$) and dibutyltin dilaurate (Bu_2SnL_2) were obtained from the Tokyo Kasei Kogyo Co. Tributyltin acetate (Bu_3SnAc) and dibutyltin oxide (Bu_2SnO) were obtained from Wako Pure Chemical Industries.

Standard butyltin solutions. An appropriate quantity of each chloride was dissolved in purified benzene or pure methanol (Dojin Chemical Lab. Co., Spectrosol).

Ultraviolet irradiation. A quartz test-tube (15 mm o.d.) was placed centrally between two 10-W mercury lamps, 80 mm apart.

Other reagents and apparatus were the same as those used previously [1, 16].

Procedures

Determination of distribution ratio of monobutyltin and dibutyltin species. In a 30-ml centrifuge tube with a fitted stopper, 5 ml of 3.99×10^{-4} M $BuSnCl_3$ or 3.77×10^{-4} M Bu_2SnCl_2 in benzene was shaken with 5 ml of 2.1 M sulfuric acid, 1×10^{-4}—3 M in sodium iodide, for 1 min. After centrifugation, an aliquot of the organic phase was pipetted into a 10-ml volumetric flask, and 1 ml of 6.0×10^{-3} M SATP in ethanol, 1% in ascorbic acid, and 1 ml of 10% pyridine in ethanol were added in that order. Benzene was added to make up to volume. The absorbance of the benzene solution was measured at 440 nm for Bu_2Sn^{2+} and at 430 nm for $BuSn^{3+}$ against a reagent blank. The wavelength of maximum absorbance (λ_{max}) and the molar absorptivity (ϵ) for each butyltin—SATP complex were as follows: Bu_2Sn—SATP, λ_{max} = 435 nm, ϵ = 7000 mol^{-1} cm^{-1}; BuSn—SATP, λ_{max} = 424 nm, ϵ = 7900 mol^{-1} cm^{-1}.

Determination of distribution ratio of tributyltin species. Tributyltin does not form a colored complex with SATP, hence atomic absorption spectrometry (a.a.s.) was used: 10 ml of 1.55×10^{-2} M Bu_3SnCl in benzene was shaken with an equal volume of 2.1 M sulfuric acid for 1 min in a 50-ml centrifuge tube with a fitted cap. The concentration of tin in the aqueous phase was determined by a.a.s. using the instrumental conditions described previously [11], except for the following gas flow rates: acetylene, 5 l min^{-1} at 0.4 kg cm^{-2}, nitrous oxide, 7 l min^{-1} at 2 kg cm^{-2}.

Recommended procedure for determination of tin(IV)

In a 50-ml separatory funnel were placed a 10-ml sample containing various organotin compounds and inorganic tin(IV) and a spike solution of

tin(IV) labeled with ^{113}Sn. The solutions were adjusted to 2.1 M in sulfuric acid and made 0.1 M in sodium iodide, and 10 ml of benzene was added. The contents were shaken for 1 min, and the organic phase was discarded. The aqueous phase was washed once with an equal volume of benzene, and a 5-ml portion of the aqueous phase was placed into a 50-ml centrifuge tube with a fitted stopper, together with 4 ml of 5 M sodium perchlorate, 1 ml of 5 M sodium iodide, and 10 ml of benzene. After shaking for 30 s, a 5-ml portion of the organic phase was pipetted into a 30-ml centrifuge tube with a fitted cap. A substoichiometric amount of SATP in ethanol (1 ml of 10^{-4} M SATP) and 0.1 ml of 10% pyridine in ethanol were added with mixing after each addition. The contents were shaken for 1 h with 5 ml of a pH 3.9 buffer solution which was 10^{-4} M in tartrate. An exact 3-ml portion was taken from the organic phase obtained and the γ-activity of $^{113}Sn(^{113m}In)$, a, was measured by a NaI(Tl) scintillation counter. If the activity obtained from the tin(IV) spike solution alone is expressed as a_s then the inorganic tin content, M_x, in the sample is calculated by $M_x = M_s\,[a_s/(a-1)]$ where M_s is the carrier tin(IV) content in the spike [1].

RESULTS AND DISCUSSION

Interferences on the substoichiometric separation of tin(IV)

Few metal ions interfere with the substoichiometric determination of tin(IV) [1]. Butyltin compounds, however, were found seriously to interfere with the determination of inorganic tin(IV). The trends of interference by Bu_3SnCl, Bu_2SnCl_2, and $BuSnCl_3$ are shown in Fig. 1. The interferences do not show any simple trends. The positive errors may be ascribed to the interfering reaction of the organotin with SATP, but the negative errors suggest an additional extraction of inorganic tin(IV) with the organotin compounds. For the present purpose more effective separation of tin(IV) from the organotin compounds had to be achieved.

Extractive separation of butyltin compounds and inorganic tin(IV)

The extraction behavior of the various iodides into benzene was investigated. The extraction equilibrium for a compound is expressed as follows:

$$Bu_{(4-n)}Sn^{n+} + nI^- \overset{\text{acid}}{\rightleftarrows} Bu_{(4-n)}SnI_{n,\,org} \quad (n = 1\text{—}4)$$

$$K_{ex} = [Bu_{(4-n)}SnI_n]_{org}/[Bu_{(4-n)}Sn^{n+}]\,[I^-]^n$$

where K_{ex}, and the subscript org denote the extraction constant and the organic phase, respectively. At a constant concentration of sulfuric acid, the slope of the plots of log D (distribution ratio of the tin species) vs. log $[I^-]$ would be expected to be 4, 3, 2, and 1 for inorganic tin(IV), $BuSn^{3+}$, Bu_2Sn^{2+}, and Bu_3Sn^+, respectively. As shown in Fig. 2, the slopes for tin(IV) (n = 3.9), $BuSn^{3+}$ (n = 3.0), and Bu_2Sn^{2+} (n = 2.2) are in good agreement with the predicted values. The distribution ratio of Bu_3SnCl was as high as

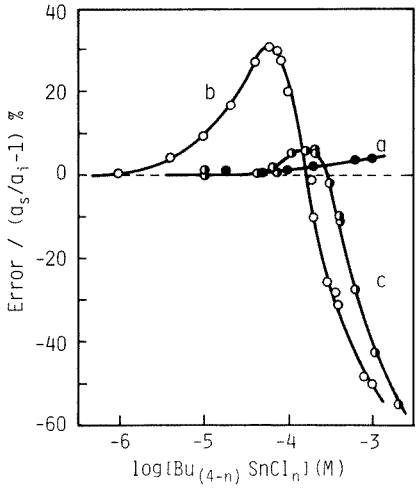

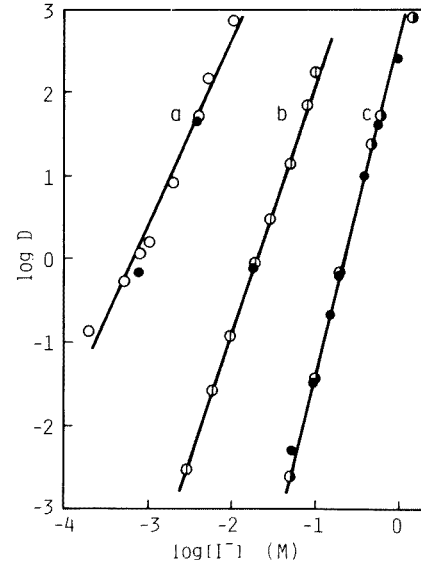

Fig. 1. Interferences of (a) Bu_3SnCl, (b) Bu_2SnCl_2, (c) $BuSnCl_3$ on the substoichiometric determination of inorganic tin(IV) after extraction from a 0.5 M NaI—2 M H_2SO_4 solution [1]. [Sn(IV)] = 4.1×10^{-5} M; [SATP] = 2.0×10^{-5} M.

Fig. 2. Extraction of (a) Bu_2Sn^{2+}, (b) $BuSn^{3+}$, (c) Sn(IV) in the NaI—2.1 M H_2SO_4—benzene system. (•) Ordinary extraction from the aqueous phase to benzene (other plots are obtained by the back-extraction technique).

$10^{2.5}$ even without iodide ions in the aqueous phase, so that any reliable iodide dependence could not be ascertained. The extractability of those compounds in the iodide system increased in the order Sn(IV) < $BuSn^{3+}$ < Bu_2Sn^{2+} < Bu_3Sn^+. These results indicate the possibility of mutual separation of these compounds using the iodide extraction system, and, for the present purpose, to separate inorganic tin(IV) from organotin compounds, by using a pre-extraction of butyltin compounds from dilute iodide solution and then of tin(IV) from a stronger iodide solution. The results of the extraction behavior in other halide system have not been included here, but the general trend of the extraction behavior in these systems was nearly the same with that in the iodide system.

Determination of inorganic tin(IV) in various organotin compounds

The accuracy and precision of the method developed was evaluated by determining tin in a synthetic mixture containing a known amount of inorganic tin(IV) and large amounts of butyltin compounds. The results are summarized in Table 1. Both the relative standard deviation and the inaccuracy are as low as 1.4% in spite of the presence of butyltin compounds at over 5000 times the amount of the inorganic tin(IV); this is considered to be very satisfactory. It was ascertained that isotopic exchange between in-

TABLE 1

Determination of inorganic tin(IV) in a synthetic mixture

Tin(IV) added (μg)	Organotin mixture (mg)	Active tin in spike (μg)	Activity from spike solution[a] (cpm)	Activity from test solution (cpm)	Tin found[b] (μg)
21.4	$BuSnCl_3$(10)	27.9	9350	5233	21.8
	Bu_2SnCl_2(50)		9323	5265	21.5
	Bu_3SnCl(50)		9295	5211	22.0

[a]Mean value (9322 ± 28) is used for the determination. [b]Mean value ± σ = 21.7 ± 0.3 μg, r.s.d. = 1.4%, deviation = +0.3 μg.

organic tin and organic tin does not occur when both species are in contact for over 24 h.

In order to test the feasibility of the method for inorganic tin(IV) in different organotin compounds, the determination of tin(IV) added to seven organotin compounds was examined. As shown in Table 2, trace amounts of tin(IV) can be determined within acceptable errors. Consequently, the present method can be applied to practical samples.

The results obtained for inorganic tin(IV) present in a commercial organotin compound (Japanese "Chemical Purity" grade) are given in Table 3; for these determinations, a known quantity of tin(IV) was added together with the active tin spike. The inorganic tin(IV) found in the chemicals seems to be produced by degradation of dibutyltin diacetate.

As a simple application of the proposed method, the decomposition of a series of butyltin compounds under u.v. irradiation was studied. A 0.05% solution of hydrochloric acid in methanol, which is generally used for leaching organotin compounds from various materials [3], was made 5.45×10^{-3} M

TABLE 2

Determination of 21.7 μg of inorganic tin(IV) added to various organotin compounds

Organotin compound	Amount added (mg)	Activity from spike[a] (cpm)	Activity from sample (cpm)	Tin found[b] (μg)
$(Bu_3Sn)_2O$	20.3	13114	7302	21.6 ± 0.1(3)
Bu_3SnAc	21.1	12765	7125	21.5 ± 0.2(2)
Bu_2SnO	21.8	12316	6815	21.9 ± 0.4(3)
Bu_2SnL_2	19.2	13344	7362	22.0 ± 0.1(3)
$Bu_2SnI(OTG)_2$	26.9	12585	6943	22.0 ± 0.2(3)
Oc_2SnCl_2	20.7	12840	7154	21.5 ± 0.2(2)
$OcSnCl_3$	25.6	12316	6828	21.8 ± 1.1(2)

[a]27.1 μg of active tin in spike. [b]Figures in parentheses indicate the number of replicate analyses.

TABLE 3

Determination of inorganic tin(IV) impurity in commercial dibutyltin diacetate

Bu_2SnAc_2 taken (mg)	Activity from spike[a] (cpm)	Activity from sample (cpm)	Total tin found[b] (μg)	Concentration[c] (%)
23.5	13434	5915	34.4	0.0543
		5914	34.5	0.0544
		5972	33.9	0.0518
14.9	12605	6003	29.8	0.0543
		5986	30.0	0.0554
		5989	29.9	0.0552

[a]27.1 μg of active tin in spike.
[b]Standard tin(IV), 21.7 μg, is added for each analysis.
[c]Mean value ± σ = 0.0542 ± 0.0013%, r.s.d. = 2.4%.

in $BuSnCl_3$, 5.02×10^{-3} M in Bu_2SnCl_2, or 5.09×10^{-3} M in Bu_3SnCl, and then irradiated for 5—60 min. An aliquot (0.1—1 ml) of the solution was pipetted into a 50-ml centrifuge tube. Then 39.0 μg of the active tin in the 2.1 M sulfuric acid—0.1 M sodium iodide solution (10 ml) was added, and the contents were shaken with 10 ml of benzene. All butyltin compounds were thoroughly extracted. Thereafter the inorganic tin produced was determined substoichiometrically.

The results are shown in Fig. 3. Since the butyltin compounds are decomposed in the sequence $Bu_3SnCl \rightarrow Bu_2SnCl_2 \rightarrow BuSnCl_3 \rightarrow SnCl_4$, the formation rate of inorganic tin(IV) increases, as is found, in the order $Bu_3SnCl < Bu_2SnCl_2 < BuSnCl_3$.

If the present extraction separation is followed by the decomposition of the extracted organotin compounds by wet ashing using an oxidizing agent or by u.v. irradiation, the organotin compounds and inorganic tin(IV) can be determined separately by the substoichiometric procedure.

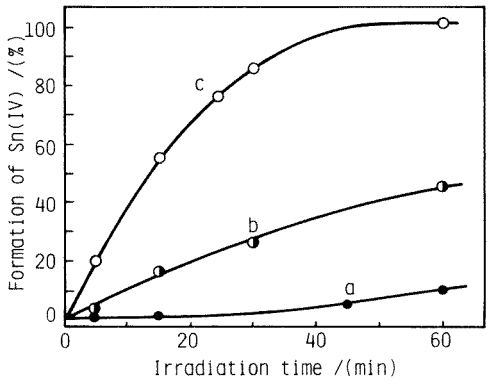

Fig. 3. Formation rate of inorganic tin from (a) Bu_3SnCl, (b) Bu_2SnCl_2, (c) $BuSnCl_3$ in 0.05% HCl—methanol under u.v. irradiation.

The authors thank Kyodoyakuhin Chem. Co. Ltd. for the supply of some of the organotin compounds.

REFERENCES

1 H. Imura and N. Suzuki, Talanta, 28 (1981) 73.
2 R. T. Skeel and C. E. Bricker, Anal. Chem., 33 (1961) 428.
3 S. Kojima, Analyst, 104 (1979) 660.
4 K. D. Freitag and R. Bock, Fresenius Z. Anal. Chem., 270 (1974) 337.
5 K. Bürger, Fresenius Z. Anal. Chem., 192 (1963) 280.
6 D. J. Williams and J. W. Price, Analyst, 89 (1964) 220.
7 Y. Tanaka and T. Morikawa, Bunseki Kagaku, 13 (1964) 753.
8 B. Herold and K. H. Droege, Fresenius Z. Anal. Chem., 245 (1969) 295.
9 K. Figge, J. Chromatogr., 39 (1969) 84.
10 T. S. Vasundhara and D. B. Parihar, Fresenius Z. Anal. Chem., 294 (1979) 408.
11 A. I. Williams, Analyst, 98 (1973) 233.
12 Y. Jitsu, N. Kudo, K. Sato and T. Teshima, Bunseki Kagaku, 18 (1969) 169.
13 G. Neubert and H. O. Wirth, Fresenius Z. Anal. Chem., 273 (1975) 19.
14 D. D. Gilbert and E. B. Sandell, Microchem. J., 4 (1960) 491.
15 A. R. Byrne and D. Gorenc, Anal. Chim. Acta, 59 (1972) 81.
16 H. Imura and N. Suzuki, Anal. Chim. Acta, 118 (1980) 129.

Analytica Chimica Acta, 126 (1981) 207—212
Elsevier Scientific Publishing Company, Amsterdam — Printed in The Netherlands

Short Communication

CARBON-13 CROSS POLARIZATION WITH MAGIC ANGLE SPINNING NUCLEAR MAGNETIC RESONANCE SPECTROSCOPY OF ORGANOSILANES BONDED TO SILICA SURFACES

D. E. LEYDEN*, D. S. KENDALL and T. G. WADDELL[a]

Department of Chemistry, University of Denver, Denver, CO 80208 (U.S.A.)

(Received 12th December 1980)

Summary. High-resolution ^{13}C-n.m.r. spectra were obtained of organosilane moieties chemically bound to the surface of silica. Techniques of cross polarization and magic angle spinning were employed. The spectra clearly confirmed some structures bound to the surface and showed that others were not as expected.

The wide application and general chemical interest in silica surfaces modified by chemical bonding of organosilanes to the surface and other reactions has stimulated the search for methods of characterization of these materials. Techniques such as infrared spectroscopy (i.r.) [1], Fourier transform infrared spectroscopy (F.t.i.r.) [2], photoacoustic spectroscopy (p.a.s.) [3, 4] and electron spin resonance (e.s.r.) [5] have been applied. Many of the applications and techniques for investigation of these materials have been presented in a recent symposium [6]. The widely recognized power of nuclear magnetic resonance spectroscopy to assist in structural elucidation and chemical characterization makes it a desirable tool for such investigations. However, until the recently developed methods of cross polarization ^{13}C-n.m.r. with magic angle spinning were developed [7—9], application of n.m.r. to solids was of extremely limited value. The technique permits the acquisition of ^{13}C-n.m.r. spectra of solids with resolution near that of solution phase samples. The effects of dipole—dipole broadening and chemical shift anisotropy in solids is effectively reduced. Cross polarization ^{13}C-n.m.r. spectra with magic angle spinning (c.p.—m.a.s.) have been obtained on a variety of solids such as fossil fuels [10] and polymers [11]. However, these materials contain the carbonaceous compounds in bulk. This communication reports preliminary results of application of c.p.—m.a.s. to chemically modified silica surfaces.

Experimental

Silanes were obtained complimentarily from Dow Corning Corporation, (Midland, MI) or from Petrarch Systems, Inc. (Levittown, PA) and were

[a]On leave from Department of Chemistry, University of Tennessee at Chattanooga, Chattanooga, TN, U.S.A.

used without further purification. Silica gel or Cab-O-Sil (Cabot Laboratories) was silylated by using 5% (v/v) of the respective silanes in toluene. The reaction mixture was stirred for about 1 h, and the silica was filtered and washed well with toluene. The product was "cured" for 8—12 h at 80°C in a vacuum oven.

The c.p.—m.a.s. spectra were acquired on a modified JEOL FX-60Q n.m.r. spectrometer operating at 11.88 MHz in the laboratory of Professor G. E. Maciel, Colorado State University, Fort Collins, CO. X-ray emission spectra were acquired using a United Scientific Corporation Spectrace 440 equipped with a Tracor NS-880 analyzer. Fourier transform infrared spectra were obtained on a Nicolet MX-1 F.t.i.r. spectrometer.

Results and discussion

An attempt was made to bond a total of seven functional groups to either silica gel or Cab-O-Sil fumed silica by silylation from toluene. The presumed silanes used are shown as (**1**—**5**)

$(CH_3O)_3Si-\overset{\alpha}{C}H_2\,\overset{\beta}{C}H_2\,\overset{\gamma}{C}H_2\overset{H}{N}CH_3$ (**1**)

$(CH_3CH_2O)_3Si-\overset{\alpha}{C}H_2\,\overset{\beta}{C}H_2-\overset{\gamma}{C}N$ (**2**)

$(CH_3CH_2O)_3Si-\overset{\alpha}{C}H_2\,\overset{\beta}{C}H_2-Cl$ (**3**)

$(CH_3CH_2O)_3Si-\overset{\alpha}{C}H_2\,\overset{\beta}{C}H_2-SH$ (**4**)

$Cl_3Si-\overset{\alpha}{C}H_2-\overset{\beta}{C}H_2-O-\overset{O}{\overset{\|}{C}}-CH_3$ (**5**)

$(CH_3O)_3Si-4\langle\overset{3}{\underset{5}{\overset{2}{\underset{6}{\rangle}}}}1CH_2Cl$ (**6**)

After immobilization of the benzyl chloride group using silane (**6**), the product was reacted with 2,4-pentanedione in an attempt to form (**7**) on the surface.

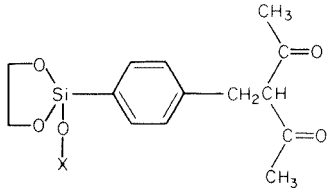

(**7**)

The "X" in structure (**7**) is to avoid implication of the details of surface bonding. Earlier F.t.i.r. and p.a.s. data had suggested that some degree of reaction had occurred [3]. The chlorine content on the silica surface after the immobilization of (**6**) and following the attempt to prepare (**7**) as determined by x-ray spectrometry indicated an approximately 50% loss, presumably by formation of (**7**). The p.a.s. ultraviolet absorption data indicated a diketone product largely in the keto tautomer although F.t.i.r. was inconclusive.

Figure 1 shows a representative c.p.—m.a.s. ^{13}C-n.m.r. spectrum taken

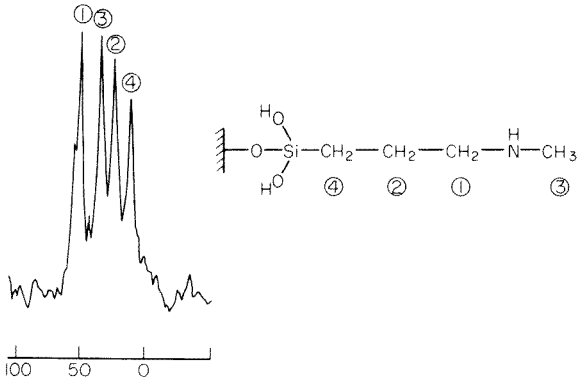

Fig. 1. ^{13}C-c.p.—m.a.s. n.m.r. spectrum of N-methylaminopropylsilane bound to silica gel (10 000 acquisitions; 5 ms contact time).

from (1) bound to silica gel. As all spectra are of similar quality, only this one is shown. The chemical shifts of the peaks formed for all samples are listed in Table 1. In most cases, the line widths at half maximum were about 75 Hz, the notable exception being the single line observed for (4). The intensities of the peaks cannot be trusted for quantitative measurement. A simple illustration is that the intensity ratio of the peaks at 18 and 39 ppm respectively for (3) changed from 1:1.2 to 1:0.95 by changing the cross-polarization contact time from 5 ms to 1 ms. The possible effects of the silica surface on chemical shifts are not known. In this work, interpretations were made without taking these effects into account because they probably are secondary to the inherent structure of the silane which is bound to the surface; however, these secondary effects are expected to contain valuable information and will be the subject of continuing studies.

Figure 1 shows the spectrum obtained from (1). From ^{13}C-n.m.r. chemical shift tables [12], reasonable assignments can be made. The peak at 10 ppm can be assigned to the carbon in the α-CH_2 group. The peaks at 24 and 50 ppm can be assigned to the β-CH_2 and γ-CH_2 resonances, respectively. Even on a semiquantitative basis, the peak at 55 ppm does not correspond to an intensity equal to the others. This resonance is likely a result of unreacted methoxy groups on the silane leading to a surface structure such as:

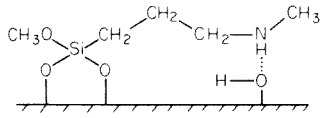

(8)

The chemical shift value of 55 ppm corresponds reasonably well to that expected for the methyl carbon of a methoxy group.

The resonances obtained from materials prepared using silanes (3) and (4) may also be assigned with reasonable confidence from chemical shift tables. The product formed from (3) yields two sharp resonance lines at 18 and 39

TABLE 1

^{13}C-n.m.r. chemical shifts from tetramethylsilane[a]

Sample[b]	Chemical shifts values of observed peaks (ppm)
(1)	10, 24, 34, 50, 55
(2)	12, 25, 45
(3)	18, 39
(4)	18 (slightly broad)
(5)	18, 60
(6)	43, 50, 70 (all weak) 127, 130, 133, 136, 139 (all strong)
(7)	31, 45, 72 (all weak) 129, 132, 136, 142 (all strong)

[a]All chemical shift values ± 0.1 ppm. [b] Sample refers to the silane after bonding to a silica surface.

ppm; these may be assigned to the α-CH_2 and β-CH_2 carbons, respectively. The product from (4) shows a single, slightly broad, and somewhat distorted peak at 18 ppm. It is conceivable that the α-CH_2 and β-CH_2 carbon chemical shift values nearly coincide purely by accident. The products of silylation with (3) and (4) were shown to contain easily detectable chlorine and sulfur, respectively, by energy-dispersive x-ray fluorescence spectroscopy.

The material formed from silylation of silica with (6) also yields a reasonable ^{13}C-c.p.—m.a.s. spectrum. Chlorine content on the surface was confirmed by x-ray fluorescence. A set of strong peaks at 127, 130, 133, 136 and 139 ppm was observed; these peaks are easily interpreted as the resonances of the aromatic carbon nuclei. Two weaker peaks are seen at 43 and 50 ppm and even yet a weaker one at 70 ppm. As an approximation, the sum of the intensity of these peaks is roughly equal to any one peak from the aromatic carbon resonance line cluster. The peaks at 43 and 50 ppm may be assigned to the methylene carbon of isomers of the chlorobenzylsilane. The solution-phase chemical shift of the $-CH_2-$ carbon in benzylchloride is reported at 46.1 ppm [13]. The peak at 70 ppm is difficult to explain but may result from a benzyl alcohol derivative as an impurity. Upon reaction of the product of silylation with (6) with 2,4-pentanedione, the peak at 50 ppm disappears and one at 31 ppm is seen. A very small shift of the other two peaks is detected. Yet, no carbon resonances for the diketone are seen. In this case, interpretation of the results is not complete. The p.a.s. and F.t.i.r. as well as loss of chlorine followed by x-ray fluorescence indicate that a reaction has taken place. There are changes in the ^{13}C-c.p.—m.a.s. n.m.r. spectrum, which are not yet interpretable.

The remaining two samples were prepared by silylation of Cab-O-Sil with (2) and (5), respectively, using commercial reagents. Again in these cases, the n.m.r. spectra gave immediate reason to question the products. In the case of the product from silylation with (2), the peak at 12 ppm can be assigned to

the α-CH_2 carbon resonance. However, the peak at 25 ppm is at too low field to be adjacent to a nitrile and more resembles one adjacent to a carboxylic acid, ester, or an amide. Fourier-transform i.r. spectra of both the product and the starting reagent show a strong amide carbonyl band at 1648 cm^{-1} and only a hint of a nitrile band at 2255 cm^{-1}. However, the continuing paradox in this case is that no amide, acid, ester, or nitrile carbon resonance was detected.

The final sample prepared from (5) also presented interesting results. The silane used is a trichlorosilane containing an ester. The ^{13}C-n.m.r. spectrum shows a peak at 18 ppm which may be assigned to the α-CH_2, and one at 60 ppm which corresponds to a highly deshielded CH_2 carbon such as one adjacent to an ester, ether, or alcohol linkage. These are the only peaks in the spectrum, and they are very intense. There is no evidence of a carbonyl carbon or adjacent methyl resonance. Infrared spectroscopy showed the starting silane reagent to contain a strong ester carbonyl band; F.t.i.r. on the product showed no such band. Thus the assignment of the peak at 60 ppm to the β-CH_2 adjacent to an alcohol is the probable result of hydrolysis of the ester catalyzed by the hydrogen chloride released during the silylation reaction. Even under reasonably dry conditions, traces of surface water will exist on silica surfaces.

Conclusions

The results presented in this preliminary report clearly show the potential of ^{13}C-c.p.—m.a.s. n.m.r. spectroscopy in the investigation of chemically modified surfaces. Although the examples presented here represent simple structures, the proof of some and challenge of other expected structures by the technique is clearly demonstrated. The potential application of the technique to monitor chemical and perhaps physical changes at the surface is indeed exciting to contemplate.

The partial support of this research by Research Grant CHE 78-23123 from the National Science Foundation and the use of the Colorado State University Regional n.m.r. Center funded by National Science Foundation Grant 78-18581 is gratefully acknowledged. The assistance of Dr. G. E. Maciel, D. W. Sindorf and D. McKay in acquisition of the spectra is sincerely appreciated.

REFERENCES

1 T. H. Elmer, in D. E. Leyden and W. Collins (Eds.), Silylated Surfaces, Midland Macromolecular Monographs, Vol. 7, Gordon and Breach, New York, 1980, pp. 1—21.
2 H. Ishida and J. L. Koenig, J. Polym. Sci., 17 (1979) 615.
3 D. E. Leyden, D. S. Kendall, L. W. Burggraf, F.-J. Pern and D. Williams, National ACS Meeting, Las Vegas, NV, Sept., 1980.
4 C. H. Lochmüller and D. R. Wilder, Anal. Chim. Acta, 118 (1980) 101.
5 T. J. Pinnavaia, J. G.-S. Lee and M. Abedin, in D. E. Leyden and W. Collins (Eds.), Silylated Surfaces, Midland Macromolecular Monographs, Vol. 7, Gordon and Breach, New York, 1980, p. 342.

6 D. E. Leyden and W. Collins (Eds.), Silylated Surfaces, Midland Macromolecular Monographs, Vol. 7, Gordon and Breach, New York, 1980.
7 A. Pines, M. G. Gibby and J. S. Waugh, J. Chem. Phys., 59 (1973) 569.
8 F. P. Miknis, V. J. Bartuska and G. E. Maciel, Am. Lab., 11 (11) (1979) 19.
9 J. J. Chang, A. Pines, J. J. Pripiat and H. A. Resing, Surf. Sci. 47 (1975) 661.
10 H. L. Retcofsky and D. L. Vander Hart, Fuel, 57 (1978) 421.
11 J. Schaefer and E. O. Stejskal, J. Am. Chem. Soc., 98 (1976) 1031.
12 D. E. Leyden and R. H. Cox, Analytical Applications of n.m.r., J. Wiley, New York, 1977, Ch. 5.
13 V. Formacek, L. Desnoyer, H. P. Kellerhals, T. Keller and J. T. Clerc, Carbon-13 Data Bank, Vol. 1, Buker Physik, Karlsruhe, 1976.

Analytica Chimica Acta, 126 (1981) 213—216
Elsevier Scientific Publishing Company, Amsterdam — Printed in The Netherlands

Short Communication

THE DETERMINATION OF ETHANOL BY ALTERNATING CURRENT TENSAMMETRY

M. C. CHENEY, D. J. CURRAN[a] and K. S. FLETCHER III*
Corporate Research, The Foxboro Company, Foxboro, MA 02035 (U.S.A.)
(Received 3rd November 1980)

Summary. A method for the determination of ethanol in vodka by phase-sensitive a.c. tensammetry is described; the only prior treatment of the sample is dilution with water and addition of KCl. The positive wave of the tensammetric response was used. Ethanol concentrations in the range 2—10% can be determined with a relative imprecision of 0.5%. Other species having surfactant properties, such as the fusel oils found in most distilled liquors, interfere.

Tensammetric waves in an a.c. polarogram are peaks which arise from voltage-dependent adsorption—desorption processes of materials which are surface-active at the mercury drop, changing the double-layer capacity of the electrode and thus the charging current. The subject has been discussed by Breyer and Bauer [1] and by Jehring [2]. Examples are also given in reviews by Smith [3, 4]. Alcohols are among the many compounds which exhibit tensammetric waves. Ethanol was among several alcohols studied in 1956 by Breyer and Hacobian [5], who used various supporting electrolytes. Schwabe and Jehring [6] studied ethanol in an acetate buffer. In these studies attention was focused on the adsorption—desorption process and establishing the summit potentials. While recent interest has been shown in using the tensammetric method for quantitative work [7, 8], it appears there are no reports on the determination of ethanol in real samples by tensammetry. In this communication, a tensammetric method for the determination of ethanol in vodka is reported.

Experimental

Equipment. A block diagram of the apparatus used is shown in Fig. 1. The potentiostat was an EG & G Princeton Applied Research (PAR) Model 173 with Model 176 current-to-voltage converter. The function generator, a PAR Model 175 Universal Programmer, was used to generate a linear ramp. The sine-wave generator was a Hewlett-Packard Model 209A oscillator. The quadrature component of the a.c. current was measured as the IR drop across a resistor in series with the cell using a PAR Model 129A lock-in

[a]Permanent address: Department of Chemistry, GRC Tower I, University of Massachusetts, Amherst, MA 01003, U.S.A.

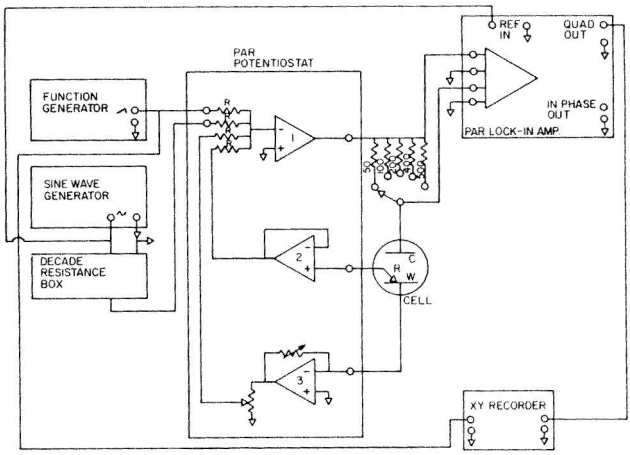

Fig. 1. Block diagram of instrumentation used for phase-sensitive tensammetry.

amplifier. A Hewlett-Packard Model 7045 X-Y recorder was used to record the capacity current versus electrode potential. A Metrohm Universal Titration Vessel served as the cell, and was equipped with nitrogen inlet and outlet tubes, the dropping mercury electrode (DME), a saturated calomel reference electrode (SCE), and a platinum counter electrode isolated in a tube containing 1 M KCl and terminated with a fine porosity glass frit.

Solutions. Standard ethanol solutions were prepared volumetrically with U.S.P. absolute alcohol (U.S. Industrial Chemicals Co.) and weighed quantities of reagent-grade KCl. Water was distilled in a Barnstead Model 210 still.

Procedure. The tensammetric wave was measured as the quadrature output of the lock-in amplifier. The peak height was maximized by adjusting the reference signal phase angle control on the lock-in amplifier, and the peak current was measured from zero current. The latter is an arbitrary but simple procedure. Calibration curves were constructed using the standard ethanol solutions. Samples (15 ml) of gin and vodka, each labeled 80 proof, were diluted with water in 100-ml volumetric flasks containing 7.46 g of KCl, to give solutions nominally 6% in ethanol. Aliquots (25 ml) of these solutions were placed in the cell and the tensammetric curves were obtained after stirring. All measurements were made with a mercury column height of 57.5 cm.

Results and discussion

The simultaneous reduction of oxygen over the potential range used in this work was shown to have no effect on the tensammetric measurement by experiments performed in the presence and absence of dissolved oxygen. Over the temperature range 18.5—31.1°C, the relative temperature coefficient of the current was 0.8%/°C for a 30% ethanol solution in 1.0 M KCl. All

subsequent work was done at ambient temperature without removing oxygen.

Positive and negative tensammetric waves, i.e., waves occurring at potentials positive and negative of the point of zero charge, were found to have summit potentials of —0.22 and —1.35 V vs. SCE for solutions 30% in ethanol and 1.0 M in KCl. This is in good agreement with reported potentials [5]. Typically, the positive wave is of greater magnitude than the negative wave and is preferred for analytical purposes. Thus, although either may be used, the positive wave was chosen. A series of positive tensammetric waves for solutions 4—20% in ethanol are shown in Fig. 2. It is noted that the summit potential of the wave shifts with concentration of surfactant, and that a baseline correction for residual current cannot be performed because the a.c. base current is also a function of the concentration of surfactant. Further, it is important to realize that a plot of peak current vs. bulk concentration has the form of an adsorption isotherm and is therefore non-linear. A saturation limit is reached where the peak current becomes independent of concentration.

A calibration curve was constructed from the peak currents obtained for the range 4—20% solutions (0.684—3.420 M ethanol) and is shown in Fig. 3. Five determinations were made for each concentration and the results averaged for the calibration curve. In general, the precision of replicates was better than ±0.5%, relative. Over the concentration range 2—10% ethanol, the data could be represented by the equation, $i = (29.62 \pm 1.04) + (1.80$

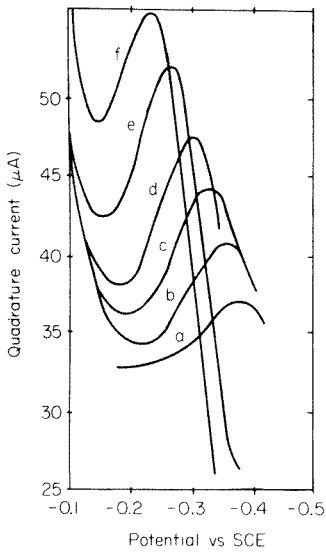

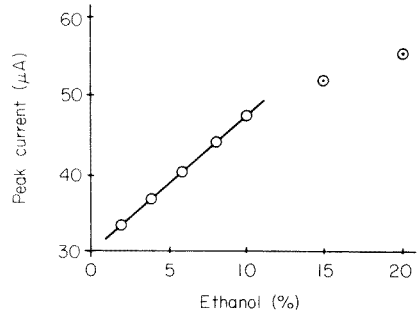

Fig. 2. Positive tensammetric waves for ethanol: (a) 4%; (b) 6%; (c) 8%; (d) 10%; (e) 15%; (f) 20%.

Fig. 3. Calibration curve for ethanol.

± 0.16) (% ethanol), (95% confidence limits, standard error of estimate = 0.242). At higher concentrations, the response begins to decrease as the saturation limit is approached. The intercept arises because the current is measured from a zero current baseline (see Fig. 2).

For the experiments with gin and vodka, 15-ml portions were treated as described in the Procedure, five aliquots being measured for replicate determinations. The percentage ethanol was obtained from the calibration graph. The results for the vodka samples (40.76 ± 0.03 μA, corresponding to 41.25% or 82.5 proof) are in good agreement with the label on the bottle. The gin result (37.98 ± 0.03 μA, 30.67% or 61.3 proof) is considerably lower than the 80 proof expected. This may reflect the fact that the tensammetric method will respond to the more strongly adsorbed molecules present in a sample at the expense of the more weakly adsorbed. For example, attempts to determine ethanol in blended whiskeys were unsuccessful. Caution is therefore needed when applying the method. However, for samples which do not contain adsorbing interferences, the method is simple and rapid.

REFERENCES

1 B. Breyer and H. H. Bauer, Alternating Current Polarography and Tensammetry, Interscience, New York, 1963.
2 H. Jehring, J. Electroanal. Chem., 21 (1969) 77.
3 D. E. Smith, in A. J. Bard (Ed.), Electroanalytical Chemistry, Vol. 1, M. Dekker, New York, 1966, pp. 1—155.
4 D. E. Smith, Crit. Rev. Anal. Chem., 2 (1971) 247.
5 B. Breyer and S. Hacobian, Aust. J. Chem., 9 (1956) 7.
6 K. Schwabe and H. Jehring, Fresenius Z. Anal. Chem., 173 (1960) 36.
7 E. Ladanyi and I. Stalder, J. Electroanal. Chem., 99 (1979) 321.
8 D. R. Canterford, Photogr. Sci. Eng., 21 (1977) 215.

Analytica Chimica Acta, 126 (1981) 217—220
Elsevier Scientific Publishing Company, Amsterdam — Printed in The Netherlands

Short Communication

LIQUID MEMBRANE ELECTRODES BASED ON QUATERNARY AMMONIUM TETRAKIS(m-TRIFLUOROMETHYLPHENYL)BORATES

C. J. COETZEE* and A. J. BASSON

Department of Chemistry, University of the Western Cape, Bellville (South Africa)

(Received 8th December 1980)

Summary. Electrodes based on the appropriate salts give linear responses for 10^{-1}—10^{-4} M tetramethylammonium and tetraethylammonium ions, with some selectivity against alkali metal ions. Use as indicator electrodes in titrations with tetraphenylborate solutions is outlined.

The use of tetra-arylborates as precipitants for the gravimetric determination of cesium in the presence of rubidium or potassium has been reported [1], and the use of the cesium and thallium tetrakis(*m*-trifluoromethylphenyl)borates as active materials in liquid membrane electrodes has been described [2]. Tetramethylammonium and tetraethylammonium tetrakis-(*m*-trifluoromethylphenyl)borates as membrane materials for ion-selective electrodes are considered here.

Experimental

All chemicals used except ethylnitrobenzene, which was distilled under reduced pressure, and the tetra-arylborate salts were of analytical-reagent grade. Sodium tetrakis(*m*-trifluoromethylphenyl)borate was prepared by the method of Meisters et al. [1]. The tetramethyl and tetraethyl salts of the tetra-arylborate were prepared by precipitation from dilute solution (aqueous 1%), separated by centrifugation, washed with ice water and dried at 110°C for 3 h.

Electrode assemblies were as described previously [3]. The organic phase consisted of a saturated solution of the salt in ethylnitrobenzene. The aqueous reference phases were 0.10 M solutions of the appropriate chlorides. After preparation, electrodes were conditioned for at least 1 h but preferably overnight, by immersion in a 0.1 M solution of the appropriate cation(s), after which they gave stable potential readings. Electrodes were usually stored in this manner when not in use. The lifetimes of the electrodes exceeded 4 months.

Results and discussion

The electrodes gave linear calibration graphs for tetramethyl- and tetraethyl-ammonium ions in pure chloride solutions in the concentration

0003—2670/81/0000—0000/$02.50

range 10^{-1}—10^{-4} M. The calibration curves could be used to determine concentrations of these cations as low as 10^{-5} M. The slopes of the calibration curves were 59.0 and 59.1 mV/pC for the tetramethyl- and tetraethylammonium ions, respectively.

The pH dependence of the electrodes was studied for the pH range 1—12. The pH of the test solutions was adjusted by addition of hydrochloric acid or sodium hydroxide solutions having the same concentration of the quaternary ammonium ion as in the test solution. The results indicated a "working range" for both electrodes between pH 1.5 and 11.0.

The response times for e.m.f. measurements were not studied in detail. In 10^{-1}—10^{-3} M solutions, stable readings were obtained within 30 s; with more dilute solutions a 1—2-min period was required to obtain stable readings. Stability of measurements was better with slow than with fast stirring.

Selectivity. The selectivity of any electrode is important as it indicates how successful an electrode would be in practice. A systematic examination of the interferences of sodium, potassium, rubidium, cesium, ammonium, tetramethylammonium and tetraethylammonium on electrode response was undertaken. Calibration curves for the primary ions in the presence of fixed concentrations (10^{-2} M) of interfering ions were prepared. Selectivity coefficients K_{CM} were calculated from these curves by means of the equation $K_{CM} = (10^{\Delta E/S} - 1)\, a_C/(a_M)^{1/z}$, where ΔE is the change in potential in the presence of the interfering ion, M^{z+}, S is the slope of the calibration curve for the primary ion, and a_C and a_M are the activities of the primary and the interfering ions, respectively. The values are shown in Table 1. The electrodes have a better degree of selectivity in the presence of alkali metal cations than previously reported electrodes of this type [2]. The general response order seems to be the same for all these types of electrode: $Cs^+ > Rb^+ > K^+ > NH_4^+ > Na^+$. Divalent ions do not have any appreciable influence on electrode behaviour.

Analytical use of the electrodes. Standard addition potentiometry [4] was applied to test the performance of the electrodes, as described previously [3]. Good results were obtained in all cases for tetramethylammonium and tetraethylammonium ions at lowest concentrations of 1.85 mg and 3.26 mg per 25 cm^3, respectively, at constant ionic strength (0.05 M NaCl).

Precipitation titrations in which the electrodes were used for end-point indication were examined. Standard solutions of sodium tetraphenylborate were used as titrant; these solutions were standardised against silver nitrate solutions using an Orion 94-16A silver-selective electrode as indicator electrode. During the precipitation titrations, the pH was not adjusted and no salt was added to adjust the ionic strength. All titrations were done with sample solutions varying between 40 and 60 cm^3.

Typical titration curves are shown in Fig. 1 for the titration of tetraethylammonium ion in various quantities, the separate titration of rubidium and potassium ions, and the titration of various mixtures of monovalent ions using the tetraethylammonium ion electrode for end-point indication.

TABLE 1

Selectivity coefficients[a] for the tetramethylammonium and tetraethylammonium electrodes

Cation	Tetramethylammonium	Tetraethylammonium
Na^+	4.0×10^{-4}	2.0×10^{-4}
K^+	1.8×10^{-2}	1.8×10^{-3}
Rb^+	3.2×10^{-2}	6.4×10^{-3}
Cs^+	1.6×10^{-1}	1.3×10^{-2}
NH_4^+	2.5×10^{-3}	2.5×10^{-3}
$(CH_3)_4N^+$	1.0×10^{0}	1.1×10^{-3}
$(C_2H_5)_4N^+$	7.0×10^{-1}	1.0×10^{0}

[a]For Mg^{2+}, Ca^{2+}, Sr^{2+} with both electrodes, $K_{CM} < 10^{-4}$.

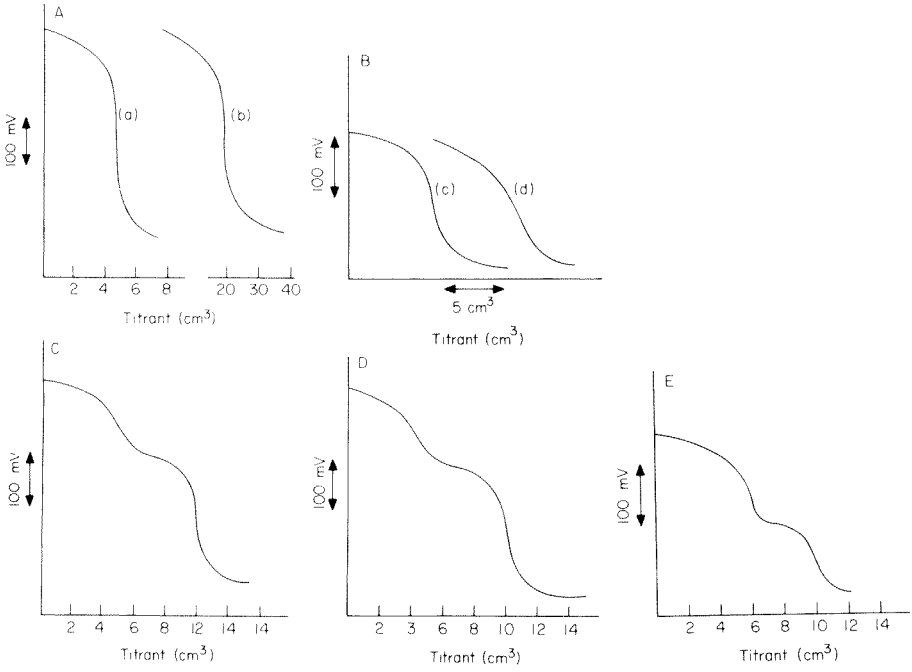

Fig. 1. Titration curves with sodium tetraphenylborate (TPB) solutions as titrant and a tetraethylammonium indicator electrode. (A) Titration of (a) 66 mg and (b) 26 mg of tetraethylammonium ion with 0.100 M and 0.0100 M TPB, respectively. (B) Titration of (c) 43 mg Rb^+ and (d) 20 mg K^+ with 0.1 M TPB. (C) Titration of 67 mg Cs^+ and 65 mg of tetraethylammonium ion with 0.1 M TPB. (D) Titration of 52 mg Rb^+ and 52 mg of tetraethylammonium ion with 0.1 M TPB. (E) Titration of 24 mg K^+ and 52 mg of tetraethylammonium ion with 0.1 M TPB.

The authors thank the South African CSIR for financial support.

REFERENCES

1 M. Meisters, C. E. Moore and F. P. Cassaretto, Anal. Chim. Acta, 44 (1969) 287.
2 C. J. Coetzee and A. J. Basson, Anal. Chim. Acta, 92 (1977) 399.
3 C. J. Coetzee and A. J. Basson, Anal. Chim. Acta, 83 (1976) 361.
4 A. Liberti and M. Mascini, Anal. Chem., 41 (1969) 676.

Analytica Chimica Acta, 126 (1981) 221—224
Elsevier Scientific Publishing Company, Amsterdam — Printed in The Netherlands

Short Communication

INDIRECT DETERMINATION OF MERCURY(II) WITH AN AIR-GAP CYANIDE SENSOR

PIOTR CZICHON*, JAROSŁAW FLIGIER and ZBIGNIEW GREGOROWICZ

Department of Analytical and General Chemistry, Silesian Polytechnic University, PL 44-101 Gliwice (Poland)

(Received 17th June 1980)

Summary. The method is based on the stability of the dicyanomercurate(II) complex at pH 0.5—1, where most other cyanide complexes decompose. The selectivity is much better than that in the direct application of mercury-selective electrodes. The method is useful in the range 5×10^{-5}—5×10^{-3} M mercury(II).

Indirect selective-electrode methods are useful in extending the number of species that can be measured, yet such applications of cyanide-selective electrodes are limited by the poor selectivity of cyanide as a reagent as well as by the solubility and stability of most cyanide complexes in the alkaline region in which the solid-state electrodes are used. Thus indirect determinations of metal ions via their cyanide complexes require pure solutions [1] or large differences in the stabilities of the cyanide complexes involved [2]. Better selectivity can be achieved in acidic solutions; at pH 0.5—1 only strong cyanide complexes, e.g., mercury(II), gold(III) and iron(II), resist decomposition. In acidic solutions, a gas-sensing cyanide electrode [3] or an air-gap sensor [4] can be used.

The present communication deals with the indirect determination of mercury(II) by means of a standard subtraction method with the air-gap cyanide sensor. Previously described mercury-selective electrodes are of the solid-state type, mainly with AgI [5—7], Ag_2S [8], Ag_2S—HgS [9], HgS or HgSe [10] or Ag_2HgI_4 [11] in the membrane, and none is particularly satisfactory. When the air-gap cyanide sensor is used as a mercury(II) detector, a response of nearly 120 mV/pHg can be obtained because of the Nernstian response of the sensor to the cyanide concentration and the composition of the dicyanomercurate(II) complex.

Experimental

Reagents. Analytical-grade reagents and deionized oxygen-free water were used. Standard solutions of mercury(II) were prepared by dissolving mercury in concentrated nitric acid and diluting the solution to the required concentration with water. A 10^{-3} M potassium cyanide stock solution was standardized by Liebig's method. The electrolyte, 10^{-2} M potassium dicyanoargent-

ate(I), was adjusted to pH 9.5 with 0.1 M borax and 0.5% (w/w) methylcellulose was added. The standard solutions and samples were acidified with 2 M sulfuric acid. Solutions (10^{-3} M) of diverse ions were prepared. The pH was adjusted with 1 M tartaric acid, 1 M sodium hydroxide, sulfuric acid (1 + 3) and commercial buffer solutions in the pH range 4—8.

Apparatus. The air-gap cyanide sensor [4] mounted in a ground-glass 19/26 joint was used with a Meratronic digital pH/mV meter; a Radiometer PHM-26c meter with a combined pH electrode was also used. For measurements, the sensor was attached to a conical glass flask of about 20-ml capacity with a ground-glass 19/26 joint.

Procedures. The air-gap cyanide sensor was prepared for measurements as described previously [4]. For each metal—cyanide system, the total cyanide concentration was 10^{-4} M, whereas that of metal ion was 5×10^{-5} M; 15.0 ml of the solution was pipetted into the conical glass flask and 1.0 ml of a pH-regulating solution was added. Immediately, the flask was closed with the sensor and the magnetic stirrer was started. Readings were made after a steady state had been reached (2—4 min), with an accuracy of 1 mV. Next the sensor was replaced by a combined pH electrode and the pH was measured (±0.01 pH). The experimental points for each metal—cyanide system covered the pH range 0.5—12.

In order to draw a calibration graph, 25.0 ml of standard cyanide solution (10^{-5}, 10^{-4} 10^{-3} M) and mercury(II) solution (0.5×10^{-5}, 0.5×10^{-4}, 0.5×10^{-3} M) in amounts of 5.0, 10.0, 15.0, 20.0 ml for each concentration were pipetted into 50-ml volumetric flasks. After dilution with water, 12 standard solutions of dicyanomercurate(II) complex were thus obtained with various excesses of cyanide. Next 15.0 ml of the solution was pipetted into the conical flask, 1.0 ml of 2 M sulfuric acid was added, and the vessel was closed with the sensor. Steady readings were obtained after 3 min.

Results and discussion

Optimal pH range. The experimental curves in Fig. 1 show that the hydrogen cyanide concentration for a metal—cyanide system is pH-dependent. For

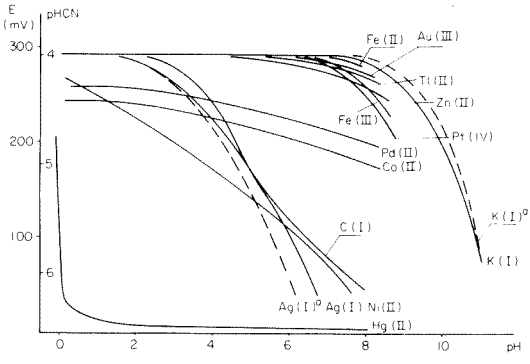

Fig. 1. The influence of pH on the hydrogen cyanide concentration of a metal—cyanide system. The dashed lines are the calculated curves for the silver(I) and potassium(I) systems.

comparison, the appropriate curves for the silver(I) and potassium(I) cyanide complexes were calculated. The possible pH range for the determination of mercury(II) with the cyanide sensor is 0.25—8. The lower value corresponds to decomposition of the mercury(II) complex yielding a hydrogen cyanide concentration at the detection limit of the sensor (pHCN $\approx$ 6) and the upper value is defined by total conversion of cyanide to hydrogen cyanide. The curves in Fig. 1 make it possible to predict selectivity: interferences will arise from metal ions whose cyanide complexes remain stable on acidification of the solution. The extremely inert iron(II)—cyanide complex does not interfere under the experimental conditions used if the pH before the addition of cyanide is less than 8—9; cyanide complexes are then not formed, and the curve is similar to that for potassium cyanide.

Calibration and testing of the sensor. The calibration graph was prepared by plotting the potential of the sensor versus the free cyanide concentration in the mercury(II)—cyanide standard solutions; under the recommended conditions, activities are essentially the same as concentrations. The calibration graphs were linear between 10^{-6} and 10^{-3} M cyanide with a slope of 115 mV/pHg. For such slopes, the optimal potential change during measurement is 55—80 mV, which corresponds to a 2.5—4 molar ratio of the cyanide standard solution to the mercury(II) content of the sample. The stability constants of cyanomercury(II) complexes [12] indicate that only the dicyanomercurate(II) complex need be considered.

For the determination of mercury(II), the procedure is the same as for calibration. If the mercury(II) concentration is not known to within an order of magnitude, preliminary tests are necessary. For this purpose, a standard cyanide solution is added to the sample, the lowest cyanide concentration being used initially, with measurements after acidification. The sample concentration is then calculated from $C_{Hg} = (C_{CN} - C'_{CN})/2$, where C_{CN} is the standard cyanide concentration in the sample, and C'_{CN} is the concentration of the excess of cyanide read off from the calibration graph.

The precision of the measurements was evaluated by determining mercury(II) at various concentration levels (Table 1).

TABLE 1

Results for the determination of mercury[a]

Hg taken (μg)[b]	Average Hg found (μg)	Relative error (%)	S.d.	R.s.d. (%)
5.0	5.3	6	0.2	4.0
20.0	20.4	2	0.85	4.2
50.0	52.0	4	2.3	4.4
100.0	103.0	3	4.7	4.6

[a]Ten determinations at each level. [b]In 25.0 ml of sample solution.

TABLE 2

Interferences from various cations in the determination of mercury (4 μg ml^{-1})

Cation[a]	Au(III)	Pd(II)	Tl(III)	Cu(I)	Cu(II)	Ag(I)	Ni(II)	Co(II)
[Me]/[Hg]	1—25	1—25	1—10^3	1—10^2	1—10^3	1—10^2	1—10^3	1—10^3
Hg found (μg ml^{-1})	4.0—4.2	4.4—4.7	4.0—4.4	4.0—5.6	4.1—4.5	4.0—6.5	4.6—5.0[b]	4.8—6.1[b]

[a]Pt(IV), Fe(II), Fe(III), Zn(II) do not interfere in the 1 × 10^3 [Me]/[Hg] ratio. [b]At a 1:1 [Me]/[Hg] ratio, the values found in presence of Ni(II) and Co(II) were 4.2 and 4.5 μg Hg ml^{-1} when potentials were measured after 30 min.

The cyanide sensor shows nearly the same dynamic properties in determinations of mercury(II) as for cyanide. In the presence of cobalt(II) or nickel(II), however, a steady-state potential was not reached even after 30 min, which period was taken as the response time of the sensor [4].

Selectivity. Interferences in this determination of mercury(II) arise from certain anions interfering with the determination of cyanide [4] and from metal ions whose cyanide complexes are not completely decomposed at pH 0.5—1 (Table 2). The steady-state potential was read off after 3—4 min, except where indicated.

Conclusions

The proposed method of determining mercury(II) may be adaptable for other metal ions which form strong complexes. Ideally, the pH requirements involve the following aspects. For best selectivity, the pH of the sample must be adjusted to the lowest value consistent with stability of the metal ion complex to be determined. The pH value, however, must be less than 8, to allow complete conversion of the excess of potassium cyanide to hydrogen cyanide.

REFERENCES

1 L. N. La Patnick, Anal. Chim. Acta, 72 (1974) 430.
2 A. Duca and F. Matei, Rev. Chim., 28 (1977) 1186.
3 M. S. Frant, J. M. Riseman and J. A. Krueger, U.S. Patent 3, 950, 231, Apr. 13, 1976.
4 J. Fligier, P. Czichon, Z. Gregorowicz, Anal. Chim. Acta, 118 (1980) 145.
5 K. Hiiro, T. Tanaka, A. Kawahara and Y. Kono, Bunseki Kagaku, 22 (1973) 1972.
6 I. C. Popescu, E. Hopirtean, L. Savici and R. Vlad, Rev. Roum. Chim., 20 (1975) 993.
7 D. Weiss, Chem. Listy, 66 (1972) 858.
8 J. Vesely, O. J. Jensen and B. Nicolaisen, Anal. Chim. Acta, 62 (1972) 1.
9 W. E. van der Linden and R. Oostervink, Anal. Chim. Acta, 108 (1979) 169.
10 M. Yamazato, S. Fukuda, M. Kato and T. Yoshimori, Denki Kagaku, 41 (1976) 789.
11 A. V. Gordievskii, A. F. Zhukov, V. S. Shterman, N. J. Savin and Yu. J. Urusov, Zh. Anal. Khim., 29 (1974) 144.
12 G. Anderegg, Helv. Chim. Acta, 40 (1957) 1022.

Analytica Chimica Acta, 126 (1981) 225—227
Elsevier Scientific Publishing Company, Amsterdam — Printed in The Netherlands

Short Communication

STANDARDIZATION OF ALUMINUM OXIDE AND DETECTION OF POLYCYCLIC AROMATIC HYDROCARBONS ON ALUMINUM OXIDE

R. J. HURTUBISE and T. W. ALLEN

Department of Chemistry, The University of Wyoming, Laramie, WY 82071 (U.S.A.)

H. F. SILVER

Chemical Engineering Department, The University of Wyoming, Laramie, WY 82071 (U.S.A.)

(Received 24th November 1980)

Summary. Luminescence methods are described for detecting polycyclic aromatic hydrocarbons (6-, 5-, 4-, and 3-ring) on aluminum oxide after separation by dry-column chromatography. A method is reported for standardizing the water content in the aluminum oxide used for dry-column chromatography. A water content of 4.74% was chosen to define the activity of aluminum oxide because there was minimum overlap among the PAH bands.

Dry-column chromatography has been used to separate polycyclic aromatic hydrocarbons (PAH) from shale oil samples and a retort water sample [1—4]. After separation by dry-column chromatography, the PAH were further separated by thin-layer chromatography and then characterized by fluorescence spectroscopy. The initial dry-column chromatography step is very useful in separating fractions that are rich in 3-, 4-, 5-, and 6-ring PAH. In this communication, an improved method is reported for detecting standard PAH on the column after separation. Also, it has been found that the activity of the aluminum oxide provided by manufacturers varies considerably in water content compared to the aluminum oxide samples used in previous work [1—4]. This communication also describes a method for standardizing the water content in the aluminum oxide.

Experimental

Reagents and materials. Individual PAH, obtained from commercial sources, were recrystallized when needed. The aluminum oxide (activity I) for dry-column chromatography was obtained from Brinkmann, Westbury, New York. Nylon lay-flat tubing (i.d. 6.62 mm) was obtained from Hall Manufacturing Corp., Mahwah, NJ. A Buchi Rotavapor-M was used for evaporation of solvents. A jar mill mixer (Norton Chemical Process Products Division, Akron, OH) was used to mix the aluminum oxide—water samples.

Standardization of aluminum oxide. A sample of 40.275 g of aluminum oxide was accurately weighed into a jar. Then 2 ml of water was added to

the aluminum oxide with a calibrated class A pipet. The mixture was shaken vigorously, placed on the jar mill mixer for 1 h and then allowed to stand overnight. Proportionately larger amounts of aluminum oxide and water could be used, depending on the experimental needs. The aluminum oxide column was prepared, and samples of coronene (1 μg), benzo[a]pyrene (5 μg), triphenylene (5 μg) and phenanthrene (5 μg) in n-hexane were added to the top of the column, as described earlier [4]. The column was then developed with 7 ml of n-hexane—ether (19:1).

Detection of PAH standards on aluminum oxide. The developed aluminum oxide column was submerged in liquid nitrogen which was contained in a styrofoam box. The column was viewed under longwave and shortwave ultraviolet (u.v.) radiation using a u.v. handlamp to detect both the fluorescence and phosphorescence of the PAH. To detect phosphorescence, the handlamp was turned off and the decaying phosphorescence of the coronene (yellow), triphenylene (light blue) and phenanthrene (yellow-green) was noted. Coronene was detected under longwave u.v. radiation and triphenylene and phenanthrene under shortwave u.v. radiation. The purple fluorescence of benzo[a]pyrene was detected under longwave u.v. radiation. The lengths of the respective PAH bands were marked while viewing them under u.v. radiation. The four bands defined the 3-, 4-, 5-, and 6-ring PAH fractions described previously [4].

Results and discussion

Standardization of aluminum oxide. Several different amounts of water were added to activity I Al_2O_3 (0% water) in duplicate to determine the activity for efficient separation of PAH according to ring size based on the standard PAH used here. The following water contents (% w/w) were used in the experimental work: 2.93%, 3.51%, 4.15%, 4.62%, 4.74%, 4.94% and 5.24%. This range was investigated because Al_2O_3 of activity II—III was used previously [1—4]. Activity II—III is defined as 3.0—6.0% water [5]. Figure 1 shows the length of the bands of the PAH standards on the aluminum oxide column versus the percent water in the aluminum oxide. The "interface" referred to in Fig. 1 was the interface of two portions of aluminum oxide, namely a 0.5-g sample of aluminum oxide added to the column with the PAH adsorbed on it and the aluminum oxide which was already in the column. This procedure was considered earlier [4]. A water content of 4.74% was chosen to define the activity of aluminum oxide because there was minimum overlap among the PAH bands and coronene migrated beyond the interface (Fig. 1). In fact, only the triphenylene and benzo[a]pyrene bands overlapped slightly. Also, the migration rates of the standards were relatively constant around 4.74% water (Fig. 1). To obtain highly reproducible migration rates, the water content should be 4.74% ± 0.02%. The effect of column diameter on migration rate has already been discussed [4]. Other researchers may want to use different or more PAH standards to fit their needs. An investigation of several PAH standards showed that those chosen

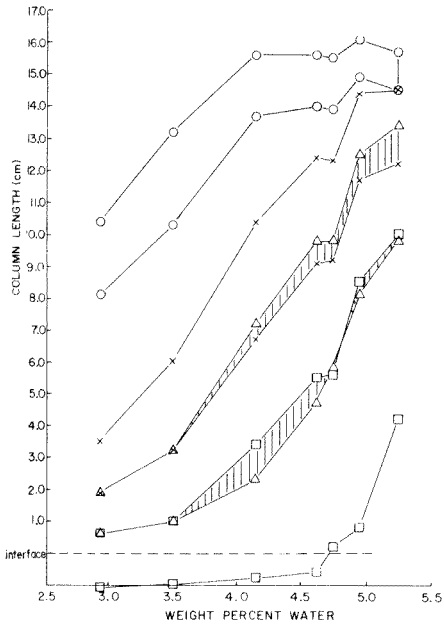

Fig. 1. Graph of length of column versus weight percent water. The vertical distance between a set of data points for a given compound represents the band length. The shaded area indicates band overlap. (○) Phenanthrene; (×) triphenylene; (△) benzo[a]-pyrene; (□) coronene. Points left to right on each plot are for 2.93, 3.51, 4.15, 4.62, 4.74, 4.94, and 5.24% water.

are very useful in investigating the 3-, 4-, 5-, and 6- ring PAH fractions in samples derived from shale oil and coal. Also, benzo[a]pyrene might be replaced with a less toxic 5-ring PAH.

Detection of PAH. The use of both fluorescence and phosphorescence to detect the PAH bands on the aluminum oxide is very simple, and the bright luminescent colors of PAH are easy to see. The nylon tubing is not affected by the liquid nitrogen and the various PAH bands can be readily cut out of the column after the column has warmed to room temperature.

Partial support of this research by the U.S. Department of Energy under contract No. DE-AC01-79ET14874 is gratefully acknowledged.

REFERENCES

1 R. J. Hurtubise, J. F. Schabron, J. D. Feaster and R. E. Poulson, Anal. Chim. Acta, 89 (1977) 377.
2 R. J. Hurtubise, G. T. Skar and R. E. Poulson, Anal. Chim. Acta, 97 (1978) 13.
3 R. J. Hurtubise, J. D. Phillip and G. T. Skar, Anal. Chim. Acta, 101 (1978) 333.
4 R. J. Hurtubise and J. D. Phillip, Anal. Chim. Acta, 110 (1979) 243.
5 L. R. Snyder, in E. Heftmann (Ed.) Chromatography: A Laboratory Handbook of Chromatographic and Electrophoretic Methods, 3rd edn., Reinhold, New York, 1975, Ch. 4.

Analytica Chimica Acta, 126 (1981) 229—232
Elsevier Scientific Publishing Company, Amsterdam — Printed in The Netherlands

Short Communication

GEL PERMEATION CHROMATOGRAPHY OF SIMPLE ANIONS IN AQUEOUS SOLUTIONS

B. MESSER, CH. YARNITZKY and G. SCHMUCKLER*

Department of Chemistry, Technion, Israel Institute of Technology, Haifa (Israel)

(Received 10th October 1980)

Summary. Semi-automatic liquid chromatographic apparatus is described for the separation of simple inorganic anions in aqueous solution, using dextran gels for the separation and differential conductivity for detection. The influence of different types of eluent on the degree and order of separation is discussed.

In the past decade, gel permeation chromatography (g.p.c.) has developed into an extremely useful tool for the separation of macromolecules and the determination of their molecular weights. It has also been shown that certain tightly cross-linked gels, such as Sephadex G-10 or G-15 [1, 2] and Biogel P-2 or P-4 [3, 4] are capable of separating simple inorganic anions such as halides, NO_3^-, NO_2^-, SCN^-, ClO_4^-, etc. The separation mechanism of inorganic salts on these hydrophilic gels is fundamentally different from that of the macromolecules, which is based mainly on steric exclusion. The size of the inorganic salt molecules is much smaller than the gel pores, and thus the predominant factor in effecting this separation is selective adsorption or desorption, which is related to hydration.

The method here proposed, despite some superficial similarities, is fundamentally different from ion chromatography, the method developed by Small et al. [5]. In ion chromatography the stationary phase is an ion-exchange resin, and the separation is based on ion-exchange selectivity; the eluents used are acids or bases of high conductivity, which necessitate suppressor columns. In contrast, the separation of ions in g.p.c. is based on ion exclusion and inclusion effects, and salt solutions are used as eluents. These eluents have a lower conductivity than either acids or bases, so that suppressor columns may be dispensed with. This is a great advantage of g.p.c., because suppressor columns have to be frequently regenerated, and they may also affect the signals of some ions, such as nitrite [6].

In the work reported here, a semiautomatic liquid-chromatography setup was developed in order to study the separation of a number of anions on a Sephadex G-15 column. Continuous monitoring by a flow-through conductometric detection system was used in order to achieve the simultaneous determination of a mixture of anions. The influence of different aqueous electrolyte and polyelectrolyte eluents on the resolution of anions is discussed.

Experimental

Apparatus. The separating column consists of a glass tube (9 mm i.d., 600 mm long) which contains the swollen aqueous Sephadex gels. The column is connected to a solvent delivery system modified to follow the elution of electrolytes by continuously measuring the differential conductivity of the effluent. The apparatus is shown schematically in Fig. 1. The conductometric detection system was designed to achieve good signal response for a variety of different eluents having a wide span of background conductivities, and for fluctuations in ambient room temperature. A conductometer (Type TH-27, El-Hama Instruments, Rosh Pina, Israel) modified as shown in Fig. 2 was used for this purpose. Determination of sample concentration in the background eluent was effected as follows: square-wave signals of 1 kHz are applied to the electrodes of the cells to eliminate polarization. The response signal is obtained by taking the difference between the centre portions of the square wave generated from the upper and lower detectors. The upper cell measures the background conductivity of the eluent while the lower cell detects both background and sample; this allows for separation of sample signal from background signal. Spurious noise is reduced by including a low-pass RC filter between the conductometer and the Radiometer RE-511 chart recorder.

The resulting chromatograms express sample concentration in terms of conductivity (μmho) as a function of time.

Materials. Deionized water was used throughout. The eluents used were aqueous 5.0 g l^{-1} solutions of various inorganic salts, organic salts and polyelectrolytes. The Cyanamer P-35 used (PMMA, American Cyanamid Co.) is a copolymer of sodium acrylate and acrylamide with a molecular weight range of 5000—7000. Sodium polystyrene sulphonate was synthesized and purified as described by Nagasawa and Horoshi [7]. Sephadex G-10, G-15 and G-25 resins were obtained in dry powder form (Pharmacia, Uppsala, Sweden).

Procedure. The eluent is introduced into the container of the solvent delivery system. It is then pumped through the packed column until a steady background conductivity is recorded on the chart for at least 5 min. The sample (100 μl) is then introduced from a syringe through the sample injection valve (Fig. 1). The flow rate of the eluent is 2 ml min^{-1} throughout.

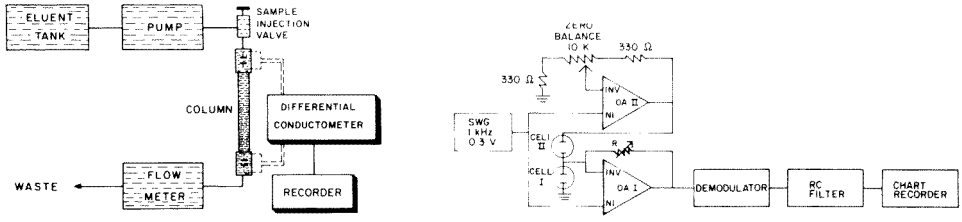

Fig. 1. Schematic diagram of the liquid chromatographic apparatus with differential conductometric detection.

Fig. 2. Modification of the conductometer for differential measurement. SWG, square-wave generator; INV, inverting input; NI, non-inverting input; BAL, balance potentiometer.

Results and discussion

The main object of this work was to investigate the effects of the type of eluent on the degree of separation of some anions. Since adsorption of electrolytes on Sephadex gels is very weak, water was first tested as the eluent for removing the ions from the column. However, incomplete separation was obtained with 100-μl samples of a mixture consisting of aqueous 10^{-3} M solutions of Na_2SO_4, NaCl, $NaNO_3$, NaSCN and $NaClO_4$ (Fig. 3). The chromatographic peaks are poorly resolved, and in all cases the peaks begin to emerge almost immediately after the void-volume blue dextran peak. All peaks exhibit a leading edge and a sharper dropping tail. A striking feature of this unresolved chromatogram is the order of elution, $SO_4^{2-} < Cl^- < NO_3^- < SCN^- < ClO_4^-$, which is the same as the lyotropic series developed by Hofmeister [8] for promoting the coagulation of lyophilic sols. The separation of anions on Sephadex gels can be greatly improved by adding an electrolyte to the eluent, as illustrated in Fig. 4. Very good resolution between the peaks is attained, and retention times are at least twice as long as those in the water elution system, whereas the order of emergence of the ions remains the same as that shown in Fig. 3.

The contrast between the chromatograms of Figs. 3 and 4 can be explained by an ion-exclusion effect [9], which is caused by the negative charges of the Sephadex gel matrix, the anions being excluded from the gel phase by electrostatic repulsion. This effect is suppressed by the addition, to the eluent, of an electrolyte, the charges of which screen the solute charges from the fixed charges of the gel. A distinction must be made between "structure-making" electrolytes, such as sodium sulphate, which have a high hydration

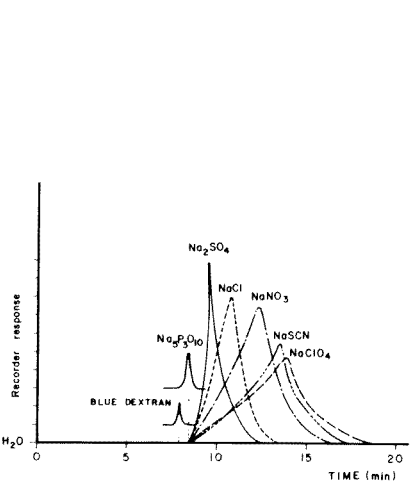

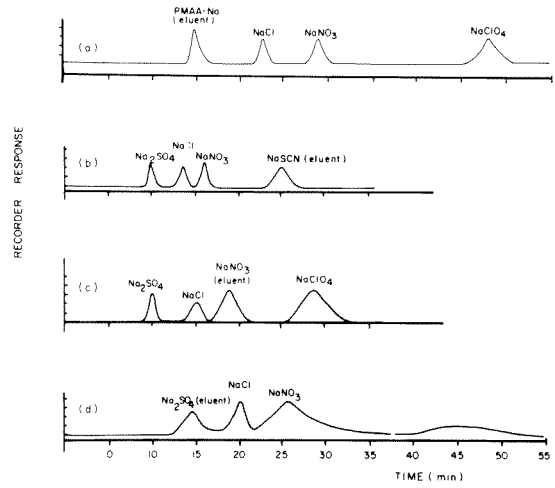

Fig. 3. A chromatogram of a salt mixture on Sephadex G-15 with water as eluent.

Fig. 4. Chromatograms of inorganic salt mixtures on Sephadex G-15 with various electrolytes (5 g l^{-1}) as eluents: (a) PMAA-Na; (b) NaSCN; (c) $NaNO_3$; (d) Na_2SO_4.

energy, and "structure-breaking" salts, such as sodium thiocyanate or perchlorate, which strongly affect the hydrated layer of the hydrophilic Sephadex gel. The effects of the different salts on the chromatograms can be seen in Fig. 4. Elution with the hydrophilic sulphate ion leads to long retention times for chloride and nitrate, whereas elution with more hydrophobic [7, 10] ions, such as nitrate or thiocyanate, produces better resolved chromatograms and shorter retention times.

The best resolution between anions is obtained with polyelectrolytes, such as Cyanamer P-35 (a sodium salt of polymethacrylic acid, PMMA) as shown in Fig. 4(a). Polyelectrolytes are water-soluble macromolecules containing ionic functionality, and have the combined advantage of being excluded from the gel pores because of their size while still screening the charges on the gel because of their own charges. Well resolved chromatograms can therefore be obtained. The effects of polyelectrolytes in gel chromatography have been studied by Stenlund [9]. He demonstrated that the presence of eluents of high molecular weight enhances the permeability of small molecules into the gel pores. This is an ion-inclusion effect, in which the eluent macromolecule is barred from the interior of the gel, thereby establishing Donnan equilibrium, which dictates the behavior of the small ionic solutes to such an extent that their transport is induced against their concentration gradients.

Conclusion

The possibility of using Sephadex gels for inorganic separations has been demonstrated. For hydrophilic anions, the ion-exclusion effect seems to predominate whereas for larger hydrophobic anions adsorption effects determine the chromatographic separation.

REFERENCES

1 T. Deguchi, J. Chromatogr., 108 (1975) 490.
2 T. Deguchi, J. Chromatogr., 120 (1976) 159.
3 P. A. Neddermayer and L. B. Rogers, Anal. Chem., 40 (1968) 755.
4 R. L. Pecsok and D. Saunders, Separ. Sci., 3 (1968) 325.
5 H. Small, T. S. Stevens and W. C. Baumann, Anal. Chem., 47 (1975) 1801.
6 W. F. Koch, Anal. Chem., 51 (1979) 1571.
7 M. Nagasawa and F. Hiroshi, J. Am. Chem. Soc., 86 (1964) 3005.
8 Water—A Comprehensive Treatise, F. Franks (Ed.), Vol. 4, Plenum, New York, 1975, Ch. 1.
9 B. Stenlund, in Advances in Chromatography, Vol. 14, M. Dekker, New York, 1976, Ch. 2.
10 H. Determann and K. Lampert, J. Chromatogr., 69 (1974) 123.

Analytica Chimica Acta, 126 (1981) 233—235
Elsevier Scientific Publishing Company, Amsterdam — Printed in The Netherlands

Short Communication

p-SULPHOBENZENEAZO-4-(2,3-DIHYDROXY-5-CHLOROPYRIDINE) AS A SPECTROPHOTOMETRIC REAGENT FOR VANADIUM IN STEELS

YOGENDU SHARMA

Department of Chemistry, Ganjdundwara College, Ganjdundwara, 207242 (India)

(Received 29th July 1980)

Summary. Vanadium(V) reacts quickly with the reagent to form a water-soluble orange-red 1:2 complex (λ_{max} = 495 nm; ϵ = 2.5 × 10^4 l mol^{-1} cm^{-1}). The complex is used to determine 0.04—1.5% vanadium in steels.

The determination of vanadium in steels is of considerable importance. The spectrophotometric determination of small amounts of vanadium(V) can be achieved with use of the reagent *p*-sulphobenzeneazo-4-(2,3-dihydro-5-chloropyridine) in an aqueous medium. The solubility of this reagent in water, the rapid development of the colour on heating, and the high molar absorptivity, make this reagent particularly useful for small amounts of vanadium in steels.

Experimental

Apparatus. A Beckman DU quartz spectrophotometer was used with matched 10-mm cells at a fixed slit-width of 0.08 mm. An expanded-scale pH meter was used with a miniature calomel—glass electrode system.

Solutions. For the standard vanadium(V) solution, dissolve 0.5850 g of analytical-grade ammonium metavanadate in 500 ml of water in a volumetric flask. Dilute with doubly-distilled water to make a working solution of 5 μg V ml^{-1}. The stock solution was standardized titrimetrically [1].

Prepare a solution (0.25% w/v) of *p*-sulphobenzeneazo-4-(2,3-dihydroxy-5-chloropyridine) in distilled water. Prepare the pH 5.0 buffer solution from 0.1 M acetic acid and 0.1 M sodium acetate.

Calibration procedure. To the vanadium solution (containing 25—270 μg of vanadium) add 5 ml of the reagent solution in a 25-ml volumetric flask, add 5 ml of pH 5.0 buffer solution and dilute to the mark with distilled water. Heat at 60—65°C for 10 min or allow to stand for 1 h, and measure the absorbance at 495 nm against a reagent blank.

Determination of vanadium (0.04—1.5%) in steels. To 100 mg of steel in a 100-ml beaker, add 5 ml of water, 5 ml of concentrated hydrochloric acid and 1 ml of concentrated nitric acid. Heat gently until dissolution is complete, evaporate almost to dryness, dissolve the residue in 5 ml of concentrated hydrochloric acid, and transfer the solution quantitatively to a 100-ml

separating funnel. To remove iron, add 10 ml of concentrated hydrochloric acid, 4 mg of ammonium iron(II) sulphate and 25 ml of 4-methylpentan-2-one. Shake the solution vigorously for 5 min, and allow to stand for 30 min. Transfer the aqueous phase to an evaporating dish and evaporate to dryness. Add a small amount of concentrated nitric acid and reheat. Dissolve the residue in distilled water and adjust the pH to about 5.5 with sodium hydroxide. Dilute to 100 ml with distilled water in a volumetric flask. Pipette a known volume (1—10 ml) of the solution into a 25-ml volumetric flask and determine the amount of vanadium by the above procedure.

Results and discussion

Effect of reaction variables. The absorption maximum of the complex occurs at 495 nm. There was no shift in this wavelength when the pH was varied from 2.5 to 9.5 or the mole ratio of vanadium to the reagent was varied from 1:5 to 5:1. Therefore all measurements were made at 495 nm. The influence of pH on the absorbance at 495 nm was examined over the pH range 1.5—10.5. A maximum, constant absorbance was obtained at pH 4.5—5.5. Therefore a pH of 5.0 was used for subsequent work.

A period of 60 min was required for full colour development at 30°C, but, on heating on a water-bath at 60—65°C, colour development was greatly accelerated and maximum colour development was obtained in 10 min; further heating (5 min) did not change the absorbance. A standard development time of 10 min was therefore adopted. The absorbance was stable for 24 h.

Calibration range and sensitivity. The molar absorptivity of the vanadium-(V) complex is 2.5×10^4 l mol^{-1} cm^{-1}, and the Sandell sensitivity is 0.0486 μg V cm^{-2}. Beer's law is valid over the concentration range 1—10.5 μg V ml^{-1}. The precision of the method was evaluated by measuring 10 identical samples each containing 5 μg of vanadium(V); the absorbance (0.38) had a standard deviation of 0.02.

Analysis of steels. The results for the determination of vanadium in vanadium-stabilized steels are given in Table 1. Determinations of vanadium in synthetic samples gave recoveries of 98%.

Effect of other ions. Synthetic solutions containing known amounts of vanadium (20 μg ml^{-1}) and various amounts of other ions and components

TABLE 1

Determination of vanadium in vanadium-stabilized steels

Sample	Vanadium certified (%)	Vanadium found (%)
Jap-852	0.52	0.494
BCS-252	0.455	0.450
NBS-123	0.04	0.038

were prepared and the proposed method was applied. An error of ±2% in absorbance reading was considered tolerable. This was achieved with up to the following concentrations: acetate, sulphate, tartrate, citrate, thiourea, Cl^-, Br^-, I^-, F^-, NO_3^- (1000 μg ml^{-1}); oxalate (700 μg ml^{-1}); Ca^{2+}, Sr^{2+}, Ba^{2+}, Mg^{2+}, Pb^{2+} (400 μg ml^{-1}) Al^{3+}, Sn^{2+}, Sb(III) (350 μg ml^{-1}): Ti(IV), Ta(V), Nb(V), Mo(VI), U(VI) (300 μg ml^{-1}); Cu^{2+}, Fe^{3+} (200 μg ml^{-1}).

Stoichiometry of the complex. The stoichiometry of the complex was investigated by Job's method of continuous variations [2] and the mole ratio method [3]; Job's method showed the stoichiometric vanadium(V): ligand ratio to be 1:2. This was confirmed by the mole ratio method. The apparent stability constant of the complex evaluated by the mole ratio method was $\log \beta_2 = 8.5 \pm 0.1$ at 30°C.

The author is grateful to the University Grants Commission for providing financial assistance.

REFERENCES

1 G. Charlot and D. Bezier, Quantitative Inorganic Analysis, J. Wiley, New York, 1957, p. xxx.
2 P. Job, Compt. Rend., 180 (1925) 928; Chim. Anal. (Paris), 9 (1928) 113.
3 J. H. Yoe and A. L. Jones, Ind. Eng. Chem., Analyt. Ed;. 16 (1944) 111.

Analytica Chimica Acta, 126 (1981) 237—240
Elsevier Scientific Publishing Company, Amsterdam — Printed in The Netherlands

Short Communication

A FLUORIMETRIC DETERMINATION OF LECITHIN-CHOLESTEROL ACYLTRANSFERASE IN BLOOD PLASMA

MASATAKE IWASAKI and CHIZUKO HAMADA

Daiichi College of Pharmaceutical Sciences, Tamagawa, Minami-ku, Fukuoka 815 (Japan)

KIYOSHI ZAITSU and YOSUKE OHKURA*

Faculty of Pharmaceutical Sciences, Kyushu University, 62 Maidashi, Higashi-ku, Fukuoka 812 (Japan)

(Received 31st October 1980)

Summary. A fluorimetric assay for lecithin-cholesterol acyltransferase in human plasma (normal and pathological) is described. The lowered cholesterol concentration in the enzyme reaction is determined fluorimetrically by using the cholesterol oxidase—peroxidase—tyramine system. The assay requires only 10 μl of plasma.

Lecithin-cholesterol acyltransferase (LCAT; EC 2.3.1.43) catalyses the transfer of a fatty acyl group from lecithin to cholesterol in plasma high-density lipoprotein. Abnormal plasma LCAT activity has been found in patients with liver diseases and diabetes [1, 2]. Several methods have been reported for the assay of LCAT. The "common-substrate" method uses an exogenous substrate prepared by incubating heat-inactivated plasma with ^{14}C- or ^{3}H-labeled cholesterol for several hours; LCAT activity in sample plasma is assayed by measuring the isotope incorporated enzymatically into the cholesterol ester after extraction of the lipids and thin-layer chromatographic separation [3—7]. In the "self-substrate" method, sample plasma is incubated with ^{14}C- or ^{3}H-labeled cholesterol and the isotope incorporated into the cholesterol ester is measured [8—13]. Alternatively, decrease in free cholesterol concentration is determined by gas chromatography [14] or by a colorimetric enzymatic method using the cholesterol oxidase (COD)—peroxidase (POD) system with 4-aminoantipyrine and phenol as chromogenic substrates [15]. In these methods (except for the colorimetric method) lecithin is not added to the incubation mixture as an exogenous substrate. Isotopic methods require complicated procedures and are unsuitable for assaying large numbers of samples: the colorimetric method can be routinely employed though it requires a large amount of plasma (0.5 ml).

Recently, a highly sensitive fluorimetric method was reported for the enzymatic assay of cholesterol in serum and in high-density lipoprotein, based on the COD—POD system with tyramine as the fluorogenic substrate of POD [16]. The LCAT-catalyzed reaction was stopped by dilution of the reaction mixture with a phosphate buffer containing the surfactant, Triton

0003—2670/81/0000—0000/$02.50

X-100: however, the surfactant enhanced the COD-mediated reaction in the cholesterol assay. This communication describes a sensitive fluorimetric method for the assay of LCAT in plasma with a simple self-substrate method utilizing the above finding. Sample plasma is incubated with dipalmitoyl lecithin (DPL) and the decrease in the cholesterol concentration in the plasma is determined fluorimetrically.

Experimental

Reagents and solutions. All chemicals were of reagent grade unless otherwise noted. Double-distilled water and isopropanol were used. DPL (120 mg; Sigma) was added to 100 ml of 20 mM Tris-HCl buffer (pH 7.5) containing 0.6 mM Na_2—EDTA and solubilized by sonication. The solution was usable for 1 week when stored at 4°C. A COD—POD solution (0.007 IU ml^{-1} and 5 purpurogallin units [17] ml^{-1}, respectively) was prepared from COD (30 μl; 23 U ml^{-1}; *Nocardia*, Miles) and 1.7 mg of POD (300 purpurogallin units mg^{-1}, Sigma), dissolved in 100 ml of 0.3 M potassiumphosphate buffer (pH 7.5). The solution was stable for more than 1 month when stored at 4°C. Tyramine hydrochloride (500 mg; recrystallized from methanol—benzene) was dissolved in 100 ml of the 0.3 M phosphate buffer (pH 7.5) and stored at 4°C. The solution was used within 1 week.

Apparatus. Fluorescence was measured with a Hitachi MPF-4 spectrofluorimeter with 10-mm quartz cells. The bandwidths were 10 nm in both the excitation and emission monochromators. The spectra were uncorrected. pH was measured with a Hitachi-Horiba M-7 pH meter at 25°C.

Human plasma. Normal and pathological plasmas from heparinized bloods were used. Plasma could be stored at 4°C for at least 3 days and at −20°C for more than 1 month without loss of LCAT activity.

Procedure. Plasma and DPL solution (5 μl each) were placed in a glass-stoppered test-tube (5 ml) and incubated at 37°C for 60 min. The incubation mixture was diluted with 3.0 ml of the 0.3 M phosphate buffer (pH 7.5) containing 0.025% Triton X-100 (Wako, Japan) to stop the enzyme reaction. COD—POD solution and tyramine solution (100 μl each) were then added and the mixture was warmed at 37°C for 20 min to develop the fluorescence (mixture A). To determine the initial concentration of free cholesterol in the plasma, the same procedure was carried out except that the plasma and DPL solution were added to the phosphate buffer, the incubation step being omitted (mixture B). The fluorescence intensities of the mixtures A and B were measured at 404 nm with excitation at 317 nm. The difference in intensity between A and B was calculated, and the loss of cholesterol determined from a standard curve prepared by treating 5-μl samples of cholesterol standard solutions (250—2500 nmol ml^{-1} in isopropanol) by the given procedure. LCAT activity was expressed as nmol of cholesterol lost per hour per ml of plasma at 37°C.

Results and discussion

Plasma LCAT was most active at pH 7.4—7.8 in 5—80 mM Tris—HCl buffer; 10 mM Tris—HCl buffer (pH 7.5) was used in the incubation. The plasma enzyme was activated more by lecithins having saturated fatty acyl chains (e.g., DPL and dimyristoyl lecithin) than by lecithins with unsaturated fatty acids [15, 18]. Although dimyristoyl lecithin enhanced the enzyme reaction more effectively than DPL, maximum reaction velocities were not achieved, and so DPL was preferred. Maximum activity was achieved with 0.8 mM DPL, the observed Michaelis constant being 0.23 mM (Fig. 1). Considerable LCAT activity was also observed in the absence of DPL, because of lecithin present in the plasma (Fig. 1). Cholesterol added to sample plasma produced neither stimulation nor suppression of LCAT activity at concentrations of 300—1000 nmol ml^{-1} even in samples with low cholesterol concentrations (750—850 nmol ml^{-1}). EDTA was used to mask the metal ions which catalyze the oxidation of lipids in the plasma [8, 19].

The enzyme activity was linear with time for at least 60 min when incubated at 37°C (Fig. 2).

When the incubation mixture was diluted with the phosphate buffer containing Triton X-100, the enzyme reaction did not restart for at least 3 h at 25°C or for 1 h at 37°C.

The fluorescence excitation (maximum, 317 nm) and emission (maximum, 404 nm) spectra for the final mixtures (A and B) were identical to those obtained with cholesterol standards. The standard curve for cholesterol was linear up to at least 2500 nmol ml^{-1} and passed through the origin.

The anticoagulants heparin and EDTA had no effect on the LCAT activity at the concentrations usually employed. Ascorbic acid and bilirubin did not affect the LCAT activity at plasma concentrations less than ca. 0.1 mg ml^{-1}, but at higher concentrations a decrease in activity was observed.

The recovery of cholesterol (1.5 and 3.0 nmol added to the incubation

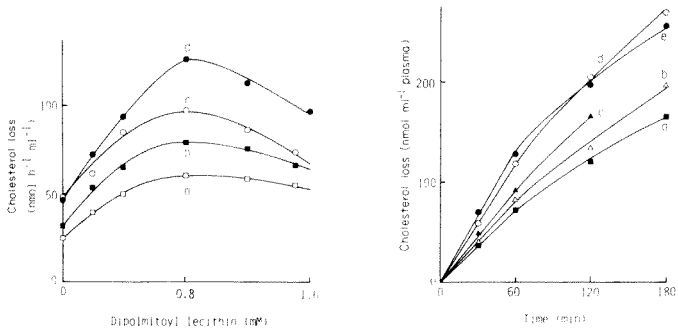

Fig. 1. Effect of dipalmitoyl lecithin concentration on LCAT activity. LCAT activity in plasma: (a) 61; (b) 79; (c) 98; (d) 126 units.

Fig. 2. Effect of incubation time on cholesterol loss. LCAT activity in plasma: (a) 72; (b) 82; (c) 92; (d) 118; (e) 128 units.

mixture) was 99 ± 2% (mean ± s.d., n = 10 in each case). The coefficient of variation was 3.6% (n = 20) at a mean LCAT activity of 135 units. Day-to-day reproducibility was demonstrated by repeating the assay for 6 days on a plasma stored at −20°C, the coefficient of variation being 4.3% (n = 18) at a mean activity of 98 units.

In a comparison with the colorimetric method [15] (n = 20) the LCAT activities by the proposed method and colorimetric method were 55—135 and 50—105 units, respectively, and the correlation coefficient was 0.840; the regression equation for the present method (x) against the colorimetric method was y = 0.717 x + 8.5. The systematic difference may arise because activities measured by the colorimetric method do not reflect maximum velocities of the enzyme-catalyzed reaction [2].

LCAT activity in normal plasma (n = 12; obtained from 22—39 year-old persons) assayed by the present method was 103 ± 20 units (mean ± s.d.). This value is in agreement with results obtained by radioassays [3, 4, 8, 12].

The present method requires only 10 μl of plasma; the procedure takes less than 2.5 h, and more than 20 samples can be assayed simultaneously. It should thus be useful for clinical investigations when only small samples are obtainable.

The supply of pathological blood from Central Clinical Laboratory of Kyushu University Hospital is acknowledged.

REFERENCES

1 Y. Muto and Y. Takahashi, Kanzo (Tokyo), 12 (1971) 630.
2 J. Makise, K. Hara and M. Kanayama, Rinshobyori (Tokyo), 27 (1979) 46.
3 J. A. Glomset and J. L. Wright, Biochim. Biophys. Acta, 89 (1964) 266.
4 O. W. Portman and M. Sugano, Arch. Biochem. Biophys., 105 (1964) 532.
5 E. A. Monger and P. J. Nestel, Clin. Chim. Acta, 15 (1967) 269.
6 K. G. Varma and L. A. Soloff, Biochem. J., 155 (1976) 583.
7 J. A. Glomset, in S. P. Colowick and N. O. Kaplan (Eds.), Methods in Enzymology, Vol. 15, Academic Press, New York, 1969, p. 543.
8 J. A. Glomset, Biochim. Biophys. Acta, 65 (1962) 128.
9 Y. Akanuma and J. A. Glomset, J. Lipid Res., 9 (1968) 620.
10 K. T. Stokke and K. R. Norum, Scand. J. Clin. Lab. Invest., 27 (1971) 21.
11 A. G. Lacko, H. L. Rutenberg and L. A. Soloff, Biochem. Med., 7 (1973) 178.
12 L. A. Soloff, H. L. Rutenberg and A. G. Lacko, Am. Heart J., 85 (1973) 153.
13 D. C. K. Roberts, J. M. Round, J. K. Lloyd and A. S. Fosbrooke, Clin. Chim. Acta, 78 (1977) 311.
14 J. P. Blomhoff, Scand. J. Clin. Lab. Invest., 33 (1974) 35.
15 T. Nagasaki and Y. Akanuma, Clin. Chim. Acta, 75 (1977) 371.
16 C. Hamada, M. Iwasaki, Y. Mibuchi, K. Zaitsu and Y. Ohkura, Chem. Pharm. Bull. (Tokyo), 28 (1980) 3131.
17 B. Chance and A. C. Maehly, in S. P. Colowick and N. O. Kaplan (Eds.), Methods in Enzymology, Vol. 2, Academic Press, New York, 1955, p. 773.
18 S. Yokoyama, T. Murase and Y. Akanuma, J. Biochem. (Tokyo), 82 (1977) 719.
19 A. V. Nichols, C. A. Rehnborg and F. T. Lindgren, J. Lipid Res., 2 (1961) 203.

Analytica Chimica Acta, 126 (1981) 241—245
Elsevier Scientific Publishing Company, Amsterdam — Printed in The Netherlands

Short Communication

DETERMINATION OF MICROMOLAR CONCENTRATIONS OF IODIDE BY ELECTROTHERMAL ATOMIC ABSORPTION SPECTROMETRY

T. NOMURA and I. KARASAWA

Department of Chemistry, Faculty of Science, Shinshu University, Asahi, Matsumoto 390 (Japan)

(Received 5th November 1980)

Summary. When a solution (at pH 3.4—4.8) containing iodide and mercury(II) nitrate in a graphite tube is heated by increasing the temperature at a uniform rate, two mercury absorption peaks appear because the decomposition temperature of mercury(II) iodide is higher than that of mercury(II) nitrate. Measurement of the second peak allows 1×10^{-6}—5×10^{-5} M iodide to be determined with good reproducibility. Equimolar concentrations of cyanide, sulfide and thiosulfate interfered, but these anions could be destroyed with hydrogen peroxide. Interfering cations were removed by extraction of 8-quinolinol complexes.

Determinations of anions by atomic absorption spectrometry have usually been performed by indirect methods, in which the absorbance of a metal which has reacted or remained after reaction with the anion is measured [1]. This is necessary, because for many anions the absorption of the resonance line is weak or the line is in the vacuum ultraviolet region [2]. For instance, iodide reacts with tris(1,10-phenanthroline)cadmium(II) to form an ion-pair which may be extracted; the absorbance of cadmium in the extract is measured [3]. Silver metal held in a flame forms silver(I) iodide which volatilizes into the flame and the absorbance of silver is measured [4]. As these indirect methods are often complicated by extraction, precipitation, filtration, etc., the accuracy and precision of the results are poorer than those achieved by a direct method.

When a graphite tube into which a solution containing mercury(II) nitrate and iodide had been injected was heated in a ramp mode, absorption peaks corresponding to the individual mercury(II) compounds appeared in sequence. Iodide could be determined by measurement of the absorbance of mercury produced from mercury(II) iodide.

Experimental

Apparatus and reagents. Mercury absorbance was measured with a Shimadzu atomic absorption spectrometer AA-650 equipped with a mercury hollow-cathode lamp (Hamamatsu TV Co. Ltd.) operated at 2 mA, a deuterium lamp for background correction, and a graphite furnace atomizer GFA-2. The temperature of the graphite tube was measured with a Baker PR-13 thermocouple.

A stock solution of potassium iodide (0.01 M) was standardized against silver(I) nitrate [5]. A mercury(II) nitrate stock solution (2×10^{-2} M) was prepared in (1 + 199) nitric acid, and standardized with EDTA using xylenol orange as indicator [6]. Working solutions were prepared by dilution with water.

Buffer solutions were prepared from 0.05 M sodium acetate and acetic acid.

Recommended procedure. Place the sample solution containing 6.4—320 μg of iodide, pH ca. 4, in a 50-ml volumetric flask, add 5 ml of 1×10^{-3} M mercury(II) nitrate solution, and dilute to volume with water. Transfer 10 μl of the solution into the graphite furnace atomizer. Measure the absorbance of mercury at 253.65 nm under the following conditions: rates of outer and inner argon flows, 1.4 l min^{-1} and 50 ml min^{-1}, respectively; current to furnace, 20 A for 30 s, then a ramp of 4.0 A s^{-1} for 30 s; spectral slit width, 0.6 nm.

Procedure for samples containing cyanide, sulfide, thiocyanate and thiosulfate. Adjust the sample solution to pH 9—10 with 10^{-2} M sodium hydroxide, add 1 ml of 3% hydrogen peroxide and heat for 10 min just below the boiling point. Neutralize with 10^{-2} M nitric acid before adding pH 4.7 acetate buffer solution, and follow the recommended procedure.

Procedure for samples containing cadmium, cobalt, copper, lead, nickel, silver, and zinc. Adjust the sample solution to pH 6.3 with 0.1 M sodium acetate, add 5 ml of ethanolic 2.5% 8-quinolinol solution and heat in a water bath for 10 min. Filter off the precipitate, dilute the filtrate with water to 50 ml and extract with two 10-ml portions of chloroform. Adjust the aqueous solution to pH 4.7 with 5 ml of acetate buffer solution and follow the recommended procedure.

Results and discussion

Measurement conditions for the graphite furnace. The mercury absorbance recorded was split into two peaks (Fig. 1a) when an iodide-mercury(II) nitrate solution was gradually heated (4.0 A s^{-1}) without pre-drying, with argon flowing. A slower increase in temperature (1.0 A s^{-1}) also without pre-drying, under gas-stop conditions, separated the peaks more clearly: the first one appeared from 7 s (ca. 60°C) to 23 s (ca. 180°C) and the second one appeared after 37 s (ca. 440°C). The height of the second peak was proportional to the concentration of iodide, and that of the first decreased with increasing amount of iodide when the total amount of mercury(II) was constant. Mole ratio experiments [7] showed that the ratio of iodide to mercury(II) corresponding to the second peak was two, as would be expected if mercury(II) iodide were the species present at this temperature.

When a solution of mercury(II) nitrate or acetate was injected into the graphite tube under the same conditions, the mercury peak appeared at the same time and temperature, corresponding to the first peak reported above. This indicates that mercury(II) nitrate and acetate released mercury atoms at

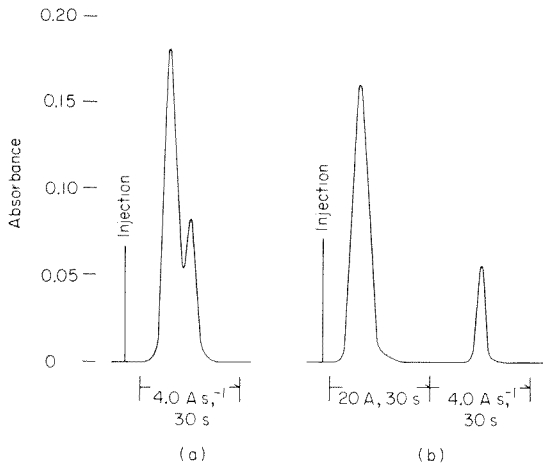

Fig. 1. (a) Mercury absorbance from 10 μl of 5×10^{-4} M mercury(II) nitrate solution which was 1×10^{-5} M in iodide atomized with a ramp of 4.0 A s^{-1} for 30 s without drying; (b) as (a) but with pre-drying at 20 A for 30 s, before heating at 4.0 A s^{-1} for 30 s: slit width, 0.6 nm; inner argon flow rate, 50 ml min^{-1}.

very low temperatures as a result of reduction by the carbon of the graphite tube [8]. Thus the mercury peak from these compounds was separated from that of mercury(II) iodide which is not reduced at such low temperatures. Therefore, pre-drying was carried out at 20 A for 30 s (ca. 150°C) and atomization in a ramp mode of 4.0 A s^{-1} for 30 s; with argon flowing under such conditions, the mercury peak from the mercury(II) which did not form the iodide appeared as a first peak during the pre-drying stage, completely separated from that of mercury produced from mercury(II) iodide, as shown in Fig. 1(b). When the drying current was 10 A for 30 s (ca. 60°C) with argon flowing, the mercury(II) nitrate was only partly decomposed during drying, and that which remained overlapped with the second peak on further heating. Mercury(II) iodide was slightly atomized, however, during drying at 25 A for 30 s (ca. 400°C).

The peak height from the mercury(II) iodide was increased with the increasing heating rate applied during ramp heating, but the reproducibility was decreased above 4.7 A s^{-1}. A ramp of 4.0 A s^{-1} for 30 s is therefore recommended.

The stopped-flow mode of introducing argon into the graphite tube gave increased sensitivity, but under such conditions the graphite tube was oxidized easily and became fragile. Thus argon at 50 ml min^{-1} is recommended to prolong the life of the tube. When the inner gas was hydrogen instead of argon, exactly the same results were obtained except that about 400 determinations per tube could be achieved compared to about 300 in argon.

Effect of pH and excess of mercury on the absorbance. The effect of pH on the absorbance was investigated with various buffer solutions because it

was assumed that the stability of mercury(II) iodide would change with pH. The optimum pH range was found to be between 3.4 and 4.8 in an acetate buffer solution. In this region, the absorbance of the reagent blank was 0.003. A large error was obtained above pH 6.0 because of the formation of mercury(II) oxide which produced a mercury signal at the same time as mercury iodide.

The absorbance was affected by the concentrations of mercury(II) nitrate solution or acetate buffer solution if they were larger than 5×10^{-3} M or 0.01 M, respectively, because mercury(II) nitrate and acetate were not evaporated completely on drying.

Calibration, reproducibility and interferences. The calibration graph was linear over the range 1×10^{-6}—5×10^{-5} M (0.13—6.4 ppm) iodide, and is described by the equation $[I^-]$ (ppm) = 52.6 (A − 0.003), where 0.003 is the absorbance of the reagent blank and A is the sample absorbance. The standard deviation was 8.8×10^{-4} (1.6%) for 5 determinations of 2×10^{-5} M iodide.

The effect of foreign ions on the determination of 2×10^{-5} M iodide was measured. A deviation greater than twice the standard deviation was considered to be an interference. The results are shown in Table 1. Interfering anions, such as cyanide, sulfide, thiocyanate and thiosulfate, which increased the iodide response, were eliminated by oxidation with hydrogen peroxide in alkaline solution. A 10-min heating time just below the boiling point of water was adequate for complete oxidation (Fig. 2). Interference of a 10-fold molar amount of bromide was eliminated by reduction of mercury(II) bromide to mercury (0) with 5 ml of 2×10^{-3} M hydroxylammonium chloride before following the recommended procedure. Interfering cations, such as

TABLE 1

Minimum interfering concentration of foreign ions for determinations of 2×10^{-5} M iodide

Ions	Molar ratio to iodide
Co^{2+}, Cu^{2+}, Ni^{2+}, Pb^{2+}, Zn^{2+}	100
Br^-, SCN^-, Cd^{2+}	10
CN^-, Ag^+	1
$S_2O_3^{2-}$, S^{2-}	0.1

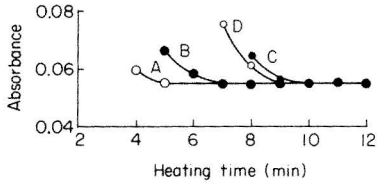

Fig. 2. Effect of heating time in a hydrogen peroxide solution, pH 9—10, on the absorbance from 2×10^{-5} M iodide solution containing 100-fold molar amounts of (A) thiocyanate, (B) cyanide, (C) thiosulfate, (D) sulfide.

cadmium, cobalt, copper, lead, nickel, silver and zinc, were eliminated by extraction of their 8-quinolinol complexes formed at pH 6.3.

REFERENCES

1 G. F. Kirkbright and H. N. Johnson, Talanta, 20 (1973) 433.
2 J. M. Manfield, T. S. West and R. M. Dagnall, Talanta, 21 (1974) 787.
3 T. Kumamaru, Bull. Chem. Soc. Jpn., 42 (1969) 956.
4 R. S. Fike and C. W. Frank, Anal. Chem., 50 (1978) 1446
5 I. M. Kolthoff and E. B. Sandell, Textbook of Quantitative Inorganic Analysis, 3rd edn., Maruzen, Tokyo, 1952, p. 544.
6 J. Körbl and R. Pribil, Chemist-Analyst, 45 (1956) 102.
7 J. H. Yoe and A. L. Jones Ind. Eng. Chem., Anal. Ed., 16 (1944) 111.
8 R. E. Sturgeon, C. L. Chakrabarti and C. H. Langford, Anal. Chem., 48 (1976) 1792.

Analytica Chimica Acta, 126 (1981) 247—251
Elsevier Scientific Publishing Company, Amsterdam — Printed in The Netherlands

Short Communication

DIFFERENTIAL PULSE POLAROGRAPHIC DETERMINATION OF TRACES OF IRON IN SOLAR-GRADE SILICON†

DONATELLA FERRI
Istituto Chimico della Facoltà d'Ingegneria, Università di Bologna, 40136 Bologna (Italy)
PIER LUIGI BULDINI*
C.N.R.-Istituto LAMEL, Via de' Castagnoli 1, 40126 Bologna (Italy)
(Received 5th November 1980)

Summary. Iron is determined, after volatilization of the matrix as hexafluorosilicic acid, by means of the polarographic iron(III) wave in a 0.1 M triethanolamine—0.1 M potassium bromate—0.5 M sodium hydroxide medium. Differential pulse polarography provides a detection limit of about 0.15 μg g^{-1} with a precision of 1—2% and linear calibration graphs up to 0.5 μg Fe(III) ml^{-1}.

Semiconductor-grade silicon is produced from the metallurgical-grade material (about 98% purity) by an expensive process involving conversion of silicon to trichlorosilane, purification, and thermal reduction with hydrogen. For extensive development of solar energy cells, silicon considerably cheaper than that now available, must be provided for crystal growth and subsequent cell fabrication. The purity of silicon required for solar cells (solar-grade silicon) is considerably less than that for semiconductor-grade silicon. Metallurgical-grade silicon is again a convenient starting product in several low-cost processes for the preparation of solar-grade silicon. Such silicon contains up to 0.5% of iron as a major impurity as well as minor impurities. Most metal impurities are at deep levels in silicon and act as traps or recombination centers with large cross-sections so that they must be removed as completely as possible. Iron is usually the impurity selected for gettering studies because of the absence of shallow trapping and its pronounced effect on silicon lifetime. At the present time, the tolerable feedstock iron content to achieve specific solar cell performance levels is accepted to be about 350 μg g^{-1} for a relative efficiency $\eta = 0.9\ \eta_0$, about 120 μg g^{-1} for $\eta = 0.95\ \eta_0$ and about 3 μg g^{-1} for $\eta \approx \eta_0$, where η_0 is the efficiency of a typical baseline device.

The iron content is usually determined by spark-source mass spectrometry, with a detection limit of about 60 ng g^{-1} [1], or by neutron activation with a detection limit of about 4 ng g^{-1} [2]; the latter method provides the lowest available detection limit. Spectrophotometry [3—5] and atomic absorption spectrometry [6, 7], as well as voltammetric techniques [8—10] have been

†Presented at the Heyrovsky Memorial Congress on Polarography, Prague, August 1980.

applied to determinations of iron in silicates, but the very sensitive polarographic determination of iron(III) in the presence of bromate has not been utilized. In alkaline triethanolamine solution containing bromate, iron(III) gives an exceptionally high polarographic current because the reduced iron(III)—triethanolamine complex is repetitively reoxidized, and the well-shaped polarographic wave is suitable for trace analysis. Although chemical methods cannot provide the high sensitivity available with sophisticated physical methods, the method described here illustrates the advantages of using inexpensive apparatus and unskilled staff, whilst reaching the detection limits required by advanced technologies.

The proposed method is based on silicon dissolution with hydrofluoric and nitric acids, volatilization as hexafluorosilicic acid, and differential pulse polarography in an alkaline triethanolamine supporting electrolyte containing bromate.

Preliminary studies

Alkaline triethanolamine solutions of variable composition are very widely used for the voltammetric determination of iron in different matrices. Zarebski [11] observed that addition of potassium bromate to the alkaline triethanolamine electrolyte greatly increased the height of iron peak although the reduction potential ($E_{1/2}$ = −1.05 V vs. SCE) of the iron(III) complex was not affected. Bromate itself shows no wave in this region, and it appears that the reduced iron(III)—triethanolamine complex is repeatedly reoxidized. The peak current is linearly dependent on the iron(III) concentration at the ppb or low ppm level.

In optimizing the working conditions, it was found that the increase in peak height depends strongly on the bromate concentration, as shown in Table 1. However, 0.1 M potassium bromate is the upper limit, because of the insolubility of the salt. The quantity of sodium hydroxide added does not influence the polarographic reduction, but if its concentration is less than 0.5 M the linear calibration range is limited to 0—0.25 μg Fe(III) ml^{-1}. With ⩾0.5 M NaOH, the linear range is 0—0.5 μg Fe(III) ml^{-1}, but higher concentrations only increase the blank values. Variation in the triethanolamine concentration between 0.05 and 1 M affected neither the polarographic response nor the linear range. Under the recommended conditions, the temperature coefficient was 4.5% K^{-1}, as reported by Zarebski [11].

TABLE 1

Variability of the d.p.p. response as a function of potassium bromate addition (Supporting electrolyte, 0.1 M triethanolamine hydrochloride—0.5 M sodium hydroxide; polarographic conditions as in Procedure)

$KBrO_3$ added (M)	0	10^{-6}	10^{-5}	10^{-4}	10^{-3}	10^{-2}	10^{-1}
Diffusion current increase	1	1.0	1.0	1.2	4.0	15.0	60.2

Experimental

Reagents and equipment. Erbatron electronic-grade chemicals were used; triethanolamine hydrochloride, potassium bromate, and Suprapur sodium hydroxide were from Merck (Darmstadt).

Reagents and solutions were stored in polyethylene bottles; polyethylene calibrated equipment was used to prevent leaching. All vessels were soaked overnight in 5 M hydrochloric acid, and rinsed thoroughly with twice-distilled water before use. Preferably, a set of equipment should be reserved for iron determinations and washed only with distilled water.

Working standards were prepared daily by diluting stock iron(III) solution (1000 μg Fe ml^{-1} from $FeCl_3$, Normex atomic absorption standard) with twice-distilled water.

The silicon samples were dissolved in PTFE test tubes in a sample dissolution device (Berghof, Tübingen, FRG) as described previously [12]. An AMEL (Milan) model 472 Multipolarograph equipped with a model 460 stand was used. The dropping mercury electrode ($m^{2/3} = 1.79$) was used with an Ingold model 303/NS saturated calomel electrode and an Ingold model Pt-805/NS platinum ring. Instrumental conditions were: pulse height 100 mV, drop time 2 s and scan 2 mV s^{-1}. A 5-ml microcell was normally used. Solutions were deaerated with pure nitrogen for 2—3 min and thermostatted at 25.0 ± 0.1°C.

Procedure. The preliminary treatment of the samples (usually as ingot pieces) based on matrix elimination has been reported [12]. After ultrasonic washing and degreasing with trichloroethylene—acetone—methanol [13], and etching with hydrofluoric—nitric acids (1 + 1), the samples are washed in running twice-distilled water, dried in a nitrogen flow and powdered finely in an agate mill.

Place 10—100 mg of samples in a PTFE test tube and add 2 ml of 65% HNO_3 and 5 ml of 12 M HF; the reaction starts spontaneously. To complete the dissolution, plug the test tube with the PTFE cone adapted for passing filtered air and insert the tube into the sample dissolution device kept at 50°C for 1 h. Then raise the temperature to 110°C for 2 h while passing a filtered air flow through the tube. Only a small residue remains. Then add 5 ml of the 0.1 M triethanolamine hydrochloride—0.1 M potassium bromate—0.5 M sodium hydroxide supporting electrolyte. Shake well to dissolve any residue, transfer the solution to the polarographic cell, deaerate for 3 min and record the polarogram from −0.75 V to −1.40 V (vs. SCE). Measure the peak height at −1.05 V and compare it with a calibration curve. Figure 1 shows a typical polarogram with the method of peak measurement. The calibration curve obtained under the recommended conditions is linear over the range 0.002—0.5 μg Fe(III) ml^{-1}.

Results and discussion

To test the proposed method, several types of silicon, both metallurgical and solar grade, were tested. Some results are reported in Table 2 with some

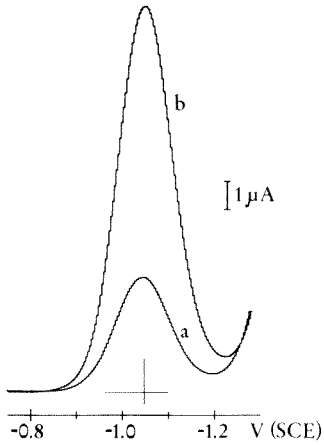

Fig. 1. Typical polarogram showing the method of peak measurement. Operating features as reported in the procedure. (a) Blank; (b) 0.1 μg Fe(III) ml^{-1}.

comparative results by a spectrophotometric procedure [14]. The results are in good agreement but the differential pulse polarographic method is far more sensitive. When the recommended conditions are used, the proposed method permits determinations of iron as low as about 0.15 μg Fe g^{-1} in the silicon sample, with a relative standard deviation of about ±2%.

When the iron content to be determined is greater than 10 μg g^{-1}, it is more convenient to use the triethanolamine—sodium hydroxide supporting electrolyte without bromate. The linear range is then larger and the sensitivity is less. In this case, the residue from the matrix volatilization is simply treated with 5 ml of 0.2 M triethanolamine hydrochloride—0.2 M sodium hydroxide and the solution is transferred to the polarographic cell. Under these conditions, the detection limit is only 2.5 μg Fe g^{-1} but the calibration curve is linear up to at least 5 μg ml^{-1}.

TABLE 2

Determination of iron in silicon samples

Sample[a]	Spectrophotometric [14]		Polarographic	
	Fe (μg g^{-1})	s_r[b] (%)	Fe (μg g^{-1})	s_r[b] (%)
Alfa 00469	60	—	57	1.1
Schuchardt SI 172	540	—	540	0.7
Merck Lab	—	—	181	1.1
B.D.H.	5344	2.3	5350	0.5
M. 3	—	—	26	2.3
M. 8	—	—	1.5	0.7
M. 10	—	—	0.6	2.5

[a]M. = Montedison SpA, Milan (Italy). [b]For 20 determinations.

No cations were found that caused interference on the iron wave in the presence of bromate. Among typical impurities found in metallurgical silicon, 200-fold amounts of chromium, copper, manganese, nickel, titanium, zinc, cobalt and lead did not interfere.

The authors thank Prof. D. Nobili and F. Zignani for their helpful suggestions.

REFERENCES

1 Performance characteristics, Mass Spectrometer type MS-7, Associated Electrical Industries Ltd.
2 General Activation Analysis Data Sheet. Multi-Element Survey Analysis of Silicon, General Activation Analysis, San Diego, CA, U.S.A.
3 H. J. Cluley and E. J. Newman, Analyst, 88 (1963) 3.
4 BS 1902, Part 2A, Chemical Analysis of High-Silica and Aluminosilicate Materials, 1964.
5 Society for Glass Technology, Chemical Analysis Committee, Glass Technol., 14 (1973) 5.
6 C. W. Fuller, Anal. Chim. Acta, 62 (1972) 261.
7 W. J. Price and P. J. Whiteside, Analyst, 102 (1977) 664.
8 E. I. Majenthal, Anal. Chem., 45 (1973) 644.
9 D. E. Campbell, S. S. Yao and J. P. Williams, Phys. Chem. Glasses, 17 (1976) 108.
10 A. A. Kaplin, Z. S. Mikhailova and L. F. Zaichko, Zh. Analit. Khim., 33 (1978) 120.
11 J. Zarebski, Chem. Anal. (Warsaw), 22 (1977) 1049.
12 P. L. Buldini, Q. Zini and D. Ferri, Anal. Chim. Acta, 124 (1981) 233.
13 P. Lanza and P. L. Buldini, Anal. Chim. Acta, 85 (1976) 69.
14 M. Taddia, Microchem. J., 22 (1977) 369.

Analytica Chimica Acta, 126 (1981) 253—257
Elsevier Scientific Publishing Company, Amsterdam — Printed in The Netherlands

Short Communication

EFFECT OF MICELLAR SYSTEMS ON THE EQUILIBRIUM OF CHEMICAL REACTIONS
Acidity and Binding Constants of Polymethylphenols in Sodium Dodecyl Sulphate

EDMONDO PRAMAURO and EZIO PELIZZETTI
Istituto di Chimica Analitica, Università di Torino (Italy)
(Received 28th October 1980)

Summary. The variations of the acidity constants in the presence of sodium dodecyl sulphate (SDS) are used to estimate the binding constants of a series of methyl-substituted phenols with the SDS micelles. The contribution of each methyl group to the transfer free energy from water to micelles is about -520 cal mol^{-1}, irrespective of the position in the benzene ring.

Molecules containing both hydrophilic and hydrophobic moieties associate in water above a certain concentration (called the critical micelle concentration, c.m.c.) to give colloidal particles called micelles [1]. Particular interest in analytical applications of micellar systems derives from their important role in solubilization processes [2] as well as from their effects on overall reaction rates and equilibria [3, 4]. These properties can be used in several techniques [5], e.g. acid—base titrations [6, 7], voltammetry [8], phosphorimetry [9], chromatography [10]. Because the partition between micellar and aqueous phases, and the variations in rates and equilibria, are related to the hydrophobicity of the substrates, it is of interest to investigate the parameters that influence hydrophobicity.

In this communication, the effect of a micelle-forming surfactant, sodium dodecyl sulphate (SDS), on the apparent acidity constants of a series of methyl-substituted phenols is described. The data allow the binding constants of phenols with SDS and the hydrophobic contribution of the methyl groups to be estimated.

Experimental

Materials and apparatus. The phenols (Erba, Merck, Aldrich) and SDS (Merck) were purified by recrystallization.

A Cary 219 spectrophotometer, a Metrohm E388 potentiometer and a Dognon-Abribat tensiometer with platinum blade were used.

pK_a measurements. The apparent acidity constants of the phenols, $K_{a(app)}$, were determined spectrophotometrically at a wavelength where the molar absorptivities for the two forms were sufficiently different. Spectral data

were utilized in the equation,

$$K_{a(app)} = 10^{-pH}(A - A_a)/(A_b - A) \quad (1)$$

where, at a given wavelength and with a constant phenol concentration ($1-2 \times 10^{-4}$ M), A_a is the absorbance in an acidic solution (0.02 M HCl), A_b is the absorbance in a basic solution (0.02—0.1 M NaOH), and A is the absorbance in buffers at intermediate and known pH values (0.1 M glycine—NaOH—0.1 M NaCl buffers were used and the pH values in the presence of SDS were checked potentiometrically).

The values of $K_{a(app)}$, at each surfactant concentration (SDS $1-5 \times 10^{-2}$ M) were averaged over 4—6 separate measurements. The deviation was ±0.05 units. The data were collected at 25.0 ± 0.5°C.

Results and discussion

Critical micelle concentration. The surface-tension measurements of the SDS systems in the presence of buffers (in the range pH 9.0—12.0) and phenols showed that the c.m.c. lies in the range $1.1-1.3 \times 10^{-3}$ M. Shifts are often caused by salts and solubilizates compared to the c.m.c. measured in distilled water (8×10^{-3} M) [1—3].

Acidity constants in the presence of surfactant micelles. Considering the dissociation of a weakly acidic substrate $HA \rightleftharpoons H^+ + A^-$, and partitioning of the different species between the micellar and aqueous pseudo-phases, the apparent acidity constant can be expressed [4] as

$$K_{a(app)} = K_W(1 + K_A[C])/(1 + K_{HA}[C]) \quad (2)$$

Here K_W is the acidity constant in the absence of surfactant, and $[C]$ is the surfactant concentration exceeding the c.m.c. K_A and K_{HA} are the binding constants with the micelles in the deprotonated and protonated forms, respectively, defined as $K = [S_M]/[S_W]([C] - [S_M])$, where subscripts M and W, to the substrate S, refer to the micellar and aqueous phases, respectively.

Recent detailed treatments, based on ion-exchange or electrostatic models, have given more complicated expressions which describe the variation of $K_{a(app)}$ over wide ranges of surfactant concentrations and in the presence of added salts [11, 12]. However, for the present conditions, eqn. (2) describes the data satisfactorily. The $pK_{a(app)}$ values increase as the surfactant concentration increases. The shift in the apparent pK_a is related to the free energy for transference from water to the micellar phase, and to the negative charge at the micellar surface.

For analytical purposes, eqn. (2) can be rewritten

$$(1 - K_{a(app)}/K_W)/[C] = (K_{HA}K_{a(pp)}/K_W) - K_A \quad (3)$$

Plots from eqn. (3) show intercepts which do not differ significantly from zero; this is as expected because the negatively charged phenoxide ions have little tendency to associate with the anionic micelles. It has recently been reported [13] that the ratio of the binding constants of duroquinone (un-

charged) and its radical anion with SDS micelles is about 600; such ratios for some naphthols and phenols and their deprotonated forms lie in the range 10—40 in non-ionic surfactant [14]. Thus eqn. (2) can be simplified to

$$K_W/K_{a(app)} = 1 + K_{HA}\,[C] \tag{4}$$

The values of K_{HA} can then be easily determined from the plots of Fig. 1 (a—d). Table 1 lists the values of K_{HA} and pK_W, which are in agreement with literature data [15].

Binding constants of phenols with SDS micelles. The free energy change involved in the solubilization, ΔG_S° [16], is related to K by $\Delta G_S^\circ = -RT \ln K$, where the standard state is taken to be a dilute solution of the solute in the buffer solution used. As micellar solubilization in the present system is primarily determined by hydrophobic interactions, ΔG_S° should be related to the number of carbon atoms; there are two contributions, one from the aromatic moiety (ΔG_{Ph}°) and one from the methyl substituents (ΔG_C°)

$$\Delta G_S^\circ = \Delta G_{Ph}^\circ + n\Delta G_C^\circ \tag{5}$$

where n is the number of methyl groups. The standard free energy of transfer to the micelle is given by $\mu_M^\circ - \mu_W^\circ = RT \ln (X_W/X_M)$, where the mole fraction $X_W = [S_W]/([S_W] + 55.5 + \text{c.m.c.})$ and the mole fraction $X_M = [S_M]/([S_M] + [C])$. For X_W, $55.5 \gg [S_W]$ + c.m.c., and for X_M, $[C] \gg [S_M]$, and so

$$\mu_M^\circ - \mu_W^\circ = \mu_{Ph}^\circ + n\mu_C^\circ = -RT \ln (55.5\ K) \tag{6}$$

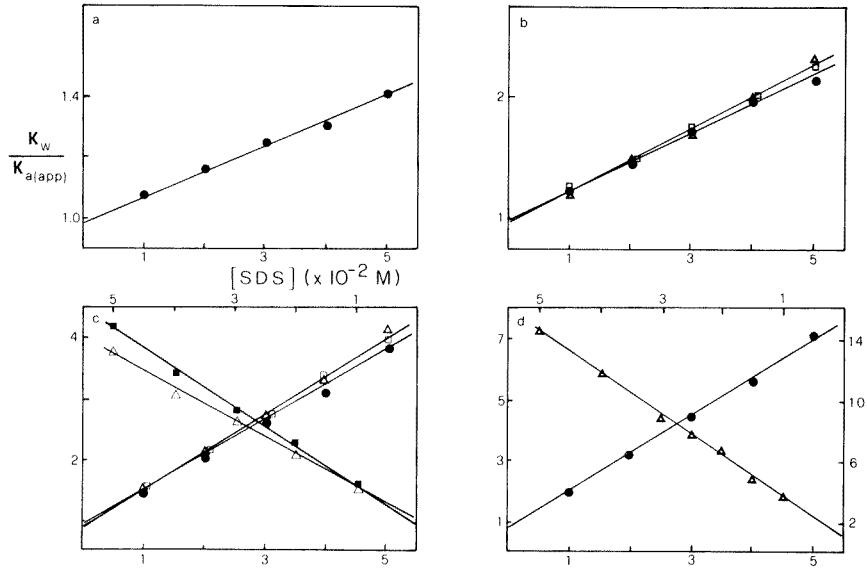

Fig. 1. Plots of eqn. (4) for the phenols investigated. The numbers relate to the compounds listed in Table 1. (a) (•) 1. (b) (•) 2; (△) 3; (□) 4. (c) Bottom scale: (•) 5; (△) 6; (□) 7; top scale; (△) 8; (▪) 9. (d) Bottom and right scale: (•) 10; top and left scale; (△) 11.

TABLE 1

Binding constants with SDS micelles and acidity constants of phenols in water (25.0°C; glycine buffer)

No.	Compound	K_{HA} (M^{-1})	pK_W	No.	Compound	K_{HA} (M^{-1})	pK_W
1	Benzene-1-ol	8 ± 2	10.02	7	2,5-Dimethyl-	64 ± 6	10.39
2	2-Methyl-	21 ± 3	10.32	8	2,6-Dimethyl-	57 ± 5	10.64
3	3-Methyl-	24 ± 3	10.09	9	3,5-Dimethyl-	64 ± 7	10.20
4	4-Methyl-	24 ± 3	10.25	10	2,4,5-Trimethyl-	125 ± 15	10.79
5	2,3-Dimethyl-	58 ± 5	10.45	11	2,3,5,6-Tetramethyl-	270 ± 30	11.3
6	2,4-Dimethyl-	63 ± 6	10.53				

The plot of Fig. 2 shows that eqn. (5) is valid and that the incremental free energy of transfer per methyl group is about −520 cal mol^{-1}. The binding constants of the isomers are very close, suggesting that the methyl groups are in similar environments.

Other examples of solubilization with SDS have been reported for alkanes [17] (−771 cal mol^{-1} for each additional carbon atom) and recently for arenes (benzene, methylbenzene and 1,4-dimethylbenzene) where an incremental free energy of −575 cal mol^{-1} was estimated [18]; the latter is very close to the present findings. Data on the interactions of methylbenzoic acids with SDS are similar to the present results [7]. The values of transfer free energy for several nonionic, zwitterionic and ionic surfactants (at relatively high ionic strength) into their micelles have been reported as approximately −700 cal mol^{-1} [19]. Since the incremental free energy for phenols with cationic micelles is lower (ca. −310 cal mol^{-1} per methylene [20]), the differences can be attributed to location of the solubilizates in a medium far from hydrocarbon-like, i.e., the interactions are mainly due to surface processes.

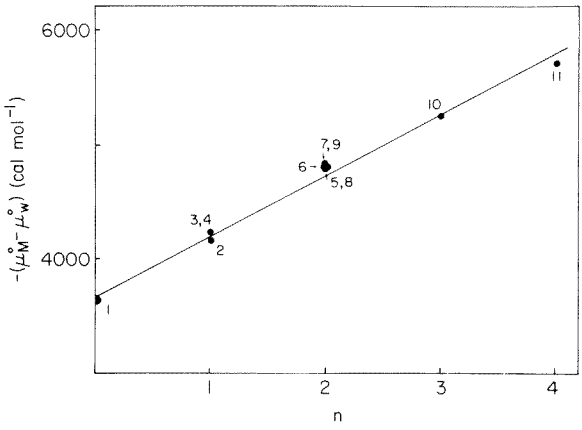

Fig. 2. Transfer free energies of phenols as a function of the number of methyl groups. The numbers relate to the compounds listed in Table 1.

The intercept of the plot of Fig. 2 allows the transfer energy transfer for a phenoxy moiety from water to micelle to be estimated as ca. -3650 cal mol^{-1}. Since the value for benzene is -4530 cal mol^{-1} [18], it follows that the hydroxyl group contribution to $\mu_M^\circ - \mu_W^\circ$ is about $+880$ cal mol^{-1} (compared with the value of $+1340$ cal mol^{-1} assigned to the contribution in the free energy transfer for aliphatic alcohols from aqueous solution to pure liquid alcohol [16]).

A systematic investigation of the hydrophobic contribution of several groups is currently under investigation.

REFERENCES

1 M. J. Rosen, Surfactants and Interfacial Phenomena, J. Wiley, New York, 1978.
2 P. H. Elworthy, A. T. Florence and C. B. McFarlane, Solubilization by Surface Active Agents, Chapman and Hall, London, 1968.
3 J. H. Fendler and E. J. Fendler, Catalysis in Micellar and Macromolecular Systems, Academic Press, New York, 1975.
4 I. V. Berezin, K. Martinek and A. K. Yatsimirskii, Russ. Chem. Rev. (Eng. trans.), 42 (1973) 787.
5 W. L. Hinze, in K. L. Mittal (Ed.), Use of Surfactant and Micellar Systems in Analytical Chemistry, Solution Chemistry of Surfactants, Plenum Press, New York, Vol. 1, 1979, p. 79.
6 A. L. Underwood, Anal. Chim. Acta, 93 (1977) 267.
7 E. Pelizzetti and E. Pramauro, Anal. Chim. Acta, 117 (1980) 403.
8 T. C. Franklin and M. Iwunze, Anal. Chem., 52 (1980) 973.
9 L. J. Cline Love, M. Skrilec and J. G. Habarta, Anal. Chem., 52 (1980) 754.
10 D. W. Armstrong and R. Q. Terril, Anal. Chem., 51 (1979) 2160.
11 F. H. Quina and H. Chaimovich, J. Phys. Chem., 83 (1979) 1844.
12 N. Funasaki, J. Phys. Chem., 83 (1979) 1999.
13 M. Almgren, F. Grieser and J. K. Thomas, J. Phys. Chem., 83 (1979) 3232.
14 L. K. J. Tong and M. C. Glesmann, J. Am. Chem. Soc., 79 (1957) 4305.
15 Y. Yukawa, Handbook of Organic Structural Analysis, Benjamin, New York, 1965.
16 C. Tanford, The Hydrophobic Effect, Wiley—Interscience, New York, 1973.
17 A. Wishnia, J. Phys. Chem., 67 (1963) 2079.
18 M. Almgren, F. Grieser and J. K. Thomas, J. Am. Chem. Soc., 101 (1979) 279.
19 K. S. Birdi, in K. L. Mittal (Ed.), Micellization, Solubilization and Microemulsions, Plenum Press, New York, 1977; Vol. 1, p. 151.
20 C. A. Bunton and L. Sepulveda, J. Phys. Chem., 83 (1979) 680.

Analytica Chimica Acta, 126 (1981) 259—261
Elsevier Scientific Publishing Company, Amsterdam — Printed in The Netherlands

Short Communication

REACTION OF α,α,α-TRIFLUOROACETOPHENONE WITH AMMONIA

W. JAMES SCOTT[a] and PETR ZUMAN*

Department of Chemistry, Clarkson College of Technology, Potsdam, NY 13676 (U.S.A.)

(Received 29th September 1980)

Summary. Increase in the reduction waves of α,α,α-trifluoroacetophenone in the presence of ammonia or ethylamine is caused by chemical reaction. Either the Schiff base is reduced at potentials similar to that of the parent compound or the rate of dehydration of geminal diol of the ketone is catalyzed by amines.

In the course of study [1] of polarographic reduction of α,α,α-trifluoroacetophenone I it was observed that reduction waves in ammonia—ammonium chloride buffers were considerably higher than waves in borate buffers of the same pH. As ketones are known [2] to yield reduction waves in ammonia buffers corresponding to condensation products, behavior of ketone I in the presence of ammonia was investigated in some detail.

Experimental

Apparatus, chemicals, solutions and procedures were the same as in the preceding paper [1].

Results

At pH 9.3, addition of ammonia—ammonium chloride buffer to a solution of ketone I in a borate buffer, results in an increase of the wave of the reduction of the unprotonated form $C_6H_5COCF_3$, previously [1] denoted as i_A. The plot of i_A against $\log[NH_3]$ has the shape of a dissociation curve with inflexion point at $\log[NH_3] = -0.75$. Similarly, when ammonia—ammonium chloride buffers were diluted with water the $i_A - \log[NH_3]$ plot had an analogous shape with an inflexion point at $\log[NH_3] = -0.64$ (Fig. 1).

An increase in the total wave-height is accompanied by a change in the wave-shape. The regular limiting current, parallel with the zero-current line, which is observed in borate buffers, changes at higher ammonia concentration to a sloping limiting current, decreasing with increasingly negative potentials (Fig. 2). Such shapes are frequently observed for waves where a chemical reaction preceding the electron transfer occurs as a surface reaction [3]. As

[a]Present address: Technicon, Tarrytown, NY 10591, U.S.A.

0003—2670/81/0000—0000/$02.50

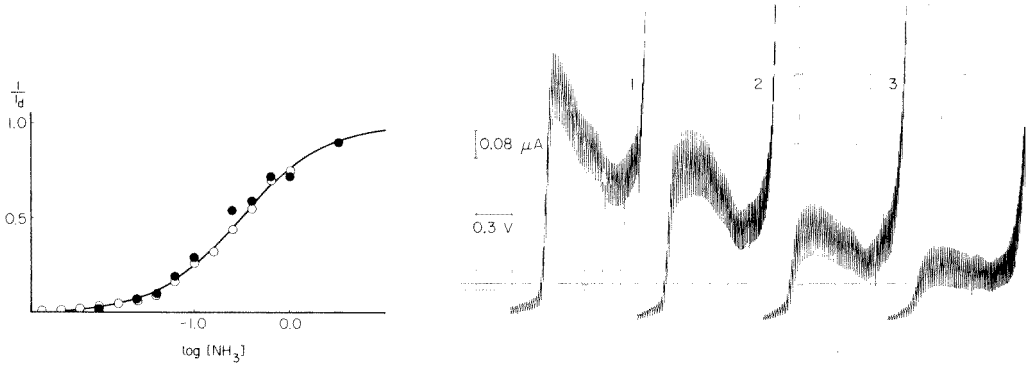

Fig. 1. Dependence of d.c. polarographic currents for 1×10^{-3} M α,α,α-trifluoroacetophenone in 5% ethanol (v/v) on ammonia concentration; •, ammonia—ammonium chloride buffer; ○, ammonia added to 0.05 M borax; experimental points, theoretical dissociation curve for monobasic acid.

Fig. 2. Dependence of d.c. polarographic curves of 1×10^{-3} M α,α,α-trifluoroacetophenone on ammonia concentration in the presence of 5% ethanol (v/v); ammonia—ammonium chloride (pH 9.2) buffer added to 0.05 M borax (pH 9.2); all curves start at −1.2 V measured vs. mercurous sulfate electrode; molar concentration of ammonia: (1) 3.3; (2) 0.25; (3) 0.06; (4) 0.01.

the wave i_A increases with increasing ammonia concentration, it becomes difficult and then impossible to measure the height of the more negative wave i_p, which corresponds [1] to reduction of acetophenone generated at the electrode surface in the reduction of the trifluoroketone I.

The wave i_A which in 1×10^{-3} M solutions of trifluoroacetophenone I in borate buffer pH 9.3 measures 1.5 μA, increases in the presence of 1 M ammonia to 7 μA, which represents more than 20% of the theoretical diffusion current corresponding to a two-electron reduction. Nevertheless, even in 1 M ammonia buffer the wave-height is practically independent of mercury pressure and thus corresponds to a kinetic current.

A qualitatively similar increase is observed in buffers consisting of ethylamine and ethylammonium chloride, but the limiting current of the resulting wave i_A is parallel with the zero current line and wave i_p remains measurable.

Observed increase in currents in the presence of ammonia indicates a change in the hydration—dehydration equilibria due to formation of a carbinolamine or a Schiff base. Two interpretations are possible: Either Schiff base is also reduced in wave i_A or more free carbonyl form $C_6H_5COCF_3$ is available for reduction in the presence of amines.

Reduction of the Schiff base at a similar potential to that observed for the parent carbonyl compound resembles the situation observed for reduction of chloral in the presence of amines [4, 5]. For simple aldehydes and ketones, the C=N bond is reduced always at more positive potentials than the C=O bond. The reduction wave i_A, nevertheless, corresponds to hydrogenolysis of

the C—F bonds rather than reduction of the carbonyl group. The increase in wave i_A can be thus attributed to the formation of a Schiff base, less strongly hydrated than ketone **I**. Either the C—F bond is activated by adjacent C=O and C=N bonds similarly, or reduction of C=N from the Schiff base of the fluoroketone occurs at potentials similar to that of C—F reduction in the parent ketone.

Alternatively, the increase in wave i_A can be caused by amine catalysis of the dehydration of $C_6H_5C(OH)_2CF_3$.

A similar increase in limiting current for carbonyl reduction in a hydrated compound has been reported for reduction of formaldehyde in the presence of ammonia, amines and amino acids [6—9]. The attribution of the increase to formation of reducible methylol derivatives (carbinolamines).

The general problem of interaction of amines with strongly hydrated aldehydes and ketones will be further investigated.

REFERENCES

1 W. J. Scott and P. Zuman, Anal. Chim. Acta, 125 (1981) 71.
2 P. Zuman, Collect. Czech. Chem. Commun., 15 (1950) 839.
3 S. G. Mairanovskii and L. I. Lishcheta, Collect. Czech. Chem. Commun., 25 (1960) 3025.
4 P. J. Elving and C. E. Bennett, J. Electrochem. Soc., 101 (1954) 520.
5 P. Zuman, W. Szafranski and D. Visioli, J. Org. Chem., submitted.
6 L. Matoušek, Ph.D. Thesis, Charles Univ., Prague, 1951.
7 Y. I. Turyan and B. P. Zhantalai, Kinet. Katal., 3 (1962) 325.
8 Y. I. Turyan and B. P. Zhantalai, Zavod. Lab., 28 (1962) 1431.
9 Y. I. Turyan and T. A. Cheremukhina, Zh. Anal. Khim., 19 (1964) 815.

Analytica Chimica Acta, 126 (1981) 263
Elsevier Scientific Publishing Company, Amsterdam — Printed in The Netherlands

Erratum

F. V. Mirzoyan, V. M. Tarayan and E. Kh. Hairyan, Sensitive Spectrophotometric Determination of Germanium as Methylene Blue 12-Molybdogermanate.
Anal. Chim. Acta, 124 (1981) 185—192.

p. 191. The last paragraph should read:

The accuracy was checked on germanium-containing standard minerals (No. 791—76, 3.1×10^{-4}% Ge and 792—76, 1.1×10^{-4}% Ge), and also by standard addition to various germanium-containing iron ores (4.3×10^{-4}—1.1×10^{-3}% Ge), following a preliminary separation of germanium(IV) as germanium tetrachloride. The results were all satisfactory.

ANALYTICA CHIMICA ACTA, Vol. 126 (1981)

AUTHOR INDEX

ACA announcements

ANNOUNCEMENT OF MEETING

6th INTERNATIONAL CONFERENCE ON COMPUTERS IN CHEMICAL RESEARCH AND EDUCATION

The 6th ICCCRE will be held in the Washington, DC area on July 11–16, 1982, and will cover broad areas of computer applications in chemical research and education. There will be lectures in the mornings and evenings, with afternoons open for informal discussions and poster sessions. There will be no parallel sessions. Among the topics to be included are: Chemical Synthesis, Structure Elucidation, Structure/Activity Relationships, Theoretical Chemistry, Chemical Graph Representations, Pattern Recognition, Factor/Cluster Analysis, Computers in the Labs, Computers in the Classroom, Chemical Graph Searching, and U.S. Government Activities in the Field of Computers in Chemistry.

The international organizing committee will consist of S. Heller, Chairman (U.S.A.), V. Koptyug (U.S.S.R.), J. Zupan (Yugoslavia), S. Sakaki (Japan), J.T. Clerc (Switzerland) and P. Lykos (U.S.A.).

Since the conference is expected to have limited facilities, attendence will be held to 150 participants. There will be a spouse program.

For more information contact: Dr. Stephen R. Heller, Chairman, 6th ICCCRE, EPA, MIDSD, PM–218, 401 M Street, S.W., Washington, DC 20460, U.S.A. Tel: (202) 755–4938; Telex: 89–27–58.

CALENDAR OF FORTHCOMING MEETINGS

May 11–15, 1981 Avignon, France	**Vth International Symposium on Column Liquid Chromatography** Contact: Prof. G. Guiochon, Ecole Polytechnique, Laboratoire de Chimie Analytique Physique, Route de Saclay, 91128 Palaiseau Cedex, France. (Further details published in Vol. 118, No. 1)
May 12–15, 1981 Frankfurt am Main, G.F.R.	**5th European Experimental NMR Conference** Contact: 5th EENC, H. Caspari, Iwan Stranski-Institut der Technischen Universität Berlin, Strasse des 17 Juni 112, D-1000 Berlin 12, G.F.R.
May 18–20, 1981 Jekyll Island, Georgia, U.S.A.	**11th Annual Symposium on the Analytical Chemistry of Pollutants** Contact: Prof. Dr. Roland W. Frei, The Free University, De Boelelaan 1083, 1081 HV Amsterdam, The Netherlands.
May 20–22, 1981 Eger, Hungary	**Symposium on the Analysis of Steroids** Contact: Prof. S. Görög, c/o Hungarian Chemical Society, 1061 Budapest VI., Anker köz 1, Hungary.
May 26–28, 1981 Washington, DC, U.S.A.	**3rd International Symposium on Rapid Methods and Automation in Microbiology** Contact: Dr. Richard C. Tilton, Chairman, ISRMA Planning Committee, University of Connecticut Health Center, Department of Laboratory Medicine, 263 Farmington Avenue, Farmington, CT 06032, U.S.A.
June 1–5, 1981 Metz, France	**International Conference on Elemental Analysis** Contact: conference administrators, S. International, 27 Rue du Mans, 92400 Courbevoie, Paris, France. Tel. (01) 333 44 10.
June 1–5, 1981 Stresa, Lago Maggiore, Italy	**2nd European Symposium on Organic Chemistry** Contact: Prof. Giorgio Modena, Istituto di Chimica Organica, Via Marzolo, 1, 35100 Padova, Italy.

June 9–11, 1981 Scarborough, Great Britain	**The 34th Chemists' Conference** Contact: J. Davey, Teesside Laboratories, British Steel Corporation, P.O. Box 11, Grangetown, Middlesbrough, Cleveland TS6 6UB, Great Britain (Further details published in Vol. 124, No. 2)
June 15–29, 1981 Toronto, Canada	**6th International Conference on Modern Trends in Activation Analysis and Exhibition** Contact: Prof. R.E. Jervis, Chairman, Organizing Committee, 6th ICMTAA, Department of Chemical Engineering and Applied Chemistry, University of Toronto, Toronto, Ontario, Canada M5S 1A4.
June 16–17, 1981 Venice, Italy	**1st International Symposium on Chromatography in Biochemistry, Medicine and Environmental Research** Contact: Dr. A. Frigerio, Italian Group for Mass Spectrometry in Biochemistry and Medicine, c/o Istituto di Ricerche Farmacologiche "Mario Negri", Via Eritrea 62, 20157 Milan, Italy. Tel: 35.54.546.
June 18–19, 1981 Venice, Italy	**8th International Symposium on Mass Spectrometry in Biochemistry, Medicine and Environmental Research** Contact: Dr. A. Frigerio, Italian Group for Mass Spectrometry in Biochemistry and Medicine, c/o Istituto di Ricerche Farmacologiche "Mario Negri" Via Eritrea 62 20157 Milan, Italy. Tel: 35.54.546.
June 22–25, 1981 Berkeley, CA, U.S.A.	**2nd International Topical Meeting on Photoacoustic Spectroscopy** Contact: Optical Society of America, Photoacoustic spectroscopy, 1816 Jefferson Place, NW, Washington, DC 20036, U.S.A.
June 22–26, 1981 Veldhoven, The Netherlands	**4th International Symposium on Affinity Chromatography and Related Techniques** Contact: Dr. T.C.J. Gribnau, Organon Scientific Development Group, P.O. Box 20, 5340 BH Oss, The Netherlands. (Further details published in Vol. 118, No. 1)
June 23–27, 1981 Karl–Marx–Stadt, G.D.R.	**Tagung Festkorperanalytik** Contact: Dr. K. Danzer, Technische Hochschule, Karl–Marx–Stadt, Sektion Chemie und Werkstofftechnik, PSF 964, 9010 Karl–Marx–Stadt, G.D.R. (Further details published in Vol. 118, No. 2)
June 30–July 2, 1981 Amsterdam, The Netherlands	**International Conference on Ion and Plasma Assisted Techniques** Contact: CEP Consultants, 26 Albany Street, Edinburgh EH1 3QH, Great Britain.
July 5–10, 1981 Jerusalem, Israel	**Fourth International Conference on Surface and Colloid Science** Contact: The Secretariat, Fourth International Conference on Surface and Colloid Science, c/o Conventions (Kopel Tours) Ltd., P.O. Box 3054, Tel Aviv 61030, Israel.
July 5–10, 1981 Swansea, Wales	**The Third Swansea Summer School of Automatic Chemical Analysis** Contact: Prof. D. Betteridge, Department of Chemistry, University College of Swansea, Singleton Park, Swansea SA2 8PP, Great Britain.
July 6–9, 1981 Strasbourg, France	**27th IUPAC Symposium on Macromolecules** Contact: Secretariat, Macro 1981, Société de Chimie Industrielle, 28, rue Saint-Dominique, 75007 Paris, France.
July 12–17, 1981 Exeter, Great Britain	**5th International Conference on NMR Spectroscopy** Contact: Dr. J.F. Gribnau, Royal Chemical Society, Burlington House, London W1V 0BN, Great Britain.
July 13–17, 1981 Srinagar, India	**International Conference on the Application of the Mössbauer Effect** Contact: Dr. V.G. Bhide, National Physical Laboratory, Hillside Road, New Delhi, 110012, India.
July 13–17, 1981 Durham, Great Britain	**International Symposium on Advances in Polymer Characterization** Contact: Dr. W.J. Feast, Chemistry Department, University of Durham, South Road, Durham DH1 3LE, Great Britain

July 14–16, 1981 Cambridge, Great Britain	**International Conference in Microscopy and X-Ray Diffraction – Inter/Micro '81** Contact: McCrone Research Institute Ltd., 2 McCrone Mews, Belsize Lane, London NW3 5BG, Great Britain.
July 19–24, 1981 Tokyo, Japan	**8th International Congress of Pharmacology** Contact: Int. Union of Pharmacology, IUPHAR, Pharmakologisches Institut im Neuenheimer, Feld 366, D-6900 Heidelberg, G.F.R.
July 20–23, 1981 Prague, Czechoslovakia	**22nd Prague Microsymposium on Characterization of Dynamic and Geometrical Structure of Polymer Systems by NMR Spectra** Contact: B. Sedláček, Institute of Macromolecular Chemistry, Czechoslovak Academy of Sciences, Heyrovského n.2, CS–162 06 Praha, Czechoslovakia.
July 20–23, 1981 Oxford, Great Britain	**7th International Symposium on Synthesis in Organic Chemistry** Contact: Dr. John F. Gibson, Royal Society of Chemistry, Burlington House, London W1V 0BN, Great Britain
July 28–31, 1981 New Hampton, NH, U.S.A.	**30th Anniversary Meeting of the Gordon Research Conference on Statistics in Chemistry and Chemical Engineering** Contact: Dr. Alexander M. Cruickshank, Director, Gordon Research Conferences, Pastore Chemical Laboratory, University of Rhode Island, Kingston, RI 02881, U.S.A. Tel. (401) 783–4011.
Aug. 2–6, 1981 Fort Collins, CO, U.S.A.	**International Symposium on Organometallic Chemistry Directed to Organic Synthesis** Contact: Dr. L.S. Hegedus, Department of Chemistry, Colorado State University, Fort Collins, CO 80523, U.S.A.
Aug. 3–7, 1981 Denver, CO, U.S.A.	**30th Denver Conference on Applications of X-Ray Analysis** Contact: Mrs. Mildred Cain, Denver Research Institute, University of Denver, Denver, CO 80208, U.S.A. Tel: (303) 753–2141.
Aug. 9–14, 1981 Toronto, Canada	**10th International Conference on Organometallic Chemistry** Contact: Dr. H.C. Clark, V-P Academic, University of Guelph, Guelph, Ontario, Canada N1G 2W1.
Aug. 9–14, 1981 Maryland, U.S.A.	**6th International Conference on Chemical Education** Contact: Dr. Marjorie Gardner, Division Director, Division of Science Education Resources Improvement, National Science Foundation, Washington, DC 20550, U.S.A.
Aug. 16–21, 1981 Vancouver, Canada	**28th Congress International Union of Pure and Applied Chemistry** Contact: Congress Secretariat, 28th IUPAC Congress, c/o The Chemical Institute of Canada, 151, Slater Street, Suite 906, Ottawa, Ontario, Canada K1P 5H3.
Aug. 17–21, 1981 Meriden, NH, U.S.A.	**Gordon Research Conference on Ion Exchange** Contact: Dr. A.M. Cruickshank, Director, Gordon Research Conferences, Pastore Chemical Laboratory, University of Rhode Island, Kingston, RI 02881, U.S.A. Tel. (401) 783–4011, or (401) 783–3372.
Aug. 20–21, 1981 Helsinki, Finland	**Symposium on Harmonisation of Collaborative Analytical Studies** Contact: Dr. H. Egan, Laboratory of the Government Chemist, Cornwall House, Stamford Street, London SE1 9NQ, Great Britain.
Aug. 23–28, 1981 Espoo, Finland	**Euroanalysis IV – Triennal Conference of the Federation of European Chemical Societies** Contact: Professor L. Niinistoe, Department of Chemistry, Helsinki University of Technology, SF–02150 Espoo 15, Finland. (Further details published in Vol. 109, No. 1)
Aug. 23–28, 1981 Canberra, Australia	**Sixth Australian Symposium on Analytical Chemistry** Contact: Hon. Secretary, Miss B.J. Stevenson, P.O. Box 1397, Canberra City, A.C.T. 2601, Australia.

Aug. 23–28, 1981 New York, NY, U.S.A.	**National American Chemical Society Meeting** Contact: American Chemical Society, 1155 Sixteenth Street, NW, Washington, DC 20036, U.S.A.
Aug. 30–Sep. 5, 1981 Vienna, Austria	**XI International Congress of Clinical Chemistry – IV European Congress of Clinical Chemistry** Contact: Congress Secretariat, Interconvention, P.O. Box 35, A-1095 Vienna, Austria. Tel. (0222) 42 13 52.
Sep. 1–3, 1981 Houston, TX, U.S.A.	**"EXPOCHEM '81"** Contact: Dr. A. Zlatkis, Chemistry Department, University of Houston, Houston, TX 77004, U.S.A. Tel. (713) 749–2623
Sep. 1–4, 1981 Siofok, Hungary	**3rd Danube Symposium on Chromatography** Contact: Hungarian Chemical Society, H–1368 Budapest, P.O.B. 240, Hungary. Tel: Budapest 427–343. (Further details published in Vol. 115)
Sep. 1–4, 1981 Aberdeen, Scotland	**ESTA 2 – The Second European Symposium on Thermal Analysis** Contact: Dr. F.P. Glasser, Chairman of the Organising Committee, ESTA 2, Department of Chemistry, University of Aberdeen, Meston Walk, Old Aberdeen, AB9 2UE, Scotland.
Sep. 4–8, 1981 Tokyo, Japan	**9th International Conference on Atomic Spectroscopy and XXII Colloquium Spectroscopicum Internationale** Contact: The Japan Society for Analytical Chemistry, 9th ICAS/XXII CSI, Gotanda Sanhaitsu, 26-2 Nishigotanda 1-chome, Shinagawa-ku, Tokyo 141, Japan. (Further details published in Vol. 118, No. 1)
Sept. 9–11, 1981 Chicago, IL, U.S.A.	**2nd International Symposium on Radiopharmacology and Exhibition** Contact: Dr. Lelio G. Colombetti, Pharmacology Department, Loyola University, Stritch School of Medicine, Maywood, IL 60153, U.S.A.
Sept. 9–11, 1981 Coventry, Great Britain	**International Conference on Advances in Flow Measurement Techniques** Contact: Conference Organizer, BHRA Fluid Engineering, Cranfield, Bedford, Great Britain.
Sept. 20–25, 1981 Philadelphia, PA, U.S.A.	**8th Annual Meeting of the Federation of Analytical Chemistry and Spectroscopy Societies (FACSS)** Contact: Richard J. Knauer, Publicity Chairman, ARMCO INC., P.O. Box 1697, Baltimore, MD 21203, U.S.A.
Sep. 21–24, 1981 Loughborough, England	**Particle Size Analysis Conference** Contact: P.J. Lloyd, PSA 81 Conference, Particle Technology Group, Chemical Engineering Department, University of Technology, Loughborough, Leics. LE11 3TU, Great Britain. (Further details published in Vol. 120)
Sep. 22–25, 1981 Leipzig, G.D.R.	**Analytiktreffen 1981 – Strukturanalytische Methoden in der Stereochemie** Contact: Sektion Chemie der KMU Leipzig, Liebigstrasse 18, DDR–7010 Leipzig, G.D.R.
Sep. 28–Oct. 1, 1981 Barcelona, Spain	**16th International Symposium on Advances in Chromatography** Contact: Professor A. Zlatkis, Chemistry Department, University of Houston, Houston, Texas 77004, U.S.A.
Sep. 29–Oct. 2, 1981 Basle, Switzerland	**ILMAC'81 – 8th International Exhibition of Laboratory, Chemical Engineering, Measurement and Automation Techniques in Chemistry** Contact: D. Gammeter, Secretariat, ILMAC '81, Postfach, CH–4021 Basle, Switzerland. Tel: 061–2620 20.
Oct. 27–29, 1981 London, Great Britain	**Petroanalysis 81** Contact: Miss I.A. McCann, Conference Officer, Institute of Petroleum, 61 New Cavendish Street, London W1M 8AR, Great Britain. (Tel: 01–636 1004, Telex: 264380)

(continued from back cover)

Short Communications

Elsevier Scientific Publishing Company, 1981

Printed in The Netherlands.

CONTENTS

(continued on inside page of cove